Diffusion of polyelectrolytes in dispersions of nanoparticles

Caterina Dolce

Thèse de doctorat

Pour l'obtention du grade de

Docteur de l'Université Pierre et Marie Curie

École doctorale de Chimie Physique et Chimie Analytique de Paris Centre

Diffusion of polyelectrolytes in dispersions of nanoparticles

Caterina DOLCE

Directeur de thèse : Guillaume MÉRIGUET

Présentée et soutenue publiquement le *24 Novembre 2016* devant un jury composé de :

M. Eric BUHLER ..... *Rapporteur*

M. Armel GUILLERMO ..... *Rapporteur*

Mme Barbara HRIBAR LEE ..... *Examinatrice*

M. François RIBOT ..... *Examinateur*

Mme Véronique GILARD ..... *Examinatrice*

M. Guillaume MÉRIGUET ..... *Directeur de thèse*

You must do the thing you think you cannot do

Eleanor Roosevelt

Remerciements

Ce travail de thèse a été réalisé au sein du laboratoire PHENIX (PHysicochimie des Electrolytes et Nanosystèmes InterfaciauX) de l'Université Pierre et Marie Curie (UPMC) sous la direction de Guillaume Mériguet. Je souhaite le remercier, tout d'abord pour m'avoir donné l'opportunité de faire ce parcours de thèse, pour ses qualités d'encadrement assujetti par ses grandes connaissances scientifiques. J'ai beaucoup appris grâce à lui, profitant de sa disponibilité permanente qui m'a permis d'apporter de nombreuses réponses à mes questions, auxquelles il a toujours su répondre de façon très didactique et scientifiquement stimulante. Je le remercie également de m'avoir appris ce qu'est un travail scientifique, et de m'avoir apporté un éclairage sur la bonne façon d'aborder un problème scientifique. Par ailleurs, un grand merci pour ses qualités humaines qui ont contribué à faire de ces trois années un parcours si agréable, une grande expérience de vie, une croissance scientifique, professionnelle, et humaine. J'ai eu la chance de l'avoir eu en tant qu'encadrant.

Je remercie sincèrement Eric Buhler et Armel Guillermo d'avoir accepté de rapporter ma thèse, et Barbara Hribar Lee, Véronique Gilard, et François Ribot d'avoir accepté de faire partie de ce jury de thèse.

Je remercie Pierre Levitz directeur du laboratoire Phenix qui m'a permis de realiser ma thèse au sein du laboratoire.

Je remercie le Professeur Marie Jardat, Directrice de l'équipe MEM, qui en plus d'avoir été un très bon guide pour cette équipe, a réussi tous les jours à créer, alimenter, et maintenir la cohésion de groupe.
Je remercie les bureaux des projets européens de l'UPMC, de la délégation Paris B du CNRS, et de l'UTC de Compiègne. Pour m'avoir accueilli pendant ma mission doctorale de valorisation de la recherche en partenariat européen. En particulier, j'adresse mes remerciement les plus chaleureux à Stéphanie Rossard, responsable des projets européens de l'UTC, pour la passion et l'enthousiasme qu'elle m'a bien transmise.
Je remercie Isabelle Grillo pour m'avoir accueilli à l'ILL et pour son aide et ses précieux conseils durant les manips sur D33 ; Un merci également à Isabelle Correia pour son aide précieuse et sa disponibilité pendant les mesures RMN.

En ce qui concerne mon laboratoire d'accueil, la liste est longue et j'espère sincèrement que je n'oublierai personne. Vous avez tous contribué à mon enrichissement personnel pendant ce parcours.

Dans le domaine de la gestion du laboratoire, je remercie beaucoup Brigitte et Gérard, pour leur efficacité dans l'organisation de toutes les missions auxquelles j'ai participé, ainsi que pour

leur gentillesse et disponibilité quotidienne.

Un grand merci à Anne-Laure pour ses conseils et son soutien sur la RMN ; Emmanuelle pour ses conseils utiles et sa disponibilité ; Jean pour ses intéressantes histoires, sa disponibilité pour répondre à toutes les questions scientifiques et techniques, et aussi pour avoir été présent pendant les longues journées au laboratoire ; Nicolas pour la bonne humeur apportée dans le laboratoire ; Natalie pour m'avoir initié aux petits angles, pour avoir permis de faire les premiers tests pendant son beam time ; Amandine pour l'aide dans le laboratoire et pour m'avoir aidé à améliorer mon français pendant les agréables déjeuners ensemble .

Merci également à tous ceux avec qui j'ai pu partager mes pauses thé, déjeuner et couloir : Serge, Vincent, Damien, Virginie, Benjamin, Mathieu, Jean-Pierre, Olivier, Ana, Augusta, José, et tous les autres.

Enfin je remercie tous mes collègues et amis pour les bons moments passés, le soutien, la compréhension, l'aide, les conseils, et les échanges sur les plus différents sujets. Tout d'abord Steph, pour avoir été un parfait compagnon de bureau pour ces trois années, pour m'avoir bien supporté, ainsi que pour sa présence durant tous les moments que ce soit dans le laboratoire ou en dehors (la liste sera trop longue) ; Willy, ami et collègue, toujours prêt à écouter, à aider avec sa gentillesse et sa bonne humeur qui ont permis à rendre si agréable les journées ; Pauline B. pour sa gentillesse permanente, sa disponibilité et sa force tranquille qui m'ont beaucoup encouragé ; Pauline S. pour ses nombreuses contributions pour le laboratoire et pour tous ; Adelchi pour sa gentillesse, sa disponibilité et pour son aide dans la traduction de nombreux mots en français que je ne connaissais pas ; Anastacia chère amie et compagnon de laboratoire. Maintenant, je dois arrêter avec les périphrases et me contenter des faire une liste de tous mes chères collègues et amis qui m'ont accompagnée et ont été présents pendant cette période passée au laboratoire : Xu, Fabien, Sébastien, Vivien, Lisa, Allan, Yasine, Jamoowantee, Nadia, Véronica, Nebewia, Alberto, Gabriele ; Aux anciens thésards : Clarisse, Antoine, Simon, Raphael, Amaël, Dario, Davide, Clément... et aux thésards venus de loin mais toujours si proche Clébert et Grégor.

C'est avec une heureuse nostalgie que je repenserai à tous les moments passés ensemble et en général à l'ensemble de ces trois années.

A Derek, la personne qui a été à mes côtés de moi tous les jours, qui m'a encouragé et donné le soutien dont j'avais, j'ai et j'aurai besoin.

Infine un ringraziamento speciale alla mia famiglia che mi ha permesso di realizzare gli studi, che mi ha sempre supportato e accompagnato nelle mie scelte senza mai giudicare ed essendo sempre presente in ogni momento di questo percorso.

Contents

Introduction

Polyelectrolytes are a particular class of polymer with ionizable repetition units that dissociate in polar solvent (such as water) leading to macro-ions and counterions [1–7]. Because of the electrostatic interactions and the presence of counterions, polyelectrolyte solutions have a number of properties remarkably different from solutions of uncharged polymers [6].

Solutions and materials made of polyelectrolytes are widespread in several industrial, biological and environmental processes [8–11]. In the industry, they are used as stabilisers, scale inhibitor, thickening agent, dispersant, or paper coatings [8, 12–14]. For example the sodium polyacrylate, thanks to its electrostatic and steric properties, is a standard dispersant used in paper industry [15]. Polyelectrolytes are also dispersants of choice for ceramic powder suspension [16]. One of their major role is played in biology, as DNA and RNA are polyelectrolytes. In environmental processes, natural organic polyacids play also a main role, such as the facilitated transport of heavy metal or radionuclide ions [17], or in the production of potable water based on coagulation and flocculation of suspended solids and colloids [18].

In most of the aforementioned applications polyelectrolytes play a crucial role. However, because the presence of other compounds, their static and dynamical properties can be consdiderably modified. For a better insight into these processes, both from a scientific and application oriented point of view, the properties of polyelectrolytes in presence of other compounds have to be studied in more detail. In particular, polyelectrolytes are commonly present in nanosized particles suspensions [4, 19–21].

In this thesis, we focus on the modification of the dynamics properties of short polyelectrolytes in suspensions of charged nanoparticles [4]. The change in the diffusion of short polyelectrolytes in the presence of charged obstacles is a fundamental issue and, the dynamics of polyelectrolytes in dispersion of nanoparticles is hardly described and understood, particularly for the smaller chains. This situation occurs in different fields, and it is of interest for the understanding of several scientific issues. For example, the dynamics of proteins in biological

samples, which are charged and crowded media, is strongly slowed due to the presence of other objects with respect to their dynamics in vitro [22]. In aquatic environments, as lake and river, humic substances, which are one of the major organic constituent that carry on nutritive substances, are polyelectrolytes that diffuse through membranes and nanoparticle systems [23]. The dynamics of polymers in suspensions of nanoparticles is also fundamental to many industrial fields such as tribology or in designing fabrication methods for nanocomposites [24].

Then, the diffusion of polyelectrolytes in suspension of nanoparticles, can be seen as a particular case of the more general problem of the diffusion in crowded system [25, 26]. If the particle and polyelectrolyte have opposite signs, electrostatic adsorption is observed, which reduces drastically the mobility of the polyelectrolytes. In the systems where both the particles and polyelectrolytes have charge of the same charge, the adsorption is precluded. The diffusion is still expected to decrease due to the excluded volume of obstacles, but additional interactions, for instance electrostatic interactions, between diffusing polyelectrolytes and crowding particles can lead to a further hindrance. In the latter context, this thesis aims to assess the parameters that affect the diffusion of short polyelectrolyte in suspensions of nanoparticles.

The questions we intend to tackle in this work are:

- *How does the diffusion depend on the properties of the crowding medium?*
- *What is the effect played by the steric obstruction?*
- *How does the electrostatic interactions affect the dynamical properties of the charged chains?*
- *Can we find a model to consider these effects?*

To address these questions, we design an experimental system made of carboxylate molecules of various sizes, from a simple carboxylate (propionate) up to polyelectrolytes (sodium polyacrylate, PAANa), diffusing in aqueous dispersions of silica nanoparticles of different size and surface charge. Both polyelectrolytes and nanoparticles are negatively charged at high pH.

In these systems, the interactions between nanoparticles and polyelectrolyte are important to the colloidal stability of the mixtures but also to the dynamic properties of polyelectrolyte chains. The interactions between these objects are of several types, for example van der Waals interaction, hydrophobic effect, but the electrostatic interaction has a major role in suspensions

of charged objects. This contribution differs from the direct Coulomb interaction, because if it always depends on the charge of the objects, it is screened by the electrolyte present in solution. The distance of screening, called Debye length κ^{-1}, decreases with the added salt concentration. It is therefore possible to modulate the electrostatic interaction, on the one hand by changing the charge of the objects and secondly by varying the salt concentration.

Moreover, the dynamics of polymers is particularly influenced by their conformation and their concentration. In this thesis, we restricted the study to the dilute regime, i.e. the polymer concentrations is below the critical concentration $c^\star$ above which the polymer chains overlap. Furthermore, we work in the colloid limit, i.e. the polymers are small compared to the colloidal particles.

Among weak polyelectrolytes, polyacrylic acid (PAA) has a specific interest since it is widely used in household and industry products as a scale inhibitor or thickening agent [12, 13]. Despite a noticeable number of studies have been devoted to polyelectrolytes, especially PAA, the vast majority have so far focused on long chain polyelectrolytes since they are compatible with scaling approaches or infinitely long chain descriptions [27, 28]. However, some applications use short chain polyelectrolytes [29, 30], for which the validity of the theoretical developments and scaling laws needs to be examined, especially for systems where the length of the chain is in the order of few persistence lengths. The study of the simple carboxylates has been suggested by the necessity to reduce the complexity of the diffusers, mostly to eliminate the intra-chains interactions which impact dynamics. Furthermore, a simpler system is more suitable for comparison with simulation systems and with theoretical models.

To study this system, we take advantage of the diffusion NMR technique [31–33]. NMR is a versatile technique to study the conformation and structure of polymer chains [34]. Diffusion NMR allows to study the Brownian movement of molecules in a time scale on the order of 10-1000 ms and over distances of 10 to 100 μm [35, 36].

Outline

This thesis starts with an introduction of the main properties and models used to describe and characterise the experimental systems of polyelectrolytes and nanoparticles. The fundamental

quantities used in this work, and the basic models used to describe the conformation and the diffusion coefficient of the polymeric chains are introduced in ***chapter 1***.

The models used to study the dynamics in crowded media are presented in ***chapter 2*** . Finding a suitable model that describes well the dynamics of polyelectrolytes in charged crowded system is a challenging problem since the properties of the diffuser have to be considered in addition with the effect of all interactions. We present a method to calculate numerically the diffusion coefficient of a charged point-like diffuser in a charged crowded system, solving the diffusion equation in a DLVO potential.

The diffusion nuclear magnetic resonance (NMR) is the technique used in this thesis to investigate the self-diffusion of polyelectrolytes in crowded system. ***Chapter 3*** is then dedicated to the theoretical concepts of NMR, from the principles of the technique, to the development of the model used for the data analysis.

Chapter 4 describes the design and properties of the experimental systems used: the diffusers, carboxylate molecules of various sizes, and the obstacles, silica nanoparticles of different sizes and surface charges.

In ***chapter 5*** thanks to the ^{1}H NMR, we study the structural changes of polyelectrolytes via the chemical shift δ, and the variation of their dynamics by the study of the diffusion coefficient. The spectra of oligomers and polyelectrolytes are studied in different conditions, to investigate the chain conformation. The effect of molecular weight, concentration and interactions on the dynamics of polyelectrolytes are investigated. Through the two NMR observables used (chemical shift and diffusion coefficient), we want to assess the consequences of the ionisation and to investigate the influence of the polyelectrolyte molar mass.

The impact of charged obstacles on the dynamics of the oligomers and polyelectrolytes is investigated in ***chapter 6*** , by the study of the self-diffusion coefficient as a function of the volume fraction of obstacles ϕ. The effect of the properties of the medium such as ionic strength and pH are investigated. The results are discussed in the light of theoretical models to understand the role played by the pure obstruction and the interactions.

Polyelectrolytes are also used to the formation, stabilisation, or aggregation of nanoparticles [4]. The stability of the suspension of nanoparticles is governed by the combination of different types of interactions. For instance, the polyelectrolyte adsorption on nanoparticle surface can result in the stabilisation of the nanoparticles by the steric and electrostatic repul-

sion [16], if there is no bridging between the particles. Conversely non-adsorbing polyelectrolytes can cause the aggregation of nanoparticles due to the depletion phenomenum [37, 38]. In the last months of this thesis, we took advantage of beam time on the D33 spectrometer of the Laue-Langevin Institute (Grenoble) to study the structure of these systems by SANS, and to investigate the phase behaviour of silica particles in the presence of polyelectrolytes. This will be presented in the ***chapitre 7***.

Chapter 1

Colloids and polyelectrolytes

Contents

1.1 | Introduction

This chapter introduces the main theoretical concepts for colloids, and in particular for polymers and polyelectrolytes. The general description of these systems includes the definition of main quantities as the characteristic lengths, the dispersity, the critical concentration, that we will use in the next chapters to characterise our systems. The basic models to describe the structure and the dynamics of an ideal and real chain will be introduced, with the aim to point out the scaling laws that we will use for the interpretation of the experimental data.

For the readers interested in a complete theoretical description of polymer chains, we suggest de Gennes and Rubinstein and Colby textbooks [39, 40]. For an extended description of colloidal systems Hunter's textbook is a valuable reading [41].

1.2 | Colloids

In this thesis, we study systems constituted by polyelectrolytes with a maximum length of $\sim$ 40 nm and nanoparticles, systems are also defined as colloidal systems. In this section we introduce the basic concepts of colloidal system, which will be useful for the comprehension of the main properties of systems studied.

A colloidal dispersion is a suspension of particles in a solvent [41]. The dimensions of the colloidal particles are within the range of 1 nm to 10 μm. The units dispersed through the solvent are larger than the molecules of the solvent and interact simultaneously with the surface of a single colloidal particle causing a Brownian motion.

The study of colloidal properties has an important role in many domains ranging from biology to industry. In biology, protein and polysaccharide solutions have been studied using the methods of colloid science [42]; in medicine, modern colloidal micro-capsule techniques allow controlled release of drug [43]; in industry, the specific absorptive properties of colloids can be used to remove or concentrate industrial products or in wastewater treatment [44]. These are just a few examples of the vast application of colloidal systems [45]. Other examples of colloidal systems are inks, paints, foams, soils, smoke and aerosols.

The properties of colloidal system are affected by their size, their shape, their electrical charge, and the type of interaction with the solvent and the neighbouring particles. We will see how the variation of the interactions between the objects can alter properties as the dynamics and the phase behaviour of the system. In colloidal systems there are two main interactions: electrostatic repulsions, which repel the objects each other, and attractive forces, which tends to bind particles together. The attractive interactions might be of the nature of van der Waals interaction. It mainly arises from instantaneous induced dipoles, even if a particle has no permanent charge.

The repulsive force due to Coulomb interactions between colloidal particles of the same charge leads to a positive potential energy, and is often used to stabilise colloidal suspensions. Due to the important role played by the electrostatic interactions in our systems, we will dedicate the next sections to a brief summary on these interactions, pointing out the attention on the principal quantities that we will use to characterise our system in the next chapters.

1.2.1 | Electrostatic potential around a macroion

For charged objects, like polyelectrolytes or charged colloidal particles, the electrostatic interactions play an significant role that affects structural and dynamic properties. The electrostatic potential ψ, originated by a charged object at the distance r, depends on the local volume density of charge in that position $\rho(r)$ by Poisson's equation [4, 41]:

$$\nabla^2\psi(r) = -\frac{e}{\varepsilon_0\varepsilon_r}\rho(r) \tag{1.1}$$

where the Laplace operator ∇^2 is equal to $\partial^2/\partial x^2 + \partial^2/\partial y^2 + \partial^2/\partial z^2$. ε_0 is the vacuum permittivity, and ε_r is the relative permittivity of the medium of dispersion. The charge density is related to the ionic concentrations as follows:

$$\rho(r) = e\sum_j z_j c_j(r) \tag{1.2}$$

where z_j is the valency of ions j, $c_j(r)$ is the concentration of species j at the position r. In a mean field approach, the concentrations of species j may be expressed thanks to the Boltzmann distribution:

$$\rho(r) = e\sum_j z_j c_j(r) = e\sum_j z_j c_0 \exp\left(-\frac{z_j e\psi(r)}{k_B T}\right) \tag{1.3}$$

where c_0 is the concentration of species j in the bulk solution when $\psi = 0$, and $z_j e\psi(r)$ represents the work done to bring an ion j up from the bulk solution to the position r. It is assumed that the only work done is a purely electrical one. If the electrostatic energy is small compared to thermal energy ($|z_j e\psi(r)| \ll k_B T$), the linearization of the previous equation leads to a Debye-Hückel (DH) theory [46]:

$$\nabla^2\psi(r) = \kappa^2\psi(r) \tag{1.4}$$

where κ is the screening parameter, whose reciprocal κ^{-1} is known as the Debye-Hückel screening length. More specifically, κ^{-1}, which has the unit of length, corresponds to a distance over which the screened electrostatic interactions become non-significant:

$$\kappa^2 = \frac{e^2}{\varepsilon_0\varepsilon_r k_B T}\sum_j z_j^2 c_j = 4\pi\ell_{\mathrm{B}}\sum_j z_j^2 c_j \tag{1.5}$$

where ℓ_B is the Bjerrum length: the distance at which the electrostatic interaction between two elementary charges is equal to the thermal energy $k_B T$ (this length will be presented in Eq. 1.28). Using the previous expression, equation 1.4 has the following solution for the electrostatic potential for a spherical particle of radius R_{o}:

$$\psi(r) = \frac{Ze}{4\pi\varepsilon_0\varepsilon_r(1+\kappa R_{\mathrm{o}})}\frac{\mathrm{e}^{-\kappa(r-R_{\mathrm{o}})}}{r} \tag{1.6}$$

According to this model, the electrostatic potential is reduced due to the presence of additional neutralizing charges in solution, by the dependence from the κ parameter.

Therefore, the charge of charged colloidal particles is balanced by the presence of ions of opposite sign (counterions). The Fig. 1.1 shows schematically the behaviour of the electrostatic potential ψ_0 in the vicinity of a positively charged particle, and the neighbour ions behaviour. The negative counterions are attracted towards the particles by the electric field generated by the positive charges, but they are also subject to thermal motion which tends to distribute them uniformly through the surrounding medium. As result, a few negative ions are bound strongly to the particle surface and their concentration falls off gradually away from the particle until

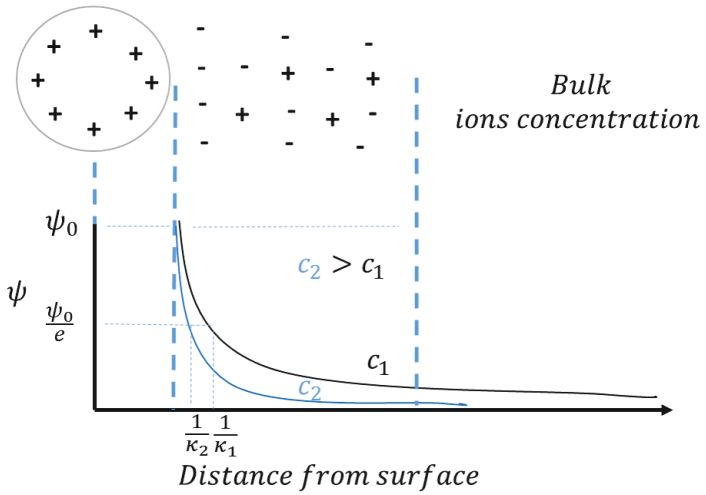

Figure 1.1: The electrostatic potential near an positively charged colloidal particle in function of the distance from colloidal particle, at different electrolyte concentration $c_2 > c_1$.

approaches the bulk concentration.

This charge arrangement is called electrical double layer around the particle. It depends on the electrolyte concentration [41]. The double layer refers to two parallel layers of charge surrounding the object. The first layer comprises ions adsorbed onto the object due to chemical interactions. The second layer called diffuse layer, it is composed of ions attracted to the surface charge via the coulomb force, it is made of free ions that move in the fluid under the influence of electric attraction and thermal motion.

A high electrolyte concentration causes the shrinking of the diffuse double layer closer to the particle, so that the electrostatic potential falls off more quickly with the distance Fig. 1.1.

Equation 1.6 is limited to weak value of electrostatic potential ($|z_j e\psi(r)| \ll k_B T$), but colloidal systems can be highly charged and this equation cannot be used. In the latter case, Poisson-Boltzmann equation (Eq. 1.1 and 1.3) can be solved numerically. Since the electrostatic potential decreases with the distance r from the surface, at a certain distance the potential is small enough so that equation 1.6 starts to be valid. However the charge Z has to be replaced by an effective charge Z_{eff}, that takes into account the condensation occuring at short distances. In the present, for high surface charges, Poisson-Boltzmann equation was solved numerically using the PB program developed by Per Linse (Lund University) and the long range behaviour has been fitted to derived the effective charge Z_{eff} [47, 48]. The solutions of the Poisson-Boltzmann

equation, and the fit of the long-range behaviour are reported in Fig. 1.2.

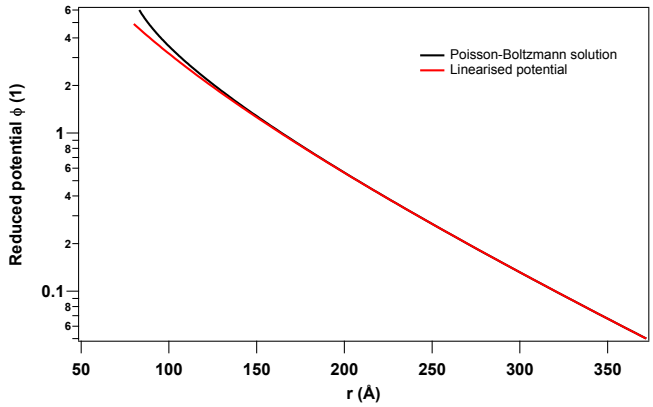

Figure 1.2: Solution of the Poisson-Boltzmann equation, compared with the fit of the long-range behaviour.

Electrostatic interactions between particles

In the present work, we will focus on particles and polyelectrolytes bearing electrostatic charge of the same sign. As a result, the electrostatic repulsions will keep them apart and the long-range linearised expression of the electrostatic potential can be used as a good approximation [49]. The screened Coulomb potential (or Yukawa potential) can be used to describe the interactions between two particles [50–52]. Considering two charged particles of radii R_1 and R_2 respectively, the interaction can be written as a function of the centre-to-centre distance r (Fig. 1.3):

$$\frac{U(r)}{k_B T} = \ell_B \frac{z_1 e^{\kappa R_1}}{1+\kappa R_1} \frac{z_2 e^{\kappa R_2}}{1+\kappa R_2} \frac{e^{-\kappa r}}{r} \tag{1.7}$$

where κ is the inverse screening Debye length (Eq. 1.5), z_i the charge of the particle i, ℓ_b the Bjerrum length (Eq. 1.28). This equation is often refered to as DLVO equation (Derjaguin-Landau [53]-Verwey-Overbeek [51]). For small ions, since the ionic radii are often small compared to κ^{-1}, the corresponding terms in κR_{ion} in 1.7 was neglected.

1.2.2 | Van der Waals potential

In the previous section we have discussed the repulsive forces arising from Coulombic interactions, but so far we have not discussed the attractive force, that cannot be neglected when the repulsion is reduced. The attractive force might be of the nature of van der Waals interaction,

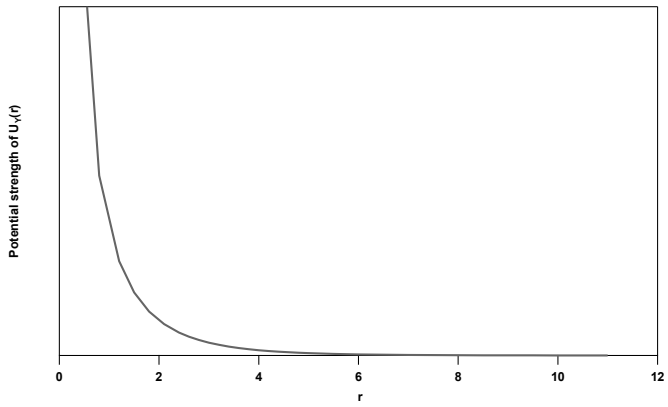

Figure 1.3: Form of the screened Coulomb potential.

responsible for example of the condensation of gases into liquids. However, in the case of two colloidal particles, this force displays a rather long range, comparable with the Coulomb interaction.

The attractive van der Waals potential, which for two particles with the same radius R_o was approximated in 1937 by Hamaker [54] integrating London's equation for the dispersion interaction energy between atoms over two spheres [55]. It has the form:

$$U_{\mathrm{vdW}}(h) = -\frac{A}{6}\left[\frac{2R_o^2}{h^2+4R_oh} + \frac{2R_o^2}{h^2+4R_oh+R_o^2} + \ln\left(\frac{h^2+4R_oh}{h^2+4R_oh+R_o^2}\right)\right] \tag{1.8}$$

where A is the Hamaker constant and h the distance between the surface of the particles ($h = r - 2R_o$, r distance center-center and R_o radius of the nanoparticle). The value of the Hamaker constant for silica in aqueous medium is $A = 8.3\times10^{-21}$ J (2.01 k_BT at 298 K) [56, 57]. For example, the value of the van der Waals interaction for two silica particles with a surface-surface distance of 6 nm is of the order of 0.3 k_BT.

1.3 | Polymer

This section is dedicated to an introduction on polymer systems, their properties and the fundamental models to describe them. Let's start with the definition of polymer and with the introduction of some parameters useful to characterise the system. A polymer is a molecule consisting of many repeating elementary units, called monomers which are connected by covalent bonds [40]. The number of monomer in a polymer is called degree of polymerisation,

N. A polymer can contain between 20 and 10 billion of monomers [40], and those with a small number of monomers (less than 20) are called oligomers. The monomer size a, ranges from a few Ångströms for synthetic polymers to a few nanometers for homopolymers. The distance between one end of the polymer chain and the other, when the polymer is stretched out, is called contour length or maximum length l_{max}. It is the product between the degree of polymerisation and the monomer length:

$$\ell_{max} = N \cdot a \tag{1.9}$$

The molecular mass M of a polymer is equal to N times the molecular mass M_m of its monomer:

$$M = N \cdot M_m \tag{1.10}$$

Polymers are not monodisperse in nature, but they are characterized by a distribution of molecular mass expressed in terms of quantity called dispersity of the chain, $Đ_{\mathrm{M}}$ [58]. It is defined as ratio of the weight-average molar mass M_w to its number-averaged molar mass M_n [59]:

$$Đ_{\mathrm{M}} = \frac{M_w}{M_n} \tag{1.11}$$

If all polymers in a given sample have the same degree of polymerisation the chain is monodisperse and $Đ_{\mathrm{M}}$ =1.

For a linear chain of homopolymer, the weight- and number-average molar mass M_w and M_n are respectively:

$$M_w = \frac{\sum_i m_i M_{mi}}{\sum_i m_i} = \frac{\sum_i N_i M_{mi}^2}{\sum_i N_i M_{mi}} \tag{1.12}$$

$$M_n = \frac{\sum_i N_i M_{mi}}{\sum_i N_i} = \sum_i N_i M_{mi} \tag{1.13}$$

where m_i is the total mass of the polymer constituted by monomers of mass M_{mi} ($m_i = N_i M_{mi}$), N_i is the fraction of monomer of mass M_{mi}. $\sum_i N_i = 1$ because the number distribution is normalized.

Therefore M_n and M_w describe the same polymer distribution with different weightings: M_n is the number average mass of molecules, and M_w is the mass average mass of molecules. In a

mixture of molecules, because M_w is always greater than M_n, $Đ_M$ is greater than 1.

Through different techniques as light scattering and the size-exclusion chromatography, we will have access at the different average molecular masses, to characterise our system.

1.3.1 | Concentration regimes

Polymer solutions can be classified in different regimes depending on their concentration c respect to the overlap or critical concentration c^*. If the polymer concentration is below $c^\star$, the solution is called dilute. In dilute solution, the average distance between chains is larger than their size, then the chain is isolated and the polymer-polymer interaction is weak. When the concentration of the polymer solution is close to $c^\star$, the mean spacing between molecules approaches the molecular diameter. If the polymer concentration is above $c^\star$, the solution is called semidilute. In this regime, polymers are not isolated chains because coils overlap and entanglement phenomena are present.

The geometrical definition of $c^\star$, that we will use to determine the concentration regime in which to work, depends on the conformation and size of the chain [60]. The ambiguities to determinate this parameter depend on the choice of the size. The radius of gyration is often used for coiled conformations, whereas the contour length is used for rod-like chains. In the present study, since changes of conformation will be considered and since the hydrodynamic radius R_h will be measured, we use R_h, which is an indirect measure of the conformation, to estimate $c^\star$ [61]:

$$c^\star = \frac{M_w}{N_A \cdot (2R_h)^3} \tag{1.14}$$

where N_A is the Avogadro constant. The hydrodynamics radius defines the size of the polymer in solution with the pervaded solvent. The polymer and the pervaded solvent move as one compact object, and R_h describes the radius of an object formed by the real chain and the solvent. For the specific case of polylectrolytes another value of the critical concentration has been proposed by Dobrynin and Rubinstein , however the model is not longer valid for the short chains treated in this thesis. So in the next chapters we will use the definition in Eq. 1.14 to define the value of critical concentration.

1.3.2 | Ideal chain

After having introduced some quantities to characterise polymers, here we are going to introduce the simplest model to describe their behaviour. These models, despite their simplicity, will allow us to obtain from our experimental data structural and conformational information of the system.

To characterise polymers, it is possible to use descriptions and models independent on chemical details and on interactions among the monomers. An useful model of polymers, that can be seen as reference for understanding the behaviour of real polymers, is the ideal chain [40]. The ideal chains are defined as chains having no interactions between monomers, and they are long enough to form an isotropic random coil. The random coil can take all possible conformations because the monomer subunits are oriented randomly.

The simplest theoretical description of an ideal chain is provided by the freely jointed chain model FJC. In this model, the polymer is described by a series of points linked by vectors of fixed length a_0 without correlations between their directions. Furthermore, the interactions between monomers, that are far apart along the chain, are not considered, consequently the overlap of different parts of the chain is possible. The chain can be described by an end-to-end vector $\vec{R_e}$. It is the sum off all monomer vectors of the chain, $\vec{a_i}$, and it is equal to the difference between the first $\vec{r_1}$ and the last point $\vec{r_N}$ of the polymer chain:

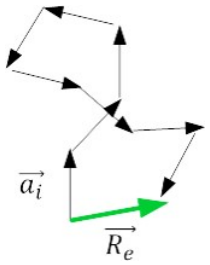

Figure 1.4: Freely jointed chain model.

$$\vec{R_e} = \vec{r_N} - \vec{r_1} = \sum_{i=1}^{N-1} \vec{a_i} \tag{1.15}$$

where N is the total number of monomers.

The root mean-square end-to-end distance R_e, is another quantity useful to describe the random coil formed by an ideal chain:

$$R_e^2 = \sum_{i,j=1}^{N-1} \langle \vec{a_i} \cdot \vec{a_j} \rangle = \sum_{i=1}^{N-1} \langle \vec{a_i}^2 \rangle + 2 \sum_{i=1}^{N-1} \sum_{j=i+1}^{N-1} \langle \vec{a_i} \cdot \vec{a_j} \rangle \tag{1.16}$$

where the ensemble average denotes an average over all possible states of the system, i.e. all possible bond orientations. In this model, all cross-products of equation 1.16 vanish for $i \neq j$, because two different vectors have a completely independent orientation:

$$\langle \vec{a_i} \cdot \vec{a_j} \rangle = 0 \tag{1.17}$$

Consequently, the characteristic length of a freely jointed chain polymer grows proportionally to the square root of the number of monomers:

$$R_e = a_0 \sqrt{N-1} \tag{1.18}$$

From this equation, we obtain one main property of ideal chain: R_e is proportional to the product of the number of vectors with the power of $1/2$.

Another important quantity to describe the polymer is the radius of gyration R_g. We will obtain this size by using the small angle neutron scattering technique in chapter 7. R_g is the average square distance between monomers and polymer's centre of mass:

$${R_g}^2 = \frac{1}{N} \sum_{i=1}^{N} (\vec{R_i} - \vec{R_{\text{cm}}})^2 \tag{1.19}$$

For an ideal chain, the average radius of gyration follows the same scaling law as the end-to-end distance. This is not true for real chain in all concentration regimes [62].

$$R_g = \frac{a_0}{\sqrt{6}} (N-1)^{1/2} \tag{1.20}$$

To sum up, the different radii described so far have been:

- R_h: the size of the polymer with the solvent that pervades it
- R_e: the end-to-end distance
- R_g: the average distance between the polymers and the polymer's centre of mass

We will obtained R_h from the NMR diffusion measurements (chapter 6), and R_g from the SANS measurements (chapter 7). The simple models introduced and the scaling law obtained,

will be used as reference models to interpret the behaviour of the experimental systems. Other models of ideal chains exist in literature, like the freely rotating chain or the worm-like chain model. Each model makes different assumptions, but every one ignores interactions between remote monomers that cannot be neglected in real polymer [40]. In the next section we introduce a model for the description of real chains.

1.3.3 | Real chain

In this section, we introduce a simple way to describe a real chain. In the ideal chain model, introduced in the previous section, one of the main hypothesis is to neglect the interaction of remote monomers. Furthermore, in the ideal model the overlap of different parts of the chain is allowed. However, this is not possible in a real chain where two monomers cannot overlap, this effect is called the *excluded volume effect*. We will see in the next chapters, the impact of the variation of volume effect on the dynamics of the chain [63]. The excluded volume effect derives from the fact that each monomer occupies a specific space that prevents other monomer from coming too close. This implies the existence of a finite volume around each point of the chain inaccessible to the other monomer.

Another hypothesis of the ideal chain, not longer valid for real polymer, is the independence between two adjacent monomers. In reality, due to chemical restrictions the orientation of two consecutive bonds are correlated and this makes the Eq. 1.17 invalids on a small scale. However, on a large scale Eq. 1.17 is valid, because the correlations between more distant vectors decay.

The model used for the ideal chain, can be adapted and used for a real chain. Practically, an equivalent freely jointed chain with uncorrelated and larger segments can be defined [39, 64]. Instead of considering a real chain consisting of bonds with fixed bond angles, Kuhn considered an equivalent ideal chain with connected segments, called Kuhn segments, that can orient in any random direction. The fixed bond length a is thus replaced, by the distance, called Kuhn length a_K, between two uncorrelated bonds:

$$a_K = n \cdot a \tag{1.21}$$

where n is the smallest distance without correlation between two bonds, thus a_K correspond with the a_0 of FJC model. a_K is also connected with rigidity of the chain expressed through

the persistence length, parameter that will be defined soon. Consequently, the number of independent segments N_K is:

$$N_K = \frac{N}{n} \tag{1.22}$$

Using the parameter a_K and N_K instead of a_0 and N, the FJC model can be used to describe a real chain according to the hypotheses introduced at the beginning of the section:

$$R_e = a_K (N_K)^{1/2} \tag{1.23}$$

However, depending on the real interactions among the monomers and the solvent, the scaling equation 1.18 or 1.23 must be rewritten with a more general expression which consider the dependence on the number of monomers:

$$R_e = \langle R_e^2 \rangle^{1/2} = a_0 N^{\nu} \tag{1.24}$$

$$R_e = a_K (N_K)^{\nu} \tag{1.25}$$

Where ν is the scaling exponent (or Flory parameter) that describes the dependence of the polymer conformation on the monomers' number. To calculate the value of the exponent ν, the following arguments developed by Flory , can be used [64]. It should be pointed that for a polymer in solution, its conformation depends on the type and quality of solvent. Indeed, the interactions polymer-solvent can be positive or negative. For a good solvent, interactions between polymer and solvent molecules are energetically favourable, so the polymer coils tends to expand. For a poor solvent, the interaction intra chains are preferred at the interactions with the solvent, and the polymer coils tends to contract. The conformation of a real chain in a good solvent is determined by the balance of an effective repulsion energy, that tends to swell the chain, and the decrease of entropy due to the deformation. From a minimisation of the chain free energy, constituted by the repulsive energy (the energy of the excluded volume interaction) and the elastic or entropic term (the energy required to stretch totally an ideal chain), a general expression is found:

$$R_{e,g,h} \sim N^{\nu} \tag{1.26}$$

For a chain in a good solvent, $\nu = 3/5$. Finally, despite the overestimations and inaccuracies of method, Flory's theory is useful, simple and provide an universal power law dependence of the polymer size on the number of monomers, proved experimentally [62].

To get an insight into the conformational properties of a chain, other characteristic parameters have to be described. An important mechanical property of a real chain is the persistence length P [65], which is considered to be one half of the Kuhn length. The persistence length defines the chain rigidity and it is a measure of how far a polymer chain persists in a given direction. As a result, the higher the persistence length, the stiffer the chain and the larger the radius of the polymer [66]. A polymer with a short persistence length is flexible over relative short distances.

The models of the previous sections describe flexible chains with l_{max} longer than P. In this case the orientation of the extremities is governed by the thermal motion, that folds the chain and reduces the distance between two ends. Conversely if l_{max} is shorter than P, the chain is a rigid rod. For a uncharged polymer the value of P arises only from the intrinsic persistence length P_0, namely the rigidity of the chain backbone. In the case of polyelectrolytes, in addition to P_0 there is the electrostatic persistence length P_e that arises from the repulsion between neighbouring ionic sites. We will detailed the P_e for polyelectrolytes in the next section.

1.4 | Polyelectrolytes

1.4.1 | Definition and applications

Polyelectrolytes are polymer composed of macromolecules in which a substantial portion of constitutional units contains ionizable groups [1]. In a polar solvents, as water, these groups dissociate, releasing counterions into the solutions and leaving charges on the polymer chain [67]. Examples of polyelectrolytes include polystyrene sulfonate, DNA, proteins, humic substances, and other polyacids and polybases.

Polyelectrolytes show a complex behaviours, with unique properties that differ from their neutral counterpart, due to the coupling of electrolyte and polymeric properties [7]. For instance, the electrostatic attraction between oppositely charged macromolecules is useful for the fabrication of multilayer films of polyelectrolytes, DNA and proteins [5, 68]. The electrostatic attraction

between DNA and histones is responsible for the building of chromosomes[69], and the electrostatic complexation between polyelectrolytes and proteins is used for protein separation [5]. Moreover, polyelectrolytes are useful in proton-exchange membrane, and in other systems as batteries, electro-chromic devices, solar cells, and sensors [70].

The structural properties of polyelectrolytes have been examined in dilute solutions from theoretical, experimental and numerical perspective in literature [6, 39, 67, 71]. Therefore, in the case of low volume fractions, the scaling concepts developed for single chain may be applied to solutions of equivalent chains [39, 72], and thanks to the equivalent chain model, the static properties of polyelectrolytes in solution can be described with the concepts developed for neutral polymer physics, that we have introduced in the previous sections [39, 63].

In the next sections, we introduce some properties and models valid for polyelectrolytes, and taking advantage of the scaling laws developed for the not charged chains.

Strong and weak polyelectrolytes

According to the nature of ionic groups and behaviour of polyelectrolytes with the pH variations, they fall into two distinct categories: strong and weak polyelectrolytes [73]. For strong polyelectrolytes the distribution of charge is not sensitive to pH variations, whereas for weak polyelectrolytes the amount of charged sites varies as a function of pH of the solution. For the weak polyelectrolytes, the system on which we will work, the charging process and the associated structural and dynamics properties have to be known and controlled in order to take advantage of the polyelectrolytes in potential applications. For example, the modification of the state of charge of a polyelectrolyte makes it possible to tune its hydrophobicity, which is useful for the decolorisation of dye solutions [9]. Another example is the power conversion efficiency in polymer solar cells, which is governed by the protonated state of the conjugated polyelectrolytes [11].

1.4.2 | Chain conformation

The knowledge of P can be of particular importance, because it governs the shape of aggregates when polyelectrolytes are added in a suspension of particle of opposite sign [74]. The conformation of a polyelectrolyte chain is due to the balance between electrostatic interaction

and chain's elasticity [67]. The predominance of the intra- or inter-chain electrostatic interactions depends on the concentration regime of the system. In a case of dilute solution the intra-chain interaction are predominant. The charges along the polyelectrolyte chain engender repulsive interactions between monomers of identical charge and make the polyelectrolyte more extended than the corresponding uncharged polymer. The electrostatic repulsion leads to an intrinsic electrostatic stiffness that increases the value of the persistence length P that, in the case of polyelectrolytes, consists in a sum of two contributions:

$$P = P_0 + P_e \tag{1.27}$$

where P_0 is the intrinsic persistence length, due to the rigidity of the chain backbone already introduced for the polymer, and P_e is the electrostatic persistence length arising from the repulsion between neighbouring ionic sites [66]. The value of P, found via full atomistic molecular dynamics simulations for a single and isolated weak polyelectrolyte (PAA) of 50 monomers, ranges from P = 0.4 nm (for a non-ionised polyelectrolytes, β=0) to P = 1.3 nm (for a fully ionised polyelectrolytes, β=1) [66]. Experimentally, the persistence length of long chain PAANa (M_w > 15 kDa) was also determined by X-ray scattering measurements by Muroga et al. [75].

For polyelectrolytes at infinite dilution, the size-dependence of the chain on the number of monomers can be estimated from a minimisation of the total free energy with respect to polyelectrolyte size R [40, 64]. The total free energy consists in a neutral polymer term, which contains a short range excluded interactions, and an electrostatic interaction energy term. The electrostatic term is proportional to the Bjerrum length ℓ_{B}, that is the distance at which the electrostatic interaction between two elementary charges is equal to the thermal energy k_BT.

$$\ell_{\mathrm{B}} = \frac{e^2}{4\pi\varepsilon_0\varepsilon_{\mathrm{r}}k_{\mathrm{B}}T} \tag{1.28}$$

where e is the elementary charge, ε_0 is the vacuum permittivity, ε_r the relative static permittivity, and k_B the Boltzmann constant.

When the distance between two charges is lower than ℓ_{B}, the electrostatic interactions are predominant. After the minimisation of the total energy term the equilibrium size of polyelectrolyte chain is obtained:

$$R_{e,g,h} \propto N(l_B a^2)^{1/3} \tag{1.29}$$

The electrostatic repulsion between the monomers, balanced with the elasticity of the chain, swells the chain and extends the conformation. From these properties, we found that $R \propto N^1$. Thus, the size of the polyelectrolyte rises with the number of monomers steeper than for neutral polymers, where $R \propto N^{\frac{3}{5}}$ Eq. 1.26. The elongation and deformation of the chain with the electrostatic repulsion is nonuniform, it decreases towards the chain's end, and it is faster than the linear increase of the chain size with the degree of polymerisation as proved by dynamics simulation [76].

1.4.3 | Counterion condensation

For a solution of polyelectrolytes, the charge has to be adjusted with the concentration of counterions, which cannot be neglected as the long-range Coulomb interactions attract the dissociated counterions, as seen in the previous section. To calculate the charge felt in the vicinity of the polyelectrolyte by ions of other polyelectrolyte chains, it is necessary to assess the condition for the counterion condensation.

The condensation of counterions on a charged polyelectrolyte can be expressed in term of the Manning parameter ξ [77]. Considering a polyelectrolyte chain, the effective strength of the interactions between charges separated from each other by the length a along the chain is determined by ξ:

$$\xi = \ell_{\mathrm{B}}/a \tag{1.30}$$

- for $\xi > 1$, the system is energy dominated (over the thermal energy), and the counterion condensation occurs.
- for $\xi < 1$, the system is entropy dominated and the counterions maximize the accessible volume. No condensation occurs and Debye-Hückel approximation of the linearisation of Poisson-Boltzmann equation can be used.

This parameter will be used in the next chapter to estimate the condensation of counterions on the polyelectrolyte chains.

1.5 | Polymer-colloid mixtures

Since in this thesis, we focus on the mixtures between polymer and nanoparticles, the rich phase behaviour of this mixtures has to be considered [4, 78–82]. Indeed, polymers and polyelectrolytes can alter the stability of colloidal suspensions through different phenomena such as adsorption, steric effect, polymer bridging, electrical effects, and depletion interaction. The effect of these phenomena, depends on the relative size polymer-colloid [82]. Three regimes can be defined:

- colloid-polymer mixtures in which the polymers are relatively large compared to the colloids, this regime is relevant for mixtures of polymer or polysaccharides mixed with proteins and it is often denoted as the *protein limit*: $R_g \gg R_o$ where R_g is the radius of gyration of the polymer and R_o the radius of the particle
- The intermediate case known as equal sized limit: $R_g \approx R_o$
- And the *colloid limit* where the polymers are small compared to the colloids :$R_g \ll R_o$

In the present work, only the third case will be investigated.

The most widely exploited effect of non-ionic polymer on colloid stability is called steric stabilization [83–85]. Steric stabilization results from the mutual repulsion which occurs when polymer chains, irreversibly adsorbed on the particles, begin to interact. The interaction between the chains will be repulsive if polymer segment-solvent interactions are more favourable than segment-segment interactions, or attractive in the opposite case. In a good solvent, the polymer chains will tend to repel, favouring interaction between the polymer segments and the solvent, and the chains will be well extended. In a poor solvent, the chains are attracted and the effect inverted.

It is possible for the polymer chain to attach itself onto another particle in process called bridging [9, 86]. This process of polymer bridging causes a destabilization of the suspension but is observed mainly in the protein limit, when the length of the chain is high enough. Polymers of various types are used, but the most common are high molar mass polymers, such high molar masses produce long tails which promote the bridging process.

A common way to induce aggregation in a colloidal system is the use of polyelectrolyte of opposite charge as flocculating agents [29, 83, 87]. They adsorb by an electrostatic mechanism, enhanced by van der Waals attractions, section 1.2.2, or hydrogen bonding. The interaction between approaching particles can then occur simply by charge neutralization, with polymer covered patches on one surface interacting with the oppositely charged polymer on the second particle. In the present study, we will not investigate this phenomenon since we will focus on polyelectrolytes and particles of the same sign.

Another remarkable effect is the *depletion* effect [19, 37, 88, 89]. This effect involves soluble non-adsorbing polymers, which influences interactions by modifying the effective osmotic pressure Π of the solvent between approaching particles.

1.5.1 | Depletion effect

Consider two colloidal spheres of radius R_o in a solution of non-adsorbing polymers (radius of gyration R_g). The non-adsorbing polymers are excluded from the vicinity of the particle. This zone is the depletion layer where the concentration of polymer is reduced due to the cost of the loss of configuration entropy of a polymer chain in that region. The mechanism that is responsible for the effective attraction between the colloidal spheres originates from the presence of this depletion layer.

In Fig. 1.5, the depletion layers of each particle is outlined by dashed circles around the spherical particles. When the depletion layers overlap, the volume available for the polymer chains increases. Then, the entropy of the polymer increases when the particles are closer. This effect can then be seen as an attractive force between the spheres. In term of osmotic pressure Π, when there is no overlap of depletion layers the osmotic pressure on the spheres due to the polymers is isotropic. For overlapping depletion layers the osmotic pressure Π on the spheres is unbalanced: higher from the outer region which induces an effective attraction between the spheres.

Oosawa and Asakura [90] first proposed an evaluation of this interaction considering the depletants as hard spheres. Later, Vrij [91] considered depletants as polymers of radius of gyration R_g. The corresponding effective interaction can be evaluated as the product of the osmotic pressure of the depletants polymer molecules Π_d with the volume of the depletion layer.

1.2 Colloidal Interactions 13

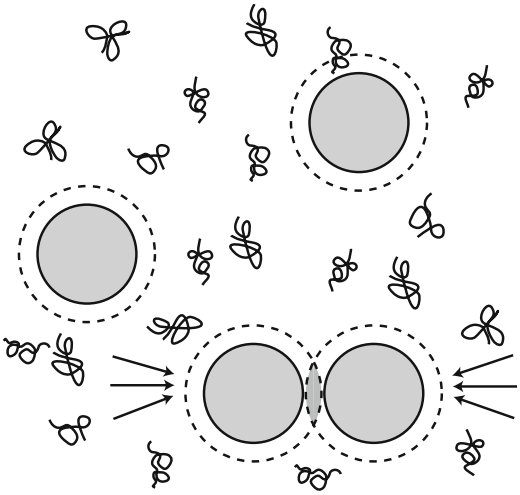

Fig. 1.7 Schematic picture of colloidal spheres in a polymer solution with non-adsorbing polymers. The depletion layers are indicated by the *short dashes*. When there is no overlap of depletion layers (*upper two spheres*) the osmotic pressure on the spheres due to the polymers is isotropic. For overlapping depletion layers (*lower two spheres*) the osmotic pressure on the spheres is unbalanced; the excess pressure is indicated by the *arrows*

Figure 1.5: Schematic picture of colloidal spheres in a polymer solution with non-adsorbing polymers. The depletion layers are indicated by the short dashes. Picture extracted from [82].

In a first approximation, the osmotic pressure of the depletants is equal to $\Pi_d = c_p k_B T$ where c_p is the concentration of the polymers. The overlap volume of the depletion layer depends on the radius of the particle R_o, the depletion layer thickness Δ_d, and the distance between the surface of the interacting particles h. The depletion potential can be written with the following expression:

$$\frac{V_{\text{depletion}}}{k_B T} = -\frac{\Pi_d}{k_B T} \cdot V_d = \begin{cases} \frac{\pi}{6} q_p^3 \Delta_d^3 \left(1 - \frac{h}{2\Delta_d}\right)^2 \left(2 + \frac{3R_o}{\Delta_d} + \frac{h}{2\Delta_d}\right) & 0 < h \leq 2\,\Delta_d \\ 0 & h \geq 2\,\Delta_d \end{cases} \tag{1.31}$$

where c_p is the concentration of the polyelectrolyte, Δ_d the depletion layer thickness, h the surface separation distance between the particles. Then, in a system where the concentration of particle is fixed, the strength of the attraction increases linearly with the polymer concentration. Furthermore, the range of depletion depends on $2\,\Delta_d$, that increases with the radius of the polymer as seen in Fig.1.6. Indeed, Δ_d is defined as:

$$\Delta_d = R_o \left[\sqrt[3]{1 + \frac{6R_g}{R_o\sqrt{\pi}} + 3\left(\frac{R_g}{R_o}\right)^2} - 1 \right] \tag{1.32}$$

However, Eq. 1.31 have to be adjusted in case the depletants are polyelectrolytes. For the same molar concentration, polyelectrolytes exhibit much larger osmotic pressures than neutral polymers because of the presence of counterions; each counterion can then contribute as much to

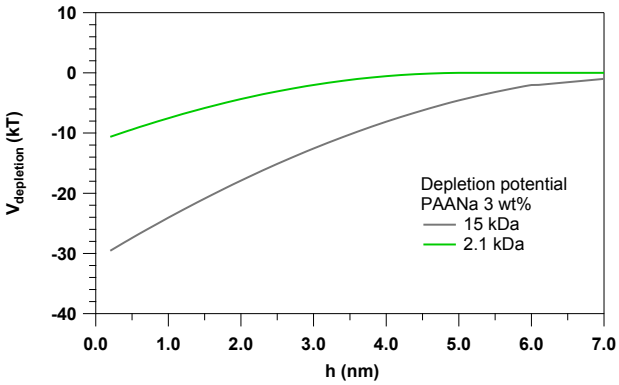

Figure 1.6: Reppresentation of the depletion potential between silica particles as a function of the distance h between them, with R_o = 7.79 nm in presence of PAANa 2.1 kDa and 15 kDa at pH 2 and concentration of 3 *wt%*.

the osmotic pressure as each polymer molecule [92]. The osmotic pressure have to be corrected with the concentration of unbounded counterions as [93].

$$\Pi_d = c_p(1 + Z_{\text{eff}})k_BT \tag{1.33}$$

For a weak polyelectrolyte, the effective charge Z_{eff} has to consider the ionisation degree β and the proportion of condensed counterions. As a result, the depletion effect for a weak polyelectrolyte is expected to be much stronger at high pH values.

Then, considering the counter-ions the depletion potential has the value of $\sim 60\ k_BT$ at the distance $h = 3\ nm$ between the particles. We will see in chapter 7 the impact of this force on the stability of the silica nanoparticles.

1.6 | Dynamics of polymers

In this section we introduce the main theories that describe the self-diffusion of polymer and polyelectrolyte. The polymer chain, even in the absence of an external force, diffuses through the medium due to the thermal fluctuation of the solvent molecules with a resulting random motion, called Brownian motion. Many dynamic theories for solutions of neutral polymers have been developed in literature [39, 72, 94, 95]. In this section, we will present some basic models that will we use for the description of our experimental data.

The self-diffusion coefficient measures the mean-squared distance travelled by a particle during a time τ:

$$D = \frac{\left\langle |r(t+\tau) - r(t)|^2 \right\rangle}{6\tau} \tag{1.34}$$

where the $\langle\rangle$ is an average over different trajectories [40, 71]. The self-diffusion coefficient may be expressed in terms of a friction coefficient f, i.e. the resistance that the diffuser feels when it moves through the solvent:

$$D = \frac{k_B T}{f} \tag{1.35}$$

where k_B is the Boltzmann constant and T the temperature.

For a sphere of radius R at infinitely dilute solution, the Stokes relation for the friction coefficient is used in Eq. 1.35, and the Stokes-Einstein relation is obtained:

$$D^\circ = \frac{k_B T}{f} = \frac{k_B T}{6\pi\eta R} \tag{1.36}$$

where η is the solvent viscosity and $^\circ$ indicates the infinity dilution. When the diffuser is not spherical, the R of this equation refers to the hydrodynamics radius R_h. Because the diffusion depends on the structural properties and the interactions in the system, we will obtain the structural information about the chain and in particular the R_h , starting from the diffusion coefficient.

So far the description have been limited to the case of a spherical particle. In what follows, we will see how the previous description is adapted in the case of a polymer chain. In principle, the diffusion coefficient of a polymer chain can be written in the same form as the previous model for a spherical particle, however, for a polymer chain the relation between the diffusion coefficient and the degree of polymerisation N (or the molecular weight M) have to be considered:

$$D = D(N) = \frac{k_B T}{f(N)} \tag{1.37}$$

Then, to adapt the models of diffusion to a polymeric chain it is necessary to develop a form for $f(N)$ than considers the polymer details. The most important models for $f(N)$ are described in the next sections. The aim of the next sections is to give a general view of the scaling models found in literature, that will be used as reference models to understand and characterise the

dynamics of the system studied in the next chapters.

1.6.1 | The Rouse model

The Rouse model describes the dynamics of an ideal chain (see section 1.3.2). The single chain diffusion is represented by Brownian motion of beads separated by springs, see Fig. 1.7, where each monomer interacts with the solvent as an independent single particle. The excluded volume effects and the long-range interactions between monomers are not considered [96].

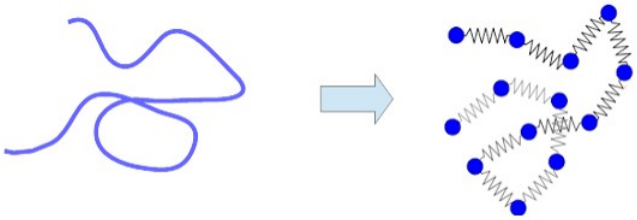

Figure 1.7: Representation of the Rouse Model. A chain of N monomers is mapped onto a bead-spring chain of N beads connected by springs.

In this model, the diffusion coefficient D decreases with the number of beads, because the total friction coefficient is the sum of the individual resistance coefficients f:

$$D_{\text{Rouse}} = \frac{k_B T}{f}\frac{1}{N} = \frac{D_m}{N} \propto \frac{1}{N} \tag{1.38}$$

The diffusion coefficient of the polymer varies as the diffusion coefficient of a single monomer D_m, divided by the number of monomers. Despite this is a simple model that neglects many real effects present in the chain, it will be a useful reference model.

1.6.2 | The Zimm Model

An important model that includes the hydrodynamic interaction mediated by the solvent between different parts of the chain is the Zimm model [97]. It can be seen as an extension of the Rouse model, that takes into account the hydrodynamic interactions. But what exactly are the hydrodynamic interactions? When a polymer moves in solution, the solvent gives a viscous resistance to the particle, because of the drag of the surrounding solvent. This viscous resistance that acts on the solvent molecule and decays with the distance r from the particles as $1/r$, is the

hydrodynamic force. Furthermore, when the polymer moves, it drags the solvent that pervades its volume. In the Zimm model, this volume filled with the solvent is treated as part of the chain in diffusion.

The diffusion of a polymer in this regime is obtained using the Stokes-Einstein relation (Eq. 1.37). In the approximation of infinite dilution, the friction coefficient $f(N)$ varies with N:

$$D_{\text{Zimm}} \approx \frac{k_B T}{f(N)} \approx \frac{k_B T}{6\pi\eta R(N)} \propto \frac{1}{N^{\nu}} \tag{1.39}$$

where ν depend on the polymer chain conformation in solution [98]. We will use this dependence to characterise the conformation chains in solution. ν varies between 0.6 and 0.5 for flexible linear random coils [99], around $\frac{1}{3}$ for highly branched or collapsed linear polymers [100], and approaching 1 for rigid rods.

1.6.3 | Kirkwood-Zimm

A more detailed model that takes into account the hydrodynamic interactions is the Kirkwood-Zimm model [101, 102]. In this description, the hydrodynamic interactions between monomers are considered by the use of a Oseen tensor. The diffusion coefficient is composed by a term related to diffusion coefficient of the monomer, and a term related to the polymer diffusion coefficient which depends on the hydrodynamic radius [101]:

$$D(N) = \frac{D_{\text{m}}}{N} + \frac{k_B T}{6\pi\eta} \left\langle \frac{1}{R_{\text{h}}} \right\rangle \tag{1.40}$$

the first term correspond to the diffusion coefficient found in the Rouse model, Eq. 1.38. The second term is related to the R_h thus defined:

$$\left\langle \frac{1}{R_{\text{h}}} \right\rangle = \frac{1}{N} \sum_{i \neq j} \left\langle \frac{1}{\|\vec{r_i} - \vec{r_j}\|} \right\rangle \tag{1.41}$$

where $\vec{r_i}$ is the position of monomer i.

For large N the average value for R_{h} is expected to scale with N^{ν} as in the previous Zimm model. In this limit, both models agree to neglect the monomer diffusion term.

In the next paragraph, without entering in the details of the models, we will introduce some phenomena and problems concerning the study of the dynamics of polyelectrolytes.

1.7 | Dynamics of polyelectrolytes

In contrast to the structural properties, the dynamical properties of the polyelectrolytes are still challenging [103–105]. The difference with neutral polymers is related to the difficulty to apply the theory and the scaling model to systems in which long range forces are present. The dynamics we are focusing on in the present work is the chain large-scale self-diffusion (for simplicity named hereafter only diffusion), on a time-scale of 10–1000 ms and spatial scale of 1–10 μm. From a theoretical point of view, the study of the polyelectrolytes chain self-diffusion coefficient should contribute to test the applicability of the theories developed for neutral polymers to polyelectrolytes [106, 107].

Many factors affect the dynamics of polyelectrolytes: the charge density of the chain, the concentration that controls the average distance [108], the size or the degree of polymerisation of the diffuser [109]. Moreover, the details of the local chain structure control the phenomena of counterions condensation, that modifies the long range part of the interactions.

Despite there is still unclear phenomena in the behaviour of polyelectrolytes, simulations methods have been a great help to grasp some information [76, 102–104].

In Brownian dynamics simulation, i.e. simulation where the medium is replaced by a simple random noise and a friction term, it was demonstrated that the diffusion coefficient decreased monotonically with the increase of the Coulomb interactions [104]. Also in an hybrid mesoscale simulation, that combines the molecular dynamics method with the multi-particle collision dynamics approach, it was shown that the dynamics depends on the coupling effects of hydrodynamics and Coulomb interactions, that affect the conformational changes of the chain and the counterions condensation [110].

Because of the complexity and the interest of the dynamics of polyelectrolytes alone, chapter 5 is devoted to the investigation of the phenomenon.

Summary of Chapter 1

In this chapter, we have introduced the main parameters and models used to describe and characterise the experimental systems, and to interpret the experimental observations.
After a general introduction on colloidal systems, we have focused on the description of the electrostatic interactions around a macroion solving the Poisson-Boltzmann equation in the Debye-Hückel approximation, and solving numerically the equation in the non linear regime. Thanks to this last method, we have calculated the effective charge of the macroions, fitting the long-range behaviour of the solution obtained numerically.
A general description of polymers and polyelectrolytes that includes the definition of the characteristic quantities: characteristic chain lengths, dispersity, molecular mass, critical concentration, persistence length, necessary to characterise the chain has been done. The basic models to describe the structure of an ideal (freely jointed model) and real chain (Kuhn model) had allow us to describe, through a scaling law, the relation between the generic radius of the polymeric chain and its degree of polymerisation $R_{e,g,h} \sim N^{\nu}$.
The same concepts introduced for the neutral polymer have been adapted to the case of polyelectrolytes. For these systems, the radius of the chain increases faster than for the neutral chain, with the degree of polymerisation.
When polyelectrolytes and colloid nanoparticles are mixed, phenomena as the steric effect, polymer bridging, and depletion interactions may affect the stability or not of the system. These effects depend on the relative size polymer/colloid. Our systems lie in a regime called the colloid limit, i.e. the polymers are small compared to the colloids. In this regime, an important effect is the depletion. This effect involves soluble non-adsorbing polymers, which influence interactions by modifying the effective osmotic pressure between approaching particles, and resulting in attractive forces between the particles even in the presence of repulsive interactions.
For the polyelectrolytes, the dynamical properties are still challenging. The difference with neutral polymers is related to the difficulty to apply the theory and the scaling model to systems in which long range forces are present. From a theoretical point of view, the study of the polyelectrolytes chain self-diffusion coefficient should contribute to test the applicability of the theories developed for neutral polymers to polyelectrolytes.

Chapter 2

Diffusion in crowded colloidal systems

Contents

2.1 | Introduction

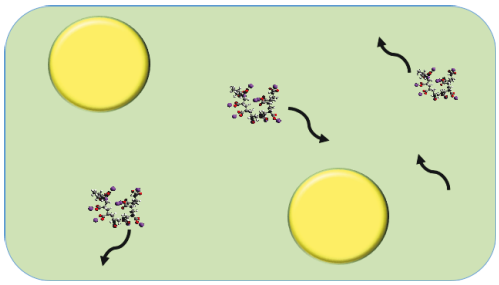

Figure 2.1: Translational diffusion of polymers in a colloidal system.

The diffusion in crowded media is a challenging problem since the properties of the diffuser have to be considered in addition with the interactions between diffuser, obstacles and solvent. It occurs in various contexts, ranging from intracellular biological processes [111, 112], protein-DNA system [113], enzyme-catalysed regulation [114], porous media, colloidal slurries or glass [115], to the functioning of fuel cells and gel electrophoresis. To study this fundamental problem, the behaviour of polymers in a crowded media Fig. 2.1, can be used as model to study the phenomena and mechanisms that come into play [116], and to understand how the diffusion depends on the properties of the obstacles. In particular, we are considering a polymer-nanoparticle mixtures in which the nanoparticles are relatively large compared to the polymer. This regime is know as colloid limit. In the opposite case, know as protein limit, polymers are relatively large compared to the colloids. This regime is relevant for mixtures of polymer or polysaccharides mixed with proteins [117].

The diffusion we refer to in this work is the self-diffusion (for simplicity named sometime only diffusion), which is also named translational diffusion: it is the random thermal motion of molecules in a pure liquid at thermal equilibrium [31]. It can be thought of as Brownian motion without an applied force and without an average net displacement. The self-diffusion must not be confused with the mutual diffusion, that is related to the mass flux to average out the inhomogeneities to achieve the thermal equilibrium in a multicomponent system.

In complex media, the self-diffusion coefficient might depend on time. In other words, the mean-squared displacement $\langle |r(t+\tau) - r(t)|^2 \rangle$ can have a time dependence that is not linear in τ. This phenomenon is called *anomalous* diffusion [118–120]. This is especially the case when the diffuser can be trapped in a cage of obstacles. However, in such media a diffusive behaviour

can sometimes be recovered at short and long time compared to the time needed for the cage to rearrange. The short time limit can be probed by scattering techniques such as quasi-elastic neutron scattering [121]. In the present study, since diffusion NMR probe large length scales compared to the nanoparticle size, the long-time regime is explored. In addition, the range of concentration of obstacles explored is limited to a volume fraction of the order of 0.2, so that the diffuser are never trapped but only slowed down. As a result, no anomalous diffusion was observed experimentally.

The description of the self-diffusion in crowded systems poses considerable theoretical problems, mostly to find an expression for the effective self-diffusion coefficient in terms of the geometry of the system, concentration, volume fraction, and size of the obstacles [122–127]. Due to the presence of obstacles, the value of the diffusion coefficient of the diffusers is modified and in general decreases toward a lower value compared to the value of the self-diffusion coefficient in a pure solvent. The decrease of the diffusion coefficient may be attributed to two mechanisms:

- The first mechanism, often referred to as the tortuosity or obstruction effect, is the increase in path length due to obstruction [128]. This effect is a consequence of the obstruction effect caused by the obstacle, i.e. an obstacle particle reduces a certain fraction of the total volume available for the diffuser.

- The second mechanism is related to interactions between diffusers and obstacles, which may lead to a further decrease of the effective self-diffusion coefficient.

To obtain the self-diffusion coefficient, we have to consider the diffusion equation. If $c(\vec{r}, t)$ is the number of particles per unit volume located at $\vec{r}$, and D is the diffusion coefficient, the flux of particle $\vec{J}(\vec{r}, t)$ is given by Fick's first law:

$$\vec{J}(\vec{r}, t) = -D\nabla c(\vec{r}, t) \tag{2.1}$$

Because of the mass conservation the following equation is valid:

$$\frac{\partial c(\vec{r}, t)}{\partial t} = -\nabla \cdot \vec{J}(\vec{r}, t) \tag{2.2}$$

This equation states that $\partial c(\vec{r},t)/\partial t$ is the difference between the incoming and outcoming flux from the point located at $\vec{r}$. Using the Eq. 2.1 and 2.2 the Fick's second law is obtained:

$$\frac{\partial c(\vec{r},t)}{\partial t} = D\nabla^2 c(\vec{r},t) \tag{2.3}$$

where ∇^2 is the Laplace operator. To obtain the diffusion coefficient for a diffuser in a medium composed of immobile, impenetrable objects, mathematically the problem consists of solving $\nabla^2 c(\vec{r},t) = 0$, i.e. solving the Laplace's equation in the void space with the relevant boundary conditions. If there is an interaction potential between the diffusers and the obstacles the Eq. 2.3 equation presents an additional term including the interaction potential (see Eq. 2.11). This is the general approach that will be followed in the models presented issued from literature.

The investigation on the diffusion in crowded media starts with the studies of the dynamics of solvent molecules in colloidal systems [129–132] and those of the diffusion of small molecules in crowded systems [127, 133, 134]. The research on the dynamics of polymers in crowded media begins with the pioneering studies by de Gennes, Muthukumar and Baumgartner, focused on homopolymers in a random medium composed of fixed obstacles [122–124]. These studies have revealed the existence of two extreme regimes, based on the ratio of polymer radius and distance between obstacles. When the radius of the polymer is smaller than the distance between the obstacles, polymers diffusion does not feel the strong spatial constraints imposed by the obstacles [125]. In this regime, the Zimm's model, that has been introduced in section 1.6, is still appropriate to describe the dynamical diffusion of the chain [71], then the diffusion coefficient D is proportional to N^{ν}. In the opposite regime, i.e. when the radius of the polymer is larger than the distance between the obstacles, the dynamics is strongly affected by the strong spatial constraints [135]. In this regime the de Gennes reptation model can be used to describe the system [71], it predicts that $D{\sim}N^{-2}$. This regime happens for long diffusion time and reflects a diffusion in dense medium [125].

The systems that we have studied in this thesis are close to the first limit, when i.e. the radius of the polymer R is smaller than the distance between the obstacles. The systems studied are in the colloidal limit, the obstacles are larger compared with the polymers (section 1.5). No change of conformation of the chain is needed for the polymeric chain to diffuse through the obstacles.

In this section, some simple models issued from the literature for the description of small molecules in crowded systems will be introduced. These simple models, despite taking into

account only some of the complex phenomena present in the real system, are useful reference models of comparison and for understanding the real behaviour observed.

2.2 | Model based on obstruction effects

In this section, an overview on the main diffusion models based on obstruction effects are presented. These models, which can be seen as reference models, will be used to interpret and understand the system studied in the next chapters.

The main concept of the obstruction effect is the following: the obstacles are regarded as motionless relative to diffusers, based on the assumption that the obstacles self-diffusion coefficient is appreciably smaller than the one of the diffusers. The presence of the fixed obstacles leads to an increase in the mean path length of the diffusing molecules between two points in the system. The obstruction concept was first introduced by Fricke [136], who studied the electric conductivity and capacitance of spheroids dispersed in a solvent. Later, it has been addressed by Wang, who, to study the self-diffusion of water in protein solutions, has derived an expression for the effective diffusion coefficient of solvent molecules as a function of the volume fraction of identical spheroidal obstacles [129].

The model here presented, called Maxwell-Fricke, allows to obtain a dependence of the diffusion coefficient on the volume fraction of spherical obstacles. It is based on the mathematically analogous properties of electric conductivity and permeability [136–138]. For the conductivity, the potential is replaced by $c(\vec{r}, t)$, the current density by $\vec{J}$, and the conductivity by D. The following equation was given [139]:

$$D = D_0 \frac{1 - \phi'}{\left(1 + \frac{\phi'}{\chi}\right)(1 - \phi)} \tag{2.4}$$

where D_0 is the self-diffusion coefficient at infinite dilution, ϕ' is the volume fraction of obstacles with the diffusers bound to the obstacle, ϕ is the volume fraction of obstacles, and χ is a factor related to the shape of obstacles ($\chi = 0$ for oblate spheroids, $\chi = 1.5$ for rods, and $\chi = 2$ for spheres). For $\phi' = \phi$ the following expression is found:

$$D = D_0 \frac{1}{1 + \frac{\phi}{\chi}} \tag{2.5}$$

This model, that depends on the obstacles volume fraction, is valid mostly for small-sized diffusers as solvent in dilute solutions or for small diffusing particles in dilute obstacles solutions. It has been shown that it predicts accurately the diffusion coefficient of water in suspensions of latex and silica particles at low concentration [138]. However, it has many limitations for large diffusers and semi-dilute or concentrated solutions.

Mackie-Meares [140, 141] employed the physical concept proposed by Fricke to describe the diffusion of electrolytes in a membrane separating two solutions at different concentrations of electrolytes. When the obstacles are very small, with a size similar to the diffusers, the continuum method used previously cannot be used. They proposed a model based on a simple cubic lattice to describe the solution, with similar size sites for diffusers and obstacles. The obstacles were pictured as blocking with a fraction ϕ of sites. They assumed that the sites occupied by the obstacles are permanently unavailable, because the obstacles could be considered fix. The complete flux equation contains three terms. One determined by the concentration difference across the membrane, another determined by the variation of the activity coefficient of the electrolyte across the membrane, and a third concerned with the rate of hydrostatic flow through the membrane. The diffusion coefficient for a small diffuser is given by the following equation:

$$D = D_0 \left(\frac{1 - \phi}{1 + \phi} \right)^2 \tag{2.6}$$

This model gives satisfactory results over a wider range of concentrations than the model of Maxwell-Fricke, and it does not provide a diffuser shape dependence, so its result is more general. The divergence between model and experimental data found at high concentration, was attributed to the interactions between larger diffusers and obstacles. The previous model can be approximated in the following way for small ϕ:

$$D = D_0 (1 - 4\phi) \tag{2.7}$$

Both models treated so far are valid mostly for solvent and small-sized diffusers in dilute and semi-dilute solutions and they have limitations for larger diffusers, as in the system treated

in this thesis for which the models present in the next chapter are more appropriate.

2.2.1 | Cell models

A family of models, or solving method, that allows to obtain the self-diffusion coefficient for small molecules in a crowded system is the cell model [131, 133, 142]. The cell model is useful for describing the self-diffusion of small-molecules, larger than solvent molecules, in crowded systems. It was originally conceived as a theory of simple liquids [143] and used in colloid and polymer chemistry to describes systems with highly charged particles [127]. In the cell model, the total volume of the system containing N_o obstacles, is divided into n simple shape cells. Usually the shape of the cell reflects that of the obstacles. The obstacles are assumed fixed and the diffusive motion of diffusers is independent of that of the obstacles. In the next subsection, different results obtained using this solving method are presented.

Uncharged obstacles

For systems with monodisperse uncharged spherical obstacles, Jönsson et al. have found an expression to describe the diffusion coefficient of small molecules as a function of the volume fraction of obstacles. By using the cell model, the Fick's equation, and the boundary equation issued from the principles of irreversible thermodynamic, the following equation for D is found [144]:

$$D = \frac{D_0}{1 + \frac{\phi}{2}} \tag{2.8}$$

where ϕ is the volume fraction of obstacles. The equation is derived for a system at infinite dilution, but it applies well also for concentrated systems, as proved by experimental and simulation results [144]. It is valid when the displacement profile is Gaussian. The Eq. 2.8 can be written for small ϕ in the following way:

$$D = D_0\left(1 - \frac{\phi}{2}\right) \tag{2.9}$$

This model was also tested by Blees and Leyte, for the self-diffusion of small molecules in a low volume fraction of colloidal particles [134, 145]. Then, the Jönsson et al. model gives accurate

results for low volume fractions of diffusers, ie when the self-diffusion is independent of the symmetry of the system. The slight deviations found a high concentration of obstacles have been attributed to a non-Gaussian displacement profile of the diffuser [145].

Venema et al. [131], in a work concerning the analysis of the self-diffusion of solvent molecules in a colloidal crystal ie where the obstacles are fixed in a crystalline structure, extend the results found by Jönsson et al. . As Jönsson et al. model, Venema et al. model considers only the obstruction effects. The advantage of this model is to obtain a value of the self-diffusion coefficient valid for all volume fractions. The self-diffusion coefficient of the solvent molecules is calculated as function of the volume fraction of fixed spherical particles. By solving the Laplace equations and by using an expansion of the probability distribution for the diffuser in term of spherical harmonics, the following expression for the effective self-diffusion coefficient is found:

$$D = D_0\left(1 - 0.5\phi + 0.25\phi^2 - 0.125\phi^3 + 0.0625\phi^4\right) \tag{2.10}$$

The first two terms on the right-hand side of Eq. 2.10 coincide with the model found by Bell [133]. Bell has found a simple expression for the self-diffusion coefficient of diffuser in the presence of spherical colloidal obstacles using a cell model. The partial differential diffusion equation, that unlike the Eq. 2.1 can also include a potential term (Smoluchowski equation [146]), have been solved in spherical symmetry:

$$\vec{J}(\vec{r}, t) = -D\left[\nabla c(\vec{r}, t) + c(\vec{r}, t)\nabla\psi\right] \tag{2.11}$$

where ψ is a dimensionless reduced potential.

For an impenetrable uncharged spherical particles (ψ outside of the particle is zero, and the $\Delta\psi$ inside the particle is ∞) the expression for the diffusion coefficient is the following:

$$D = D_0\left(1 - \frac{\phi}{2}\right) \tag{2.12}$$

where ϕ is the volume ratio of obstacles. This expression is mainly valid only at moderate volume fraction of obstacles, in contrast to the Eq. 2.8 where the formula should be valid over the full range of volume fraction of the colloidal particles.

Another simple solution is provided by Bell, for a constant value of the potential ψ inside the particle. In this case the problem concerns a penetrable particle and the solution found is the

following [133]:

$$D = D_0 \frac{1 + \frac{1}{3}(1 + 2\phi)\left[\exp(-\Delta\psi) - 1\right]}{\left\{1 + \frac{1}{3}(1 - \phi)\left[\exp(-\Delta\psi) - 1\right]\right\}\left\{1 + \phi\left[\exp(-\Delta\psi) - 1\right]\right\}} \tag{2.13}$$

The model presented so far, are compared in figure 2.2 with a set of experimental data obtained from the NMR diffusion data. The experimental data are related to the diffusion coefficient of the propionic acid (PA) as a function of the volume fraction of silica nanoparticles. In the graph the Jönsson (Eq. 2.8), Venema (Eq. 2.10), and Bell's model (Eq. 2.12) are reported together with the diffusion coefficient of the PA as a function of the volume fraction of obstacles. It is observed that all models overlap each other in the range of concentration studied. Also Venema's model, Eq. 2.10, that is expanded until the fourth order in ϕ, has the same behaviour that the models developed until the first order in ϕ. The Mackie-Meares model (Eq. 2.6), was not reported in the figure because not suitable for the relative size diffuser/obstacle studied. Indeed, it is suitable when diffusers and obstacles have the same size.

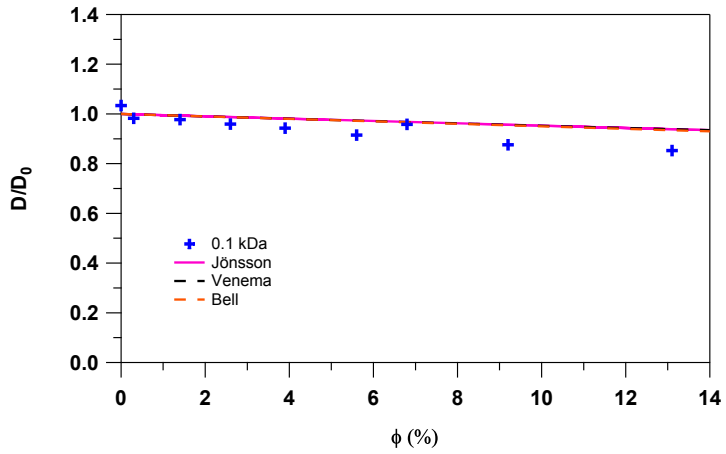

Figure 2.2: Normalized diffusion coefficient of the propionic acid 0.1 kDa (concentration 0.1 *wt%*, blue crosses) versus the volume fraction ϕ of silica LS. The theoretical curves reported are: Jönsson's model Eq. 2.8 (pink line); Venema's model Eq. 2.10 (black line); Bell's model Eq. 2.12 (dotted orange line). T= 298 K, pH $\approx$ 8.

Because the similarity of the models with the experimental data, the Jönsson et al. will be chosen as model of reference for the interpretation of the experimental data shown in the next chapters.

Charged obstacles

Regarding the physical processes that come into play in the dynamics of small molecules in charged crowded systems, we can generalize two phenomena that affect the dynamics. The first, treated in the previous section, is the obstructing effect or excluded volume interactions [25]: the obstacle particles exclude a fraction of the total volume and lengthen the diffusion paths for the diffusing molecules [134]. The second, is the specific interaction between small molecules and obstacles, which can lead to a counter-intuitive effect on the diffusion behaviour [147]. For example the diffusion coefficient of a particle among fixed attractive crowders, should decrease with the strength of the attraction because the crowders impede the motion of diffusers. Instead, in this system it has been observed that a weak attraction to the crowders leads to a higher diffusion coefficient [148]. This behaviour was understood in terms of the effective excess chemical potential landscape experienced by the diffuser: the roughness of this landscape decreased when a small attractive interaction is added, resulting in a faster diffusion. Below, two models that consider the electrostatic interaction between diffusers and obstacles are introduced.

Using Bell's suggestion for counterion Eq. 2.12, the volume fraction ϕ can be replaced by an effective volume fraction that considers the interactions in the case of charged objects. Practically, the radius of the nanoparticle R_o can be replaced by $R_o = R_o + \kappa^{-1}$:

$$D = D_0 \frac{1}{1 - \frac{\phi}{2}\left(1 + \frac{\kappa^{-1}}{R_o}\right)^3} \tag{2.14}$$

where κ^{-1} is the Debye length (Eq. 1.5). In this case the equations for the charged object are still solved in the case of an impenetrable uncharged particles because the values of the potentials in the equations have been not changed. Then, to adapt the previous equations to a case of charged particles we have just replaced the ϕ with an effective value that takes into account roughly the interactions of the particle.

To be more accurate, Smoluchowski equation (Eq. 2.11) can be solved with an interaction potential. For example, Bell and Dunning [149] and later Chan and Halle [150] have used the Poisson-Bolzmann interaction potential to investigate the diffusion of counterions. The same method was used to investigate the counterion diffusion in different systems: linear polyelectrolytes [151, 152] or hydrogel [153].

In section 2.5, we will discuss the results of this approach using a screened Coulomb potential as an interaction parameter between diffuser and obstacles.

Authors	Applications	Limitations
Waggoner et al. [139]	Small-sized diffusers Dilute solutions	Large diffusers Semi-dilute solutions
Mackie and Meares [140]	Small-sized diffusers Semi-dilute solutions	Large diffusers Concentrated solutions
Jönsson et al. [144]	Neutral obstacles Dilute concentration	Concentrated solutions
Venema et al. [131]	Concentrated solutions	High order in ϕ
Bell [133]	Charged obstacles Dilute concentration	Concentrated solutions

Table 2.1: Summary of the diffusion models presented in section 2.2 and 2.2.1.

2.3 | Models based on chemical binding

In this approach, the diffuser molecules can bind to the obstacles and hence do not diffuse. This hypothesis has been studied by Wang, who has found a simple expression for the self-diffusion coefficient [129] of water in suspension of proteins taking into account the effect of hydration of proteins:

$$D = D_0\left(1 - \frac{C_1}{C_t}\right) \tag{2.15}$$

where C_1 is the concentration of diffusers bound to the obstacles, and C_t is the total concentration of diffusers. The solution has been obtained solving Fick's equations, considering the obstacles fixed and the rate of exchange between free and bound diffusers instantaneously fast. However, one problem of this formulation found later in literature, is that the diffusers concentration is obtained over the free volume unoccupied by particles rather than over the total volume.

Another way to consider the charges effect when the diffuser can be bound to the obstacle, is to use a two state model (free or bound state). If there is a fast exchange (compared to the

characteristic time of observation) between the two states, then the diffusion coefficient can be evaluated as a weighted average of the diffusion coefficient of the two diffusion coefficients:

$$D = p_{\text{bound}} D_1 + p_{\text{free}} D_2 \tag{2.16}$$

where $p_i = c_i/(c_{\text{bound}} + c_{\text{free}})$. This kind of equation has been used to determine protein-ligand binding constant [154] and counterion condensation [155].

In case of binding to obstacles, Jönsson et al. find an expression for the diffusion coefficient, related to the concentration of interacting diffusers c_1, and free diffusers c_2, and to their diffusion coefficient D_1 and D_2 [144]:

$$D = D_2 \cdot \frac{1}{1 - \phi\left(1 - \dfrac{c_1}{c_2}\right)} \left(\frac{1 - \beta\phi}{1 + \beta\dfrac{\phi}{2}} \right) \tag{2.17}$$

with β:

$$\beta = \frac{1 - \dfrac{D_1 c_1}{D_2 c_2}}{1 + \dfrac{1}{2}\dfrac{D_1 c_1}{D_2 c_2}} \tag{2.18}$$

In the limit of $c_1 = 0$ the Eq. 2.17 is reduced to 2.8. This expression coincides with the Eq. 2.15 if the definition of concentrations is equalised.

2.4 | Models based on other effects

Other models that consider other interactions like the hydrodynamic interactions, or based on different physical concept as the free volume theory exist, but they are not presented here because they are not used for the analysis of the data in this thesis [138].

2.4.1 | Free volume theories

In free volume theories, diffusion occurs via the rearrangement of obstacles that creates voids where the diffusers are able to pass. The free volume theories are then based on the assumption that the free volume is the major factor controlling the diffusion rate of molecules [156, 157]. The diffusion rate is then related to the probability of the formation of voids in the dispersion of

obstacles [158–160]. The probability of hole formation can be estimated from the free energy of hole formation, but the latter quantity is difficult to assess unambiguously, which is the reason why the free volume theory approach was not used in the present work.

2.4.2 | Colloidal approach

There exists many studies on the effect of the increase of volume fraction on the diffusion coefficient of colloidal particles [161]. Different methods of resolution of Smoluchowski's equation (Eq. 2.11) exist. Some of them include the effect of hydrodynamic coupling often called hydrodynamic interactions (HI) [162]. This effect is caused by the velocity of solvent induced by the displacement of other particles on the dynamics of the particle under study. It is then very difficult and cumbersome to evaluate this effect precisely and is often reduced to its pairwise and far-field approximation, namely the Oseen tensor.

In the the case of hard spheres without hydrodynamic interactions, the following dependence on the volume fraction ϕ is found by several methods [163, 164]

$$D = D_0(1 - 2\phi) \tag{2.19}$$

If HI are present, the self-diffusion coefficient is increased [165], but if only far field contribution are taken into account the correction is too strong ($D = D_0(1 - 0.09\phi)$). As put forward by [166], for hard spheres, an improved treatment of hydrodynamics leads only to a 5 % change of the coefficient [162, 165]. Charged particles, due to the electrostatic repulsion, are in average further apart, and as a result the effect of hydrodynamic coupling is expected can be described by the far-field contribution as a reasonable approximation. Generally, hydrodynamics lessens the effect of direct interactions. This observation has been confirmed for charged systems by mode coupling theories calculations [167–169] Brownian Dynamics [170, 171] and MPCD simulations [172]. The effect for the diffusion coefficient is a relative enhancement of the diffusion of the order of 5 to 8%. The effect of hydrodynamic interactions will not be considered in the present study due to the complicated computations involved, but it should be included to have a fully quantitative assessment.

The diffusion in concentrated colloidal dispersions have also been investigated extensively by numerical simulations such as Brownian Dynamics [22, 173, 174], Stokesian dynamics [175]

and Multi-Particle Collision Dynamics [176, 177]. However, if the latter techniques can contain both a high complexities in terms of interaction potential but also of hydrodynamics coupling their implementation and use are time consuming and lie out of the scope of the present work.

The long-time self-diffusion of charged colloidal particles in mixtures have been hardly studied: by mode-coupling scheme including hydrodynamic interaction [178] or using the Generalized Langevin Equation [179–181]. They have used the DLVO or Yukawa potential (Eq. 1.7), and found that if the particles bear the same charge, the increase of the radius of the larger particle has a stronger effect on the diffusion of the larger particle than on the smaller one. However, this effect is found to be quasi independent of the concentration ratio between large and small particles. Instead, as in our systems where the diffusers are smaller than the obstacles, the small particle diffusion shows a strong dependence on the large particle concentration, as we will see in our experimental results.

2.5 | Cell-model for the diffusion in the DLVO potential

2.5.1 | Method

Bell [133] proposed to apply a weak macroscopic gradient of tagged diffusers and to solve Smoluchoswki equation in the stationary state.

$$\vec{J}(\vec{r},t) = -D\left[\nabla c(\vec{r},t) + c(\vec{r},t)\nabla\tilde{\psi}\right] \tag{2.20}$$

$$\nabla\cdot\vec{J} = 0 \tag{2.21}$$

where $\tilde{\psi} = \psi/k_BT$ is the reduced interaction potential between the obstacles and the diffusers. The main application of the previous equation was with the Poisson-Boltzmann potential (section 2.2.1). Since we are interested in the diffusion of polyelectrolytes in a dispersion of colloidal particles, a more suited potential is the DLVO potential (Eq. 1.7).

To solve the previous equations, a cell model with a radius R_c is considered at a center of which a spherical charged obstacle of radius R_o is placed. The corresponding volume fraction of

obstacles can then be easily evaluated as:

$$\phi = \left(\frac{R_o}{R_c}\right)^3 \tag{2.22}$$

Bell [133] has shown that for the following boundary conditions of the interaction potential:

$$\tilde{\psi}(r = R_c) = 0 \quad ; \quad \frac{d\tilde{\psi}}{dr}(r = R_c) = 0 \tag{2.23}$$

then the diffusion coefficient writes

$$\frac{D}{D^\circ} = \frac{\chi(R_c)}{\left\langle e^{-\tilde{\psi}} \right\rangle} = \chi(R_c) \frac{\frac{4}{3}\pi R_c^3}{\int_{R_o}^{R_c} e^{-\tilde{\psi}(r)} 4\pi r^2 dr} \tag{2.24}$$

where χ is the solution of the following first order differential equation:

$$r \frac{d\chi}{dr} + \chi(r)\left(1 + \chi(r) - r\frac{d\tilde{\psi}}{dr}\right) - 2 = 0 \tag{2.25}$$

$$\chi(R_o) = 0 \tag{2.26}$$

The boundary condition (Eq. 2.26) comes from the impenetrability of the obstacle which corresponds to a zero flux condition at this boundary. Unfortunately, there are only a limited number of cases for which either the function χ or the integral $\left\langle e^{-\tilde{\psi}} \right\rangle$ exhibit an analytic form apart form the hard sphere case.

In what follows, we will then use the following DLVO interaction potential (Eq. 1.7)

$$\tilde{\psi}(r) = \ell_B \frac{z_1 e^{\kappa R_1}}{1 + \kappa R_1} \frac{z_2 e^{\kappa R_2}}{1 + \kappa R_2} \frac{e^{-\kappa r}}{r} \tag{2.27}$$

for which the Fehlberg fourth-fifth order Runge-Kutta method, with degree four interpolant of the `Maple` software was used to integrate Eq. 2.25 .

2.5.2 | Applications

In this part, we consider a dispersion of silica particles with $R_o = 8$ nm and variable charge Z_{eff}. The volume fraction ϕ varies from 0 to 0.2. The value of κ is fixed to 1 nm^{-1}. The reduced diffusion coefficient $D/D_\circ$ of a point-like anion of charge $z = -1$ is then computed thanks to the method described in the previous section.

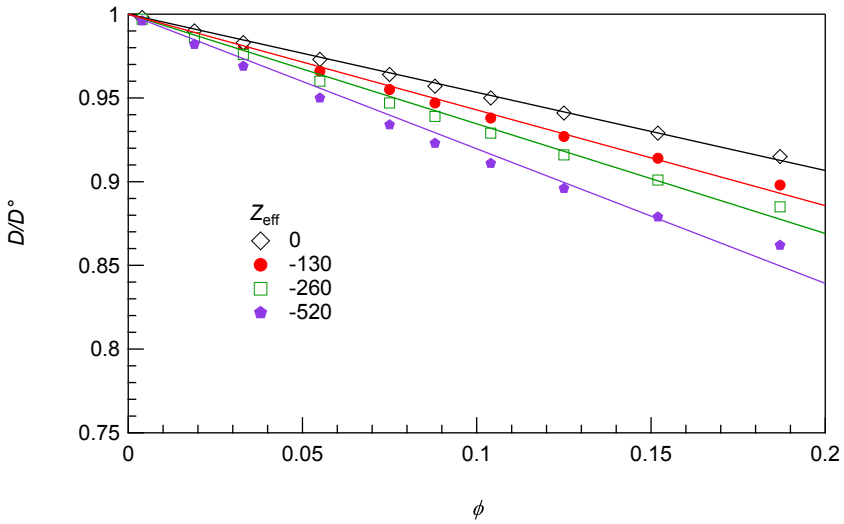

Figure 2.3: Effect of the charge of the obstacle on the diffusion of a point-like counterion. Normalised diffusion coefficient versus the volume fraction of obstacles at difference charge, calculated using the method described in section 2.5.

In Fig. 2.3, the effect of the increase of the volume fraction is shown. Even for uncharged particle the diffusion coefficient of the ion decreases linearly. The slope of this decrease is −0.47, which is in fair agreement with the model of Jönsson (−0.5, Eq. 2.9). As the charge of the particle increases, the slope becomes steeper and deviations from the linear behaviour start to appear for the larger values of the volume fraction.

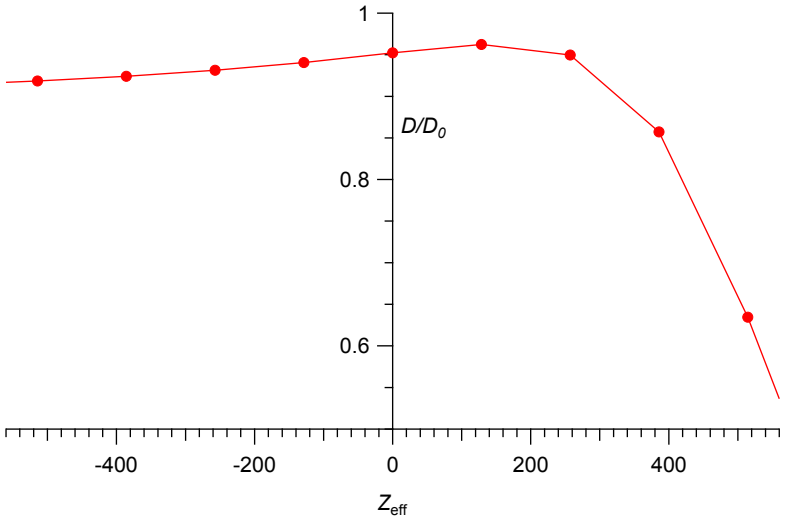

Figure 2.4: Effect of the charge of the obstacle on the diffusion of a point-like coion, ϕ = 10 %. Normalised diffusion coefficient versus the charge of obstacles. See text for parameters.

In Fig. 2.4, the effect of the charge of the nanoparticle and its sign is investigated. For

negatively charged particles, the anion is a coion of the particle, and the diffusion coefficient decreases slowly as the absolute value of the charge increases. This effect has been already observed in Fig. 2.3. When the charge of the particle is reversed, the diffusing ion, that now is a counterion, is attracted towards the particle. This observation is confirmed at high values of charge, where the diffusion coefficient of the ions drops rapidly. In this regime, the ion is trapped in the close vicinity of a particle and it can hardly diffuse among the other particles. An intermediate regime is observed at small values of positive charge, where a small increase of the diffusion coefficient is found compared to the pure obstruction. This small rise might be caused by the small accumulation of ions, which without being trapped by a too strong interaction, are close to the particle . This accumulation makes more likely trajectories close to the particle, and promotes a faster diffusion.

Summary of Chapter 2

The description of the diffusion of charged objects in a crowded media is a challenging problem, since the properties of the diffuser have to be considered in addition with the interactions present. To study this fundamental problem, the behaviour of polymers in a crowded media is used as model to study the phenomena that come into play. In particular, we consider a polymer-nanoparticle mixture in which the nanoparticles are relatively large compared to the polymer, i.e. the colloid limit.
Due to the presence of obstacles, the value of the diffusion coefficient of the diffuser changes compared to the value in a pure solvent. The modification of the diffusion coefficient may be attributed to the obstruction effect and to the interactions between diffusers and obstacles.
To calculate the diffusion coefficient, one has to solve the diffusion equation in the void space with the opportune boundary conditions, but in the presence of interactions an additional term including the interaction potential have to be considered.
The models based on obstruction effects, where obstacles are regarded as motionless, allow to obtain for uncharged obstacles, a simple dependence of the diffusion coefficient on the volume fraction of spherical obstacles. In particular Jönsson's model ($D = D_0/(1 + 0.5\phi)$) [144], calculated using a cell model approach and valid for uncharged obstacles in the dilute regime, will be used as reference model for the interpretation of the experimental data. The models based on the chemical bonding have not been considered, they are not relevant if obstacles repel the diffuser.
In the case of charged obstacles, the effect of the interactions have to be considered. In a first approximation, the model obtained for uncharged obstacles can be adapted, modifying the volume fraction to take into account the interactions. To be more accurate, the Smoluchowski equation can be solved with an interaction potential to obtain the diffusion coefficient. Since we are interested in the diffusion of polyelectrolytes in dispersions of colloidal particles, we solve the Smoluchowski equation with the DLVO potential. Using a cell model approach and the boundary condition of impenetrable obstacles, the problem has been solved numerically. The diffusion coefficient decreases linearly with the volume fraction of obstacles. The decrease is steeper as the charge of the obstacles increases.

Chapter 3

Nuclear Magnetic Resonance

Contents

3.1 | Introduction

Nuclear Magnetic Resonance (NMR) is the technique used in this thesis to investigate the self-diffusion of polyelectrolytes in crowded system, and to study the conformation of the chain. In particular, the application of specific pulse sequences makes it possible to use NMR, traditionally dedicated to the characterization the chemical structure of the molecules, to monitor the diffusion of chemical species. This specific use of NMR gives rise to numerous applications: deformulation of complex mixtures [182–184], investigation of the interaction of nanoparticles and ligands[185, 186], the determination of the size of micronic droplets due to the confinement effect on the diffusion [187], ... Diffusion NMR is then a perfect complementary technique to scattering measurements to understand how the structure of materials affect the dynamics [188, 189]. One of its greatest successes is diffusion Magnetic Resonance Imaging which gives access to the structure of white matter of the brain [190], and also it is a non-invasive technique [191]. NMR is then a powerful technique to studying both the structural and dynamics properties of molecules. Because of the central role played by NMR in this work, this chapter introduces the main principles and characteristics of the technique.

Why chose NMR to study the self-diffusion of the polyelectrolytes, and what are its main advantages compared to the other diffusion techniques?

One of the great advantage of the technique is that the information is isotope selective, namely it is possible to obtain specific properties for a specific site or part of a complex system, and mostly it allows to separate clearly the solute-solvent signal [32]. Indeed, NMR relies on the interaction between the nuclear spin and magnetic field, that is characteristic of the specific nucleus and of the chemical environment [192].

Diffusion NMR monitors the Brownian displacement of specific molecules on 10-1000 ms timescale (10-100 μm spatial scale) [31, 193], and it allows to obtain a diffusion coefficient between 10^{-14}–10^{-9} m^2 s^{-1}. In contrast to fluorescence correlation spectroscopy (FCS), that measures the diffusion coefficients thanks to fluorescent moieties in the diffusing species [27, 194], NMR does not need the grafting of additional external species that might alter the dynamics [195]. Furthermore, diffusion NMR is not affected by the limitations of the dynamic light scattering (DLS), from which diffusion coefficients can also be determined. While DLS is not suited for small molecular weights, it measures concentration fluctuations and hence

collective (mutual) diffusion coefficients [196], and more for small molecules in crowded media. Conversely diffusion NMR is efficient for small molecules in crowded systems.

In this chapter, we introduce the theoretical concepts of NMR, the bases of the experimental technique, the pulse sequences used to obtain the desired information and we conclude with some experimental details about the technique.

3.2 | Magnetic momentum

For a comprehension of the NMR technique, the main concepts of the NMR are presented in this section. This section, which can be skipped by people not interested in the fundamental of the technique, starts from the explication of the nuclear magnetism to understand the origin of the NMR signal.

Magnetic nuclei are characterized by an intrinsic angular momentum known as spin, whose magnitude is:

$$S = \hbar \sqrt{I(I+1)} \tag{3.1}$$

where I is the spin quantum number. The angular momentum vector $\vec{S}$ has $2I + 1$ projections onto an generic axis (called z axis). This z component, called I_z is quantized, and it is equal to:

$$I_z = m_I \hbar \tag{3.2}$$

where the magnetic quantum number m_I has $2I + 1$ values in integral steps between $+I$ and $-I$. The magnetic momentum $\vec{\mu}$, the quantity that interacts with the magnetic field causes the NMR signal, is directly proportional to $\vec{S}$:

$$\vec{\mu} = \gamma \vec{S} \tag{3.3}$$

where the proportionality constant γ is the gyromagnetic ratio, specific of a nucleus. Once an observation direction z is fixed, the values of $\vec{\mu}$ onto that direction are:

$$\mu_z = \gamma I_z = \gamma m \hbar \tag{3.4}$$

The $2I + 1$ orientations of the spin have the same energetic levels, but when a magnetic field $\vec{B}$ is applied the degeneracy is removed and the energetic levels are splitted. The energy of interaction between the magnetic moment $\vec{\mu}$ and the external magnetic field $\vec{B}$ is equal to:

$$E = -\vec{\mu} \cdot \vec{B} = -\mu_z B = -m_I \hbar \gamma B \tag{3.5}$$

in case z coincides with the direction of the magnetic field. Therefore, $2I + 1$ energetic states appear because m_I has $2I + 1$ values equally spaced with an energy gap equal to $\hbar\gamma B$. This last effect is known as Zeeman effect.

For a nucleus with spin $I = \frac{1}{2}$, as the hydrogen nucleus, nucleus on which we have performed the measurements, the Zeeman effect causes two energetic levels, related to two different I_z values ($\pm\hbar/2$). A state called spin-up for $m_\uparrow = 1/2$ in the same direction to the magnetic field, and a state called spin-down for $m_\downarrow = -1/2$ in the opposite direction to $\vec{B}$. The absorption of energy, which is equals to the difference of energy between the two states, causes a transition between the two states and originates the resonance condition, which is thus:

$$\Delta E = h\nu = \hbar\gamma B \tag{3.6}$$

where ν is the frequency of the electromagnetic radiation, equal to:

$$\nu = \frac{\gamma B}{2\pi} \tag{3.7}$$

For magnetic field of the order of few teslas, this frequency falls in the radio-frequency region of the electromagnetic spectrum ($\nu \sim 100$ MHz). However, the exact resonance frequency of a nucleus in a molecule is characteristic of the chemical environment of the nucleus. This phenomenon, detailed in the next section, is at the origin of the chemical shift and it will give us information on the arrangement of atoms in the molecule.

3.3 | Chemical shifts

The chemical shift, which is the small shift of resonance frequency due to the chemical environment of the nucleus, is a very efficient empirical tool to detect changes in electronic

environment that may arise from chemical reactions or bonding [192, 197].

The chemical shift makes NMR an attractive technique to characterise and distinguish different types of hydrogen in a molecule. The study of the dependence of this parameter on the local properties of the system will allow us in chapter 5 and 6, to investigate the structural properties of polyelectrolytes.

The exact resonance frequency of a nucleus in a molecule is determined by its neighbours in the molecule and by its environment, which affects the local electron distribution, hence the magnetic field shielding. Thanks to the latter effect, it is possible to distinguish a same atom in a different group, to observe structural changes of a molecule, and also it provides information on the environment within the molecule and around.

The chemical shift arises because the magnetic field perceived by a nucleus differs from the external field B_0, because of the proximate electrons generate a magnetic field $B^{'}$ that modify B_0. Therefore the field perceived by the nucleus B is equal to $B = B_0 - B^{'}$. The real field experienced by the nucleus can be expressed as:

$$B = B_0(1 - \sigma) \tag{3.8}$$

where σ is a parameter, called shielding constant, characteristic of the nucleus environment. As result of nuclear shielding, the resonance condition becomes:

$$\nu = \frac{\gamma B_0(1 - \sigma)}{2\pi} \tag{3.9}$$

The nuclear shielding is affected by phenomena like the local dia- (σ>0) and paramagnetic (σ<0) shielding (arising from the electrons close to the nucleus), and the remote currents. The local shielding is dependent on the electron density around the nucleus: the larger the electron density, the stronger the shielding and the smaller the chemical shift. Other effects include the hydrogen bonding, the local electron field arising from charged or polar groups, and the paramagnetic shifts produced by unpaired electrons [192].

For convenience, the chemical shift δ is defined in terms of the difference in resonance frequencies between the nucleus of interest ν, and a reference nucleus ν_{ref}. The difference is divided by ν_{ref}. This parameter, called chemical shift δ, which is a dimensionless parameter, molecular dependent and independent of the magnitude of the magnetic field, is :

$$\delta = \frac{\nu - \nu_{\text{ref}}}{\nu_{\text{ref}}} \tag{3.10}$$

The amplitude of this shift is often rather small and the common unit used is ppm. The dependence of δ on the properties of the solution, like the value of pH, is a valuable source of information on the change occuring in the system as it will discussed later on.

In the next section, we will focus on an NMR fundamental process, the nuclear relaxation.

3.4 | Relaxation

Before dealing with diffusion NMR, it is necessary to introduce the nuclear relaxation processes, because relaxation times of the system under study have to be known before performing the diffusion experiments in order to set-up correctly the parameters of the sequence and to analyse correctly the data that could be distorted by the effect of the relaxation phenomena. In addition, relaxation measurements can be a very efficient tool to probe the colloidal dispersion [198]. When the hydrogen nucleus interacts with an externally applied magnetic field, the ratio of population of spins in the two levels ($n_\uparrow$ and $n_\downarrow$) is governed by the Boltzmann distribution:

$$\frac{n_\uparrow}{n_\downarrow} = \exp^{\Delta E/kT} \tag{3.11}$$

where ΔE is the energy gap between the two levels as in Eq. 3.6, and T is the temperature. Transitions between adjacent spin levels can be induced by the application of a radiofrequency pulse (RF) at the Larmor frequency Eq. 3.7, of the nuclei under study. Upon cessation of the RF pulse, the spins will return to the value of equilibrium population in a process known as NMR relaxation [199].

The time to restore the equilibrium along the z-axis, i.e. to restore the equilibrium of the spin population, is called longitudinal relaxation time or T_1. The time needed for the decay to zero of the transverse xy magnetisation, or loss of coherence between levels, is the transverse relaxation time or T_2. T_2 is always smaller than T_1, since there can not be magnetization remaining in the xy plane if the system has returned to thermal equilibrium.

The relaxation processes occur due to the fluctuations of the field experienced by the nuclei. In the absence of paramagnetic impurities, the mechanism of proton relaxation is the ^{1}H-^{1}H

dipolar interaction and it is then especially sensitive to the relative motions of nuclei [200]. The next sections is devoted to the methods used for their measurements.

3.4.1 | Methods

Measurement of T_1

The knowledge of these relaxation times is necessary to set-up correctly the time parameters in diffusion measurements. So before performing the diffusion experiments in a new system, measurements of the relaxation times have been performed.

The relaxation to the z axis, the so called longitudinal relaxation, is caused by the loss of the energy absorbed during the resonance process by the nuclear spins, and for the magnetisation achievement of its equilibrium value. The spin-lattice relaxation time T_1 can be measured using a pulse sequence consisting in an inversion of the magnetization, followed by its recovery [201]:

$$180^\circ - \tau - 90^\circ - \text{acquisition}$$

The first pulse inverts the magnetisation along the negative z axis, and during the variable delay τ the spin-lattice relaxation along the z axis occurs. The 90° brings back the z magnetization onto the xy to be detected.

$$M_z(\tau) = M_0 \left[1 - 2\, \mathrm{e}^{-\frac{\tau}{T_1}}\right] \tag{3.12}$$

This sequence is repeated for different τ values to map the process of return to the equilibrium of the magnetisation, and to obtain the decay rate. A delay time of at least $5T_1$ is necessary between repeated measurements, to ensure that the sample has returned to equilibrium.

Measurement of T_2

The transverse, or spin-spin, relaxation time is due to the intra- or intermolecular magnetic field, and to the spatial inhomogeneities of the magnetic field that cause a loss of the phase coherence of the magnetization. The characteristic time of this relaxation process T_2, can be obtained with a sequence

$$90^\circ - \tau - 180^\circ - \tau - \text{acquisition}$$

This sequence called spin-echo or Hahn echo [202] refocuses the phase shift caused by field inhomogeneity or by the chemical shift thanks to the 180° pulse.

After the 90° pulse, the total magnetization, coming from different spatial regions, precesses at different frequencies. After the time τ, the 180° pulse flips the magnetization to a symmetrical position in the *xy* plane. After another interval τ, all magnetizations come back into phase. Therefore, the NMR signal decays rapidly after the first 90° pulse and reappears at 2τ.

The NMR intensity of each line in the spin echo spectrum is given by:

$$I(2\tau) = I(0)\exp^{-2\tau/T_2} \tag{3.13}$$

If the whole experiment is repeated with different τ delays, like for T_1, one can show that the diffusion of the species in the field heterogeneity may contribute to the decay of the signal, then the decay cannot be ascribed only to the transverse relaxation [199]. To solve this problem, Carr and Purcell [203] suggested the use of a series of n 180° pulses separated by 2τ to minimize the effect of diffusion. Later, Meiboom and Gill [204] corrected the previous pulse sequence by changing the phase of the 180° with respect to the initial 90° to avoid the cumulation of the imperfection of the pulses. The resulting pulse sequence, now commonly known as CPMG, has been used. T_2 is obtained from a plot of $I(2n\tau)$ versus $2n\tau$.

The measurement of T_2 is necessary to choose the time interval in the sequence used to obtain the diffusion coefficient, whose measurement method is described in next section.

3.4.2 | Results

We have not focused on the analysis of the relaxation times, but we have made a preliminary analysis of the relaxation times in order to subsequently prepare the diffusion measurements. The relaxation times T_1 and T_2 have been determined for solution at 1 % wt at pH$\simeq$ 8 using the pulse sequences described above. For T_1, whatever the length of the polyelectrolyte constant values were found: $1/T_1(CH_2) = 2.0\ s^{-1}$ and $1/T_1(CH) = 3.0\ s^{-1}$. For T_2 however, the value of $1/T_2$ increase significantly with the length of the polyelectrolyte, from $1/T_2(CH_2) = 5\ s^{-1}$ for PAANa 2.1 kDa to $1/T_2(CH_2) = 20\ s^{-1}$ for PAANa 15 kDa. A similar increase is observed for methine protons. The difference of behaviour between T_1 and T_2 can be explained by the different timescale probed by these two observables [199]. While T_1 is sensitive to the dynamics

at the Larmor frequency, T_2 is sensitive to the low frequency dynamics (long time limit). For polymers, if the Larmor frequency is of the order of hundreds of MHz, T_1 probes the internal dynamics of the chain or Rouse dynamics, while T_2 probes the global dynamics of the chain. The internal dynamics seems then to be similar whatever the length of the chain, while the global dynamics strongly depends on the size [205].

3.5 | Diffusion NMR

In this section the principle of diffusion NMR and the pulse sequences used to obtain the value of the diffusion coefficient are presented [31, 193, 206].

A general method to measure the translational diffusion of molecules is the Pulsed field gradient NMR (PFG-NMR) sequence. In PFG-NMR, nuclei are labelled by precession frequencies according to their location in the sample. Then, when the nucleus moves during the diffusion time, the new position can be detected because of alteration of the signal [31]. Historically, the alteration of the NMR signal due to the diffusion of the sample was observed for the first time by Hahn [202]. He observed an huge reduction of the NMR signal in a spin-echo sequence caused by the diffusion inside an inhomogeneous magnetic field. After Carr and Purcell adjusted the Hahn's NMR sequences, to reduce the effect of the inhomogeneous magnetic field on the transversal relaxation [203]. A further refinement has been done by Stejskal and Tanner with the Pulsed Field Gradient Spin Echo (PFG-SE) [207].

Here, we will explain the effects of the magnetic field gradient on a couple of spins by two examples. In the first example, the effect of the gradient magnetic field is explained in the case of two fixed spins. In the second example, the effect of the gradient on system of spins in presence of a diffusion process is shown.

In Fig. 3.1, it is shown the effect of two magnetic field gradients on the precession of a couple of spins, the two coloured disks in the figure. The arrow inside the disk is the magnetic momentum of the spin. In the top of Fig. 3.1, the green arrows are the total magnetic field perceived by the spins in different periods. Below, the frequency of precession of every spin is shown.

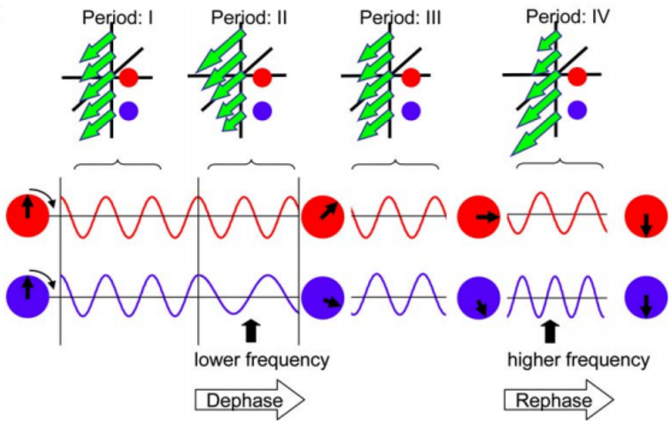

Figure 3.1: Effect of a couple of magnetic field gradients on the precession of two spins. In the first period only the static magnetic field is on, and both the spins precess with the same Larmor frequency. In the second period, the gradient causes a dephasing of the spins. In the third period, when the gradient is off, the spins precess with the Larmor frequency but with a different phase. In the fourth period, when a gradient equal in intensity and duration but opposite in direction to the first one is applied, the spins are completely rephased. Reproduced from [208].

- In the period I, the two spins perceive the same static magnetic field, as a consequence they precess at the same Larmor frequency.
- In the period II, a field gradient is applied, so the spins are affected by different magnetic fields as function of their position. As a consequence the spins precess with different frequencies.
- In the period III, when the gradient is turned off, the magnetic field is homogeneous in the space. However, because of the phase shift accumulated in the period II, the spins precess with a difference phase.
- In the IV period, another gradient with an opposite polarity, along the negative z axis, is applied. When a gradient, with the same intensity and duration time than the first is applied, if the spins are motionless they will be completely rephase at the end of this time.

If the spins are diffusing, the second gradient will not rephase completely the spins, as shown in Fig. 3.2 [208].

These two examples show the general idea of a diffusion measurement. In the next section the main sequences used to determine the self-diffusion will be presented.

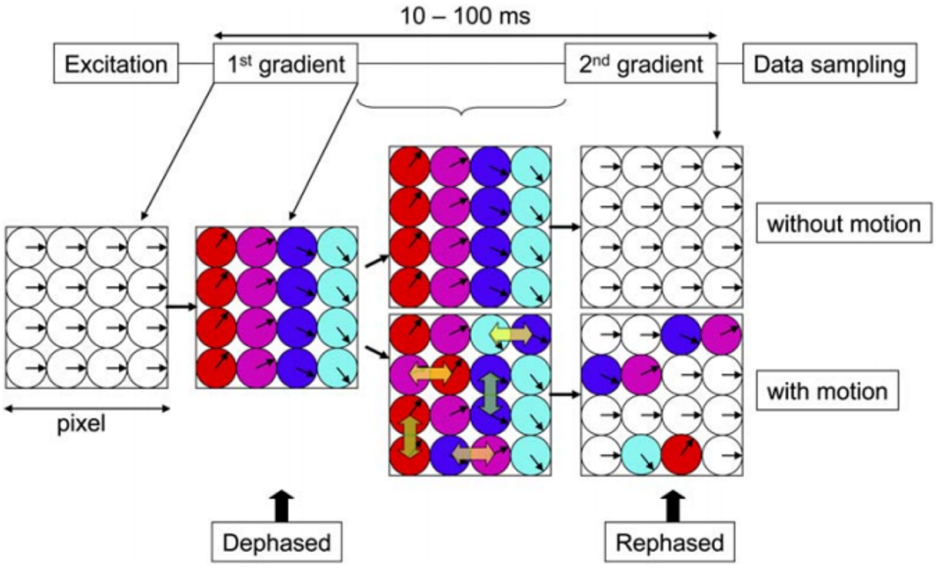

Figure 3.2: Effect of two bipolar magnetic field gradients on a sample of spins. The dephasing of every spin is function of the position of the spin. When the spins diffuse during the application of the two gradients Δ, the second gradient is not able to rephase completely the magnetisation. This causes a decrease of the NMR signal compared with the case where the spins are without motion. Reproduced from [208].

3.5.1 | Diffusion pulse sequences

Pulsed field gradient spin-echo sequence

The most common and simplest sequence used in pulse field gradient diffusion NMR is the Pulsed Field Gradient spin-echo sequence (PFG-SE) proposed by Stejskal and Tanner [206, 209].

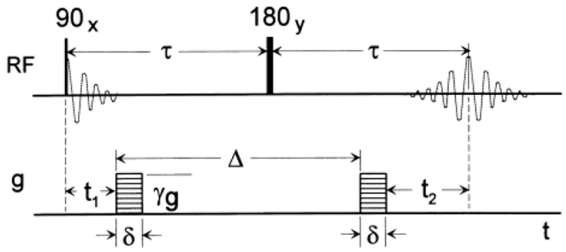

Figure 3.3: Sequence of Stejskal and Tanner or PFG-SE [207]. Reproduced from [206].

They proposed a sequence with two gradients applied in the same direction, plus two radiofrequency pulses of 90° and 180° to form a Hahn echo as shown in Fig. 3.3. First a 90° pulse rotates the magnetization from the z axis to the xy plane. Then, a magnetic field gradient

of intensity g and duration δ, is applied causing a phase shift of the spins as a function of their position $\varphi(z) = \gamma g \delta z$. Later, a 180° pulse is applied to inverse the phase shift. Finally, a last gradient equal to the first one is applied. If the spins do not move during the delay Δ between the two gradients, the phase shift during the application of the second gradient is the exact opposite of the first phase shift $\varphi'(z) = -\gamma g \delta z$. However, if z' differs from z, because the diffusion, the echo signal is reduced. The amplitude of the NMR signal measured at the echo time is given by:

$$I(b) = I_0 \mathrm{e}^{-\frac{2\tau}{T_2}} e^{-bD} \tag{3.14}$$

where I_0 is the unattenuated intensity and b is the diffusion sensitivity factor:

$$b = (\gamma g \delta)^2 T_D = q^2 T_D \tag{3.15}$$

In Eq. 3.15, $q = \gamma g \delta$ has the dimension of a wavevector at which the correlation of the diffusive displacement is done and T_D is a diffusion delay or correlation time. Its exact expression depends on the pulse sequence but in a first approximation it can be considered that $T_D \simeq \Delta$. For the PFG-SE pulse sequence, the exact expression is $T_D = \Delta - \frac{\delta}{3}$.

As seen in Eq. 3.14 the intensity of the signal I depends on T_2. For polymers, T_2 can be rather short and the diffusion delay Δ has to be long enough to observe a significant decay of the signal.

Pulsed field gradient stimulated echo sequence

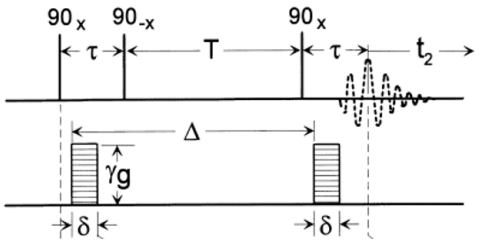

Figure 3.4: PFG-STE sequence [210]. Reproduced from [206].

A variation of the spin-echo sequence is the pulsed field gradient stimulated echo sequence (PFG-STE) [210]. The main advantage of the PFG-STE compared to the PFG-SE is that the magnetisation is stored along the the longitudinal axis and decays with T_1 [210]. Since T_1 is longer than the transversal relaxation time T_2, it allows longer diffusion time. As it shown in

Eq. 3.14, the signal intensity when the SE sequence is used depends strongly on T_2. Contrarily to the PFG-STE sequence, the amplitude of the NMR signal is mainly related to T_1:

$$I(b) = \frac{I_0}{2} \mathrm{e}^{-\left(\frac{2\tau}{T_2} + \frac{T}{T_1}\right)} \mathrm{e}^{-bD} \tag{3.16}$$

The attenuation factor due to nuclear spin relaxation has been modified according to the time during which the magnetization is transversal (τ) and longitudinal (T). The amplitude of the unattenuated intensity I_0 is reduced by a factor of two, because only half of the signal is refocused.

The PFG-STE sequence still need some corrections to eliminate contributions that can alter the NMR spectrum, as will be explained in the next paragraph where we introduce the sequence used for our experiments.

Bipolar pulse pair-longitudinal eddy current delay sequence

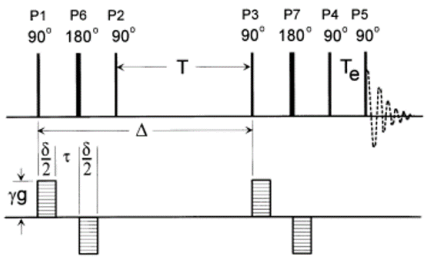

Figure 3.5: The BPP-LED pulse sequence incorporating bipolar gradient pulses [211]. The bipolar gradient pulses cancel the generation of the eddy currents. The two 90° pulses delay the acquisition in order to the eddy currents to dissipate. Reproduced from [206].

One problem of the use of the magnetic field gradient, is the generation of Foucault currents, or eddy currents, that change anomalously the intensity of the signal and alter the NMR spectrum. To minimise these effects, a bipolar pulse pair - longitudinal eddy current delay BPP-LED, is often used Fig. 3.5 [211]. The main parts of this sequence are two: a bipolar pulse pair gradient (BPP) and a longitudinal eddy current delay (LED). Every gradient is replaced by a couple of shorter bipolar gradients, with a different polarity and separated by a 180° pulse. The eddy current, generated by the first pulse, will be approximately cancelled by the effects of the second gradient pulse which is of opposite polarity. Another solution to dissipate the eddy currents is to delay the acquisition until they have dissipated. To achieve this goal, two 90° pulses separated

by an time interval T_e, the longitudinal eddy current delay, are applied before the acquisition process. The signal distortion is decreased by this settling period for eddy currents prior to signal acquisition [211].

Another significant interest of the use of bipolar gradients is to remove the effect of constant backgrounds gradients that might exist in the sample [212, 213] for example due to the inhomogeneity of the magnetic susceptibility.

Despite more recent sequences exist, this sequence is quite effective and suitable for systems used, so we will use it, to perform our experiments, with some corrections to prevent experimental problems.

Other sequences

Several other NMR pulses sequences have been proposed in the literature to measure self-diffusion coefficients since the Wu et al. sequence. Most of them have concatenated other sequences or block of pulses to the main diffusion sequence, in order to add a functionality. This functionality can be the suppression of the water signal [214] using WATERGATE block (WATER suppression by GrAdient-Tailored Excitation) [215], the enhancement of the signal selectivity using an INEPT (Insensitive Nuclei Enhanced by Polarization Transfer [216]) block [217], the suppression of chemical exchange [218] etc. It must be noted, that the diffusion measurement displayed in 2D map named DOSY, concatenated with another sequence, is mostly used as a tool in the separation and identification of products, not specifically to the study of diffusion processes. More interestingly for our purpose, is the development of sequences that suppress the convection artefacts. As for example the convection effects. During the measurements, the data quality could also by affected from convection effects. Since in the spectrometer, the tube is heated at the bottom, the temperature regulation might induce temperature gradients that may cause a convection in the sample. This effect is evidenced either by phase shift at high gradient strengths [219] or by a downward curvature in the curve of the signal versus b [206]. This effect was not observed in our experiments certainly due to the relatively high viscosity of aqueous solutions. To eventually solve this problem, Jerschow et al. have proposed a double stimulated echo sequence that suppress the signal arising from coherent displacement of nuclei [220]. This sequence is very efficient and necessary for highly

sensitive sample (low viscosity liquid and high temperature systems). However, the amount of measured signal is significantly lower than using the PFGSTE sequence. In our case, where the concentration of polyelectrolyte is low, it would increase significantly the acquisition time. Moreover, the viscosity of our sample is not critical to use this kind of pulses sequence. To finish with this rapid overview of the recent PFG sequences, one has to mention the development one single-scan measurement [221]. Based on gradient encoding during acquisition, they allow very fast measurements in concentrated systems. This is a great advantage in evolving systems. In our case, we have decided to use the Wu et al. sequence that is the most suitable to our diluted polyelectrolyte systems.

3.6 | Implementation of the experiments

To obtain the diffusion coefficient, the PFG stimulated echo sequence that we have used in our experiments is the BPP-LED [211, 222] described in section 3.5.1 , with a water presaturation (see § 3.6.1): `ledbpgppr2s` Bruker sequence.

The pulse gradient duration δ and the diffusion delay Δ were fixed and the field gradient amplitude g was varied. The diffusion coefficient was obtained from a fit of the resultant signal intensity as a function of b:

$$I(b) = I(b = 0)\, \mathrm{e}^{-bD} \tag{3.17}$$

where $I(b)$ is the measured intensity, $I(b = 0)$ the unattenuated signal intensity, D the diffusion coefficient. The value of the gradient has been calibrated with the value of the self-diffusion coefficient of HOD in D_2O [223, 224]. For this pulse sequence, the diffusion sensitivity factor b is equal to

$$b = \gamma^2 \delta^2 g^2 \left(\Delta - \frac{\delta}{3} - \frac{\tau}{2} \right)$$

where γ is the gyromagnetic radius of the observed nucleus, g is the gradient strength (the variable parameter), δ is the length of the gradient, Δ is the diffusion delay, and τ is a delay for the gradient recovery.

3.6.1 | Solvent signal suppression

A phenomenon that could strongly limit the ability to observe the signal of interest and to measure accurately the diffusion coefficient is the signal arising from solvent. In aqueous solutions, as in our experiments, the strong water signal could cover the polyelectrolyte signal and create a strong baseline distortion in the NMR spectra. To avoid these effects, two techniques can be used. The first is the substitution of light water (H_2O) by heavy water (D_2O). This method was not chosen in order not to change the physical-chemical properties of the system, especially the dynamics ones than are affected by the change of viscosity of the medium. The second one is to adapt the pulse sequence to suppress the signal coming from the solvent. Plenty of pulse sequences are available [214, 225] to achieve the suppression but we chose one of the simplest, the presaturation. At the beginning of the pulse sequence, a long and low power pulse at the frequency of the water signal is applied. The consequence of this pulse is to equalize the population of spins. As a result, no contribution to the magnetization comes form the water spins. This procedure has known drawbacks, such as the decrease of resonances close to the water signal and the saturation of labile protons[214], but none of them affect our systems, which is the reason why we chose it.

3.6.2 | Non-Gaussian brownian diffusion

The mono-exponential decay of the signal described by Eq. 3.17 is correct if the distribution of the displacements is Gaussian and if the sample is not polydisperse. The effect of dispersity (Eq. 1.11) are discussed in § 3.6.3. Non-gaussian diffusion can be seen as dependence of the diffusion coefficient on time or a mean squared displacement that does not scale with t [26, 118, 119, 226]. This time dependence is not explored by default by the pulse sequences used since the diffusion delay Δ is fixed to keep the relaxation effect constant while the gradient amplitude g is varied. To check the Gaussian decay, we have done some preliminary measurements at fixed g values and variable Δ, ie fixed wavevector $q = \gamma g \delta$ and variable diffusion time, and no variation of the diffusion coefficient was found. This result proves that non-Gaussian effects are negligible in the regime studied.

3.6.3 | Dispersity effects

Polymer systems often display a notable distribution of molar mass [58]. They are characterised by a range of molecular weights that give to a corresponding molecular size distribution and then, a distribution of self-diffusion coefficients. Therefore, due to this dispersity Eq. 1.11, at high b values the signal deviates from a simple single exponential and a mono-exponential fit leads to a significant underestimation of the average diffusion coefficient $\langle D \rangle$. To fit the data satisfactorily, it is then necessary to take this departure into account [61, 227–230], using for example the following second order expansion:

$$I(b) = I(b=0) \int_0^\infty P(D) \exp(-bD) \mathrm{d}D \simeq I(b=0) \exp\left(-b\langle D\rangle + \frac{1}{2} b^2 \left(\langle D^2\rangle - \langle D\rangle^2\right)\right) + \cdots \tag{3.18}$$

where the first cumulant $\langle D \rangle$ is the average diffusion coefficient, and the second term ($\langle D^2 \rangle - \langle D \rangle^2$), gives access to the width of the distribution.

Furthermore, when a specific mass distribution is assumed, e.g. a Log-Normal distribution or a Gamma distribution, the dispersity $Đ_\mathrm{M} = M_w/M_n$ can be estimated via the value of the second cumulant [61, 227] (see § 3.6.3), or by the complete integration of the distribution [230]. Diffusion NMR measurements can then be used to determine polymer molecular mass distributions [231, 232]

General effect of size dispersity

In this section the expression used to analyse NMR data is calculated, taking into account the dispersity of the system. First, a general expression independent of the type of mass distribution is found.

The signal $I(b)/I_0$, with the assumption that there are not interactions between coils of different molar mass (dilute system), has a mass average dependence of the type [233]:

$$\frac{I(b)}{I_0} = \frac{\sum_i f_i M_i \exp(-bD_i)}{\sum_i f_i M_i} \tag{3.19}$$

where f_i is the number of polymer of mass M_i and diffusion coefficient D_i. Equation 3.19 may be expanded as a power series up to the second order in bD_i ($bD_i < 1$), $\mathrm{e}^x = 1 + x + \frac{x^2}{2!} + \cdots$:

$$\frac{I(b)}{I(b=0)} = 1 - b\frac{\sum_i f_i M_i D_i}{\sum_i f_i M_i} + \frac{b^2}{2}\frac{\sum_i f_i M_i D_i^2}{\sum_i f_i M_i} \tag{3.20}$$

Further, Eq. 3.20 can be logarithmised and then expanded into series up to the second order, $\ln(1+x) = x - \frac{x^2}{2} + \cdots$, where $x = -b\frac{\sum_i f_i M_i D_i}{\sum_i f_i M_i} + \frac{b^2}{2}\frac{\sum_i f_i M_i D_i^2}{\sum_i f_i M_i}$. Upon disregarding terms of third and fourth order in D_i one obtains

$$\ln\frac{I(b)}{I(b=0)} = -b\frac{\sum_i f_i M_i D_i}{\sum_i f_i M_i} + \frac{b^2}{2}\left[\frac{\sum_i f_i M_i D_i^2}{\sum_i f_i M_i} - \left(\frac{\sum_i f_i M_i D_i}{\sum_i f_i M_i}\right)^2\right] \tag{3.21}$$

or in terms of $\langle D\rangle_w$:

$$\ln\frac{I(b)}{I(b=0)} = -b\langle D\rangle_w + \frac{b^2}{2}\left[\left\langle D^2\right\rangle_w - \langle D\rangle_w^2\right] \tag{3.22}$$

To apply the Eq.3.22, it is necessary to use a specific diffusion distribution to explicit the $\left\langle D^2\right\rangle_w$. This point is developed in the next paragraph.

Case study of the log-normal distribution

A common distribution function used to describe the molar mass distribution is a log-normal distribution [61, 227]:

$$P(x) = \frac{1}{x\sigma\sqrt{2\pi}}\exp\left(-\frac{(\ln(x) - \ln(x_0))^2}{2\sigma^2}\right) \tag{3.23}$$

where x is a general variable, x_0 is a median value and σ is a measure of the width of distribution. In probability theory, a log-normal distribution is a continuous probability distribution of a variable whose logarithm is normally distributed. This means that the logarithm of x is normally distributed. Then we can write the momentum s of the distribution as:

$$E\left(x^S\right) = e^{S\mu + \frac{1}{2}S^2\sigma^2} \tag{3.24}$$

where $\mu = \ln x_0$ is the mean and σ is the deviation of the distribution. Because the following scaling law for the diffusion coefficient can be assumed (this statement is verified in the chapter 5) [233]:

$$D(M) \approx M^{-\nu} \tag{3.25}$$

The μ and σ^2 of Eq.3.24 can be written as:

$$\mu = \ln(M_0) \quad \text{and} \quad e^{\sigma^2} = \frac{M_w}{M_n} = Đ_M \tag{3.26}$$

If M_n and M_w, and $\langle D\rangle_w$ and $\langle D^2\rangle_w$, are express in integral form, we obtain:

$$M_n = \frac{\int MP(M)dM}{\int P(M)dM} \quad M_w = \frac{\int M^2P(M)dM}{\int MP(M)dM} \tag{3.27}$$

and using integral definition of $\langle D\rangle_w$ and $\langle D^2\rangle_w$:

$$\langle D\rangle_w = \frac{\int MP(M)D(M)dM}{\int MP(M)dM} \quad \langle D^2\rangle_w = \frac{\int MP(M)D^2(M)dM}{\int MP(M)dM}$$

Using Eq. 3.27 and 3.26 in Eq. 3.22, the final expression that we will use to fit data is obtained [155]:

$$\ln\frac{I(b)}{I(b=0)} = -b\langle D\rangle_w + \frac{b^2}{2}\langle D_w\rangle^2\left[\left(\frac{M_w}{M_n}\right)^{\nu^2} - 1\right] \tag{3.28}$$

To fit our experimental data the Eq. 3.28 is used. Where $I(b)$ and $I(b = 0)$ are the area of a resonance peak in the NMR spectra with and without gradient pulse; $\langle D\rangle_w$ and ν are free parameters of the fit; $\frac{M_w}{M_n}$ is the dispersity $Đ_\mathrm{M}$ fixed with the value found by SEC measurements (section 4.1.2).

Then, from the Eq.3.28, it could be possible to estimate the dispersity once known the parameter ν that correlates the diffusion coefficient with the molecular weigh, Eq.3.25. Using the value of ν obtained in section 5.3.1, the value of dispersity have been obtained and compared with those obtained using SEC measurements (section 4.1.2). The values found (1.60 ± 0.05, 1.70 ± 0.03, 1.65 ±0.04, and 2.00 ± 0.09 for the 2.1, 5.1, 8, and 15 kDa respectively) are in good agreement with the value found by the Sadron Institute for the same system, section 4.1.2 (1.54, 1.64, 1.78, 1.95). So this method, that has not been tested for other systems, could be an easy way to characterise also the dispersity once knew the conformational properties of the chain related to ν.

3.6.4 | Sequence parameters

The experiments of diffusion NMR were carried out on a Bruker Avance DRX 500 NMR spectrometer operating at 499.76 MHz for ^{1}H, with a maximal magnetic gradient field achievable

of 57×10^{-2} T m^{-1}. Data were recorded in 90% H_2O – 10% D_2O mixture (residual HOD, peak at 4.7 ppm) for locking purpose. The temperature was controlled by a Bruker BCU, and set to have a sample temperature of 298.0 K. ^{13}C and ^{23}Na experiments were also performed using the broadband channel of the BBO probe.

To obtain the diffusion coefficient, the pulse gradient duration δ was 5 ms, value at least 10 times shorter than the transverse relaxation time T_2 of the longest chain studied (see § 3.4.2). This condition is necessary to avoid a significant bias of the distribution due to of the relaxation of the magnetization during encoding and decoding periods. The diffusion delay Δ was 0.200 s. According to the results of § 3.4.2, we conclude that there are no significant effects arising from the T_1 weighting on the diffusion coefficient.

The field gradient amplitude g was varied with 16 increments, from 2 % to 80 % of the maximum field gradient amplitude. Sine-shaped gradient pulses were used as default (maximum effective gradient of 28×10^{-2} T m^{-1}). In order to assess the effect of the gradient amplitude and shape, also a smooth square-shaped gradient pulse has been tested (maximum effective gradient of 40×10^{-2} T m^{-1}). The variation of the average diffusion coefficients $\langle D \rangle$, obtained with the two gradient shapes, is below the uncertainty of measurement ($\simeq 2\%$). Increasing the effective gradient value leads to a better description of the diffusion coefficient dispersion, but the average diffusion coefficient value $\langle D \rangle$, is unaffected. For each sample four spectra were acquired, and to obtain each spectrum sixteen measurements were averaged. The number of scans chosen allow to respect the complete phase cycling of the pulse sequence in order to select only the meaningful coherences [200].

Summary of Chapter 3

This chapter is dedicated to the theoretical concepts of NMR.
Nuclear magnetic resonance (NMR) is the technique used to investigate the self-diffusion of polyelectrolytes, and to study the conformation of the chain. It monitors the Brownian displacement of specific molecules on 10-1000 ms timescale [35] (10-100 μm spatial scale), and it allows to obtain a diffusion coefficient between $10^{-14} - 10^{-9}$ m^2 s^{-1}.
The NMR signal is caused by the interaction of the magnetic momentum μ of the nucleus with the magnetic field B. The resonance frequency (chemical shift) of a nucleus in a molecule, is characteristic of the environment. The chemical shift makes NMR an attractive technique to characterise and distinguish a same atom in different groups, and to investigate the structural properties of a molecule.
The diffusion coefficient can be also measured using NMR, by using magnetic field gradients. Basically, a nucleus is labelled by a precession frequency according to its location and when the nucleus moves during the diffusion delay, the new position can be detected because of the attenuation of the signal. The Pulsed field gradient (PFG) sequence that we have used in our experiments is the bipolar pulse pair-longitudinal eddy current delay sequence (BPP-LED), with a solvent signal presaturation. This sequence reduces the strong water signal, and allows to explore a large time delay ($\sim$ 100 ms) by storing the the magnetization along the longitudinal axis of the magnetic field. Although, other sequences have been proposed in literature, this one is particular suitable for our dilute system.
To analyse the diffusion NMR data, a data analysis that considers the dispersity of the molecular mass of the diffuser has been developed. Indeed, a mono-exponential decay of the signal is correct only if the distribution of the displacements is Gaussian and if the sample is not polydisperse. The model proposed, calculated using a log-normal distribution of the molar mass, allows to estimate the mean diffusion coefficient and the dispersity of the system.

Chapter 4

Chemical and physical properties of the systems

Contents

In this chapter, the experimental systems used in this thesis are introduced and described, together with the techniques used to characterise them.

The experimental systems consist mainly of two objects: diffusers and obstacles both negatively charged at high pH. The diffusers are carboxylated molecules of various sizes, from simple carboxylates to short polyelectrolytes (sodium polyacrylate, PAANa). The study of the simple carboxylates has been suggested by the necessity to reduce the complexity of the diffusers, mostly to eliminate the intra-chains interactions which modify the dynamics. Furthermore, a simpler system is more suitable for comparison with simulations and with theoretical models. The obstacles are silica nanoparticles of different sizes and surface charges.

4.1 | Chemical systems

4.1.1 | Oligomers

Three carboxylates molecules have been used in this work, with the aim of comparing their diffusive behaviour with the one of the polyelectrolytes. The carboxylatic acid used in the present study are the propionic acid $C_2H_5(COOH)$ from Alfa Aesar; the glutaric acid $C_3H_6(COOH)_2$ from Alfa Aesar; and the 1,3,5-pentanetricarboxylic acid $C_5H_9(COOH)_3$ from TCI America. The chemical structures are represented in Fig. 4.1. These oligomers, that will be called hereafter C1, C2, and C3 or PA, GA, PCA, can be considered respectively as the monomer (M_w = 74 Da), the dimer (M_w = 132 Da), and the trimer (M_w = 204 Da) of the polyacrylic acid.

4.1.2 | Polyelectrolytes

The polyelectrolyte used is work is the sodium polyacrylate (PAANa) and its conjugate acid the polyacrylic acid (PAA) [234]. It is a weak polyelectrolyte, which has a specific interest since it is widely used in household and industry products as a scale inhibitor or thickening agent [8, 12, 13, 15, 16]. In addition, the PAA can be seen as a model for natural organic polyacids which are at play in various environmental processes, such as the facilitated transport of heavy metal or radionuclide ions [17, 18].

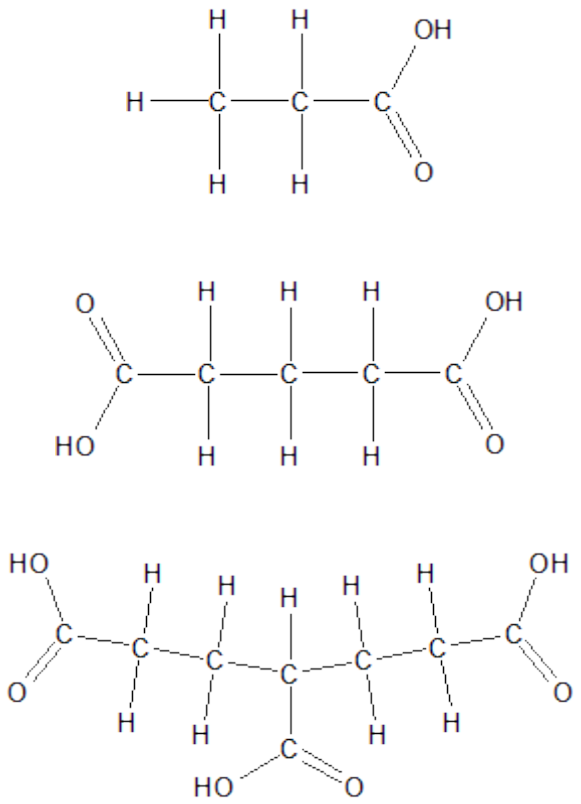

Figure 4.1: From the top: chemical structure of the propionic acid, glutaric acid, and 1,3,5-pentanetricarboxylic acid.

PAANa $[\text{-}C_2H_3(COONa)\text{-}]_n$ of different molecular weights (M = 2.1, 5.1, 8 and 15 kDa), purchased from Sigma-Aldrich, are used in this thesis. The chemical structure of the PAA is represented in Fig. 4.2.

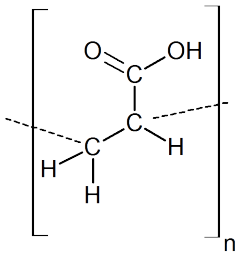

Figure 4.2: Chemical structure of the PAA.

Structural characterisation

In the following, the PAANa with a specific molecular weight, will be labelled with M i.e. the approximate weight averaged molecular weight given by the provider. A more precise

characterization of the molecular weight have been performed using size exclusion chromatography (SEC) by the Institute Charles Sadron (Strasbourg - France). The measurements have been carried out in an aqueous solution of sodium nitrate (0.1 mol L^{-1}), to minimise ionic effects, with an Ultimate 3000 RSLC system. Shodex OH-pak 30 cm columns have been used (802.5HQ, 804HQ,806HQ and 807HQ) in series. Molar masses determined with SEC do not come from a calibration with standard sample but from absolute measurements with Multi-Angle Light Scattering (MALS) coupled with the SEC, since the optical refraction index increment of PAANa is known [12].

The values of the weight-average molecular weight M_w, and the number-average molecular weight M_n thus obtained are reported in table 4.1, together with other specific quantities of the systems. From the ratio between M_w and M_n the dispersity $Đ_M$ of the sample is obtained Eq. 1.11.

Another important quantity to evaluate the size of the chain is the weight averaged degree of polymerization N_w. It is obtained from the molecular mass of polymer and of the monomer M_m (94 g mol^{-1}) [75, 235] $N_w = M_w/M_m$. R_h is the hydrodynamic radius obtained from NMR measurements at pH $\sim$ 8, using Stokes-Einstein equation, Eq. 1.36, whith the solvent viscosity at 298 K (10 % D_2O and 90 % H_2O, 930 μPa s) [236], as also calculated by [237]. The maximum end-to-end distance ℓ_{max} is calculated from monomers' number N_w and length a, $l_{max}= N_w\ a$. The value of a was obtained by SAXS experiments (a = 0.252 nm) [75, 235].

The PAANa solutions were prepared at weight fraction of $\sim$ 1% in MilliQ water, in a range of concentrations studied below the estimated $c^\star$.

Evaluation of the critical concentration

To estimate $c^\star$, as described in Eq.1.14, the hydrodynamic radius R_h has been used. $c^\star$ can also be evaluated using M_n instead of M_w in Eq. 1.14, to have a more conservative estimate, and the concentrations used are still lower than that estimated. Viscosity measurements have been performed on the smallest (2.1 kDa) and largest (15 kDa) polyelectrolytes. Using the inverse of the intrinsic viscosity $[\eta]^{-1}$ to estimate $c^\star$, as suggested for example by Litmanovich et al. [238], we get respectively 220 kg m^{-3} and 40 kg m^{-3} still above of the range of concentration used.

This has been confirmed by the linear dependence of the self-diffusion coefficient on the concentration (cf Fig. 5.12). Indeed, when $c > c^\star$, the expected concentration dependence is a power law [239]. We will see later on, that in the regime of concentration studied the effect of inter-chain interactions is weak compared to the intra-chain interactions, and thus that the modification of the diffusion coefficient of the chain without obstacles can as a consequence be ascribed to the changes of conformation. All the quantities here described are reported in the table 4.1.

M (kDa)	M_w (kDa)	M_n (kDa)	N_w	R_h (nm)	ℓ_{max} (nm)	$c^\star$ (kg m^{-3})	$Đ_\mathrm{M}$
2.1	2.7	1.8	22	1.2	6	324	1.54
5.1	5.8	3.5	54	1.7	14	245	1.64
8	8	4.5	85	2.2	21	156	1.78
15	13.7	7.1	160	2.6	40	162	1.95

Table 4.1: Structural features of PAANa with different molecular mass M (label value from the provider). M_w is the weight-average molecular weight, M_n is the number-average molecular weight, N_w is the weight averaged degree of polymerization, R_h is the hydrodynamic radius obtained from NMR measurements at pH $\sim$ 8, ℓ_{max} is the max end-to-end distance obtained from monomers' number and length, and $c^\star$ is the overlap concentration obtained from Eq. 1.14. $Đ_\mathrm{M}$ is the dispersity as defined in Eq. 1.11.

4.1.3 | Nanoparticles

The nanoparticles used in this work as obstacles are silica nanoparticles of different size and surface charge: Ludox LS colloidal silica (30 wt %) suspension in H_2O and Ludox TM colloidal silica (40 wt %) suspension in H_2O provided by Sigma-Aldrich.

Before characterising and using the nanoparticles, it has been necessary to purify them and to decrease the amount of salt initially present in the commercial dispersions. The silica nanoparticles dispersions have then been purified with a dialysis process: 20 mL of the commercial suspension was loaded in a Spectra/Por molecular porous membrane tubing (molecular weight cut-off: 6000 – 8000 Da, pore size $\simeq$ 2 nm). The filled membrane was placed in solutions of 200 mL of water solution with a weight fraction of 2 % of Poly(ethylene glycol) (PEG) and 1 mM NaCl. In this process, the particles are confined in the dialysis tubing while water and ions can cross the membrane. As a result, the salt concentration of the dispersion decreases. However, to prevent the water ingress in the membrane, the osmotic pressure (or the chemical potential of water) is equilibrated with the PEG. Changing the concentration of PEG makes it

possible to modify the concentration of silica nanoparticles. The evolution of the purification process of silica suspensions has been monitored by measurements of the electrical conductivity of the external bath during 5 days.

The conductivity experiments were performed with a Quadtech 7600 Plus Precision LCR Meter. From the molar conductivity of sodium chloride $\Lambda_{NaCl} = 126.39 \times 10^{-4}$ m^2 S mol^{-1}, the concentration of ions in the external bath is estimated and reported Fig. 4.3.

The fluctuations observed in the signal are caused by natural daily temperature change of the experimental setup. As seen in Fig. 4.3, at least than 3 days are needed to achieve a stationary concentration of ions in the external bath. When the stationary state is reached, the conductivity gives the ionic concentration in equilibrium with the suspension of silica particles. With the hypothesis that mainly sodium and chloride ions contributes to the conductivity, the concentration of ions at equilibrium is found to be 7.6×10^{-3} mol L^{-1}.

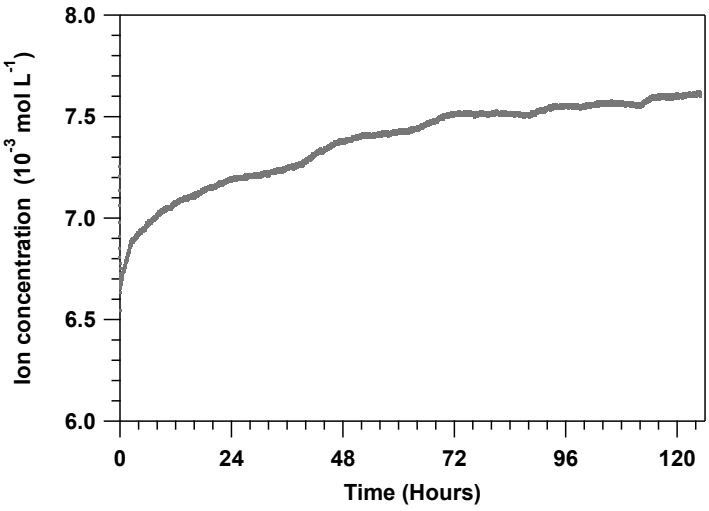

Figure 4.3: Ionic concentration (mol L^{-1}) versus time of the external bath of the dialysis setup at room temperature.

The same procedure was followed for the silica TM and a similar equilibrium concentration of ions was found (8×10^{-3} mol L^{-1}).

4.2 | Physical properties of the experimental systems

In this section, preliminary characterisations of the experimental systems, together with a brief overview of basic principles of methods used are desribed.

4.2.1 | Size characterisation: light scattering

Static light scattering (SLS) and dynamical light scattering (DLS) are useful experimental tools used for the characterization of macromolecules in solution [240, 241]. From a thermodynamic point of view, the light scattering can be seen as the coupling of the incident light field to the spontaneous concentration fluctuations that exist in solution [242]. These techniques have been used here, to determine the size of the macromolecules and to verify the stability of the system of obstacles [242].

SLS and DLS experiments, were performed with a Zetasizer NanoZS instrument, (Malvern). The digital correlator allows to simultaneously measure static and dynamic light scattering. Measurements were carried out at 173°. A HeNe gas laser with a wavelength of 633 nm was the light source. Polystyrene cuvettes (filled to a depth of between 10 mm to 15 mm and minimum sample volume of 1 mL) have been used. Measurements were performed at 25 °C. For comparison the DLS measurements have also been made with Vasco nanoparticle size analyzer (Cordouan Technologies) at an angle of 135°. This instrument uses a laser diode at 658 nm.

Static light scattering measurements were attempted on polyelectrolytes. If a correct order of magnitude for the size was obtained, the very low signal due to the small size of scatterers prevented us to get quantitative results. This results are presented in the Appendix A.

Dynamical light scattering

The light scattering is used to determine the diffusion coefficient of the particles by the analysis of the temporal fluctuations of scattered light. The time-dependent fluctuations of the scattered light intensity arise from Brownian motion of the dispersed particles [4, 241]. The rate of the intensity fluctuation is measured by a digital correlator, which basically measures

the correlation function $\langle I(\tau)I(0)\rangle$. The rate of decay for the correlation function is related to the diffusion coefficient of the scatterer. The faster the diffusion, the faster the decay of the correlation. For large correlation times, the position of the particles is totally uncorrelated: the final plateau is equal to the square of the average intensity $\langle I\rangle^2$. At short correlation times, the particles' positions is fully correlated: the correlation value is equal to the average of the square intensity $\langle I^2\rangle$.

Mathematically, the correlation function is related to dynamic structure factor, $S(q,\tau)$ of the particle studied. In the simplest case, monodisperse particles without interactions, the dynamical structure factor is related to the diffusion coefficient of the particles:

$$S(q,\tau) = S(q)e^{-Dq^2\tau} = S(q)e^{-\Gamma\tau} \tag{4.1}$$

where q is the scattering vector equal to $4\pi n_s/\lambda_0 \sin\frac{\theta}{2}$ (n_s solvent refraction index and θ angle of measurement), τ is the relaxation time, and $\Gamma = Dq^2$.

In real samples, there often exists a size distribution of the particles and hence there is a distribution of times of relaxation, $F(\Gamma)$. The dynamical structure factor can be written with the following expression:

$$S(q,\tau) \propto \int_0^\infty F(\Gamma)e^{-\Gamma\tau}d\Gamma \tag{4.2}$$

$S(q,\tau)$ is then formally the Laplace transform of the distribution $F(\Gamma)$. One simple way to obtain the diffusion coefficient value is the cumulant analysis, i.e. log of $S(q,\tau)$ is developed as power series of τ.

$$\ln S(q,\tau) \approx 1 - k_1\tau + k_2\frac{\tau^2}{2!} + \cdots \tag{4.3}$$

where the k_i are called cumulants. For a monodisperse case, $k_1 = \Gamma = Dq^2$. For a polydisperse system, $k_1 = \langle\Gamma\rangle$, and $k_2 = \langle\Gamma^2\rangle - \langle\Gamma^2\rangle^2$ is the variance of the distribution.

The diffusion coefficient distribution can also be recovered with an inversion of equation 4.2. Several numerical solutions of this ill-conditioned problem exists and are implemented in the DLS software. When the suspensions investigated are dilute enough, so that no significant interaction exists between the scattering particles, an hydrodynamic radius can be determined

from the diffusion coefficient by the use of Stokes's law:

$$R_{\mathrm{h}} = \frac{k_B T}{6\pi\eta D} \tag{4.4}$$

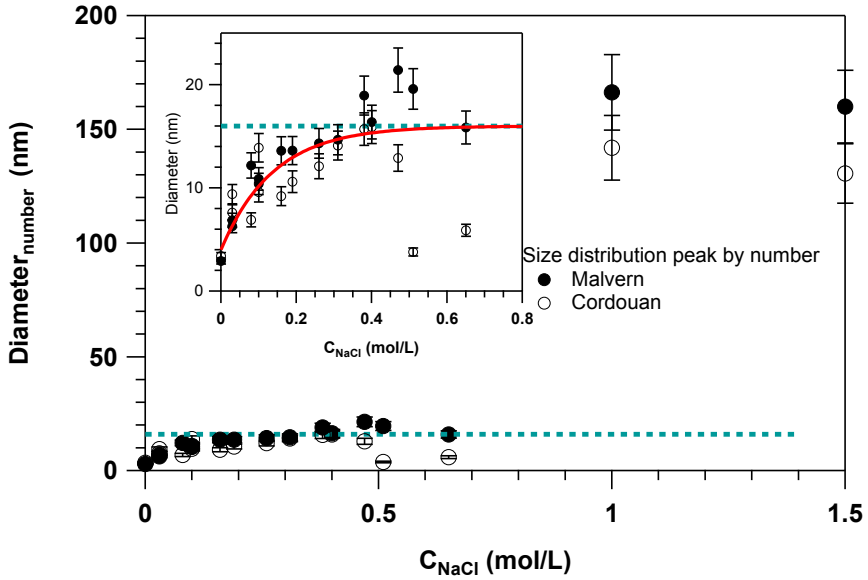

Figure 4.4: Diameter of Ludox LS colloidal silica in H_2O suspension at the volume fraction of 3%, as a function of the molarity of NaCl. T=298 K and a pH~ 9. Data obtained with the Zetasizer NanoZS instrument, Malvern (black points), and with the Vasco gamma (empty black points). The diameter given by the furnisher is shown (blue dotted line). The sub-window is a zoom in the smaller concentration regime.

Silica nanoparticles The size of the nanoparticles has been checked by DLS, as a function of the salt concentration. The data, obtained with two DLS instruments (Zetasizer NanoZS from Malvern and Vasco from Cordouan-Tech.) at pH ~ 9 and T = 298 K, are reported in Fig. 4.4 where the number averaged diameters are plotted. This distribution has been chosen because it is the less sensitive to the presence of few high molecular mass impurities. Furthermore, in the present case, the results obtained by the number distribution are very close to those of the volume distribution.

The data obtained with the two instruments are consistent. In Fig.4.4, the diameter is shown to increase slowly with the increase of salt until a concentration of 0.4 mol L^{-1} of added NaCl. The salt reduces the electrostatic repulsion between the particles and the hydrodynamic diameter can determined as the plateau value, d = 16 nm. For higher salt concentration, above 1 mol L^{-1} in the present case, an abrupt increase of the order of ten times of the plateau value is observed, the particles are aggregating.

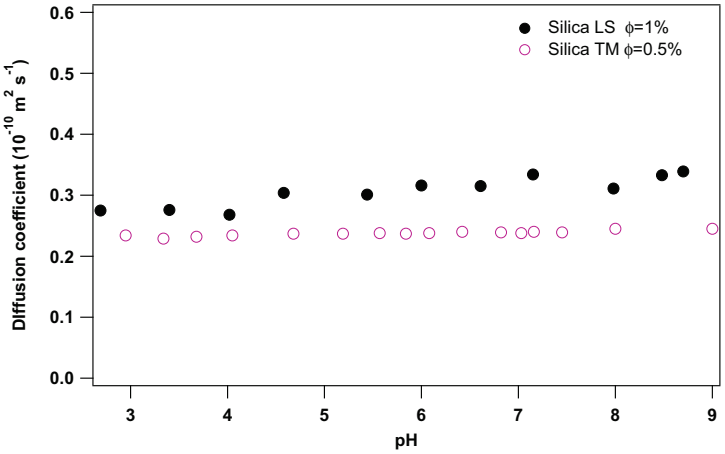

Figure 4.5: Diffusion coefficient of the silica nanoparticles as a function of the pH, measured by DLS using the Zetasizer NanoZS. Silica ludox LS a $\phi = 1\%$ (black points), and silica Ludox TM $\phi = 1\%$ (purple circles). T=298 K.

The same analysis was performed for the silica TM particles and a diameter of 28 nm was determined.

Before choosing the experimental conditions for the diffusion experiments, it is necessary to know the behaviour of the silica particles in that conditions. In Fig. 4.5, the diffusion coefficient of the silica particles LS and TM is reported as a function of the pH. The value of the diffusion coefficient does not change notably with the pH, so the formation of aggregate of the nanoparticle in the range of pH explored is excluded. This observation is made for relatively fresh suspensions, as we will show in chapter 7 that on the long run aggregates form in acidic conditions. The data shown are related to the nanoparticles with a volume fraction around 1%, but the same results have been found for a volume fraction ten times higher. So in the whole range of nanoparticles studied and in all pH conditions no aggregation is observed.

4.2.2 | Charge characterizations

Potentiometric titration

The potentiometric titration has been used to characterise the ionization behaviour of polyelectrolytes and nanoparticles [4]. In particular to determine the protonation state, the surface charge density, and to assess the charge properties of the polyelectrolyte with the pH.

The dissociation constant K_a of a weak acid HA can be described according to the law of mass action as:

$$K_a = \frac{[\mathrm{H^+}]\,[\mathrm{A^-}]}{[\mathrm{HA}]} \tag{4.5}$$

or introducing pK_a and pH:

$$\mathrm{p}K_a = \mathrm{pH} - \log \frac{[\mathrm{A^-}]}{[\mathrm{HA}]} \tag{4.6}$$

The previous equation is the Henderson− Hasselbalch equation, where $[A^-]$ is related to the fraction of deprotonated sites β, and [HA] to $1-\beta$. The Eq. 4.6 can be rewritten as:

$$\mathrm{p}K_a = \mathrm{pH} + \log \frac{\beta}{1-\beta} \tag{4.7}$$

Experimental details The titration measurements were performed with the titrator DT1200 from Dispersion Technology at room temperature. The proportion of ionised sites, or the deprotonation degree β, is calculated with the following procedure. First, the fraction of protons bound to the polymeric chain or the particle is obtained from the difference between added protons (amount of reagent) and measured protons (value of pH). From the plateau at high pH, the maximum number of (de)protonable sites is obtained. Finally, the deprotonation degree is computed by dividing the number of deprotonated sites by the plateau value. At low and high pH values, due to instrumental limitations, significant deviations appear. As a result, the chain is considered fully protonated at pH=3 ($\beta = 0$) and fully deprotonated ($\beta = 1$) at pH=9, as found in the literature [27].

Polyelectrolytes Since PAA is weak polyelectrolytes, the number of charged sites along the chain varies as a function of the pH of the solution. It is thus important to determine the ionisation degree as a function of pH.

The samples of polyelectrolytes were prepared at ~ 1 *wt%* and diluted 10 times using MilliQ water, the final molarity of the polyelectrolyte units was around 0.01 mol L^{-1}. The initial pH of this system is ~ 9. The titrant was HCl (0.1000 ± 0.0002 mol L^{-1}, Carl-Roth). Small doses (down to 3 μL) of titrant were added, followed by delays of 20-120 s for stabilisation of pH.

In Fig. 4.6, the ionisation of PAA for 4 different molecular weights M_w is shown. The curves show a sigmoidal increase of the fraction of deprotonated sites β with pH, in agreement with lit-

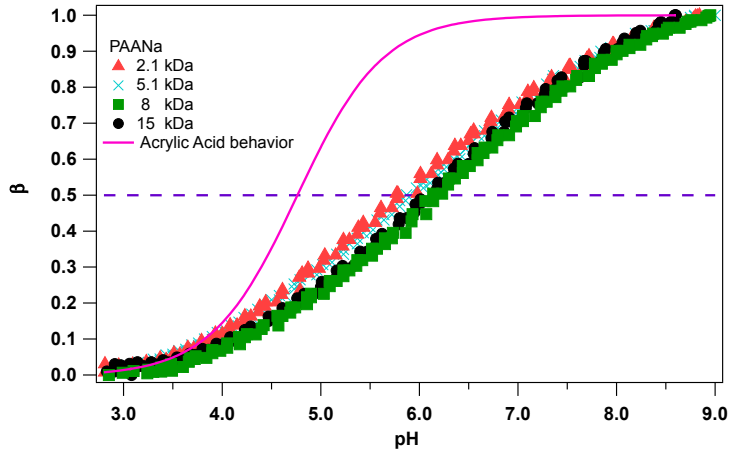

Figure 4.6: Fraction of deprotonated sites β as a function of pH. Titration for different molecular size PAANa: 2.1 kDa (red triangle), 5.1 kDa (blue cross), 8 kDa (green square), 15 kDa (black circle). The behaviour of the monomeric acid, the acrylic acid, is also shown (pink line). The dashed violet line marks $\beta = 0.5$. $T = 298$ K.

erature data [27, 243]. However, the protonation of polyelectrolytes is strongly influenced by the state of charge of nearby sites and the Henderson-Hasselbalch equation (Eq.4.7) [244, 245], has to be corrected in order to describe properly the protonation behaviour for polyelectrolytes [246]. The variation of deprotonated sites β with the pH then deviates from the Henderson-Hasselbalch curve. Several models have been developed to describe this deviation: the smeared out charge model [246], the Poisson-Bolztmann description [243], the "neighbour effect" model [247], or Monte-Carlo simulations either with implicit or explicit counterions [248–250].

An intermediate approach is to use the smeared-out charge model [246], where a mean contribution of the electrostatic effect is included in a modified Henderson-Hasselbalch equation by the term $\epsilon\beta$, where ϵ is an average interaction parameter:

$$\mathrm{pH} = \mathrm{p}K - \epsilon\beta + \log\frac{\beta}{1-\beta} \tag{4.8}$$

Other descriptions might include either higher order terms in β [73] or fractional power [251]. In the model proposed in Eq.4.8, the same ionisation values should be found, regardless of the length of the chain at low ionisation state, which is not what is observed experimentally in the present case. In this low pH region, the difference might then be explained by non-electrostatic interactions such as H-bonds or van der Waals interactions.

The simpler approach used here is to consider the pH value for which half of the ionised sites ($\beta = 0.5$) as an estimate of an effective pK, noted as pK_β.

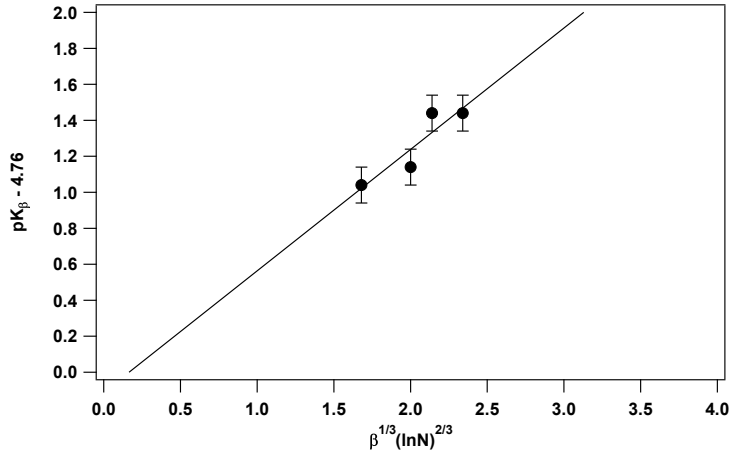

Figure 4.7: Difference between the experimental pK_β of the PAANa 2.1, 5.1, 8 and 15 kDa (N=22, 55, 85, 160 respectively) from the degree of ionization β, and the pK of the propionic acid (N=1). The black line indicates the deviation computed from Ullner's scaling law (Eq. 4.9) [249, 250].

The effect of the chain length is clearly noticeable in Fig. 4.6. The effective pK_β increases with the size of polyelectrolytes (pK_β = 5.8 ± 0.1, 5.9 ± 0.1 , 6.2 ± 0.1, and 6.2 ± 0.1 for the 2.1, 5.1, 8, and 15 kDa PAANa respectively). This effect is related to the difficulty to ionise high molecular weight polyelectrolytes, because of the increase of the electrostatic potential with M_w [27, 248]. These values are slightly lower than values of pK_β found by Laguecir et al. [27], certainly due to the difference in concentration and salinity between the samples. Ullner et al. [249, 250] have studied the phenomenon using Monte-Carlo simulations and a scaling approach, they have suggested the following law for the deviation from the non-charged pK=4.76:

$$\Delta \mathrm{p}K \sim \beta^{\frac{1}{3}} (\ln N)^{\frac{2}{3}} \tag{4.9}$$

where ΔpK is equal to pK_β - pK_a.

The deviations of pK_β values from the non-charged pK_a (4.76 [249, 250]), the pK value of the acrylic acid, and the Eq. 4.9 are reported in Fig. 4.7. A rather fair agreement between the data and Ullner's relation is shown.

When the polyelectrolyte is diluted in water solution at 1 *wt%*, the pH of the solution is around 8, and according to Fig. 4.6, the fraction of the sites deprotonated β is around 90%, for all sizes studied. Among the deprotonated sites, not all of them are charged due to the condensation of sodium counterions. To assess the extent of this phenomenon, the following reasoning may be considered. The distance between neighbouring monomers is a = 0.252 nm [75, 235], far

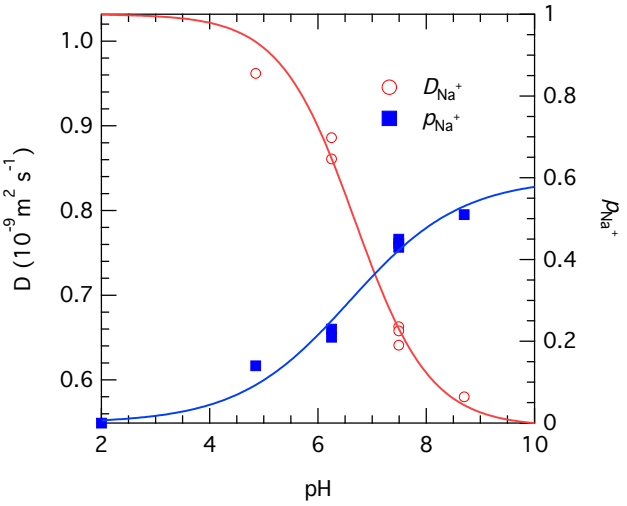

Figure 4.8: Sodium diffusion coefficient determined by ^{23}Na NMR and the calculated condensation ratio p_{Na^+}. PAANa 5.1 kDa at 1 *wt%*. $T = 298$ K.

below the Bjerrum length, $\ell_B = 0.71$ nm at 298 K. ℓ_B is the distance at which the electrostatic interaction between two elementary charges is equal to the thermal energy (Eq. 1.28). When the distance between two charges is lower than the ℓ_B, the electrostatic interactions are predominant. When the Manning parameter ξ, that compares the two lengths [252] (Eq.1.30), is > 1, Coulomb interaction dominates over the thermal energy and the counterion condensation occurs, in our case $\xi = \ell_B/a = 2.84$. The value of $\xi \simeq 3$ shows that the length of three repeating units is close to the Bjerrum length, and suggests then that 2/3 of the sites are compensated by the condensation of a sodium counterions when the chain is completely deprotonated.

A more quantitative estimate of the condensed sodium ions can be obtained by measuring their diffusion coefficient D_{Na^+}. Using the free ion diffusion coefficient $D^\circ_{Na^+}$ and the diffusion coefficient of the polyelectrolyte D_p, the condensation ratio p_{Na^+} of the sodium can be estimated as:

$$p_{Na^+} = \frac{D^\circ_{Na^+} - D_{Na^+}}{D^\circ_{Na^+} - D_p} \tag{4.10}$$

The ^{23}Na NMR diffusion measurements were performed on the 5.1 kDa sample varying pH and the results are reported in Fig. 4.8.

For a salt free solution of PAANa at pH 8, p_{Na^+} is close to 0.5 and there is 10 % of protonated carboxylic sites and 90% of deprotonated sites (Fig. 4.6). The charge of the deprotonated sites is compensated by the sodium ions either free or condensed (the concentrations of hydroxide

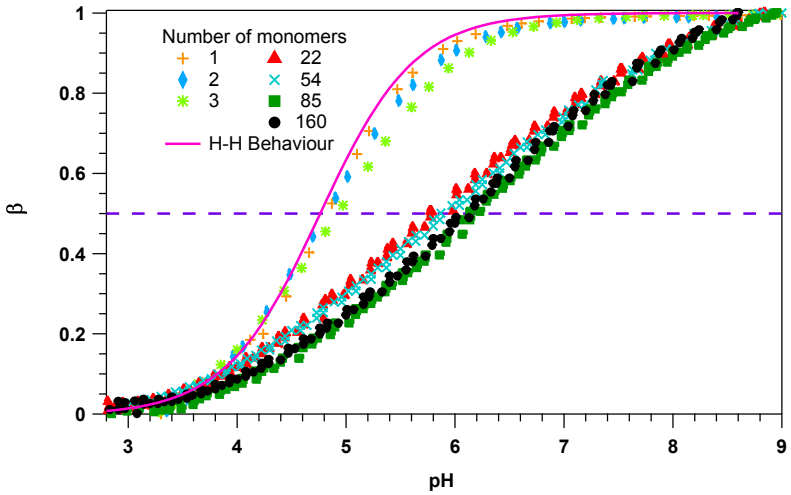

Figure 4.9: Fraction of deprotonated sites β as a function of pH for carboxylated molecules of various number of monomers: propionic acid (N=1, orange vertical-cross); glutaric acid (N=2, blue rhombus); 1,3,5-pentanetricarboxylic acid (N=3, green multi-cross); PAANa 2.1 kDa (N=22, red triangle); PAANa 5.1 kDa (N= 54, light blue cross); PAANa 8 kDa (N=85, green square); PAANa 15 kDa (N=160, black points). The dashed violet line marks β = 0.5. H-H is the Henderson-Hasselbalch behaviour. T = 298 K.

and hydrogen ions are negligible). As a result, 45% of deprotonated sites are free charged carboxylate groups, while the remaining 55% have a condensed sodium ion. This result is in agreement with previous conductimetric study of the same samples [17].

Oligomers The same titration experiments were performed for the oligomers. Because their simple structure, we expect that, instead of the longer polyelectrolytes, the fraction of deprotonated sites follows the Henderson-Hasselbalch behaviour. By the comparison with the behaviour of the PAA, it is possible to point out the effect of the length of chain.

The results of the titration of these three carboxylates are reported in Fig. 4.9 together with those obtained for the PAA. The oligomers, as the polyelectrolytes, shown a sigmoidal increase of the fraction of deprotonated sites β with pH. However for the oligomers the deprotonation process is steeper than for the polyelectrolytes, as a lower pK_β proves (p$K_\beta \approx 4.9$). There are fewer charged nearby sites that influence the protonation of oligomers and as a result in Fig. 4.9, the sigmoidal shape of the titration curve follows the classical Henderson-Hasselbalch behaviour.

In Table 4.2, the values of the pK_β obtained for all carboxylate molecules studied are shown.

N	1	2	3	22	54	85	160
pK_β	4.9 ± 0.1	4.9 ± 0.1	4.9 ± 0.1	5.8 ± 0.1	5.9 ± 0.1	6.2 ± 0.1	6.2 ± 0.1

Table 4.2: pK_β related to β=0.5 in Fig. 4.9, for the carboxylated molecules with different number of monomers N.

Silica Thanks to the potentiometric titration experiments, the surface charge of the silica particles and its variation with the pH of the solution is studied. The titration measurements have been performed using HCl solutions as titrant (0.100 mol L^{-1}). From the value of the specific surface area given by the manufacturer (~215 m^2 g^{-1}), the amount of titratable charge can be converted into the surface charge density of silica as a function of the pH (Fig.4.10).

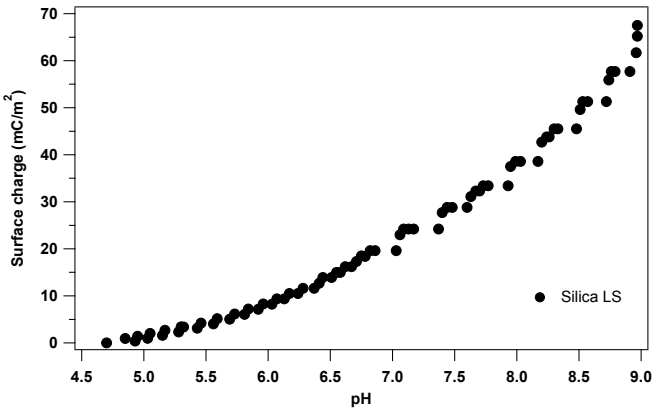

Figure 4.10: Surface charge of the Silica LS at 0.1 % ϕ as a function of the pH. T = 298 K.

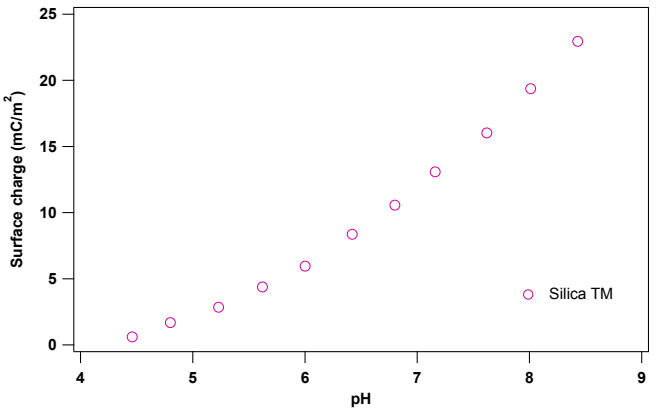

Figure 4.11: Surface charge of the Silica TM at 3 % ϕ as a function of the pH. T = 298 K.

The same analysis has been performed for the Silica TM at ϕ = 3 %. The surface charge of this particle as a function of the pH is shown in Fig. 4.11, the surface area used is 140 m^2 g^{-1} as given by the manufacturer.

To sum up for the two nanoparticles the surface charge varies with the same behaviour as function of pH.

Respectively at pH 8.5, for the Silica LS the surface charge is 70 mC/m^2 and for the Silica TM the surface charge is 25 mC/m^2. These results are summarised in Table 4.3. This variation of the surface charge density with the particle radius is established for silica nanoparticles. Recently, is has been attributed to the change in the surface concentration of H^+ ions [253].

Silica	LS	TM
diameter (nm)	16	28
surface charge density (mC m^{-2})	70	25

Table 4.3: Diameter of the silica nanoparticles, and surface charge at pH 8.5 provided by Sigma-Aldrich: Ludox LS and Ludox TM.

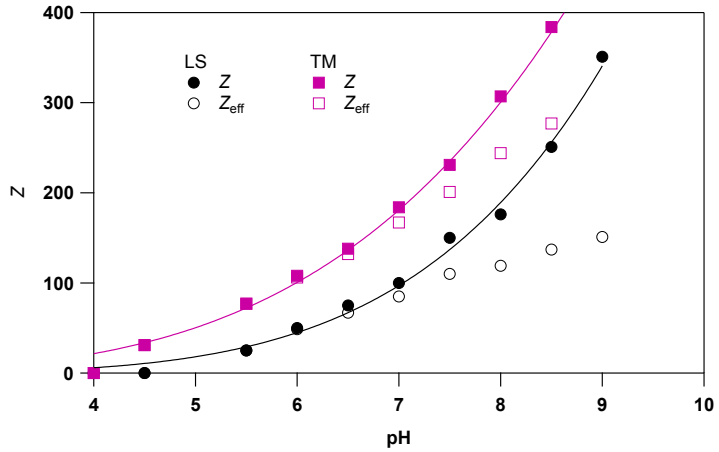

Figure 4.12: Charge of the Silica LS (black symbols) and TM (purple symbols) as a function of the pH, and effective charge (empty symbols) calculated using the long-range behaviour of the Poisson-Boltzmann equation (section 1.2.1).

Finally, from the surface charge density of the nanoparticles both the structural charge and the effective charge can be computed. The effective charge, defined as the value of the charge so that the Poisson-Boltzmann electrostatic potential can be approximated by its linearised form was computed as described in section 1.2.1. The results have been plotted in Fig. 4.12. As expected for low surface charges, the effective charge coincides with the value of the structural charges since the Poisson-Boltzmann equation can be linearised. However, at high pH values, when the particles are highly charged the deviation is substantial. In addition, even if the surface charge density measured is higher for the smaller particle both the structural and effective charge

are higher for the largest particles. Stronger electrostatic interactions are then expected to occur for the larger TM particles than for the smaller LS ones.

Electrokinetic potential ζ

The electrokinetic potential ζ is the electrostatic potential where the slip between a solid particle with respect to bulk solution is postulated to occur [56]. ζ is a then a physical property related to the intensity of the electrostatic potential close to the surface of the particle and is then used as an indicator of colloidal stability of charge stabilised systems [41, 56, 254].

The eletrokinetic potential cannot be determined directly but, it can be calculated from measurable quantities such as the eletrophoretic mobility. This calculation is straightforward only for large objects compared to the Debye lenght κ^{-1}(Eq. 1.5), and small value of the potential, ie corresponding to values for which the Poisson-Boltzmann equation can be linearised. In the latter case, a simple expression of ζ with the velocity of a moving particle v in a electric field E and the properties of the medium (dielectric constant ε_r and viscosity η) can be found :

$$\zeta = \frac{\eta}{\varepsilon_0 \varepsilon_r} \frac{v}{E} \tag{4.11}$$

In general, no such expression can be found and several theories can be used to derive the value of ζ from the measured electrophoretic velocity v/E [56, 255, 256]. Finally, the relationship between the eletrokinetic potential and the exact potential close to surface of the particle is another difficult issue to consider [257].

In what follows, we will consequently only use ζ evaluated by equation 4.11 as a semi-quantitative indicator of the state of charge of the nanoparticles.

Experimental details The electrophoretic mobility is measured using a capillary cell equipped with a pair of electrodes in a Malvern Zetasizer NanoZS instrument . As the charged objects move in the electric field E, their velocity is measured via a laser Doppler measurement. The value of the eletrokinetic potential ζ is then computed from the velocity using equation 4.11 and the dielectric constant and viscosity of water.

Nanoparticles To verify the stability of the nanoparticle suspensions, the zeta potential of silica nanoparticles as a function of the pH has been measured. As shown in the Fig. 4.13,

the zeta potential of silica LS and TM present the highest absolute value in basic conditions. This confirms the higher stability in basic conditions as expected from the charge determined by acid-base titrations (Fig. 4.10 and 4.11). Since the surface charge changes, due to the protonation of SiO^- groups to Si-OH from basic to acidic pH, the zeta potential varies from a high negative value to zero in acidic conditions.

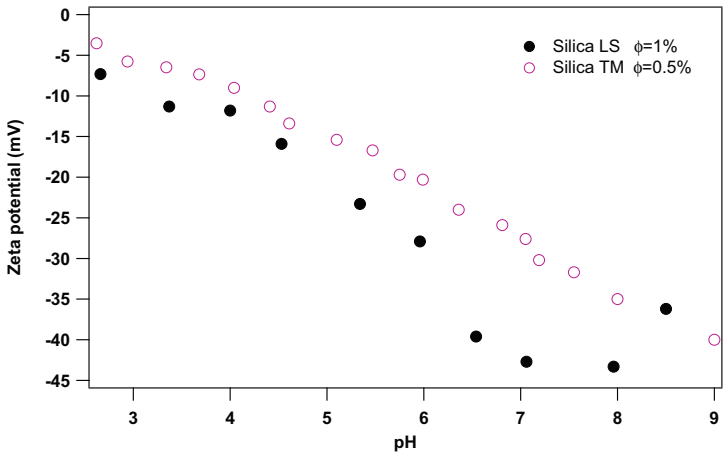

Figure 4.13: Zeta potential of the nanoparticles as a function of the pH, measured by Malvern Zetasizer Nano ZS. Silica ludox LS a $\phi = 1\%$ (black points), silica Ludox TM $\phi = 1\%$ (purple circle). T=298 K.

Summary of Chapter 4

The experimental systems consist mainly of two objects: diffusers and obstacles both negatively charged at high pH. The diffusers are carboxylate molecules of various sizes, from simple carboxylate to short polyelectrolytes (sodium polyacrylate, PAANa). The study of the simple carboxylates has been suggested by the necessity to reduce the complexity of the diffusers, and to have a system more suitable for comparison with simulation and theoretical models. The obstacles are silica nanoparticles of different sizes and surface charges.
The carboxylic acids used are the propionic acid $C_2H_5(COOH)$; the glutaric acid $C_3H_6(COOH)_2$; and the 1,3,5-pentanetricarboxylic acid $C_5H_9(COOH)_3$. These oligomers, can be considered as the monomer, the dimer, and the trimer of the polyelectrolytes studied. The polyelectrolytes used is the sodium polyacrylate (PAANa) $[\text{-}C_2H_3(COONa)\text{-}]_n$ of different molecular weights (M = 2.1, 5.1, 8 and 15 kDa), with a number of monomers from 22 to 160, and dispersity arising from 1.54 to 1.95. The nanoparticles used are silica particle with a diameter of 16 (LS) and 28 nm (TM). The dispersion of particle is stable up to NaCl concentration of 0.6 $molL^{-1}$, after the silica particles aggregate.
The fraction of deprotonated sites β of the PAANa, determined by potentiometric titrations, increases with a sigmoidal behaviour with pH, and it is strongly influenced by the state of charge of nearby sites, contrarily to the oligomers. The apparent pK obtained for these measurements increases with the size of the chain, because the difficulty to ionise high molecular weight polyelectrolytes, due to the effect of the electrostatic potential.
The surface charge of both particles increases with pH. From the surface charge density of the nanoparticle, structural and effective charges have been computed. At low pH, the effective charge coincides with the value of the structural charge. However, at high pH values, when the particles are highly charged the deviation is substantial. In addition, even if the surface charge density measured is higher for the smaller particle both the structural and effective charge are higher for the larger particles. Stronger electrostatic interactions are then expected to occur for the larger TM particles than for the smaller LS ones.

Chapter 5

Small polyelectrolytes in dilute regime

Contents

5.1 | Introduction

In this chapter, thanks to ^{1}H NMR, we will study the structural changes of polyelectrolytes via the chemical shift δ, and the variation of their dynamics by the study of the diffusion coefficient. The spectra of oligomers and polyelectrolytes are shown, explained with respect to their structure, and studied in function of their concentration, and the variation of the electrostatic interactions, by adding salt and by variation of the pH. The effect of molecular weight, concentration and interactions on the dynamics of polyelectrolytes are also investigated. We will point out also the impact of the chain length on the properties of short weak polyelectrolytes.

5.2 | Analysis of ^{1}H spectra

The spectra of the propionate at pH = 7.6, the glutarate at pH = 7.0, and the 1,3,5-pentanetricarboxylate at pH = 6.6 at $T = 298$ K are displayed in Fig. 5.1, together with the drawings of the molecular structures of the oligomers.

In the propionate spectrum, the peak centred at 2.09 ppm is related to the CH_2 group, and the peak at 0.97 ppm is associated with the CH_3 group. The area ratio of these peaks is equal to the ratio of the number of hydrogens of the associated groups. In the glutarate and 1,3,5-pentanetricarboxylate spectrum, the peaks centred at 2.13 ppm and 2.07 ppm respectively, are related to the proton of the CH_2 in the α position respect to the carboxylic acid. The second peak observed, centred respectively at 1.70 and 1.60 ppm for the two oligomers, is related to the CH_2 in β position, as the lower intensity confirms. The J-couplings patterns confirm the molecular structure reported in the graph.

The ^{1}H NMR (H_2O with 10% v/v D_2O, 500 MHz) spectra of PAANa 2.1, 5.1, 8 and 15 kDa at 1 *wt%* are shown in Fig. 5.2. In the studied PAANa, the hydrogens of two different groups have been identified. This assignment has been confirmed by DEPT-135 and ^{13}C-^{1}H HSQC experiments where the number of hydrogens attached to each carbon can be determined unambiguously, and by comparison with literature data [258]. In Fig. 5.2 the peak centred around 2.0 ppm is associated to methine groups (CH), and that around 1.4 ppm to methylene groups (CH_2). This assignment is confirmed by the ratio of the integration of the peaks. The

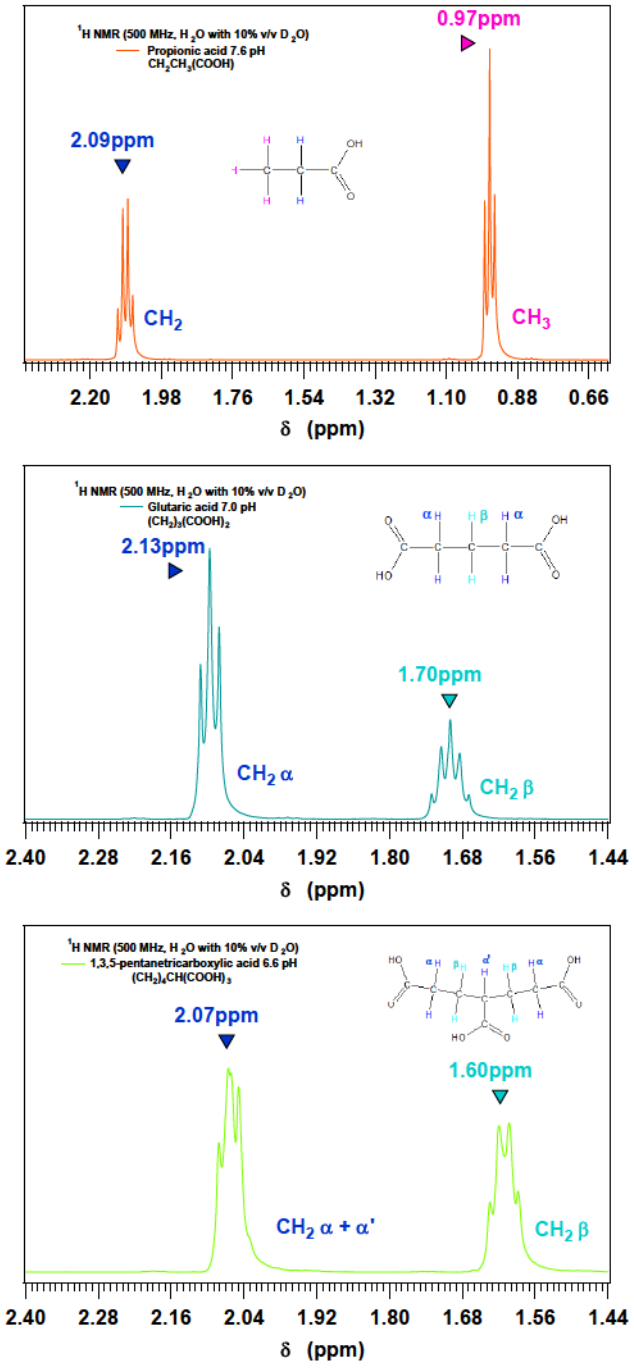

Figure 5.1: From the top: ^{1}H NMR (500 MHz) spectrum of propionate at pH 7.6 (red spectrum); ^{1}H NMR (500 MHz) spectrum of glutarate at pH = 7.0 (blue spectrum); ^{1}H NMR (500 MHz) spectrum of 1,3,5-pentanetricarboxylate at pH = 6.6 (green spectrum). T = 298 K.

splitting observed is due to the various configurations of the carboxylate groups with respect to the chain, i.e. the tacticity. The smaller polylectrolytes, 2.1 and 5.1 kDa, are characterised by thin peaks at low δ that are not present for the longer chains. These peaks are likely related with the terminal groups of the chain. This is proved by the faster diffusion coefficient found for

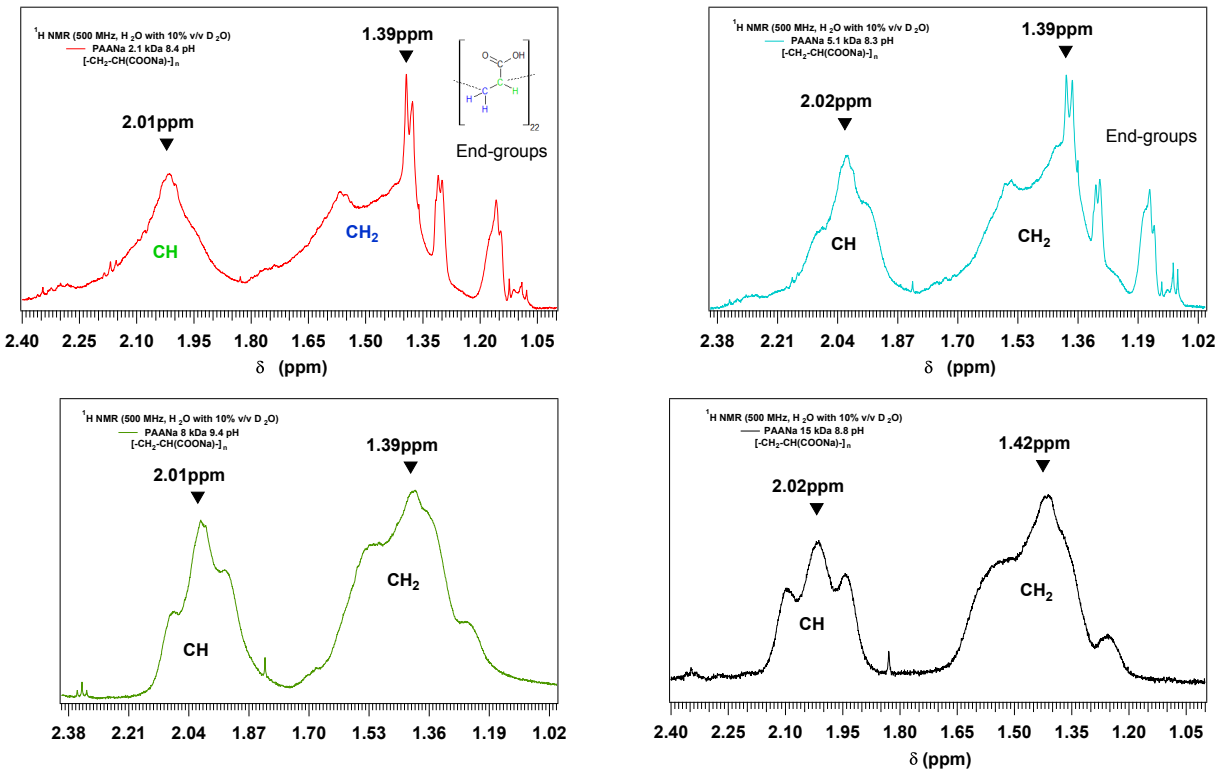

Figure 5.2: From the top graph on the left, clockwise: ^{1}H NMR (500 MHz) spectra of PAANa 2.1 kDa at pH 8.4 (red spectrum); ^{1}H NMR (500 MHz) spectrum of PAANa 5.1 kDa at pH 8.3 (blue spectrum); ^{1}H NMR (500 MHz) spectrum of PAANa 8 kDa at pH 9.4 (green spectrum); ^{1}H NMR (500 MHz) spectrum of PAANa 15 kDa at pH 8.8 (black spectrum). T = 298 K.

the terminal groups, which is 15 % larger than other peaks, as found also by Viéville et al. [59], which proposed to use this difference to determine the dispersity of poly-ethyleneoxide (Eq. 1.11, section 1.3). The diffusion coefficient of the extremity is related to the number average mass of molecules (M_n), and that of the main chain groups to the mass average mass (M_w). As explain in section 1.3 M_w is always larger than M_n, then because the inverse proportionality between diffusion coefficient and molecular weight, the diffusion coefficient of the extremity is greater than that of the main chain. Furthermore, the normalized area of the terminal group decreases by a factor 2 from the PAANa 5.1 kDa to the 2.1 kDa. This confirms the terminal group hypothesis, the larger the polyelectrolytes the smaller the weight of the terminal group with respect to the whole chain. From the comparison among the area of peaks, it is obtained that the protons of the terminal group are 8 % of the protons of the all chain. Not further investigation have been done in these last peaks, since they will not be used for further analysis, where only methine and methylene group peaks are considered.

5.2.1 | Effect of concentration on ^{1}H spectra

In this work, most of the experiments have been performed at a concentration around 1 wt%, in a regime called dilute (the detail of the regime are in section 1.3.1). Indeed, this concentration is lower than the critical concentration (32 *wt%* for the 2.1 kDa and 16 *wt%* for the 15 kDa). The variation of the chemical shift with the concentration have been investigated. The variation in concentration may modify the inter-chain interactions, and then affects the conformation of the chain.

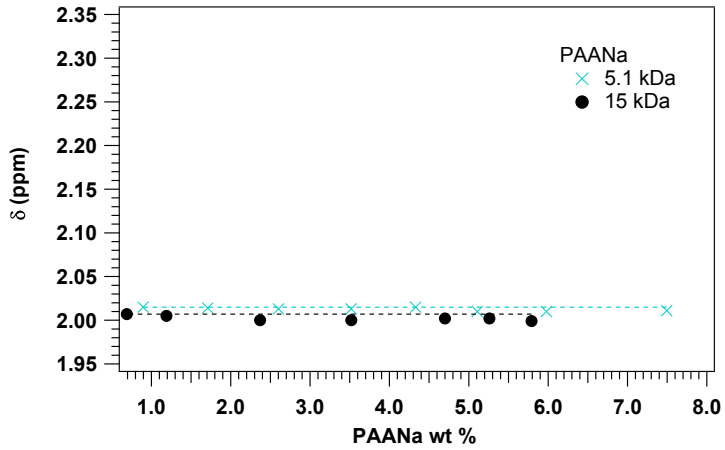

Figure 5.3: Chemical shift of the -CH- peak versus the polyelectrolyte concentration of PAANa 5.1 kDa (light blue cross) and 15 kDa (black point) at different concentrations. pH~8 T = 298 K.

In Fig. 5.3, the chemical shifts of the proton of the CH group of the 5.1 kDa and 15 kDa at 298 K and a pH~8 are reported as a function of the concentration. The chosen scale of the graph corresponds to the interval of variation of the chemical shift observed with pH (Fig.5.10). No significant variations of the chemical shift are observed in this concentration regime. It is then possible conclude that the variation of the inter-chain interaction and the change of interchain distance caused by the concentration variation, from 0.5 to 7.5 wt%, does not change the local environment of the spins notably.

5.2.2 | Effect of screening of electrostatic interactions

In this section, we study the effect of screening of electrostatic interactions on the polyelectrolytes charge distribution and structure. We modify the electrostatic interactions by salt addition.

Through the titration measurement, we check the modification on the fraction of deprotonated sites, and through the observation of ^{1}H spectra we study the effect on the structure of the chain.

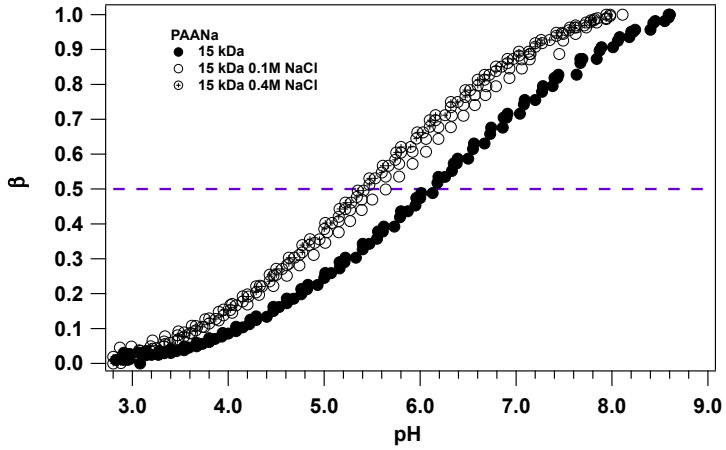

Figure 5.4: Salt effect on the fraction of deprotonated sites β, of the PAANa 15 kDa: no salt added (black point), 0.1 mol L^{-1} NaCl (black circle), 0.4 mol L^{-1} NaCl (empty black cross-circle). The dashed violet line marks β=0.5. T=298 K.

The effect of the salt addition on the fraction of deprotonated sites is shown in Fig. 5.4. The addition of 0.1 mol L^{-1} or 0.4 mol L^{-1} NaCl shifts to a lower pH the pK_β of PAANa 15 kDa, because the salt reduces the electrostatic potential and as a consequence facilitates the ionisation of the polyelectrolyte. This behaviour was also found by Monte Carlo simulations, for a weak polyelectrolyte of 100 monomers [248]. The authors found that the monomer-salt attractive interactions counterbalance the monomer-monomer repulsive interactions, and that the increase of the ionic strength makes the deprotonation process easier. The effects are prevalent for a trivalent salt, while they are weak for a monovalent salt. The weak influence of monovalent salt is confirmed by our results, since rather high concentrations of salt should be added to observe a significant effect.

In Fig.5.5 the NMR spectra of the PAANa 2.1 kDa and 15 kDa without added salt, and with 0.2 and 0.7 mol L^{-1} NaCl are reported. In Fig.5.6 all values of the proton of the CH group are shown as a function of the added salt concentratoin. The system studied are at a pH around 8 and a concentration of 1.4 wt%.

From Fig. 5.5, it seems that the addition of salt produces a slight downfield shift on δ for both chains. This can be compared to the effect of salt on the HDO resonance. As Wishart

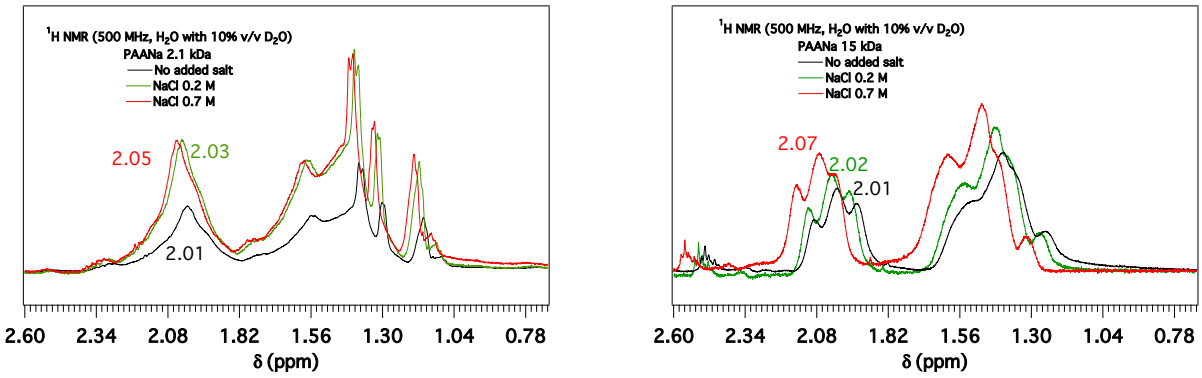

Figure 5.5: *Left:* ^{1}H NMR (500 MHz) spectra of PAANa 2.1 kDa (1.4 wt%, pH = 8) at different salt molarity. No added salt (black curve), 0.2 mol L^{-1} NaCl (green curve), 0.7 mol L^{-1} NaCl (red curve). *Right:* ^{1}H NMR (500 MHz) spectra of PAANa 15 kDa (1.4 wt%, pH = 8) at different salt molarity. No added salt (black curve), 0.2 mol L^{-1} NaCl (green curve), 0.7 mol L^{-1} NaCl (red curve). T = 298 K.

et al. found [259], the HDO chemical δ position is slighlyt affected by the increase of salt concentration (−9 ppb for 100 mmol L^{-1} salt).

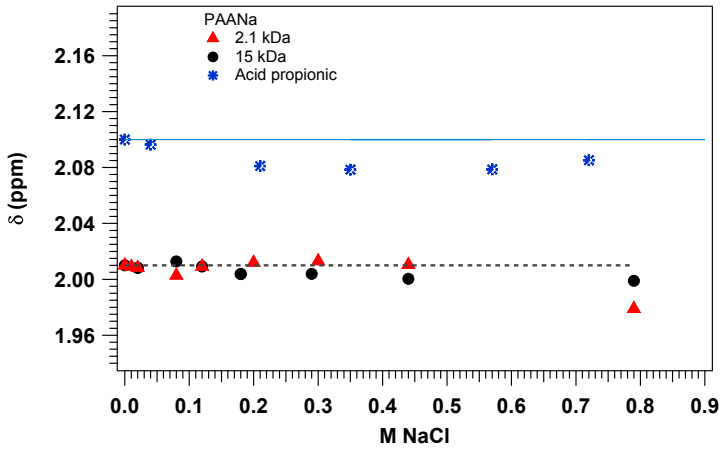

Figure 5.6: Chemical shift δ (ppm) of CH peak versus molarity of NaCl of PAANa 2.1 kDa (red triangles) and 15 kDa (∼ 1.4 *wt%*, pH 8) (black circles), and the CH_2 of the acidic propionic (0.3 *wt%*, pH 10) (blue cross). T = 298 K.

In Fig.5.6, the chemical shift of the CH peak of the PAANa 2.1 and 5.1 kDa (1.4 wt%, pH = 8), and the one of the CH_2 peak of the propionate are shown (0.3 wt%, pH = 10). The data have been corrected with the shift of the HDO reference (−9 ppb/100 mM salt). The salt does not affect the δ of the PAANa until 0.8 mol L^{-1}, where a slight diminution of δ is observed. This variation is not related to a structural modification of the chain. As we will see in Fig. 5.14, the hydrodynamic radius of the chain changes for a lower salt concentration (0.1 mol L^{-1})

and displays a constant value for higher concentration. For the propionate, δ decreases from 0.2 mol L^{-1} NaCl, and after it has a constant value.

In the next section, we will see how the variation of interactions caused by the modification of the charge of the chain, affects the conformation of the chain.

5.2.3 | Effect of the interactions: the pH

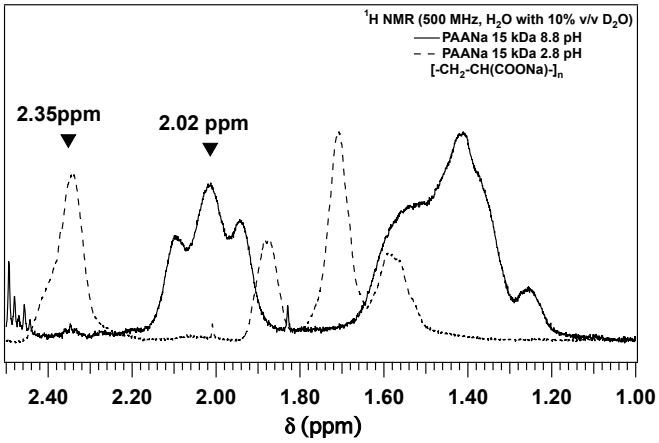

Figure 5.7: ^{1}H NMR (500 MHz) spectra of PAANa 15 Da at pH=8.8 (solid line) and pH=2.8 (dashed line). T=298 K.

In this section, the effect of pH on the ^{1}H NMR spectra of oligomers and polyelectrolytes is studied, to understand the effect of the charge modification on the chain conformation, and the influence of the chain length.

Two ^{1}H NMR spectra of the PAANa 15 kDa at two pH values are reported in Fig. 5.7. We observe that the chemical shift changes with the pH: δ decreases when the pH increases, because of the dependence on the protonation state of adjacent acidic or basic sites [260]. The first peak (CH) centred at 2.02 ppm at pH = 8.8, shifts to 2.35 ppm at pH = 2.8. Then in acidic conditions the spectrum shifts to higher δ. In basic medium, the shielding of the magnetic field is higher because the protons are richer in electrons and, as a consequence a lower δ value is observed. This behaviour has already been identified for protons located in the α position of small carboxylic acids [261]. An opposite trend is observed for ^{13}C, for which the chemical shift is seen to increase with the pH, as shown in Fig. 5.8, with a largest variation for the carboxyl carbon. This is in agreement with the previous results for small carboxylic acids [262] or

PAA [263]. The polarisation of the C–H bond could be the cause of the two opposite evolutions of the chemical shifts of ^{13}C and ^{1}H [264, 265].

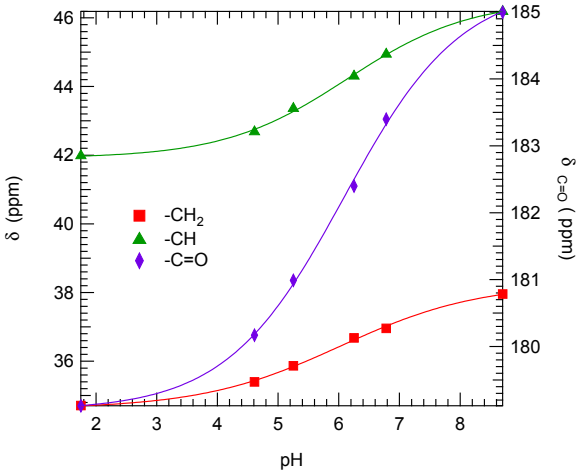

Figure 5.8: ^{13}C chemical shift of PAANa 15 Da with the pH of the solution. T=298 K

In Fig. 5.9, the chemical shifts of the protons in α position with respects to the carboxylate group of the oligomers, the propionic acid (N=1), the glutaric acid (N=2), and the 1,3,5-pentanetricarboxylic acid (N=3), are displayed. For all molecules, the chemical shift decreases with increasing pH.

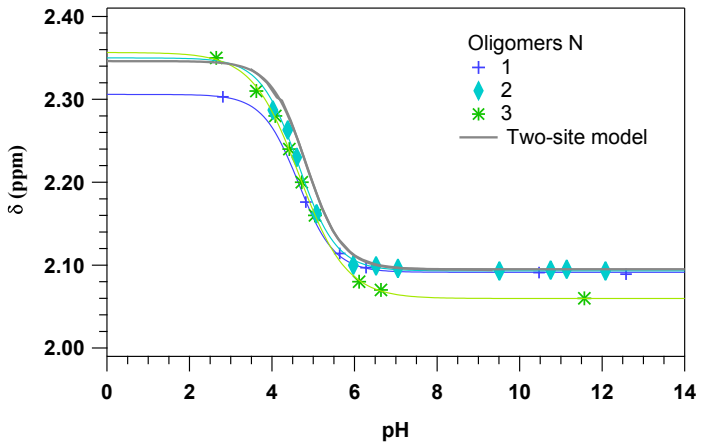

Figure 5.9: Chemical shift δ (ppm) versus pH value of α proton: propionic acid (N = 1; blue cross), glutaric acid (N = 2; blue rhombus), 1,3,5-pentanetricarboxylic acid (N = 3; green star). Data have been fitted with a sigmoidal fit. Two-site model is reported (grey line). T=298 K.

To understand the deviation of the chemical shift, the values in Fig. 5.9 can be compared with a simple two-site model. In this model, only two states of the molecule, protonated and not protonated, are considered:

$$\delta = \beta\, \delta_{\mathrm{COO^-}} + (1 - \beta\,)\delta_{\mathrm{COOH}} \tag{5.1}$$

where β is the the fraction of deprotonated sites obtained from titration measurements, $\delta_{\mathrm{COO^-}}$ and δ_{COOH} are obtained from the chemical shift measured at high and low pH respectively. It is observed that the two-site model is close to the experimental data.

To study the influence of the chain length on the pH effect, the spectra of polyelectrolytes of different molecular masses have been acquired (2.1, 5.1, 8 and 15 kDa) for different pH values. For the different PAANa, the chemical shift δ of the methine proton (CH) as a function of pH is reported in Fig. 5.10, together with the data of the oligomers. The peak position is undoubtedly affected by the pH of the solution, but the global variation of δ appears to be independent from the molecular mass. Indeed, all the data have been well fitted with a unique sigmoidal curve (dotted curve in the Fig. 5.10):

$$\delta(\mathrm{pH}) = \delta_{\mathrm{acid}} + \frac{\delta_{\mathrm{basic}} - \delta_{\mathrm{acid}}}{1 + \exp\left(\dfrac{\mathrm{p}K_\delta - \mathrm{pH}}{rate}\right)} \tag{5.2}$$

with a resulting inflection point pK_δ of 5.6±0.1 and *rate* of 0.81±0.05. The decrease of this curve is slower than the Henderson-Hasselbalch behaviour (pK=4.76 [27] and $rate = 1/\ln 10$=0.44). This departure from the Henderson-Hasselbalch equation suggests the existence of a charge regulation process during the deprotonation, as observed for β in Fig. 4.6. Conversely, for small chain as the oligomers the Henderson-Hasselbalch behaviour is found [244, 245]. The inflexion point found for the oligomers in Fig. 5.9, is around 4.7 close to the published pK_a value of 4.76 for the propionic acid.

To explore further the evolution of the chemical shift, the values in Fig. 5.10 are compared with the two-site model, where only protonated and not protonated states are considered. The ionisation ratio β determined by acid-base titration is used. The corresponding result is plotted in Fig. 5.10 (bottom). A strong disagreement is found especially in the intermediate pH region. This observation means that the chemical shift is not only sensitive to the global deprotonation state β but that another phenomenon is at play. The titration measures the macroscopic amount of protons exchanged in the solution, this number is directly related to the chain length and does not measure the counterion condensation. The NMR chemical shift δ, is a microscopic

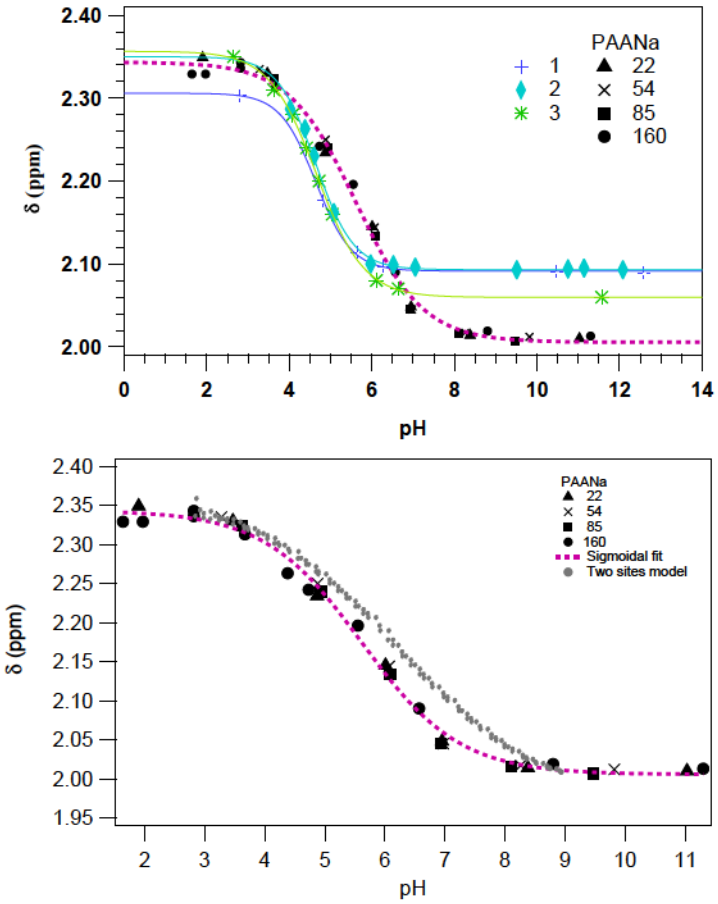

Figure 5.10: From the top: Chemical shift δ (ppm) versus pH value of α-protons: propionic acid ($N = 1$; blue cross), glutaric acid ($N = 2$; light blue rhombus), 1,3,5-pentanetricarboxylic acid ($N = 3$; green star), PAANa 2.1 kDa (black triangle), 5.1 kDa (black cross), 8 kDa (black square) and 15 kDa (black circle). Bottom: chemical shift δ versus pH value of α-protons of PAANa. Sigmoidal fit (purple dotted line), two-site model (grey points). $T = 298$ K.

measure of how the magnetic field is shielded for the nucleus and it is related to the local electric field. As discussed before, it is also correlated to the C–H bond polarisation due to the local electric field. It depends indirectly on the number of sites deprotonated and on the sodium ions condensed. As shown before, a significant fraction of the deprotonated sites is compensated by the sodium counterions, as already discussed in section 4.2.2.1. The sodium condensation decreases the electrostatic field and as result the value of pK observed for the chemical shift is lower than that for β, where the sodium condensation is not taken into account. However, this effect is not visible for the oligomers, where pK_δ and pK_β have the same value. Moreover, if the chain is long enough, there are no dependence of the δ on the polyelectrolyte length, since the chemical shift is sensitive only to the local environment.

We have shown that the determination of a ionisation midpoint might depend on the technique used for polyelectrolytes but is unambiguous for small molecules. Therefore, the NMR chemical shifts should be used with caution to determine the pK for large molecules, unlike what Bezencon et al. say, namely that the inflection point is unique whatever the method used to determine it [260].

5.3 | Self-diffusion of polyelectrolytes and oligomers

So far, NMR has enabled us to give information on the local environment through the chemical shift, but NMR is also a powerful technique to study the diffusion of the polyelectrolytes. In this section, the effect of the molecular weight, concentration and interactions on the dynamics of polyelectrolytes are investigated. To study the effect of the interactions, parameters such as the salinity and the pH of the solution are modified.

5.3.1 | Molecular weight influence

To understand the variation of the self-diffusion with the molecular mass, the diffusion coefficients of PAANa as a function of the molecular weight at pH = 6, are reported in Fig. 5.11, together with the values for the small carboxylic acids.

The values of longer chains from the literature are also reported for comparison [12, 27]. All data for the polymeric chains are well fitted with the expression $D(M) \propto M^{-\nu}$, with $\nu = 0.56$,

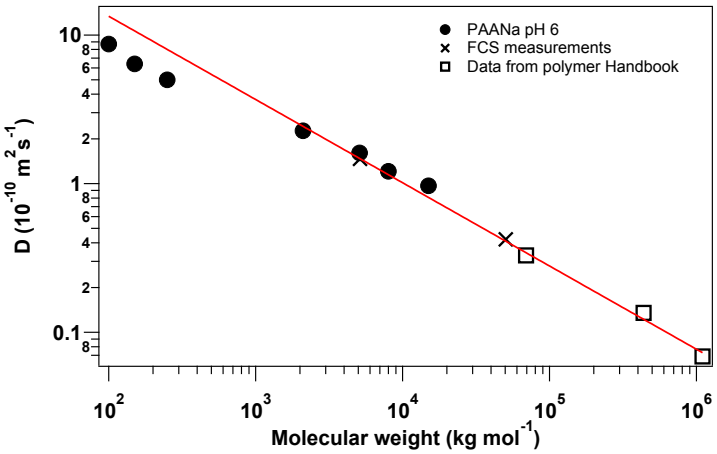

Figure 5.11: Diffusion coefficient of PAANa at pH = 6 as a function of molecular weight. Data obtained by diffusion NMR (black circle), data found in literature by fluorescence correlation spectroscopy (FCS) (black cross) [27], and in the Polymer Handbook (black square) [12]. T = 298 K.

except the points corresponding to the small carboxylic acids that depart from this law certainly due to their too small size. This value is in agreement with the literature results found by light scattering [28, 62]. To understand the physical meaning of the ν value obtained, we compare it with other ν values issued from theoretical analysis in different conformations in dilute regime:

- 0.3 is the ν value for a hard ellipsoid [233],
- 0.6 is the value for a random coil chain,
- 1 is the value for a rod-like particle [228].

From a comparison with the previous literature values, we conclude that the chain adopts a rather coiled conformation. The same analysis was carried out at pH = 1.8 and pH = 8. At pH = 1.8, the exponent ν is equal to 0.49 showing that the conformation is more compact at low pH. At pH = 8, ν = 0.67 was found, showing that the chain cannot be seen as a rigid rod, and it adopts a more flexible conformation. This last result is consistent with viscosimetric determination at low salt concentration [266].

5.3.2 | Influence of the concentration on the dynamics

In Fig. 5.12, the diffusion coefficients of PAANa 5.1 and 15 kDa, as a function of the concentration of the polyelectrolyte are shown. As discussed in section 1.3.1 and 5.2.1, the

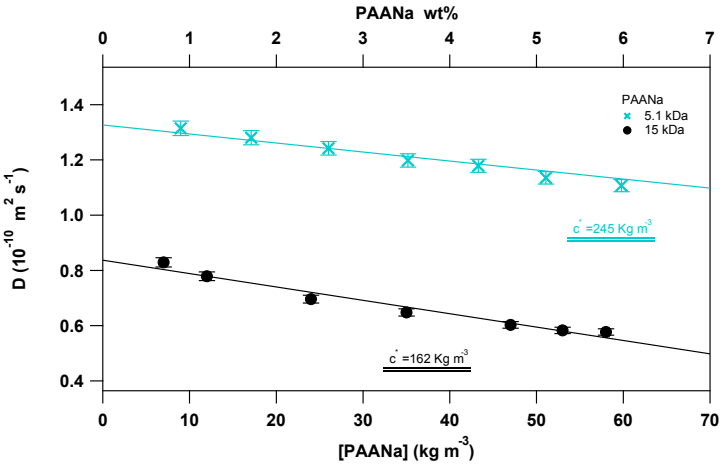

Figure 5.12: Diffusion coefficients versus the concentration of PAANa 5.1 kDa (blue cross) and 15 kDa (black point) at pH~ 8, fitted with a linear curve. T = 298 K.

range of concentration studied is below the overlap concentration $c^\star$ (see Table 4.1). In this regime, the interactions between polyelectrolyte chains are not strong but, they can still affect the self-diffusion. The diffusion coefficient decreases slightly with the amount of polyelectrolytes in a linear behaviour that was also observed by Pristinski et al. [194] and Callaghan and Pinder [99], which confirms the dilute regime ($c < c^\star$). Furthermore the decrease of the diffusion coefficient with the concentration proves that there are a still repulsive interaction between the chains [67]. Oostwal et al. also observed that, in a dilute solution, the diffusion of sodium poly(styrene-sulfonate) is weakly related to the concentration [228]. This effect comes from non negligible intermolecular electrostatic interactions, not screened in these salt free solutions, also observed by viscosity measurements [267] and in Fig. 5.13, where the viscosity as a function of the concentration is reported for the 2.1 kDa and 15 kDa at 298 K.

As observed in Fig. 5.13, the viscosity increases with the concentration of the PAANa. Since the viscosity of the suspension is a feature that takes into account the inter-chain interactions because, when it is measured, the whole solution undergoes a shear stress, the increases of the viscosity with the concentration shows the presence of intermolecular interactions. Furthermore from the viscosity dependence on the concentration, the dilute regime is confirmed, because the viscosity depends on the concentration with a power law (see the fit in Fig. 5.13) with an exponent close to 1 (respectively 1.2 and 1.0 for the 2.1 kDa and 15 kDa) [6, 65, 95]. For a dilute regime the exponent x in the power law, $\eta \approx c^x$, is close to 1, while for a semidilute regime it is close to 1/2 [6].

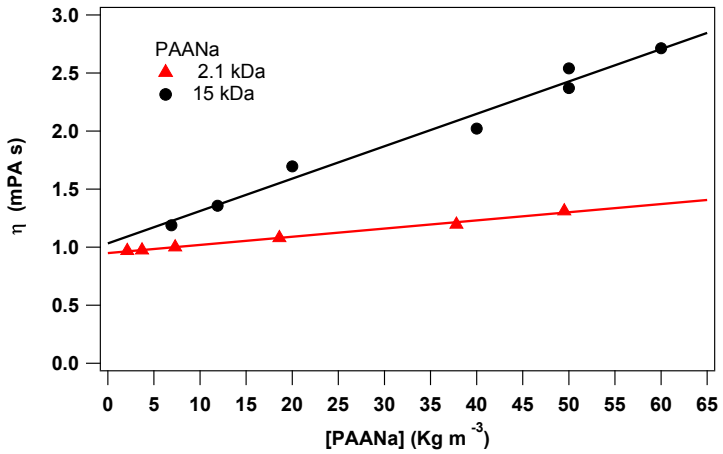

Figure 5.13: Viscosity of the sample η versus the concentration of PAANa 2.1 kDa (red triangles) and 15 kDa (black points) at pH$\sim$ 8. T = 298 K.

The stronger decrease of the diffusion coefficient with the concentration for the longer chain, confirms that the intermolecular interactions increase with the length of the chain. This is also shown in the variation of the viscosity with the molecular weight of the PAANa: in the concentration regime from 7 kg m^{-3} to $\sim$ 50 kg m^{-3} the viscosity of PAANa 2.1 kDa and 15 kDa changes respectively of 25% and 53%.

For the propionate, the concentration effect was also studied and no significant variation on the diffusion coefficient have been found until 5 wt%.

5.3.3 | Influence of the interaction on the diffusion

To investigate the effect of the electrostatic interactions on the diffusion of the polyelectrolyte, the dynamics of the polyelectrolytes is studied in different salt concentrations and pH values. Thanks to salt addition, the electrostatic repulsions of the system are screened, and thanks to the pH the charge of the chain is modified as shown in Fig. 4.6. First, the effects caused by salt addition at high pH are shown. Finally, the effect of the pH are discussed and compared with all modification of the properties of the system observed with the pH in the previous sections.

Effect of salt

The diffusion coefficients of PAANa 2.1 kDa and 15 kDa as a function of added NaCl concentration are reported in Fig. 5.14, together with the propionate.

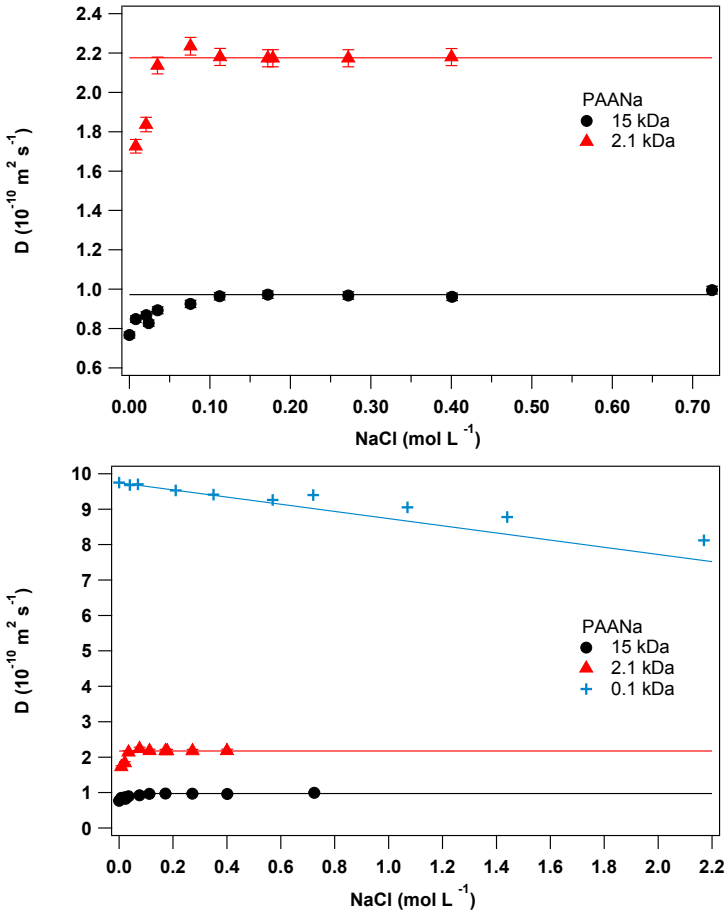

Figure 5.14: Top: Diffusion coefficient as a function of NaCl molarity at pH~8, for the 2.1 kDa (red triangle) and 15 kDa (black point) PAANa. T = 298 K. Bottom: the diffusion coefficient of the propionic acid 0.1 kDa (blue cross) as a function of the added salt is also shown. Reference lines are also reported.

The diffusion coefficient increases (the hydrodynamic radius decreases) with the concentration of added NaCl up to 0.1 mol L^{-1}, before reaching a plateau value. Surprisingly, the plateau value is observed at lower concentration (0.1 mol L^{-1}) than the θ-solvent concentration (1.5 mol L^{-1}) [28]. This initial strong increase followed by a plateau was also observed by Böhme et al. [77]. The added salt screens the intrachain electrostatic interactions, that causes a more coiled conformation and a lower hydrodynamic size [77], visible in the increase of the diffusion. This effect was also observed for polylysine [107, 268], poly(methacrylic acid) [194] and for sodium poly(styrenesulfonate) in N-methylformamide [269].

The propionate exhibit an inverse trend in Fig. 5.14 (bottom), with a decrease of the diffusion coefficient with the increase of the salt concentration. Several phenomena can be at the origin of the observed evolution. This decrease of the diffusion coefficient may be caused by the increase

of the viscosity of the water with the salt addition [236]. The ratio between the viscosity of water at the two extreme salt concentrations measured ($\eta(c_{\mathrm{NaCl}} = 2.2\ M)/\eta(c_{\mathrm{NaCl}} = 0) = 1.2$), corresponds to the inverse ratio between the correspondent diffusion coefficient ($D(c_{\mathrm{NaCl}} = 0)/D(c_{\mathrm{NaCl}} = 2.2\ M) = 1.2$). On a more microscopic level, in electrolyte solutions, the two most important factors that impede the diffusion of charged species are the relaxation and electrophoretic effect [270–272]. The hydrodynamic effect comes from the opposite motion of the counterion cloud in an electric field while the relaxation contribution is due to the electrostatic restoring force caused by the counterions.

Thanks to the comparison with this system it is possible to conclude that the increase of the diffusion coefficient observed for the PAANa is due to an effect of the salt on the intra-chain electrostatic interactions.

Effect of pH

The diffusion coefficients of PAANa 2.1, 5.1, 8 and 15 kDa as a function of pH are reported in Fig. 5.15 (top graph). The same data are normalized to the diffusion coefficient at pH∼2 in the bottom graph. The data of the PAANa 50 kDa (obtained by FCS) come from literature [27]. The diffusion coefficients decrease with a sigmoidal behaviour with pH.

At high pH, the PAANa is fully charged and the long range interactions are strong enough to stretch the polyelectrolyte chain and as a consequence reduce the polyelectrolyte self-diffusion. Especially the diffusion coefficient decreases in the pH range of 4–7. The observed increase of the hydrodynamic radius is also consistent with the evolution of the radius of gyration with the increase of the degree of ionisation β observed by Monte Carlo simulations [27, 248]. Carnal et al. [248] have simulated using the Monte-Carlo simulation an isolated weak polyelectrolyte of 100 monomers at several pH values. At a high pH, they found that an extended structure is achieved to minimise the long-range electrostatic energy and that there is a competition between the monomer-monomer repulsive interactions (the strongest interaction), and the attractive monomers-counterion interactions. This confirms that at a high pH the chain is stretched and instead it is more compact at a low pH, which was already inferred from the dependence of the ν exponent on the pH. Moreover, as seen in Fig.5.15 (bottom), the relative variation of the diffusion coefficient with the pH is size-dependent. This variation increases with the molecular

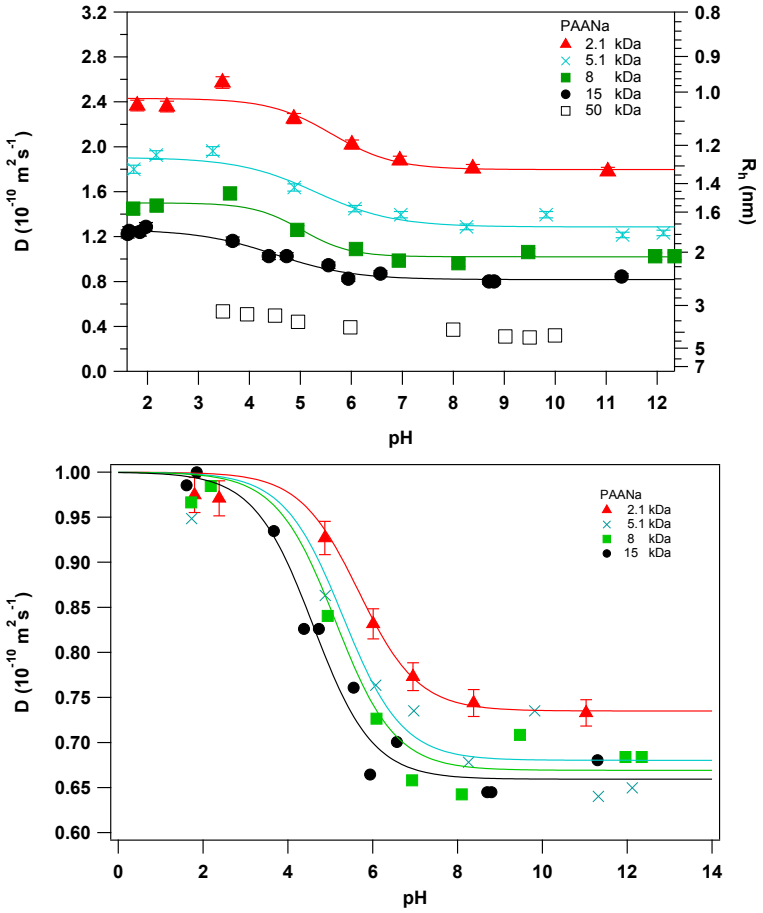

Figure 5.15: Top: Diffusion coefficient versus pH for different molecular weigh of PAANa: 2.1 kDa (N=22, red triangles), 5.1 kDa (N=54, blue cross), 8 kDa (N=85, green square), and 15 kDa (N=160 black point). The data of the PAANa 50 kDa (obtained by FCS) come from the literature [27] (N=700, empty black square). The data are fitted by a sigmoidal fit. The value of the hydrodynamic radius is reported on the right. Bottom: Data normalized to the diffusion coefficient at low pH.

weight, from 26 % for the 2.1 kDa to 34 % for 15 kDa PAANa. This trend is also observed in the data of Swift et al. [273] where the decrease of D, between acidic and basic conditions, varies from 50 % to 75% while the mass varies from 17 kDa to 55 kDa. However, contrary to Swift et al. results [273], the diffusion variation is observed even for low molecular weight PAANa (down to M_w = 2.1 kDa). In other words the impact of the chain length on the properties of short weak polyelectrolytes diffusion variation is observed even for low molecular weight PAANa.

Actually, the previous variation is even observed for small carboxylic acids like acetic Fig. 5.16, consistently with the results of Dunn and Stokes [274]. In Fig. 5.16, the diffusion coefficient of the propionic acid, glutaric acid, and 1,3,5-pentanetricarboxylic acid are reported as a function of the pH. The value found for the PA is in agreement with literature value at high pH [275], a slight deviation is found for the GA (literature value 7.9 10^{-10} m^2 s^{-1} [275]), no literature values have been found for the PCA.

For low molecular weight species, this change of diffusion could be ascribed to change of solvation between the neutral and the charged species as suggested by Dunn and Stokes [274]. As visible in Fig. 5.16 (bottom), this effect increases with the molecular weight, from 15 % for the 0.1 kDa to the 20 % for the 0.2 kDa. This solvation phenomenon occurs also for longer chains, but the main origin of the mass dependence of the swelling with pH, is related to the different scaling laws in acidic and basic media and the electrostatic interactions as discussed before. In basic medium, the diffusion dependence with mass, $D(M) \propto M^{-\nu}$, is steeper than in acidic media, where the chain has a more stretched conformation. Furthermore the mass dependence of this swelling is consistent with the electrostatic potential increases with M_w, already discussed for the ionization of the chain of Fig.4.6.

The conformational change with the pH can be discussed in the light of the persistence length P, which measures how far a polymer chain persists in given direction as described in the section 1.3.3 and 1.4.2. The higher the persistence length, the stiffer the chain and the larger the radius of the polymer. As said in section 1.4.2, the persistence length P can be divided into a sum of two contributions: an intrinsic persistence length, due to the rigidity of the chain backbone and an electrostatic persistence length arising from the repulsion between neighbouring ionic sites [66]. For an end-to-end distance larger than the persistence length, the orientations of the extremities are governed by the thermal motions that fold the chain and reduce the distance between the two ends. Comparing the values of persistence length given in section 1.4.2, with

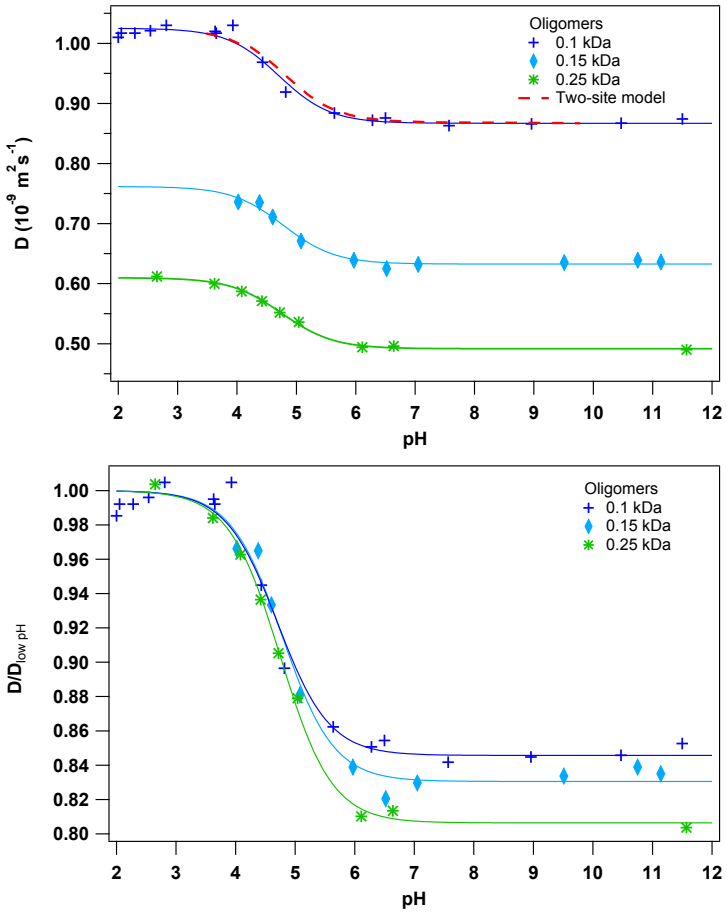

Figure 5.16: Top: diffusion coefficient of carboxylic acids vs pH: propionic acid (N = 1; blue vertical cross), glutaric acid (N = 2; light blue rhombus), 1,3,5-pentanetricarboxylic acid (N = 3; green star). The two-site model is calculated for the 0.1 kDa (red dotted line). Bottom: normalized diffusion coefficient of the previous data for the carboxylic acids vs pH. The data are fitted with a sigmoidal curve.

the dimensions of polyelectrolytes, reported in table 4.1, both the hydrodynamic radii R_h and the max end-to-end distances ℓ_{max} are in the order of few persistence lengths, which explain why they tend to behave as not folded chain. The ratio ℓ_{max}/P, which could be seen as the number of Kuhn segments of the chain, decreases with the pH consistently with the measured evolution of the diffusion coefficient. However, the small carboxylic acids are significantly below the persistence length and does not follow the same scaling laws, as already observed in Fig. 5.11.

As shown in Fig. 5.16 for the propionic acid, the diffusion coefficient of oligomers follows a two-site model. This model, introduced in the section 5.2.3, describes the behaviour of the diffusion coefficient as dependent only from protonated and deprotonated states. Indeed, the diffusion coefficients reported in 5.16 (red dotted line) for the propionic acid, have been calculated considering the fraction of protonated and deprotonated states, as calculated in the titration experiments (Fig. 4.9).

$$D_{2state} = \beta D_{basic} + (1 - \beta) D_{acid} \tag{5.3}$$

where β is the fraction of deprotonated sites. As seen for the chemical shift, this model is only valid for the short oligomers, confirmed by the agreement of the model with the diffusion coefficient, and it is not valid for the larger PAANa polyelectrolyte (Fig. 5.10 bottom).

The effect of the electrostatic screening due to the salt addition presented in the previous section, is compared with the behaviour of an uncharged chain (the system at low pH, Fig. 5.15). To decrease the electrostatic interactions two ways are possible: screening the interactions by salt addition, or discharge the chain by decreasing the pH of the solution. The diffusion of the chain at high salt concentration ($D = 0.98 \pm 0.02 \cdot 10^{-10}$ m^2 s^{-1} at $C_{salt} \geq 0.1$ mol L^{-1}, for the 15 kDa) is slower than for the uncharged chains a low pH, as shown in Fig. 5.15 (D=$1.36 \pm 0.02 \cdot 10^{-10}$ m^2 s^{-1} at pH$\sim$ 2, for the 15 kDa). This suggests a residual influence of electrostatic interactions, despite the electrostatic screening by the addition of salt. The residual interactions may be the origin of a better solvation of the chain at high salt concentration than the uncharged chain. Hence, the increased solvation effect could be responsible for the lower diffusion coefficient of the chain at high salt concentration.

In the next section, we will sum up the results of this chapter, trying to figure out the impact of the chain length.

5.4 | *What is the impact of the chain length on the properties of short weak polyelectrolytes?*

For each studied system, we have measured the variation with pH of the degree of neutralization of the PAA sample, the chemical shifts of the proton NMR peaks, and the self-diffusion coefficient. Each property is found to vary in a sigmoidal fashion with pH.

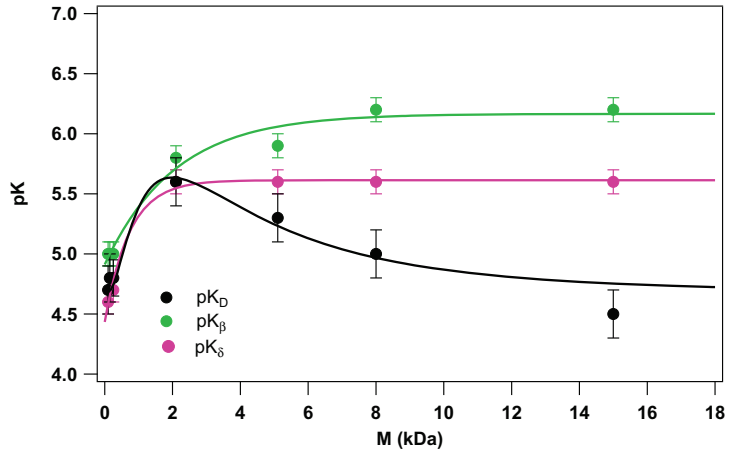

Figure 5.17: Inflection points of the previous measurements as a function of pH, versus the molecular weight. pK_D is related to the diffusion coefficient in Fig. 5.15 and Fig. 5.16 (black points); pK_β to β in Fig. 4.9 (green points); pK_δ is the inflection point of the chemical shift in Fig. 5.10 (pink points). Lines are guide to the eyes.

To have a comprehensive view of the the ionization process for the different molecular weights, the midpoint point of the sigmoidal transition is chosen in order to compare the molecular weigh dependence of the different properties. The comparison of the different pK (pK_D, pK_β and pK_δ) points out the complex interplay between the different parameters under study. The errors bars for the diffusion coefficients and chemical shift inflexion points correspond to the standard deviation from the sigmoidal fit of the diffusion data. For the titration, the error bar comes form the dispersion of experimental data close to the midpoint.

The constant value of the pK_δ proves the local character of the δ, that is independent to the molecular weight. For small carboxylic acids, the same value of inflection point pK is observed whatever the method. For longer chain polyelectrolytes, a departure is expected. The deviation between pK_δ and pK_β, already discussed in the section 5.2.3, increases with the molecular weight. Furthermore pK_D is found to be less than the other two pK, as it was already observed

in the work of Pristinski et al. [194], for a 72 kDa poly(methacrylic acid) PMAA. Here we observe that this departure is size dependent, and it increases with the molecular weight of the chain. A shorter chain is closer to a two-site model, and the different values of inflection point pK should are closer as well. If a two-site model is considered (for example a species with only one acid and one basic configuration), the same value of inflection point should be observed whatever the method.

Summary of Chapter 5

In this chapter, NMR experiments have been used to study the structural changes of carboxylate molecules via the chemical shift, and the variation of their dynamics by the study of the diffusion coefficient.
The studied systems are in dilute regime. The chemical shift δ is independent on the salt concentration, but it decreases with a sigmoidal behaviour with the pH for oligomers and for PAANa independently from the molecular mass. A similar sigmoidal behaviour has been observed also for the fraction of deprotonated sites β as a function of the pH. If both exhibit a sigmoidal variation with pH, β shows a molecular mass dependence, not seen for δ. The counterion condensation could explain the difference between β and δ.
The effect of molecular weight and of the interactions on the dynamics of polyelectrolytes have been investigated. The diffusion coefficient decreases with the molecular weight with a power law dependence $D(M) \propto M^{-\nu}$, that depends on the pH value. At high pH, the higher ν shows that the conformation adopted tends towards a flexible rod when the polyelectrolyte is fully charged. Conversely, the chain is more compact at lower pH values.
We have seen that the quantity measured, β, δ, and the D vary in a sigmoidal manner with pH. The pH at the inflection point of the sigmoidal transition is chosen in order to compare, for a given system, the different measurements and, for all data, the variation of the inflection point (pK) with the molecular weight. The comparison of the different pK_x (pK_D, pK_β and pK_δ), points out the complex interplay between the different parameters under study. The constant value of the pK_δ proves the local character of the δ, that is independent to the molecular weight. The deviation between pK_δ and pK_β, increases with the molecular weight. For small carboxylic acids, the same value of inflection points pK are observed whatever the method.
Even short polyelectrolytes singularly differ from simple carboxylic acids. They tend to behave like long chain polyelectrolytes but with noticeable differences due to their small size compared to the persistence length. Their ionization process and its effect on diffusion cannot be easily derived by a single parameter study, since several phenomena are at play.

Chapter 6

Diffusion of short polyelectrolytes in crowded charged media

Contents

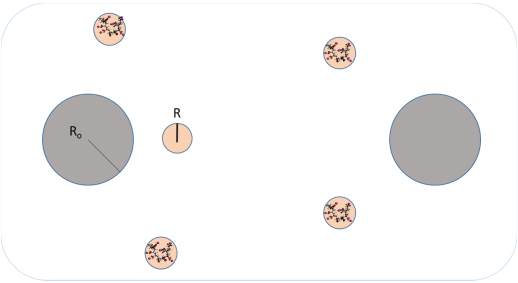

Figure 6.1: Sketch of the studied system.

In this chapter, we investigate the effects of the charged obstacles on the diffusion of polyelectrolytes. These effects will be studied by using carboxylate molecules of increasing sizes, from the simple propionic acid to the sodium polyacrylate. To point out the effects of obstacles properties, silica nanoparticles with different sizes and surface charge are used (chapter 4). As mentioned earlier, the polyelectrolytes are smaller than the nanoparticles ($R/R_o < 0.5$). Fig.6.1 is a representative sketch of the investigated system. First, the effect of the obstacles on the diffusion coefficient is studied by changing the volume fraction of obstacles, starting from the study of the oligomers to the more complex chains of polyelectrolytes. Secondly, the influence of the interactions between diffuser and obstacles, is then investigated by the modification of their interactions by salt addition or pH variation.

6.1 | Preliminary analysis of polyelectrolytes and nanoparticles mixtures

In this section, we investigate the stability of the system of polyelectrolytes and nanoparticles, in the conditions used during the NMR diffusion experiments. The samples, prepared 24 to 48 hours before the experiments, have a polyelectrolyte concentration close to 1 %. The behaviour of the system after a longer stabilisation time (more than 48 hours) and a different polyelectrolyte concentrations, will be studied in the next chapter, which focuses on the interaction between silica particles due to the polyelectrolytes, through SANS.

The stability of the system is investigated through the diffusion coefficient of the obstacles (silica nanoparticles) using DLS, and the study of their electrokinetic potential (see 4.2.2.2). This parameter is used here, to investigate if the addition of polyelectrolytes modifies significantly the

surface potential of the silica and then affects the stability of the nanoparticles. As before, the experiments have been performed at 298 K with Zetasizer Nano ZS (Malvern) and the samples have been measured less than 24 hours after mixing.

In the studied systems, the silica volume fraction is ϕ = 1% and ϕ = 5%, and 15 kDa PAANa concentration of 0.1 wt% and 1 wt% respectively. The volume fraction of the nanoparticle is measured gravimetrically from the mass of silica in a dried sample using the density of the solvent and nanoparticle.

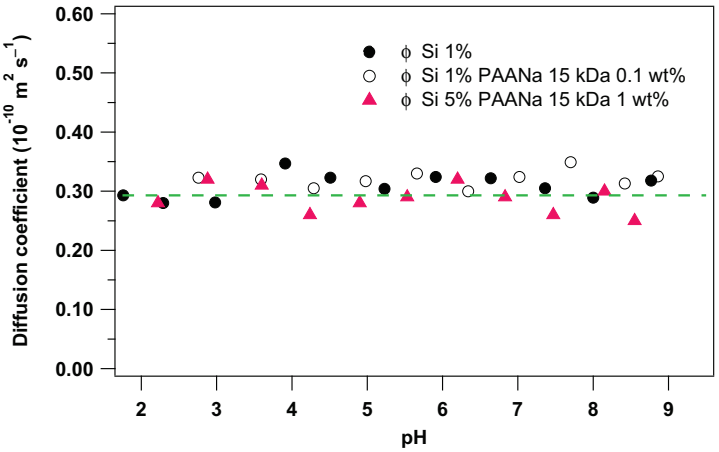

Figure 6.2: Diffusion coefficient of silica LS in H_2O suspension a different volume fraction ϕ, without and with PAANa 15 k at 0.1 % as a function of the pH. Silica ϕ=1% (black point); silica ϕ=1%, PAANa 15 kDa 0.1 % (black circle); silica ϕ=5 %, PAANa 15 kDa 1 % (pink triangle); the dotted green line is reported as eyes guide. Data obtained with Zetasizer NanoZS, Malvern. T=298 K.

In Fig. 6.2 and 6.3, the diffusion coefficient and the electrokinetic potential of the nanoparticle are reported respectively as a function of pH for the different systems studied. For all studied systems, there are no significant variation on the silica diffusion coefficient with or without PAANa. This means that the dispersion of nanoparticle is kinetically stable after the addition of polyelectrolytes.

As observed in Fig. 6.3, ζ exhibits a similar behaviour whatever the data reported: it has a value close to zero a low pH, and it decreases with the pH, as also observed by Wisniewska et al. [84]. The zero value at low pH, is due to the low charge of the silica, see section 4.1.3. Despite the decrease of pH reduces the number of ionised surface silanol groups, Fig. 4.10, the dispersion is still kinetically stable as the constant value of the diffusion coefficient proves, Fig. 6.2. Then, the particles are not aggregated in the conditions studied. As the pH increases,

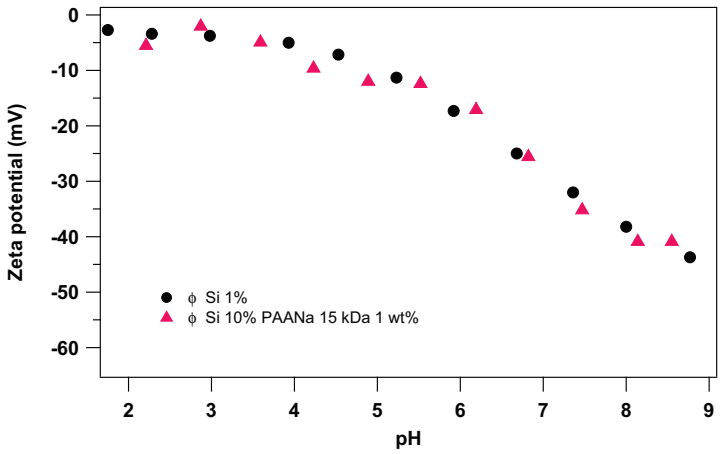

Figure 6.3: Zeta potential of silica LS in H_2O suspension a different volume fraction ϕ, without and with PAANa 15 kDa at 0.1 *wt%* as a function of the pH. Silica ϕ=1% (black point)s; silica ϕ=10 *wt%*, PAANa 15 kDa 1 % (pink triangle). Measured by Malvern Zetasizer Nano ZS. T=298 K.

the surface potential of the particle increase and the ζ becomes highly negative due to the increasing of the number of ionised sites. In other words, this behaviour is related to a higher stability of the obstacles in agreement with the increase of the fraction of charged sites a high pH. Overall, the behaviour of the electrokinetic potential does not change notably in the presence of polyelctrolyte.

In Fig. 6.4, the ^{1}H NMR spectra of the PAANa without obstacles and with different nanoparticles used in this work are reported. The data have been normalised at the maximum value. The concentration of the PAANa is around 0.5 *wt%* for all spectra, and the volume fraction of nanoparticles is around 9 % for the silica LS and TM. The spectra do not significantly differ from the spectrum without nanoparticles. The slight shift observed are due to small differences of pH between the different systems, see section 5.2.

To conclude we can say that no significant variations of the nanoparticles behaviour, and no notable aggregation of the nanoparticles are observed after the addition of the polyelectrolytes to the suspensions of nanoparticles in the regime of concentration studied, and in the time scale of 2 days between sample preparation and measurements. The systems that we are going to study in the next section by NMR are then constituted by polyelectrolytes in a suspension of homogeneous and dispersed obstacles. Furthermore, the addition of nanoparticles does not change the conformation of the polyelectrolytes.

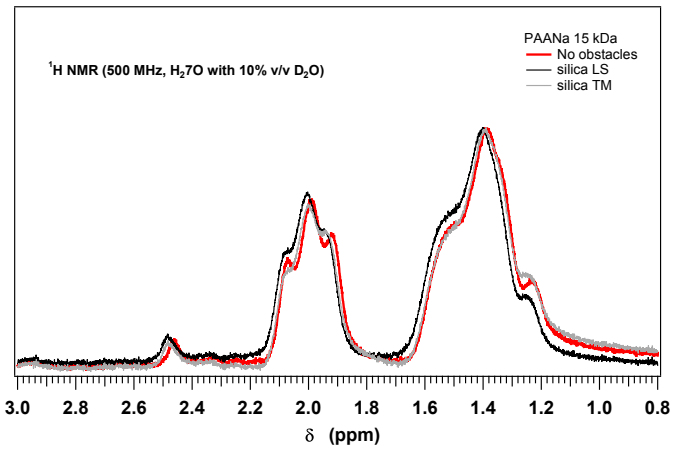

Figure 6.4: ^{1}H NMR (500 MHz) spectra of PAANa 15 kDa normalised at the CH_2 peak: without obstacles (0.7 *wt%*, red line), silica LS (0.5 *wt%*, ϕ 9.5 % black line), silica TM (0.5 *wt%*, ϕ 9.7 % gray line). T= 298 K, pH $\approx$ 8.

6.2 | Diffusion of simple charged diffusers: the oligomers

In this section, the impact of charged obstacles on the diffusion of oligomers is investigated, by the study of the self-diffusion coefficient as a function of the volume fraction of obstacles a fixed temperature (298 K) and pH ($\approx$ 8). The propionic acid (PA, 0.1 kDa), glutaric acid (GA, 0.15 kDa), and 1,3,5-pentanetricarboxylic acid (PCA, 0.25 kDa) are the oligomers studied.

Jönsson's model, which describes the behaviour of the diffusion coefficient in presence of uncharged spherical obstacles (chapter 2), will be used as a reference model and compared to the experimental data to investigate the properties that may affect the dynamics. Among the different models presented, Jönsson's curve has been chosen as reference model because it is a simple model and its evolution is not different from some of the other models proposed, as discussed in chapter 2.

6.2.1 | Experimental results

The diffusion coefficient of oligomers as a function of the volume fraction of silica LS are shown in the Fig. 6.5. The studied oligomers are propionic acid (PA, 0.1 kDa), glutaric acid (GA, 0.15 kDa), and 1,3,5-pentanetricarboxylic acid (PCA, 0.25 kDa). These systems

can be considered respectively as the analogs of the monomer, the dimer, and the trimer of the polyelectrolytes studied in the next sections. Then, these oligomers can be considered as the simplest among polyacrylic acid, without the complexity of strong intra-chain interactions, for the investigation of the impact of the obstacles on the polyelectrolytes dynamics. The experimental data are reported together with the Jönsson's curve, as a reference model (Eq. 2.8). As shown in Fig. 6.5 (top), the increase of the volume fraction of obstacle causes a linear decrease of the diffusion coefficient of all studied oligomers for the range of ϕ studied. The data in Fig. 6.5 have then been fitted with a linear dependence of the diffusion coefficient:

$$D = D_0 (1 - A\phi) \tag{6.1}$$

where D_0 is the diffusion coefficient of the molecules in the absence of obstacles.

The parameter A is 0.5 in the case of the approximation of the Jönsson model (Eq. 2.9) in the limit $R \ll R_o$, but is close to 2 for colloidal particles of the same size (see chap. 2). The D_0 found using Eq. 6.1 has been used to normalise the data reported in Fig. 6.5 (bottom), which have been fitted with Eq. 6.1. In Table 6.1, the A of the linear fit are reported (the errors are the standard deviation values issued from the linear fit). The deviation of the data from Jönsson's model (called in the graph $J(\phi)$) increases with the molecular weight, as the increase of the parameter A reported in Table 6.1 points out. Jönsson et al. have suggested [144] for an analogous system, that the disagreement is due to properties such as the size of the diffuser and the interaction between diffusers and obstacles, that are not considered in their model. Both these effects become more significant as the volume fraction of obstacles increases and when the size of diffuser increases. For the oligomers however, the minimum size ratio is of the order of $R/R_o = 1/16$ which means that the interaction effect is the most important.

However, no variations are observed between 0.15 and 0.25 kDa. This effect may be related to the effect of the electrostatic condensation for the larger of the three oligomers. The maximum effective charge for the three oligomers can been estimated using the formula proposed by Ramanathan, that has used the PB equation in the limit of small object compared with the Debye length (Eq. 1.5) $\kappa R \ll 1$ [276].

$$Z_{\max} = \frac{2a}{\ell_B} \ln \frac{1}{\kappa R} \tag{6.2}$$

The values found are respectively $Z_{\max} = 1.4$, 1.6, and 1.7 for the 0.1, 0.15, and 0.25 kDa

oligomers, that can be compared with the structural charges (1,2 and 3). For the two former molecules, the structural charges are below the calculated maximum charge but, it is no longer the case for the latter for which a counterion condensation can be expected due to its high charge density.

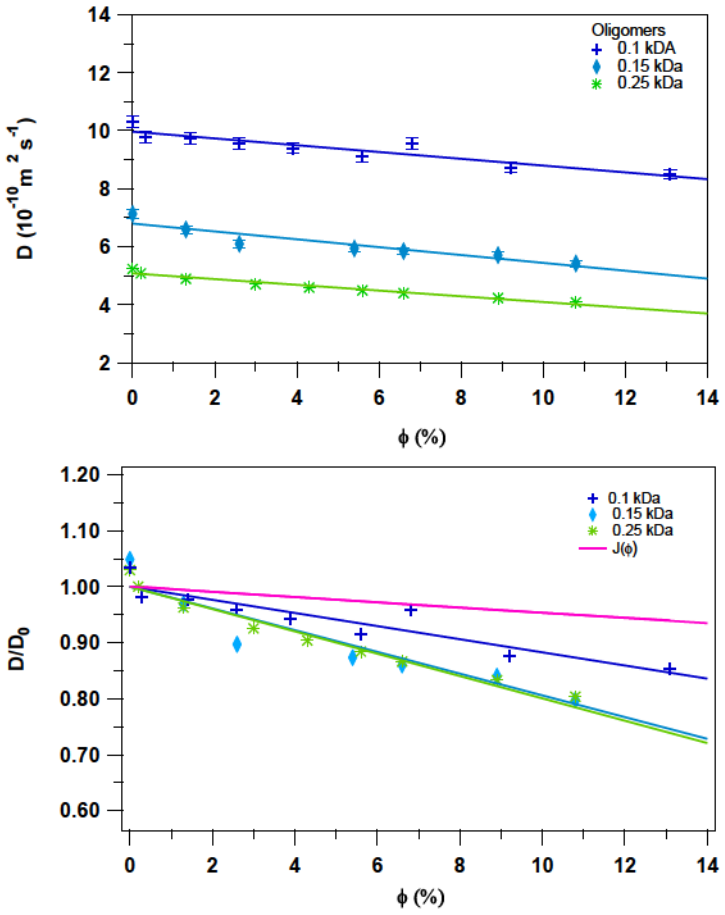

Figure 6.5: Top: diffusion coefficient of the propionic acid (0.1 kDa, concentration 0.1 *wt%*, blue crosses), glutaric acid (0.15 kDa, concentration 0.1 *wt%*, blue rhombus), and 1,3,5-pentanetricarboxylic acid (0.25 kDa, concentration 0.1 *wt%*, green stars) versus the volume fraction of silica LS. Jönsson's curve, Eq. 2.8 (pink line), is reported as reference. Bottom: normalized diffusion coefficient of top graph data. All data have been fitted with a linear curve, Eq. 6.1. T= 298 K, pH ≈ 8.

Through these experiments, we have seen that the presence of the negative charged obstacles decreases the diffusion coefficient of the oligomers. In the next section, we will try to establish the parameters that effect the dynamics of the oligomers.

	Jönsson	0.1 kDa	0.15 kDa	0.25 kDa
A	0.5	1.2 ± 0.2	1.9 ± 0.2	1.9 ± 0.2

Table 6.1: A of the linear fit, Eq. 6.1, of normalised data in Fig. 6.5.

6.2.2 | Effective volume fraction approach

In the previous paragraph, we have seen that the increase of the volume fraction of obstacles, decreases the diffusion coefficient of the oligomers. The physical size of the obstacles is one element that reduces the diffusion coefficient of diffusers, but it is not the only one. A better assessment of the accessible volume have to be done, since for example the diffusers have a finite volume and then the accessible volume for the diffusion is less than if they were point-like. The volume fraction can then be rescaled to take this effect into account considering also the excluded volume of the diffuser. ϕ_R is defined as:

$$\phi_R = \phi\left(1 + \frac{R}{R_o}\right)^3 \tag{6.3}$$

where R_o is the radius of the obstacle and R the radius of the diffuser.

The diffuser-obstacle interaction is another element that affects the diffusion. At high pH, the main interaction is the repulsive electrostatic interaction, since both the diffuser and the obstacles are negatively charged. To considered the interaction in the Jönsson's model, ϕ can be rescaled with an extra length that considers also the excluded volume due to the repulsive interaction. This contribution to the excluded volume is not straightforward to evaluate. As suggested by Bell, a first approximation of this extra length could be the the Debye length (Eq. 1.5) [133]. ϕ_κ is defined as:

$$\phi_\kappa = \phi\left(1 + \frac{\kappa^{-1}}{R_o}\right)^3 \tag{6.4}$$

where κ^{-1} is the Debye length (Eq. 1.5).

A schematic picture of the system is sketched in Fig. 6.6. R_o is the radius of the nanoparticle LS, 8 nm, and R the radius of the diffuser. $\ell = 30$ nm is the mean separation distance between two nanoparticles for a volume fraction of 8 %, which is calculated considering that the nanoparticles are equally dispersed in the suspension ($\ell = \sqrt[3]{V/N_p}$, where V is the volume of the system and N_p is the number of particles).

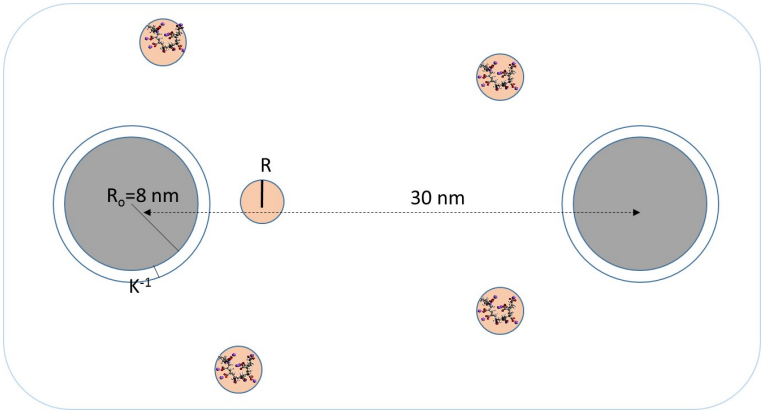

Figure 6.6: Schematic representation of the system of silica LS at $\phi \approx 8$ % with a radius $R_o = 8$ nm, and diffuser with a radius R.

In Fig. 6.7, Jönsson's equation is plotted using ϕ, ϕ_R, and ϕ_κ together with the experimental data of the PA (left) and PCA (right). ϕ_R is calculated using the hydrodynamic radius of the oligomers, R_h obtained from the D_0 of the data in Fig. 6.5 by the Stokes-Einstein equation (Eq. 1.36). The value found for PA is $R_\mathrm{h} = 0.24$ nm and $R_\mathrm{h} = 0.46$ nm for PCA.

To evaluate ϕ_κ, κ^{-1} has been calculated using the concentration of ions used to deprotonate the acid up to pH= 8 ($\sim$ 10 mM) and the concentration of the background salt of the silica suspension after the dialysis ($\sim$ 8 mM). The value found is $\kappa^{-1} = 2.3$ nm.

In Fig. 6.7, one can see that the diffuser size correction by the rescaling ϕ into ϕ_R does not improve the agreement between the experiment and the model. This result is not surprising since the diffuser is rather small compared to the obstacle. The Debye length κ^{-1} however modifies significantly Jönsson equation, and we observe an overlap between $J(\phi_\kappa)$ and the experimental data of PA. Conversely, for PCA, if both corrections produce a visible effect, but none is sufficient to reproduce the data observed. As for PA, the small size of the oligomers makes the correction due to the Debye length higher than the correction of the size.

The disagreement between the experimental data and Jönsson's model, have shown that, besides the effect of the physical volume of the obstacles that modifies the diffusion of the polyelectrolyte, there are other effects that influence the dynamics. In fact, Jönsson's model calculated using ϕ_R and ϕ_κ, have shown the influence of the physical volume of the diffuser and of the interactions.

In the next section, we will study the effects seen in this section, in case of chains with larger molecular weight.

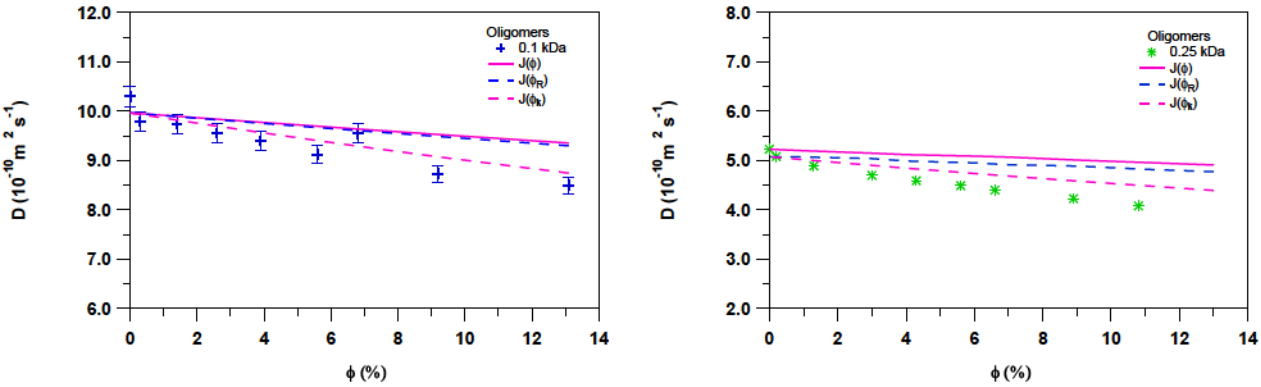

Figure 6.7: *Left:* diffusion coefficient of the PA 0.1 kDa (concentration 0.1 *wt%*) versus the volume fraction of silica LS (blue crosses). Jönsson's model Eq. 2.8 (pink line). $J(\phi_R)$ (blue dotted line), and $J(\phi_\kappa)$ (pink dotted line). *Right:* diffusion coefficient of the PCA 0.25 kDa (concentration 0.1 *wt%*) versus the volume fraction of silica LS (blue crosses). Jönsson's model $J(\phi)$ Eq. 2.8 (pink line). $J(\phi_R)$ (blue dotted line), and $J(\phi_\kappa)$ (pink dotted line). T= 298 K, pH $\approx$ 8.

6.3 | Diffusion of the polyelectrolytes

In this section, we study the impact of the obstacles on the dynamics of PAANa 2.1 kDa and 15 kDa. In these systems, because of the larger molecular size, we expect to observe a stronger effect than the one seen in the previous section.

6.3.1 | Experimental results

In Fig. 6.8, the experimental data of the PAANa 2.1 and 15 kDa are reported, together with the Jönsson's model.

As for the oligomers, the evolution of the diffusion coefficient with the volume fraction of the obtacles is also a linear function of ϕ, and the deviation of the experimental data from Jönsson's model is higher.

To understand the parameters that cause the departure of the data from the Jönsson's model, the experimental data are compared with the Jönsson's models calculated as a function of ϕ_R and ϕ_κ Eq. 6.3 and 6.4 (see Fig. 6.9). κ^{-1} used to calculate ϕ_κ was evaluated with the concentration of the background salt of the silica particle at the end of the dialysis and from the concentration of free counterions of the polyacrylate. The value of Debye length for a polyelectrolyte concentration of 1 *wt%* is κ^{-1} = 1.7 nm (Eq. 1.5).

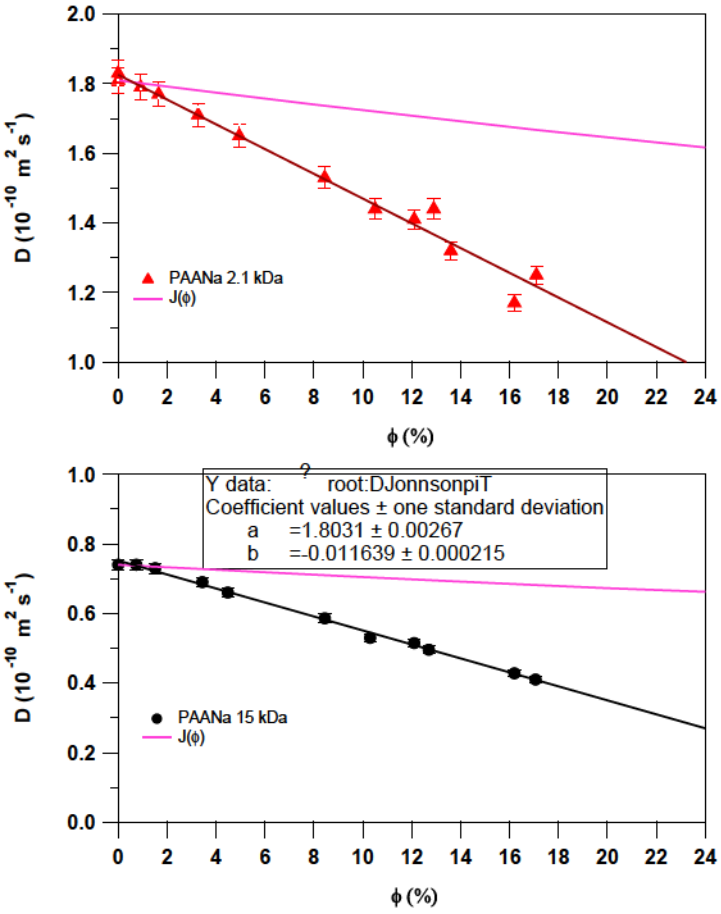

Figure 6.8: *Top:* diffusion coefficient of the PAANa 2.1 kDa (concentration 0.7 *wt%*) versus the volume fraction of silica LS (red triangles). *Bottom:* diffusion coefficient of the PAANa 15 kDa (concentration 0.7 *wt%*) versus the volume fraction of silica LS (black points). Jönsson's model (Eq. 2.8) is reported as reference curve. T= 298 K, pH ≈ 8.

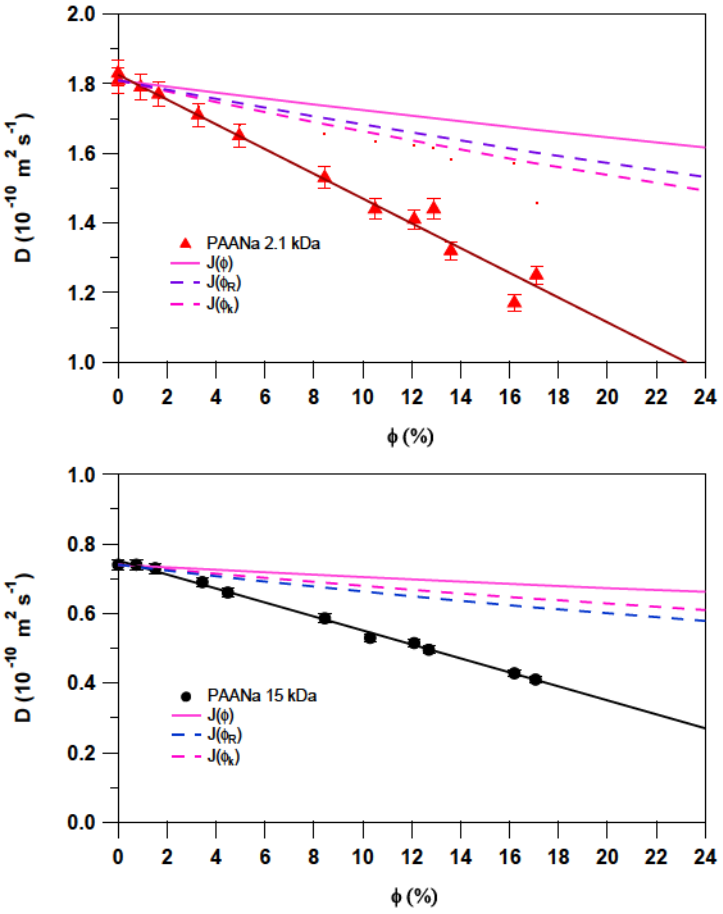

Figure 6.9: *Top:* diffusion coefficient of the PAANa 2.1 kDa (concentration 0.7 *wt%*) versus the volume fraction of silica LS (red triangles). *Bottom:* diffusion coefficient of the PAANa 15 kDa (concentration 0.7 *wt%*) versus the volume fraction of silica LS (black points). Jönsson's model (Eq. 2.8) calculated using ϕ, ϕ_R (Eq. 6.3), and ϕ_κ (Eq. 6.4) are reported. T= 298 K, pH $\approx$ 8.

As for the largest oligomers, if both corrections tends to bring the simple model closer to the experimental data, they fail to achieve a quantitative agreement. For the longer polyelectrolytes (15 kDa), the correction due to the physical volume of the polyelectrolytes is stronger than the effect of the Debye length since the radius (R_h = 2.6 nm) is larger than the Debye length, which is not the case for the smaller polyacrylate (2.1 kDa, R_h = 1.2 nm).

6.3.2 | Comparison with the DLVO cell-model

In this paragraph, we apply the Bell cell model with the DLVO potential (see section 2.5) to estimate the diffusion of the various carboxylate molecules with the charge of silica particles at pH= 8 (section 4.2.2). The diffusion coefficients of carboxylates were calculated using the cell-model to solve the Smoluchowski equation with the DLVO potential. The volume fraction of obstacle was varied from 0 to 0.2. The Debye length used for the calculation was κ^{-1} = 2 nm (Eq. 1.5). The simulated system was at pH= 8, where the charge of the silica nanoparticles of radius R_o = 8 nm is $Z_{\text{eff}} = -119$. The charge of the diffusers are respectively $z = -1$, for the propanoate ion, $z = -2$ for the glutarate ion and $z = -3$ for the 1,3,5-pentanetricarboxylate ion. As mentioned before, for this ions the size effects are neglected.

For the polyelectrolytes, the effective charge was calculated taking into account the effect of the condensation of counterion to yield the following parameters PAA 2.1 kDa: $z = -8$ and R = 1.2 nm; PAA 15 kDa: $z = -53$ and R = 2.6 nm.

The values of the slopes calculated by this method are reported in Table 6.2, together with the slopes extracted by the linear fit (Eq. 6.1) of the experimental data. When the charge of the particle is zero, the slope observed is in good agreement with the result predicted by theories of pure obstruction like Jönsson equation. For charged molecules, the slope increases monotonously with the size and the charge of the diffuser, as the trend observed for the experimental systems. The propanoate exhibit the closest behaviour to the Jönsson's curve while the larger chains are farther from this behaviour.

The agreement of the DLVO cell-model with the experimental data is only semi-quantitative since while the correct order of magnitude and global tendency are recovered, the model fails to fit satisfactorily the values of slope observed. The computed correction is too weak for the small molecules whereas it is too large for the larger polyelectrolyte. The DLVO approximation

	Jönsson	0.1 kDa	0.15 kDa	0.25 kDa	2.1 kDa	15 kDa
A_{exp}	0.5	1.2 ± 0.2	1.9 ± 0.2	1.9 ± 0.2	2.0 ± 0.1	2.7 ± 0.1
A_{DLVO}	0.47 ± 0.02	0.99 ± 0.02	1.37 ± 0.02	1.57 ± 0.02	2.43 ± 0.04	5.51 ± 0.07

Table 6.2: A of the linear fit, Eq. 6.1 and Bell-DLVO model.

might be stronger for the smaller diffusers that are able to explore more easily the region where the approximation fails, and where the real electrostatic potential is higher. For the larger particles, additional effects can be involved, since these molecules are not only larger but, also flexible which might enhance their ability to diffuse, and their diffusion coefficient is not so small compared to the one of the obstacles .

Even if the DLVO cell-model does not achieve a entirely satisfying description of the observed results, it is still a valuable benchmark to compare with. In the remainder of the chapter, we will vary the other parameters of the interaction potential to assess their respective influence.

6.4 | Effect of the change of interactions on the diffusion of polyelectrolytes

6.4.1 | Type of obstacles

One way to change the interactions, is to change the silica nanoparticles that act as obstacles for the diffusers. As seen in chapter 4, changing silica LS nanoparticles, used in the beginning of this chapter, by silica TM nanoparticles modifies not only the size of the obstacles, their radius is 14 nm instead of 8 nm for silica LS, but also their charge. At pH= 8, the long distance effective charge of silica TM is $Z_{\text{eff}} = -244$ instead of $Z_{\text{eff}} = -119$ for silica LS.

In Fig. 6.10, the diffusion coefficients of the 2.1 kDa and 15 kDa, as a function of the volume fraction of the silica TM and LS, are reported. From the graph, the effects caused by the two types of nanoparticles on the diffusion coefficient of polyelectrolytes appears to be very close.

The theoretical slopes were calculated by the Bell cell-model with the DLVO potential as for the smaller LS silica nanoparticles. The values of the slopes issued from a linear fit of the experimental data and of the calculations are reported in Table 6.3.

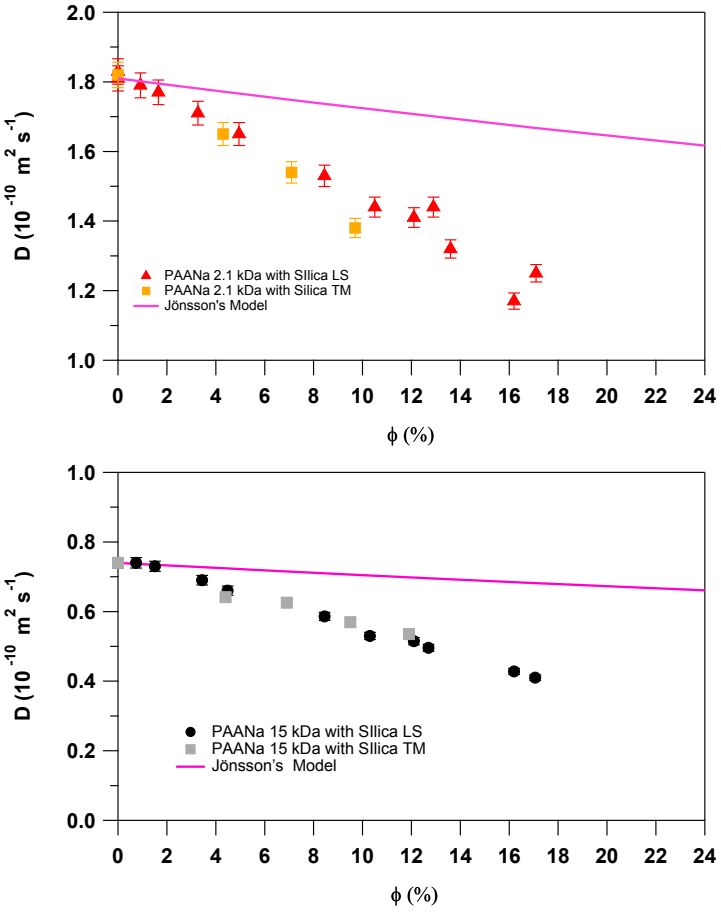

Figure 6.10: *Top:* diffusion coefficient of the PAANa 2.1 kDa (concentration 0.7 *wt%*) versus the volume fraction of silica LS (red triangles) and silica TM (orange squares). *Bottom:* diffusion coefficient of the PAANa 15 kDa (concentration 0.7 *wt%*) versus the volume fraction of silica LS (black points) and silica TM (grey points). Jönsson equation (Eq. 2.8, pink line), is reported as reference. T= 298 K, pH $\approx$ 8.

	2.1 kDa		15 kDa	
	A_{exp}	A_{DLVO}	A_{exp}	A_{DLVO}
LS	2.0 ± 0.1	2.43 ± 0.04	2.7 ± 0.1	5.51 ± 0.07
TM	2.5 ± 0.3	1.35 ± 0.01	2.3 ± 0.2	2.54 ± 0.04

Table 6.3: Slopes issued from the linear fit of data in figure 6.10 (A_{exp}), and theoretical slopes calculated by the Bell cell-model with the DLVO potential (A_{DLVO}).

While no significant difference is observed experimentally, the values calculated by the cell-model suggest a smaller effect of the larger particles. Despite the larger electrostatic charge of the silica TM nanoparticles, the easier diffusion among these obstacles can be explained by the difference of effective volume fractions (see § 6.2.2). For silica LS particle (R_o = 8 nm), both the effective volume fraction taking into account the excluded volume of the diffuser (ϕ_R/ϕ = 2.3 for

PAA 15 kDa), and the effective volume fraction taking into account the Debye length ($\phi_\kappa/\phi \simeq 2$) are larger than for the silica TM particles ($\phi_R/\phi = 1.7$ for PAA 15 kDa, and $\phi_\kappa/\phi \simeq 1.5$). The diffusion is then expected to be faster in a suspension of larger obstacles as the cell-model results suggest, with a decrease of the slope by a factor close to two.

The experimental results surprinsingly do not show any significant difference between the two types of obstacles which implies a contribution to the phenomenon that is not considered in our model.

To explore further the role of the interactions, we will now modulate the electrostatic repulsion with the addition of salt to act on the range of this repulsion and later on with the change of pH to affect the amplitude.

6.4.2 | Screening the interaction by salt addition

In this section, we want to understand the role played by the interaction between diffuser and silica. With this purpose, we change the interaction by screening the charge of the objects with the salt addition, hence reducing the range of the electrostatic repulsion by decreasing κ^{-1}. The diffusion coefficients of the PAANa 2.1 kDa and 15 kDa are studied as a function of the volume fraction of obstacles, in the presence of an added monovalent salt, NaCl. In a second part, the diffusion coefficient of the 15 kDa polyelectrolyte is studied as a function of the added salt concentration at a fixed nanoparticle volume fraction.

In Fig. 6.11, the diffusion coefficients of the PAANa 2.1 kDa (0.7 wt%, top graph) and 15 kDa (0.7 wt%, bottom graph) with 0.1 mol L^{-1} of added NaCl are reported as a function of the volume fraction of silica LS. To point out the effect of the screening of the interactions, the data are compared with the diffusion coefficients without added salt (called also salt-free). In the presence of added salt, the diffusion coefficienf decreases linearly with the increase of the volume fraction of obstacles. The diffusion coefficient exhibit higher values at 0.1 mol L^{-1}, than the system without added salt. For all volume fraction of obstacles, the self-diffusion of the PAANa is remarkably faster in the presence of salt. Because the salt is screening all the electrostatic interactions in the system, the effect of the salt on the PAANa intra-chain interactions, have to be separated from the effects between PAANa and silica nanoparticles.

The increase of the diffusion coefficient of the PAANa in the presence of added salt, have already been observed for the polyelectrolyte without obstacles in Fig. 5.14, where the diffusion coefficient of the PAANa as a function of the added NaCl molarity is shown. In that case, it was demonstrated that the increase of the diffusion coefficient was due to the screening of the intra-chain interactions of the PAANa. However, in the presence of obstacles, we have to consider the effect of the salt on the diffuser-obstacle interactions.

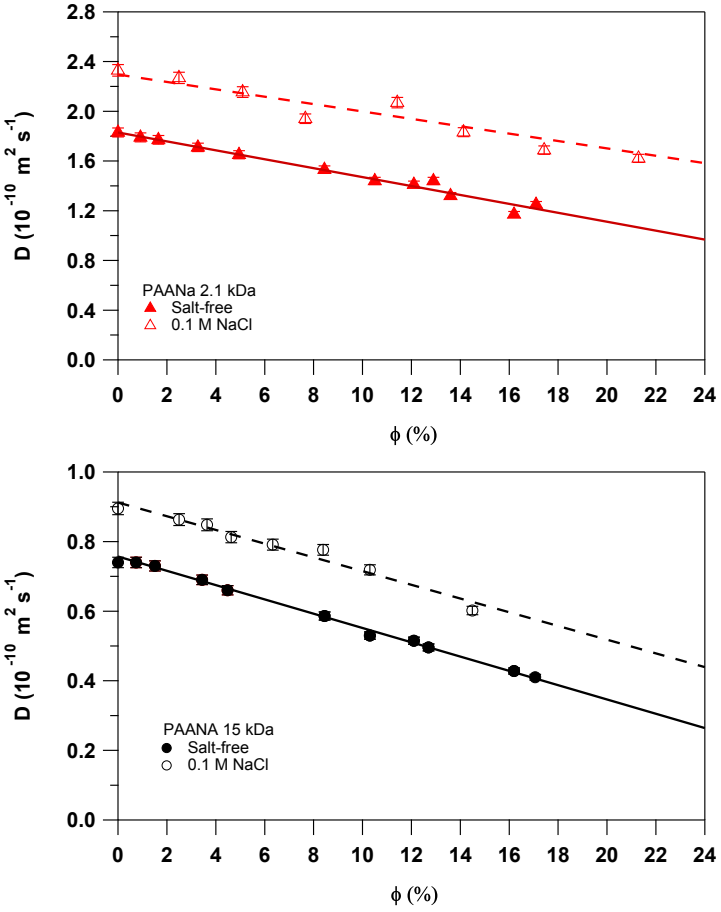

Figure 6.11: *Top:* diffusion coefficients of the PAANa 2.1 kDa (concentration 0.7 *wt%*) versus the volume fraction of silica LS in a salt-free solution (red triangles), and 0.1 mol L^{-1} NaCl (empty red triangles). *Bottom:* diffusion coefficients of the PAANa 15 kDa (concentration 0.7 *wt%*) versus the volume fraction of silica LS in a salt-free solution (black points), and 0.1 mol L^{-1} NaCl (black circles). Data have been fitted with a liner fit (solid line in a salt free solution, dotted lines data at 0.1 mol L^{-1} NaCl) . T= 298 K, pH $\approx$ 8.

To isolate the effect on the dynamics caused by the screening of the polyelectrolyte-silica interactions, the data in Fig. 6.11 are normalised to D_0, the diffusion coefficient in the absence of obstacles. D_0, which depends on the concentration of added salt, is obtained from the intercept value of the linear fit of data in Fig. 6.11. The normalised data are reported in Fig. 6.12.

In Fig. 6.12, an increase of the diffusion coefficient of the polyelectrolyte in the presence of added salt is observed. This increase can only be ascribed to the screening of the diffuser-silica nanoparticle interactions, because the effect of the salt on the intra-chain interactions of the PAANa have been removed with the normalisation. Accordingly the diffusion coefficient with 0.1 mol L^{-1} of added salt get closer to the pure obstruction behaviour (Jönsson's equation).

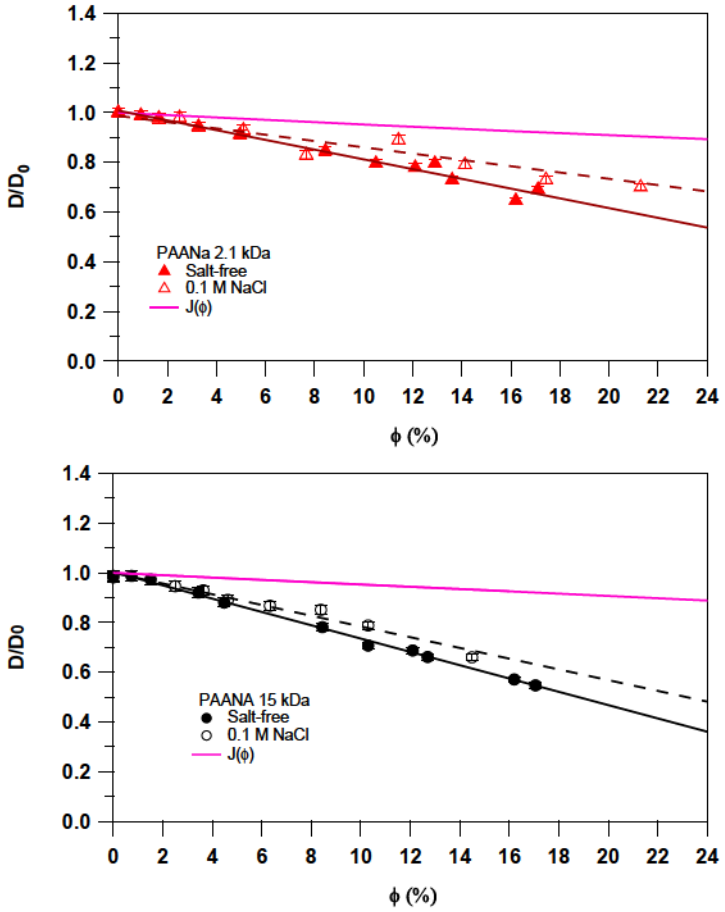

Figure 6.12: Top: normalised diffusion coefficients of the PAANa 2.1 kDa (concentration 0.7 *wt%*) versus the volume fraction of silica LS in a salt-free solution (red triangles), and 0.1 mol L^{-1} NaCl (empty red triangles). Bottom: normalized diffusion coefficients of the PAANa 15 kDa (concentration 0.7 *wt%*) versus the volume fraction of silica LS in a salt-free solution (black points), and 0.1 mol L^{-1} NaCl (black circles). Data have been fitted with a linear fit. The Jönsson's curve calculated using the ϕ (pink line) is reported as reference. T= 298 K, pH $\approx$ 8.

The normalised data in Fig. 6.12, have been fitted with the linear equation (Eq. 6.1). The values of the slope, the A of Eq. 6.1 issued from the fit, are summarized in table 6.4. For both polyelectrolyte sizes, the slope A decreases with the addition of salt. Screening of the repulsive interaction of the silica, the diffusion coefficient of the PAANa increases. When the salt is added,

the effective range of the electrostatic repulsion, the Debye length κ^{-1}, is reduced from 1.7 nm without added salt down to 1.0 nm for 0.1 mol L^{-1} NaCl (Eq. 1.5).

added salt (mol L^{-1})	2.1 kDa		15 kDa	
	A_{exp}	A_{DLVO}	A_{exp}	A_{DLVO}
0	1.9 ± 0.1	2.43 ± 0.04	2.7 ± 0.1	5.51 ± 0.07
0.1	1.3 ± 0.1	1.22 ± 0.01	2.2 ± 0.2	2.43 ± 0.03

Table 6.4: Slope, A of the linear fit, Eq. 6.1 of data in Fig. 6.12.

The slopes were also calculated with DLVO cell-model where the Debye length was changed to $\kappa^{-1} = 0.95$ nm, while keeping the other parameters constants. The corresponding slopes are reported in table 6.4. The decrease of the Debye length indeed makes the diffusion of polyelectrolyte faster thanks to the diminished range of repulsion. The effective fraction changes from $\phi_\kappa/\phi = 2$ to $\phi_\kappa/\phi = 1.4$ which leads to a significant change of the volume accessible to the diffuser where the repulsion is weakened. In addition, for this highly screened regime the agreement of the slopes calculated with the DLVO cell-model and the experimentally measured one improves. Finally, even with this notable concentration of salt added and the ensuing screening of the interaction, its consequence on the diffusion is still measurable and differs from pure obstruction.

Addition of salt at fixed obstacle volume fraction

The behaviour of the diffusion coefficient of the PAANa 15 kDa, at a fixed silica concentration (ϕ=9%), has been studied as a function of the added salt concentration (Fig. 6.13). As in the polyelectrolyte suspension without obstacles (data are also reported in the graph), the addition of salt produces the increase of the diffusion coefficient of the polyelectrolyte, However, in the presence of silica particles, the increase of the diffusion coefficient is slightly higher than in absence of silica. Indeed, in the presence of obstacles, the salt reduce the intra-chain PAANa interactions, as in the case without silica, and but also the silica-PAANa repulsions.

The addition of salt on the diffusion of the propanoate in the presence of silica LS nanoparticles was studied with a similar procedure. For this diffuser, since it is the equivalent of the monomer of the polyacrylate, no intramolecular interaction are present and only the effect of salt addition on diffuser-obstacle interaction can be investigated. The effect of the salt on the diffusion coefficient of the propanoate, have been studied in § 5.3.3.1. It was observed that,

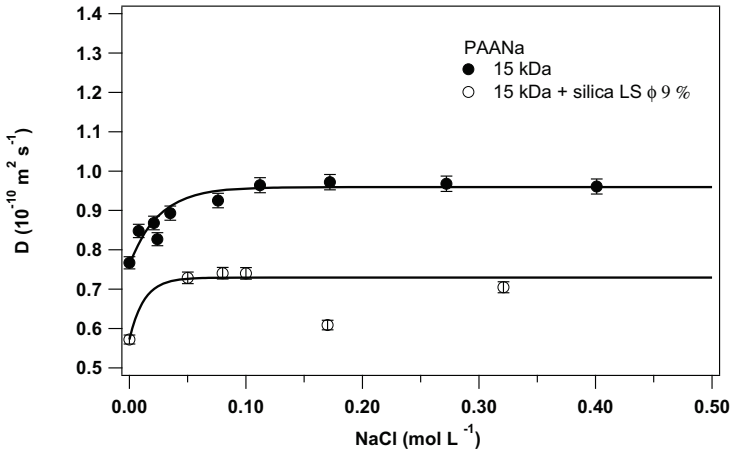

Figure 6.13: Diffusion coefficients of the PAANa 15 kDa (concentration 1.5 *wt%*) in a silica LS suspension (ϕ= 9%), as a function of the molarity of NaCl of the solution. The lines are guides to the eye. $T = 298$ K, pH $\approx$ 8.

instead of the PAANa, the diffusion coefficient decreases with the addition of salt. This effect was associated with the variation of the viscosity of the solvent.

In Fig. 6.14, the diffusion coefficients of the propanoate (0.5 wt%) with silica LS nanoparticles ($\phi = 5\%$) and without obstacles, are reported as a function of the added NaCl concentration. The diffusion coefficient also decreases with the addition of salt in the presence of nanoparticles. When diffusion coefficients are rescaled with the value at zero added salt concentration, no significant differences appear between the reduced diffusion coefficients. The effect of addition of salt on the diffusion of the propanoate among silica LS nanoparticles was also calculated using the DLVO cell-model. A change of diffusion was observed after this addition but its amplitude was of the order of 1 % (for ϕ = 5 %) which lies below the experimental uncertainty of our measurements.

6.4.3 | Changing the state of charge with pH

In this section, we study the effect of the charge variation on the dynamics of the diffuser by pH variation. Indeed by changing the pH of the solution, we change not only the charge of surface of the obstacles, as observed in Fig. 4.10, but also the charge of the diffuser since we are working with weak polyelectrolytes. As a result, the predominant electrostatic repulsion at high pH values can be progressively weakened by decreasing the pH to reach a state of uncharged

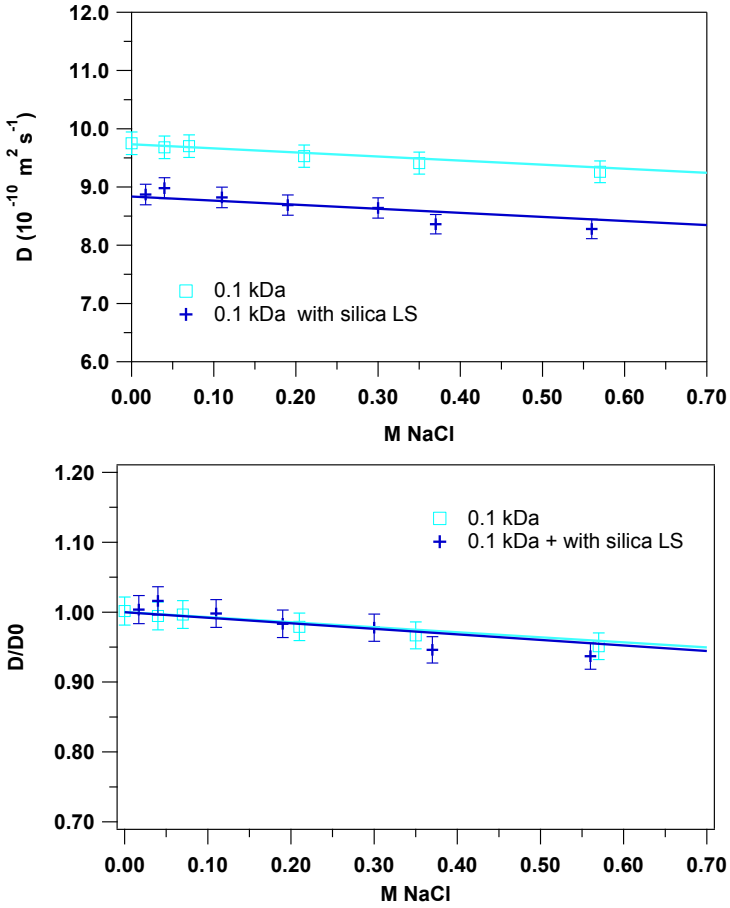

Figure 6.14: *Top:* diffusion coefficient of the acid propionic (0.1 kDa, 0.3 *wt%*) in water solution without (blue cross) and with silica LS nanoparticles (light blue square, ϕ=5%), as a function of the molarity of NaCl. *Bottom:* diffusion coefficients normalised by the salt free values.

obstacles for low pH values. For these low pH values, the regime of pure obstruction might be observed.

In Fig. 6.15 (top), the diffusion coefficient of the PAANa 15 kDA as a function of the pH is reported for three systems: without silica (black point), and with silica a two volume fractions ϕ = 3 % (black circle) and ϕ = 9% (green square). All the diffusion coefficients decreases with a sigmoidal behaviour with the pH. As observed previously, the diffusion coefficient decreases with the concentration of obstacles. For a fixed volume fraction of obstacles, the decreases of the diffusion coefficient is function of the pH: it is stronger at high pH, and achieves the lowest value at low pH. At high pH, the charged diffuser is influenced by a charged particle with the same charge; instead a low pH the diffuser is influenced mainly by the physical volume of the obstacle, since both the chain and obstacle are uncharged.

In the low pH limit, the diffusion coefficient in the presence of the silica nanoparticles

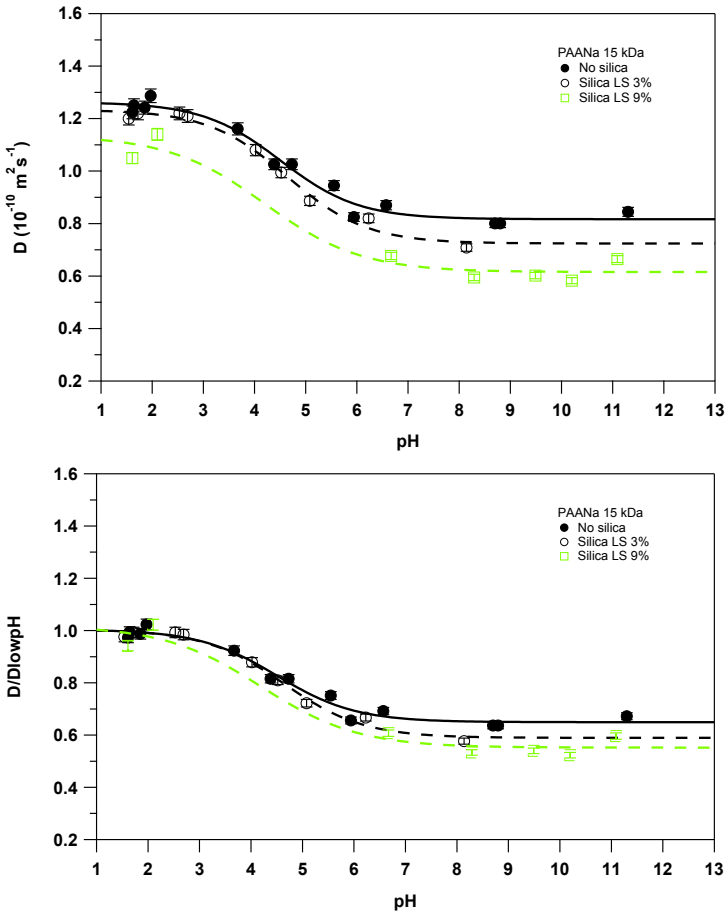

Figure 6.15: *Top:* diffusion coefficient of PAANa 15 kDa (~ 0.7 %) vs pH, without obstacles (black points), with silica LS ϕ 3 % (black circles), and silica LS ϕ 9 % (green circles). *Bottom:* previous data normalised at the corresponding diffusion coefficient a low pH. T= 298 K.

decreases of 2 % for $\phi = 3\%$ and 11 % for $\phi = 9\%$, compared to the value of the diffusion coefficient without nanoparticles. Using the expression accounting for the excluded volume of both diffuser and obstacles, $D = D_0(1 - \frac{1}{2}\phi_R)$ (Eq.6.3), we obtain comparable values with the experimental data at pH=2 for the two volume fractions of silica nanoparticles. We can conclude that at low pH the diffusion coefficient is affected mainly by the physical volume of the objected presents in solution.

If the data are normalised by the low pH value of the diffusion coefficient (Fig. 6.15, bottom), the effect of the interactions can be revealed. The difference with the diffusion coefficient without obstacles increase with the pH and with the concentration of obstacles.

To isolate the contribution of the obstacles from the effect of the change of the diffusion coefficient of the polyacrylate with pH, the diffusion coefficients of the previous graphs were divided by the latter. The reduced diffusion coefficient are reported Fig. 6.16. It is visible that

the interactions of the silica start to be significant at pH $\sim$ 5 for the less concentrated system in silica nanoparticles.

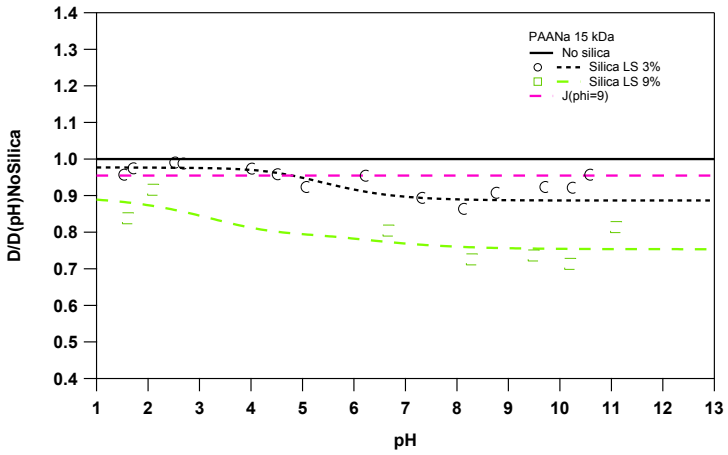

Figure 6.16: Diffusion coefficient of PAANa 15 kDa ($\sim$ 0.7 %) vs pH, normalised at the diffusion coefficient at the same pH without obstacles: system without obstacles (black line), with silica LS ϕ 3 % (black circles, dotted line), and silica ϕ 9 % LS (green circles, dotted green line), $J(\phi)$ (dotted pink line). T= 298 K.

In Fig. 6.16, the Jönsson equation $J(\phi)$ is also plotted for $\phi = 9\%$, as a reference where only the physical volume of obstacles is considered. We observe that the relative values of the diffusion coefficient are close to this model only at low pH. A higher pH values, when the electrostatic interactions become notable, the diffusion is significantly diminished and departs from this equation.

To study this effect on a simpler system, the effect of the pH on the diffusion of the oligomers is shown in Fig. 6.17. The diffusion coefficients of propionic acid, glutaric acid, and 1,3,5-pentanetricarboxylic acid in the presence of silica LS, are presented as a function of the pH (the normalised data are shown in the bottom figure). The data are compared with the measurements in absence of silica (only in the top graph). As observed previously (Fig. 6.5), the presence of silica decreases the diffusion coefficient of the oligomers at all pH. As for the system without obstacles, the diffusion coefficient has a sigmoidal behaviour with pH. However contrarily to the PAANa, the effect of pH on the silica does not seem to have a strong impact on the oligomers, the decrease of the data in presence of silica is not function of pH. In other words, whatever the value of pH the relative reduction of the diffusion coefficient due to the presence of obstacles appears constant within the experimental uncertainty. To have a different point of view on this phenomenon, this relative change was computed for the monomer (propionic acid) with the

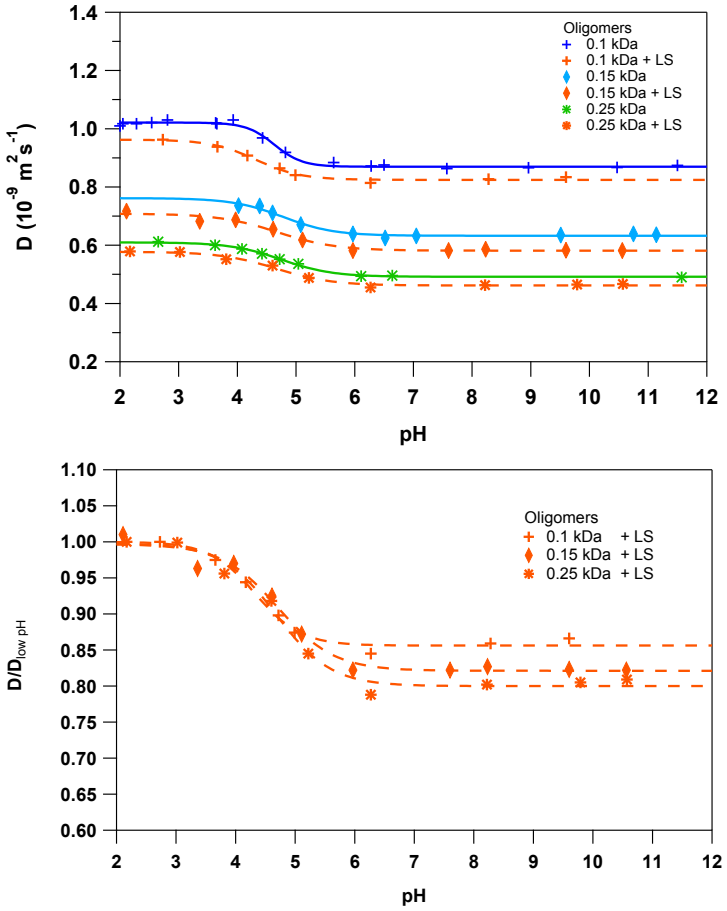

Figure 6.17: Top: diffusion coefficient of carboxylic acids vs pH: propionic acid (N = 1, 1*wt%*; blue vertical cross), glutaric acid (N = 2, 1*wt%*; light blue rhombus), 1,3,5-pentanetricarboxylic acid (N = 3, 1*wt%*; green star). Diffusion coefficient of carboxylic acids vs pH in the presence of silica LS (ϕ=5%): propionic acid (N = 1, 0.5 *wt%*; orange vertical cross), glutaric acid (N = 2, 0.5 *wt%*; orange rhombus), 1,3,5-pentanetricarboxylic acid (N = 3, 0.5*wt%*; orange star). Data have fitted with a sigmoidal curve: system without silica (continuous line) and with silica (dotted lines). Bottom: normalised diffusion coefficient of the previous data in presence of silica. T= 298 K.

DLVO cell-model at ϕ = 5%. The dependence with pH of both the effective charge of the nanoparticle Z_{eff} (Fig. 4.12) and the charge of the diffuser (Fig. 4.9) was accounted for in this modelling. The data are plotted in Fig. 6.18.

The effect calculated with the DLVO cell-model for the propanoic acid seems to exits but its extent appears to be rather small compared to the experimental uncertainty of the experiment. On top of that, so far, specific interactions such as the adsorption of the diffuser onto the silica particles have been disregarded. If at high pH, the strength of the electrostatic repulsion would act again this phenomenon [277], it is no longer the case when the charge of the nanoparticles

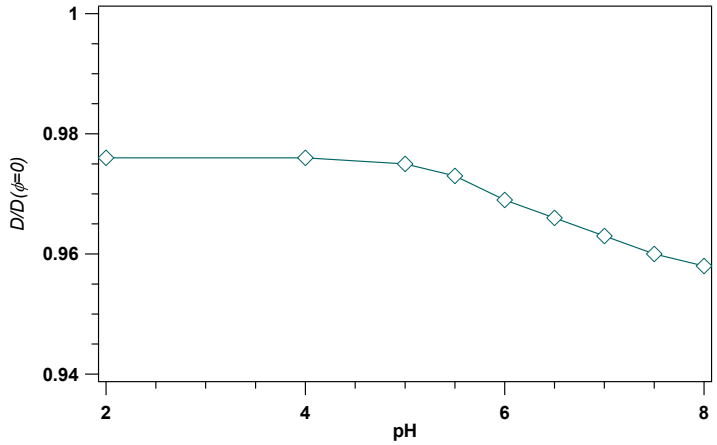

Figure 6.18: Diffusion coefficient of the propanoic in a suspension of LS silica nanoparticles (ϕ = 5%) divided by the coefficient without silica nanoparticles vs pH. Data calculated with the DLVO cell-model.

vanishes at low pH values. In the case of adsorption, the diffusion coefficient depends on the volume fraction of obstacles as described in section 2.3. However, without knowing the quantity of adsorbed oligomers is not possible to evaluate the diffusion coefficient using the model based on chemical binding.

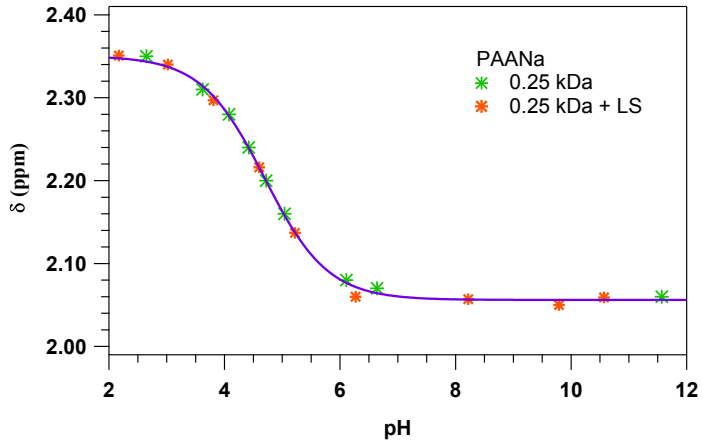

Figure 6.19: Chemical shift δ (ppm) versus pH value of α proton of the 1,3,5-pentanetricarboxylic acid, without silica (N = 3; green star), and with silica (ϕ=5%, orange star). T= 298 K.

To test the occurrence of adsorption at low pH, a closer look at the NMR spectra was performed. First, the chemical shifts of the oligmers as a function of the pH were examined. The evolution of the chemical shift of the α proton of the 0.25 kDa oligomer with and without obstacles is reported in Fig. 6.19. As for the other oligomers, the presence of silica nanoparticles

does no affect notably the chemical shift. If a significant adsorption occurred, the environment of the spins would be in average different from the environment in solution and the chemical would be affected, but it is not observed for the present system.

Another observable consequence of a strong adsorption on the NMR spectrum would be a significant decrease of the area. If the molecule are bound to the very slowly moving nanoparticles, its transverse relaxation time T_2 will fall steeply due to the slow dynamics. As a consequence, a part of the intensity of the peak will be lost in the baseline in the spectra and the integration of the peak will decrease. If adsorption is not so strong and the T_2 not short the peak will only widen. Such a widening has been detected both at high and low pH values but it can also be ascribed to the internal gradients of magnetic field due to the presence of the nanoparticles.

Summary of Chapter 6

The impact of charged obstacles on the dynamics of the polyelectrolytes have been investigated, by the study of the self-diffusion coefficient of carboxylate (from the simple propionate to the sodium polyacrylate) in a suspension of homogeneous and dispersed obstacles (silica nanoparticles with different sizes and surface charge).
The increase of the volume fraction of negative charged obstacle causes a linear decrease of the diffusion coefficient of all studied oligomers and PAANa, in the range of ϕ studied. Furthermore, the data depart from Jönsson's model, which describes the behaviour of the diffusion coefficient in presence of uncharged spherical obstacles.
A semi-quantitative agreement between the DLVO cell-model with the experimental data has been found. While the correct order of magnitude and global tendency of experimental data are recovered, the model fails to fit satisfactorily the values. However, the DLVO cell-model is still a valuable benchmark to compare the experimental data.
To assess the influence played by the interactions, they have been screened by addition of salt or modified by the variation of pH. The addition of salt, decreasing the Debye length, makes the diffusion of the PAANa faster thanks to the diminished range of repulsion, as a consequence the data are closer to the Jönsson's model. In addition, for this highly screened regime the agreement DLVO cell-model and experimental data improves.
By changing the pH of the solution, we change not only the charge of surface of the obstacles but also the charge of the diffuser, since we are working with weak polyelectrolytes. Then, the predominant electrostatic repulsion at high pH values can be progressively weakened by decreased the pH to reach a state of uncharged obstacles for low pH values, where the regime of pure obstruction might be observed.
In presence of silica the diffusion coefficient decreases with a sigmoidal behaviour with the pH. At low pH, the diffusion coefficient is affected mainly by the physical volume of the objected presents in solution. At high pH, the objects are strongly charged, so the decrease of the diffusion coefficient is higher than a low pH because the presence of the interactions. For the oligomers, the effect of pH on the silica does not seem to have a strong impact on the dynamics. It appears to be rather small compared to the experimental uncertainty of the experiment, as the DLVO cell-model suggests.

Chapter 7

Small-Angle Neutron Scattering investigation of polyelectrolyte-nanoparticle mixtures

Contents

This chapter investigates the phase behaviour of silica nanoparticles in the presence of polyelectrolytes, the PAANa. For that purpose, the system is studied by small-angle neutron scattering (SANS). SANS is well suited to study colloidal systems and their dispersion state, since it allows to probe a large range of length scales, from a few to several hundred *nm* [278].

The basic principle of SANS is the following: the neutrons go through a sample and they are elastically scattered by atomic nuclei, and the neutrons scattered at small angles are recorded. The scattering intensity depends on the scattering length densities of the system, which can be modified by changing the isotopic composition, this process is known as *contrast variation*. The difference between the scattering length densities of hydrogen and deuterium can be used to have a solvent with an isotopic composition enabling to isolate the scattering contribution of polyelectrolyte or colloidal particles in a mixed system. Then, the central role of SANS compared with other small angle techniques as small-angle X-ray scattering, is due to this contrast variation method, that allows to switch on or off a part of the system. Furthermore, the particle size, the dispersity, and other properties can be derived by fitting the scattered intensity.

One of the particularity of neutron scattering, it is that the scattering probability, proportional to a quantity called cross-section, does not scale with the atomic number. For neutrons, heavy and light elements can have comparable cross-sections. That is the reverse that for X-rays, for which the cross-section is proportional to the atomic number: the light elements are almost invisible in X-ray investigations, especially if heavy ions are presents. On the contrary, there is a priori no obstacle to observe light atoms with neutrons, this is a valuable advantage of the neutron technique.

The measurements have been performed with the spectrometer D33 (ILL) [279]. Due to the different length scales in the structure of the samples, a broad q range, from 10^{-3} to 0.5 Å^{-1} have been explored.

The chapter starts with a general introduction on the technique of neutron scattering concerning its main properties, and an introduction to SANS, with a particular attention to the contrast variation technique. After having characterised the system of polyelectrolytes and silica nanoparticles, the effect caused by the PAANa on the behaviour of the silica dispersions is investigated.

7.1 | Basic concepts of neutron scattering

The absorption, transmission and scattering of neutrons allow a non-destructive investigation of materials and the investigation of the atomic structure and dynamics of the condensed matter. The usefulness of neutrons arises from its basic properties [280–282]. The value of the mass of the neutron ($m_n = 1.68 \times 10^{-27}$ kg) makes the wavelength (λ) of thermal neutrons (average energy of 25 meV) of the order of inter-atomic distances. Thus, the interference effects can yield information on the structure of the scattering system at this lengthscale. Indeed, the neutrons can also be considered as plane waves with a de Broglie wavelength of:

$$\lambda = \frac{h}{m_n v} \tag{7.1}$$

where $h = 6.63 \times 10^{-34}$ J·s is the Planck′s constant, and v the velocity of the neutron. The neutrons used in our experiments have wavelengths λ of 8 and 13 Å, corresponding to neutrons with a mean velocity of 0.49 and 0.31 km s^{-1}.

Because the neutron is an uncharged particle, it penetrates deeply into the matter, since there is no Coulomb barrier to overcome. Therefore, it interacts strongly with the nuclei and it is thus scattered by nuclear forces, a very short range interaction. This interaction depends on the scattering length of the nucleus, quantity that we will discuss in the next section.

The difference between the incident and scattered wave vector is the scattering vector $\vec{q}$, whose magnitude is defined as:

$$q = \frac{4\pi}{\lambda} \sin\theta \tag{7.2}$$

where λ is the wavelength of the incident beam, and θ the angle between incident and scattered beam. The corresponding correlation length d can be obtained as:

$$d = \frac{2\pi}{q} \tag{7.3}$$

The q range covered during the experiments, from 10^{-3} to 0.5 $Å^{-1}$, allows to investigate a range of length from 1.3 to 630 nm. The range of q studied has been covered in three instrument settings on D33: $\lambda = 13$ Å, and $D = 12$ m (distance sample-detector) , small angle configuration; $\lambda = 8$ Å, $D = 12$ m, medium angle configuration; $\lambda = 8$ Å, $D = 2$ m large angle configuration.

7.1.1 | Scattering length

The probability of scattering is related to the scattering length b, which describes the character and the strength of the neutron-nucleus interaction [280]. The scattering length b, which can varies drastically between isotopes, depends on the particular nucleus and on the spin state of the nucleus-neutron system. To clarify the last concept, we can consider the following example. Suppose a nucleus with spin $I \neq 0$. The spin S of the nucleus-neutron system is $S^+ = I + \frac{1}{2}$, or $S^- = I - \frac{1}{2}$ since the neutron has a spin $\frac{1}{2}$. Therefore, in this case, there are two scattering lengths b_i, associated with the two possible spin states. The average of all scattering lengths b_i is called the coherent scattering length:

$$b_{\text{coh}} = \langle b_i \rangle \tag{7.4}$$

The root mean square deviation of b_i from $\langle b_i \rangle$ called the incoherent scattering length:

$$b_{\text{inc}} = \sqrt{\langle b_i^2 \rangle - \langle b_i \rangle^2} \tag{7.5}$$

The results of neutron measurements can be written as a sum of coherent and incoherent scattered intensity, proportional to b_{coh} and b_{inc}. The coherent scattering, depends on the correlation between positions of same and different nuclei, it depends on the values of b_{coh} for each nucleus, and it gives interference effects due to the correlation between the nuclei. The incoherent scattering depends only of the position of the same scattering nucleus, it depends on b_{inc}. It does not give interference effects with waves scattered by different atoms. Because we want to characterise the structure and conformation, in our experiments we will focus only on the coherent scattering. The incoherent scattering will be a background, arising mainly from the solvent.

7.1.2 | Scattering length density

At small q, that is to say large correlation distances, atomic descriptions are no longer relevant and can be replaced by coarse-grained or averaged description. For small angle scattering, the *contrast approximation* that consider a continuous scattering medium instead of atomic scatterers is a good approximation up to $q = 0.6$ Å^{-1} [283]. The atomic scattering length b is then replaced

in this coarse-grained description by the *scattering length density* (SLD), which is the volume averaged density of scattering lengths. For example, in a molecule with x_i atoms i, and molecular volume v_p, the SLD ρ_p is defined as [282]:

$$\rho_p = \frac{\sum_i x_i b_{\mathrm{coh}i}}{v_p} \tag{7.6}$$

where b_{coh_i} is the coherent neutron scattering length of atom i. b_i can vary drastically between two isotopes, as in the case of the hydrogen and deuterium. This last property is one of the main advantage of the neutron experiments, because it opens the possibility of the contrast variation. The substitution of one atom with one isotope, can change strongly the scattering length of the system and, assuming that no drastic variation of the other physical properties of the system occur, the system can be studied in the same conditions but with another point of view.

7.2 | Small-angle neutron scattering

The SANS experiment allows to extract the shape and the structural organisation of particles or aggregate dispersed in a continuum medium [284]. It is a suitable technique for many systems, ranging from small colloidal particles to proteins. From the interference of coherent scattering, correlation functions can be extracted which gives information on the shape of the colloidal scatterers (intraparticle correlation) or the organisation and interaction of the particles (interparticle correlations).

7.2.1 | Scattering intensity and contrast variation

In SANS experiments, we will study the different elements of the system by playing with the contrast matching approach. In the following we will see mathematically and experimentally the application of this approach [284, 285].

In the case of a system consisting of one type of particle (2) in a solvent (1), as in the case, treated in the next sections, were silica nanoparticle or polyelectrolytes are dispersed alone in the solvent, the scattered signal $I(q)$ measured by the detector is equal to [284]:

$$I(q) = (\rho_2 - \rho_1)^2 \phi v_2 \mathcal{S}_{22}(q) \tag{7.7}$$

where ϕ is the volume fraction of the particles, v_2 the molecular volume of one particle, ρ_i is the SLD of the particle (2) or solvent (1), and $\mathcal{S}(q)$ is a nondimensional scattered intensity depending on the intra- and inter-particle correlations.

More specifically, for homogeneous isotropic scatterers in a solvent the intra- and inter-particle interferences are not correlated and, the Eq. 7.7 can be rewritten as:

$$I(q) = (\rho_2 - \rho_1)^2 \phi v_2 \mathcal{S}_{22}(q) = (\rho_2 - \rho_1)^2 \phi v_2 S_{22}(q) P_2(q) = (\rho_2 - \rho_1)^2 c_2 v_2^2 S_{22}(q) F_2(q)^2 \quad (7.8)$$

where ϕv_2 is equal to $c_2 v_2^2$ (c_2 is the concentration of particle 2); $\mathcal{S}_{22}(q)$ is equal to $S_{22}(q)F_2(q)^2$. $S_{22}(q)$, called in the following only $S(q)$, is the structure factor that contains the interparticle correlations and $F_2(q)^2 = P_2(q)$ is the form factor of the particle that reveals the intraparticle correlation.

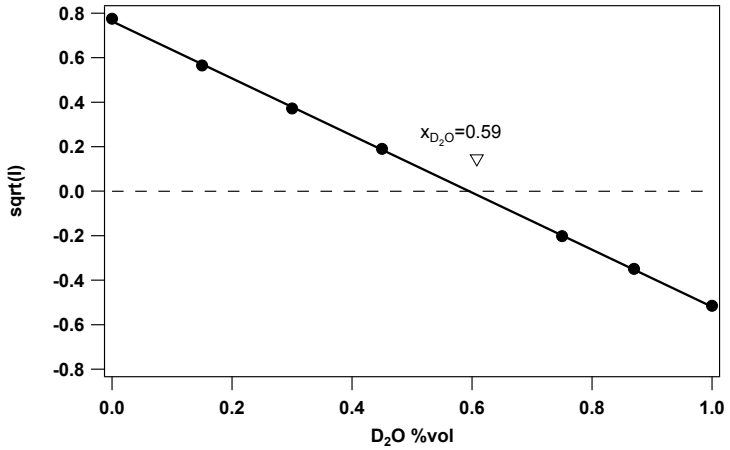

Figure 7.1: Contrast variation experiment from an aqueous solution of silca LS. Square root of the intensity versus the volume fraction of D_2O.

Changing the isotopic composition of the solvent varies the scattering density ρ_1 and the contrast between the solvent and the scatterer $(\rho_2 - \rho_1)$. It is then possible to change the intensity of the measured signal. If ρ_2 has a value that lies between ρ_{H_2O} and ρ_{D_2O}, there exists a composition for which the scattered intensity is equal to zero, called composition of the contrast match. In Fig. 7.1, the contrast match solvent composition was determined for the silica nanoparticles. The intensity of the silica signal decreases with the fraction of D_2O until it vanishes for a fraction of D_2O of 59 %. At the contrast match point, the SLD of the solvent is equal to that of the scatterer and no signal is measured. The values after the contract match point are reported in negative values to fit purpose.

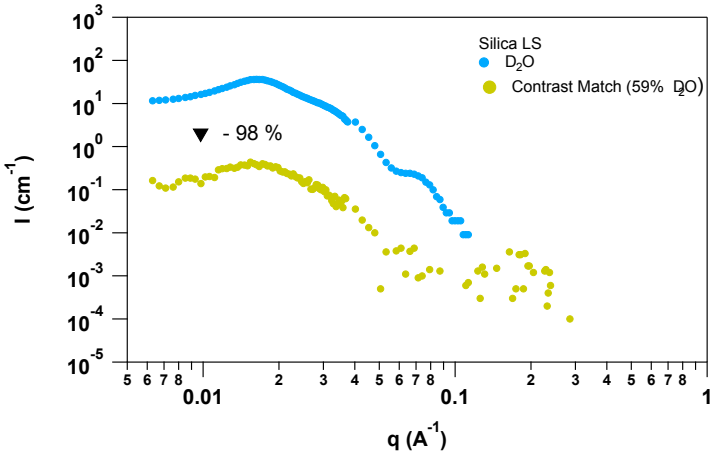

Figure 7.2: SANS data of silica LS ϕ =3% in D_2O pH 10 (blue points), and in contrast match with the solvent (59 % D_2O, 41% H_2O).

In the reality, it is difficult to match perfectly the contribution of a scatterer even if the intensity can still be substantially reduced. As shown in Fig. 7.2, the signal of the silica is reduced by 98 % in a solution of 59 % of D_2O, respect to the signal in 100 % D_2O.

In the next paragraph, we will see how to use the contrast variation technique for a mixture of three components.

Mixture of three components

When there are two scattering objects (2) and (3), as in the case of the system under study made of nanoparticles and polyelectrolytes, the situation is more complex [285, 286]. The Eq. 7.8 has to consider the interference between same and different kinds of particles:

$$I(q) = \sum_{i,j=2}^{3}(\rho_i - \rho_1)(\rho_j - \rho_1)\sqrt{c_i c_j}v_i v_j \mathcal{S}_{ij}(q) = \tag{7.9}$$

$$= (\rho_2 - \rho_1)^2 c_2 v_2^2 \mathcal{S}_{22}(q) + (\rho_3 - \rho_1)^2 c_3 v_3^2 \mathcal{S}_{33}(q) + (\rho_2 - \rho_1)(\rho_3 - \rho_1)\sqrt{c_2 c_3}v_2 v_3 \mathcal{S}_{23}(q)$$

with $\mathcal{S}_{ij}(q) = F_i(q)F_j(q)S_{ij}(q)$ when intra- and interparticle correlations can be factorized (centrosymmetric scatterers). Every term is weighted by the contrast factor of the scatterer relative to the solvent $\rho_i - \rho_1$. Looking at the Eq. 7.9, it is possible to see the usefulness of the contrast variation. Changing the value of ρ_1, the SLD of the solvent, by mixing light and heavy water, it is possible to adjust the pre-factor $(\rho_i - \rho_1)$. It is then possible to cancel one contribution in the mixture and isolate the scattering arising from only an element of the mixture

of the complex system. Below, we will see how by a suitable mixture of H/D molecules, is possible isolate each contribution.

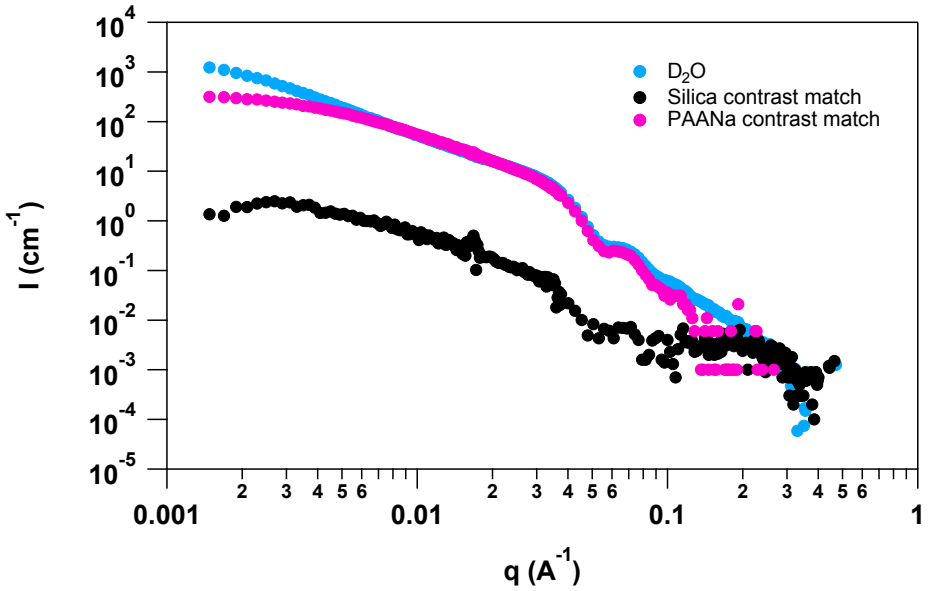

Figure 7.3: SANS data of PAANa 15 kDa 3 *wt%* and silica LS ϕ =3%, a different contrast. Full signal (D_2O, blue points); silica contrast match (59 % D_2O 41 % H_2O, pink points); PAANa contrast match (43 % D_2O 57 % H_2O, black points). pH 4, T=298 K.

In Fig. 7.3, the contrast variation technique is used for a mixture of silica LS and PAANa in water solution. The full signal, the signal coming from all scatterers, is observed when the solvent is D_2O. Mixing heavy and light water, it is possible to isolate the contribution arising only from silica or PAANa. At the silica contrast match condition, the ratio of heavy water is 59 % respect to the all solvent, the signal of the silica is almost completely hidden (as observed in Fig. 7.2 there is still a 2% of the signal coming from the silica). If the remaining signal of the silica is not predominant, then the main contribution arises from the PAANa. Conversely, at the PAANa contrast match, 43 % of D_2O at pH 4, the signal of the PAANa is masked. It is important to point out that the SLD of the PAANa is pH dependent, because the molecular volume of the PAANa changes with the pH [287, 288]. As shown in Fig. 7.4, where the SLD of the system studied are reported as a function of the pH.

The contrast variation technique offers then the possibility to study the behaviour of a same object in complex systems. In the case of a system of silica and PAANa, we will use this technique to observe only the effects caused by PAANa on the silica, masking the scattering contribution of the PAANa, or vice versa.

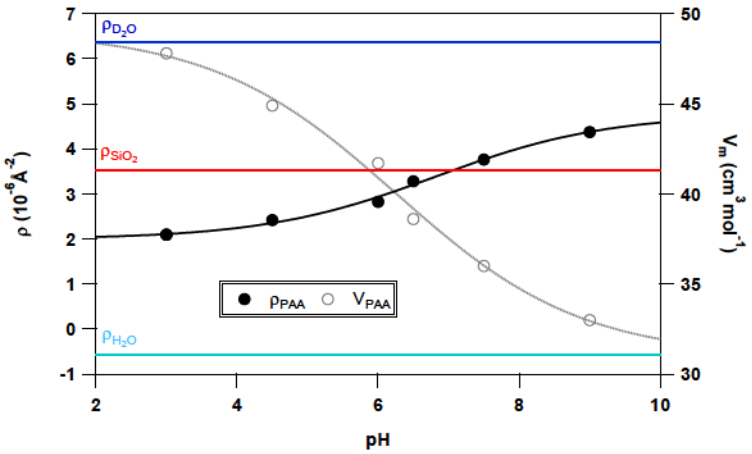

Figure 7.4: SLD of the D_2O (blue line), SiO_2 (red line), H_2O(light blue line), and PAANa (black curve), as a function of the pH. The molecular volume of the PAANa is shown (black dotted line) [287].

7.2.2 | Corrections of raw data

Before the data analysis, the reduction of raw data is a crucial step [284]. The SANS data have been treated before data analysis with LAMP, a data treatment program developed at ILL. Preliminary measurement of empty cell, incident flux, light water, and transmission have been performed at the beginning of the experiments.

The scattering from the empty cell is substracted from the total scattering signal, to remove the scattering contribution arising from the quartz cell (we have used a cell with a thickness of 1 mm). The intensity measurement have to be normalised with the value of the incident flux. The incident flux is the number of neutrons per second at the sample position for a given aperture. It is measured using the direct beam on the detector through a calibrated attenuator. The data are normalised with the value of solid angle to be corrected from geometric distortion of the measurement. A sample of light water is used for an absolute scaling and to correct the variations in efficiency of the detector. The water is used as standard because the liquid is homogeneous at the SANS scale and it has a strong incoherent scattering. As a consequence the scattered intensity does not depend on the value of the scattering wavevector q. The data are normalised with the transmission, obtained from the ratio of the intensity of the neutron beam through the sample and the white beam. Finally, the incoherent scattering, coming mainly from the hydrogen molecules of the solvent, that gives a flat background, have been subtracted. This value is estimated with the measurement at the highest scattering vector since it is independent

on q. In all analysis, we neglect the contribution to the scattering intensity arising from the small ions. This is justified because their SLD is small compared to those of main scatterer objects [289].

The data analysis and fitting of the scattering curves was performed with the `SasView` software.[1]

7.3 | Polyelectrolytes

In this section, we use SANS to study the structure of the polyelectrolytes alone [278, 290], in a q region from 0.001 to 0.3 Å^{-1}, corresponding to a correlation distances from 1.3 to 630 nm. We obtained structural information of the chain as the radius of gyration (section 1.3), and the Porod exponent that is related to the conformation of the chain.
The scattering intensity of the PAANa 15 kDa at 10 *wt%* in D_2O at pH = 2 is shown in Fig. 7.5. D_2O is used as solvent for better contrast with the polyelectrolytes and lower incoherent background scattering from the solvent.

The model used to fit the data is the polymer excluded volume model. This model describes the scattering from polymer chains subject to excluded volume effects [291, 292]:

$$P(q) = 2\int_0^1 (1-x)\, \mathrm{e}^{-\frac{q^2\ell_s^2}{6}N^{2\nu_p}x^{2\nu_p}}\mathrm{d}x \tag{7.10}$$

$$= \frac{1}{\nu_p U^{\frac{1}{2\nu_p}}}\gamma\left(\frac{1}{2\nu_p}, U\right) - \frac{1}{\nu_p U^{\frac{1}{\nu_p}}}\gamma\left(\frac{1}{\nu_p}, U\right) \tag{7.11}$$

where $\gamma(x, U)$ is the incomplete gamma function:

$$\gamma(x, U) = \int_0^U \mathrm{e}^{-t}t^{x-1}\mathrm{d}t \tag{7.12}$$

and U can be expressed in terms of the scattering vector q as:

$$U = \frac{q^2\ell_s N^{2\nu_p}}{6} = \frac{q^2 R_\mathrm{g}^2\left(2\nu_p+1\right)\left(2\nu_p+2\right)}{6} \tag{7.13}$$

[1] `SasView`, `http://www.sasview.org/`
`SasView` software is an open source, collaboratively developed software for the analysis of small angle scattering data and was originally developed by the DANSE project under NSF award DMR-0520547

The form factor is then dependent on ν_p, that is the inverse of the Porod exponent or fractal dimension ($m_{\text{Porod}} = 1/\nu_p$), the statistical segment length of the polymer chain (ℓ_s), and on the degree of polymerization N. ν_p reminds the exponent ν, described in section 5.3.1, that relates the diffusion coefficient with the molecular weight ($R_{\text{h}}(M) \propto M^{\nu}$). However, the two exponents, ν_p and ν, coincide only in the asymptotic limit of long chain ($N \to \infty$) [98]. In this model, the gyration radius R_{g}, is defined as:

$$R_{\text{g}} = \ell_s \sqrt{\frac{N^{2\nu_p}}{\left(2\nu_p + 1\right)\left(2\nu_p + 2\right)}} \tag{7.14}$$

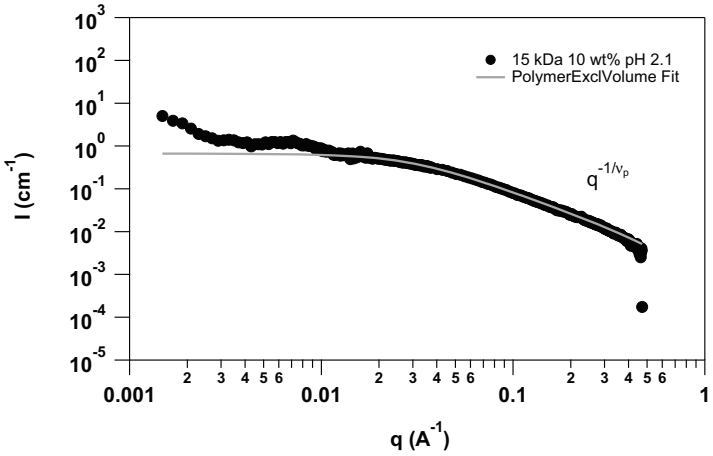

Figure 7.5: SANS data of PAANa 15 kDa (10 *wt%*) in D_2O pH 2.1, fitted to a polymer excluded volume model [292]. T=298 K.

The data are well fitted at high q ($qR_{\text{g}} > 1$), where the data vary as q^{-1/ν_p} Fig. 7.5. For rigid objects or dilute solutions where the scattering objets are separated, a high q (low correlation distances) the contribution of the intermolecular interactions vanishes, and the observed signal is then approaching the form factor. Contrarily, at low q the intermolecular correlations are not negligible, and the model is not suitable to fit the scattering data. The increase of the intensity at $q < 0.003\text{Å}^{-1}$ could be ascribed to the formation of clusters of PAA in acidic medium. Hammouda et al. [293] have seen a similar low-q shape for poly(ethylene oxide) solutions and have proposed the formation of polymer clusters. Such a behaviour is indeed expected at low pH due to neutrality charge of the polymeric chain and the possibility to form hydrogen bonds between chains. Such aggregates were not evidenced by the NMR measurements probably because the concentration used for these experiments was ten times less than for the SANS experiments.

From the fit in the high q domain, the exponent ν_p is fount to be equal to 0.60. This values suggest that the PAA chain is in a good solvent, but is not in agreement with the ν exponent determined by NMR with the scaling of the diffusion coefficient with the molar mass. A ν of 0.49 was obtained fitting the R_h of the PAANa sizes measured by NMR in chapter 5. The different value found between ν (self-diffusion) and ν_p (SANS) could be related to the difference between the two techniques used [62]. The SANS examines various length scales up to the total size, so it could be more affected by the local conformation of the chain [62]. Furthermore, Weill and des Cloizeaux [98] have shown that there exists an intermediate regime in chain length where deviation between ν and ν_p can appear. This discrepancy between the static and dynamics dependence on the molecular weight, comes from the different rate between static and dynamics properties to reach the asymptotic limit [98] with the increase of the degree of polymerisation N.

From the fit of data in Fig. 7.5, we obtain that the radius of gyration is equal of 4.6 nm and for a lower concentration (3 wt%), we found a lower R_g (3.7 nm). This decrease of R_g with the concentration could be related to the existence of some overlap or association between the chains such as the clusters observed at low q which would increase the size of the apparent scattering unit. The value at lower concentration is then more reliable. For PAA 2.1 kDa, the radius of gyration determined by the fit is 2.4 nm. The values determined by SANS are around a factor 2 higher compared to the values of hydrodynamic radii R_h determined by NMR at low pH. For PAANa, at higher pH a ratio close to $R_\mathrm{g}/R_\mathrm{h} = 1.5$ was found by Reith et al. (pH$\approx$ 8 and 1 mol L^{-1} NaCl) [62] whereas for similar conditions Volk et al. found a value of $R_\mathrm{g}/R_\mathrm{h} = 1.95$ for PAANa in good solvent ($\nu_p = 0.6$) [294]. From a theoretical point of view, Akcasu and Benmouna [295, 296] calculated a value of 1.86 for a neutral polymer in a good solvent which is fairly close to the value observed here.

Unfortunately, it was not possible to do the same experiment a high pH, because of the weakness of the signal due to the small contrast with the solvent. At high pH the SLD of the PAANa is closer to the SLD of the D_2O as clear in Fig. 7.4.

7.4 | Silica nanoparticles

In this section, the structural characteristics of the silica nanoparticle are obtained, from the fit of the form factor $P(q)$ and the structure factor $S(q)$ of SANS data. First, the form factor

of the silica is obtained, from a system where the interactions have been screened thanks to the addition of salt. Once the form factor is known, the structure factor is obtained. From the structure factor are obtained the parameters related to the interaction between nanoparticles.

7.4.1 | Form factor

To determine the form factor of the silica, the intermolecular interactions have been made negligible by adding salt to the system. The total scattering signal of silica at $\phi = 1\%$ with 10 mmol L^{-1} NaCl in D_2O is reported in Fig. 7.6. After a plateau at low q, a steep decrease is observed with a shoulder close to $q \sim 0.069$ Å^{-1}, characteristic of the radius R_o of the particle.

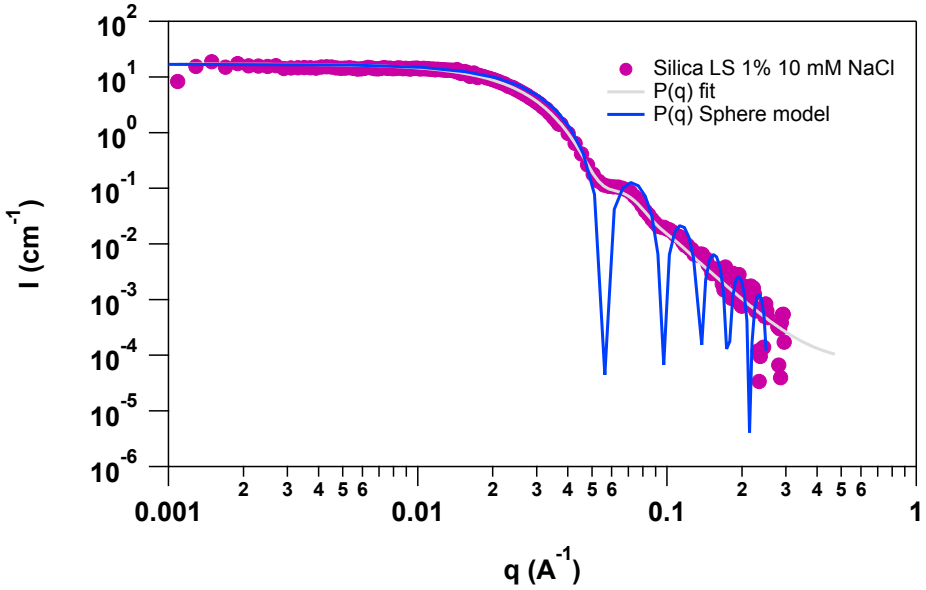

Figure 7.6: SANS data of silica LS ϕ 1% 10 mmol L^{-1} NaCl in D_2O, $T = 298$ K. Fitted to a form factor $P(q)$, using a sphere model function with particle size dispersity.

The function chosen for the form factor is the sphere model [297], also reported in Fig. 7.6:

$$F(q) = 3\frac{\sin(qR_o) - qR_o\cos(qR_o)}{(qR_o)^3} \tag{7.15}$$

with $P(q) = F(q)^2$. In the previous formulation, the effects of dispersity and of the experimental resolution in q are not considered. The dispersity reduces drastically the oscillations of the form factor, and the resolution in q contribute to the smearing of the intensity [298], as observed in Fig. 7.6 where the sphere model is compared with the experimental data. Both effects have been considered in the fit. The dispersity of the nanoparticles have been considered in the fit

through a log-normal distribution of the radius, which was introduced in section 3.6.3 (Eq. 3.23). It was possible to consider other distributions, but they give very similar numerical values of dispersity and mean radius and it is not possible to distinguish them by SANS [284]. The resolution in q is considered in the fit using the error of the q data calculated during the reduction of the experimental data. The mean radius obtained for the nanoparticle is 7.8 ± 0.1 nm, with a dispersity of 0.15. The value of the radius R_o found is in good agreement with the value found by DLS (section 4.2). Using these values of radius and dispersity, we are going to see in the next section the modification of the dispersions of silica nanoparticles at different values of pH.

7.4.2 | Structure factor: effect of the pH

Knowing the form factor of the silica nanoparticles, i.e. the intra-particle correlation, it is possible to obtain the structure factor $S(q)$, from the ratio between the scattered intensity and the form factor (this relation is valid for centrosymmetric particles [284]):

$$S(q,\phi) = \frac{I(q,\phi)}{I_{FF}(q,\phi_{FF})}\frac{\phi_{FF}}{\phi} \tag{7.16}$$

where I_{FF} is the scattered intensity corresponding to the form factor signal (see § 7.4.1). $S(q)$ contains the same information as the pair distribution function $g(r)$ which depends on the interaction potential between the objects [299]. The structure factor can be written as:

$$S(q) = 1 + 4\pi c \int_0^\infty \frac{\sin(qr)}{qr}\,(g(r)-1)\,r^2 dr \tag{7.17}$$

where c is the concentration of scatterers.

The scattering intensities of two systems of silica LS (ϕ= 3% in D_2O) at pH 2 and 9 are shown in Fig. 7.7.

A pH = 9, Fig. 7.7 on the right, a broad peak is observed experimentally a low q (q=0.016 $Å^{-1}$, corresponding to a distance of 39 nm). It is a position order, related to the repulsion between the nanoparticles [290]. This peak is not present when the interaction are screened, as observed in case of salt addition, Fig. 7.6, and in the system at pH = 2 (Fig.7.7 on the left). The distance calculated from this peak is close to that calculated if the nanoparticles are equally

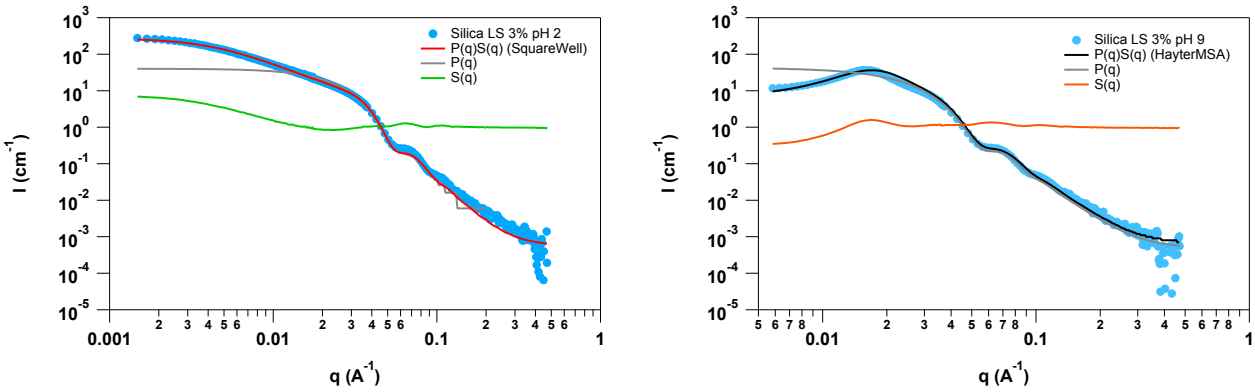

Figure 7.7: SANS data of silica LS ϕ 3 % in D_2O pH 2 (left) and pH 9 (right), T=298 K. S(q) fitted to a Square well (red line, pH 2) or Hayter-Penfold MSA implementation (HayterMSA) (black line, pH 9). Separate form and structure factor, and the resulting combined fit are shown.

dispersed in the suspension:

$$\ell = \frac{1}{\sqrt[3]{c}} = \sqrt[3]{\frac{V}{N_p}}$$

where V is the volume of the suspension and N_p is the number of particles. For a volume fraction of nanoparticle of $\phi = 3$ %, the value found is $\ell = 45$ nm. The system is governed by repulsive interactions, as expected when the nanoparticles are charged, as the low q the structure factor $S(0) < 1$ proves. The high q behaviour of the curve is unchanged since it mainly comes from the form factor of the nanoparticle.

At pH 2, Fig. 7.7 on the left, the shape and the form of the silica is unchanged, as the same behaviour of data at high q proves. However, the interactions between the nanoparticles are strongly modified. The system is governed by attractive interactions, as the low q the structure factor $S(0) > 1$ proves. Furthermore, the peak related to the structural order at pH=9, disappears.

The data have been fitted using functions that consider both form and structure factor. The form factor used, $P(q)$, is the polydisperse sphere model, reported in Fig. 7.7. The corresponding parameters, of radius R_o, dispersity, and the SLD of SiO_2 and D_2O have been fixed with the values obtained for the form factor determination (see §7.4.1).

The structure factor, S(q), reported in the figures is calculated by dividing the total measured signal by the form factor.

The data at pH = 9, have been fitted using the Hayter-Penfold MSA implementation of $S(q)$ calculation for a screened Coulomb/DLVO potential described in section 1.2.1 [300, 301]. This potential has already been used in the previous chapters. The other fixed parameters of the fit

are the dielectric constant of D_2O at 298 K ($\varepsilon_r = 77.94$) and the temperature of $T = 298$ K needed to compute the Bjerrum length ℓ_B (Eq. 1.28). A series of dialysis have been used to exchange the original H_2O into D_2O to reduce the incoherent background. The salt concentration of the external bath was fixed to 0.001 mol L^{-1} of NaCl. The Debye screening length is then $\kappa^{-1} = 9.6$ nm. The value of charge obtained from the fit is $Z = -70$. This value of charge is lower than the value derived from the Poisson-Boltzmann linear regime and used in the previous chapters $Z_{eff} = -119$(§ 4.2.2.1, Fig. 4.12). This underestimation of the charge might come from the intrinsic limitation of the MSA closure where the direct correlation function is approximated to its asymptotic value at low concentration and interaction potential [302]. Another possible origin would be the smearing of the peak due to dispersity effects not only in terms of size of particles but also in terms of interactions. The consequence of this dispersity is a less well-defined correlation [303], ie a "softening" of the static correlations [304], as observed in the present case.

To fit the data at pH = 2, we have tried to use the attractive square well interaction potential U_{sw} [305] also known as the Baxter potential [306] to calculate the structure factor. This model calculates the interparticle structure factor for a square well potential, characterised by a depth ϵ_{sw} and a width ℓ_{sw} which is defined as multiples of the particle radius [305].

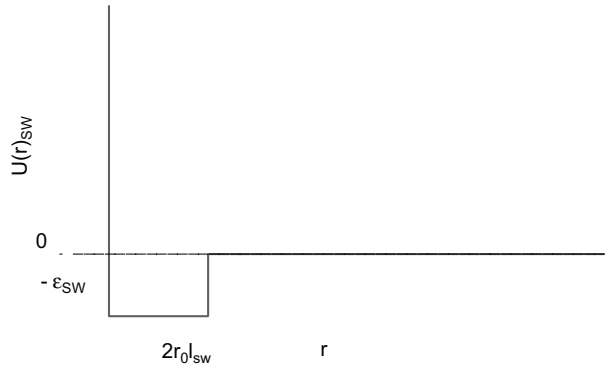

Figure 7.8: Interaction potential used in the square well model structure factor. *r* is the center-to-center distance between particles.

The use of this square-well interaction potential leads however to non physical results in terms of amplitude and range of interaction compared to the interactions at play such as van der Waals attraction § 1.2.2 or hydration forces. The detailed short range interaction between silica

surfaces and the ensuing stability have studied for long [307] but is still a debated topic [308, 309] that lies out of the scope of the present work.

The structure factor of the silica a pH 2 and 9 are compared in Fig. 7.9.

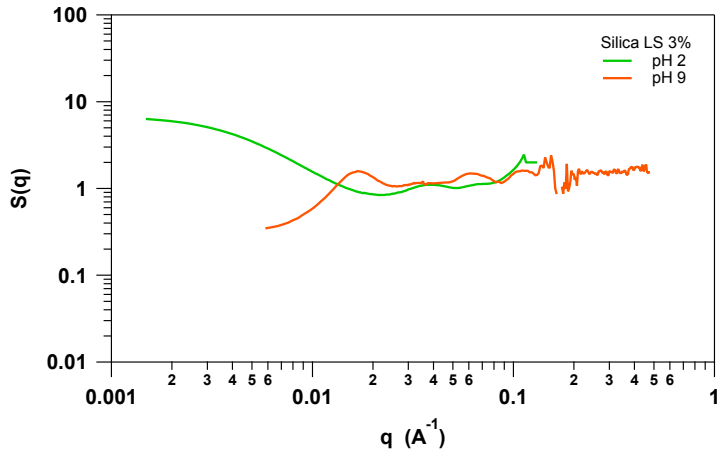

Figure 7.9: Structure factor of the silica LS ϕ 3% in D_2O pH 9 (orange line) and pH 2 (green line), T=298 K.

At high q the curves overlap, because there are no interparticle correlations at these short correlation lengths or high wavevector. From the low q limit, it is possible to obtain information related to the interactions among the objects. When $S(0) \rightarrow 1$ there is in average no interaction between scatterers, there is a balance between attractive and repulsive interactions. When they tend to a value $S(0) > 1$ there are attractive interactions, and for a value $S(0) < 1$ there are repulsive interactions [290]. At pH = 2 the attraction between the nanoparticles are predominant. Conversely, at pH = 10 the repulsive interactions predominate.

How do these interactions are modified in the presence of the polyelectrolytes? The next sections address this question.

7.5 | Effect of polyelectrolyte on silica interactions

In this section, we investigate the effect of the addition of polyelectrolytes on the interactions between silica nanoparticles. Indeed, polymers, either depleted or absorbed to the surface of colloidal particles strongly influence the interparticle interactions [82]. The systems of bare

silica and silica plus polyelectrolytes are then studied at different pH, concentration and length of polyelectrolyte.

More precisely we want to investigate the effect of attraction depletion interaction (section 1.5), induced by the presence of the polyelectrolytes. In a system where the concentration of particle is fixed, the strength of this attraction increases with the polymer concentration and the range of depletion increases with the radius of the polymer. To investigate this point, we intend to estimate the amplitude of the interparticle potential by fitting the structure factor of the silica particle, and to compare it with the value of the depletion potential.

In Fig. 7.10, scattering curves of the system of silica alone (ϕ = 3% in D_2O) and silica with added polyacrylate (H_2O/D_2O mixed at the ratio that match the signal of the polyelectrolytes at that pH, PCM) at pH = 2 (left graph) and pH = 9 (right graph) are shown. The contrast factor of the intensity $(\rho_{SiO_2} - \rho_{solvent})^2$ have been rescaled to perform a direct comparison of the curves.

At pH = 2 (left graph in Fig. 7.10), the attractive interactions between silica nanoparticles are predominant, in presence and absence of PAA. In both cases, the structure factor is larger than 1 at low q. However, the presence of the polyelectrolytes changes slightly the behaviour of the silica, decreasing the attractive interactions, as the decrease of the plateau at low q in the presence of PAA suggests. This effect induced by the addition of PAANa, could be related to the adsorption of the polymer on the surface of the silica.

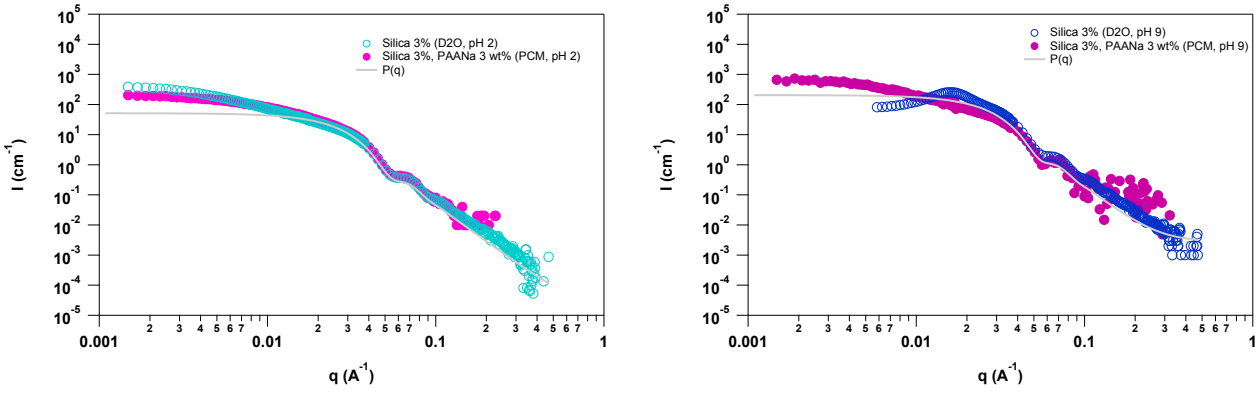

Figure 7.10: Left: SANS data of silica LS ϕ 3% (D_2O, pH 2 light blue circles), and silica LS ϕ 3% with PAANa 15 kDa 3*wt*% (PAANa contrast match PCM, 38% D_2O 62% H_2O pH 2, pink points). Right: SANS data of silica LS ϕ 3% (D_2O, pH 9 dark blue circles), and silica LS ϕ 3% with PAANa 15 kDa 3*wt*% (PAANa contrast match PCM, 71% D_2O, 29% H_2O pH 9 purple points). The silica nanoparticle form factor is shown (grey line). T=298 K.

At pH = 9 (right graph in Fig. 7.10), in the absence of PAANa the repulsive interactions

between nanoparticles are predominant, as is observed from the signal a low q (see §7.4.2). However, in the presence of PAANa the structure factor at low q becomes higher than 1, meaning that the addition of polyelectrolytes causes an attractive interaction between the charged particles that is higher than the electrostatic repulsion [278]. Furthermore, it alters the ordered spatial organization of the silica, as the disappearance of the correlation peak at $q = 0.017$ Å^{-1} shows. This effects can be explained by the effect of attractive interactions present in the system because the presence of the polyelectrolytes as the depletion [37, 82, 89, 310].

To quantify the interactions, the sum of the depletion potential and of the Yukawa potential has been calculated. The depletion potential is calculated using Eq. 1.31, with a silica radius of 7.8 nm (as obtained from the form factor Fig. 7.6), and the radius of gyration of the polyelectrolyte obtain in section 7.3. The DLVO potential was calculated using Eq. 1.7, considering the Z_{eff} of the nanoparticle (Z_{eff} reported in Fig. 4.12). Albeit differing in intensity, the depletion potential prevails both at low and high pH at short separation h. This is consistent with the overall attraction observed on the scattering curves.

The presence of polyacrylate is responsible of attractive interactions between the silica nanoparticles at high pH. To verify the depletion nature of the attractive potential, in the next section we will study the variation of this potential with the concentration of the polyelectrolytes. For an attractive depletion potential, we expect an increase of the interactions with the increase of the concentration of the polyelectrolytes, as shown in Eq. 1.31.

7.5.1 | Effect of polyelectrolyte concentration

In this section, we investigate the effect of the polyelectrolyte concentration on the stability of silica nanoparticles and to investigate the depletion nature of the attraction observed in the previous sections. We study a system at a fixed silica concentration ($\phi = 3\%$) and increasing concentrations of PAANa 15 kDa (1, 3 and 9 wt%) at pH = 2 and 9. In Fig. 7.11, the corresponding scattered intensity are shown. The mixture of silica nanoparticles and PAANa dispersed in a solvent matching the contribution of the polyacrylate (PCM), i.e. where only the nanoparticles contribute to the scattering intensity. These data are compared with those of the bare silica in D_2O.

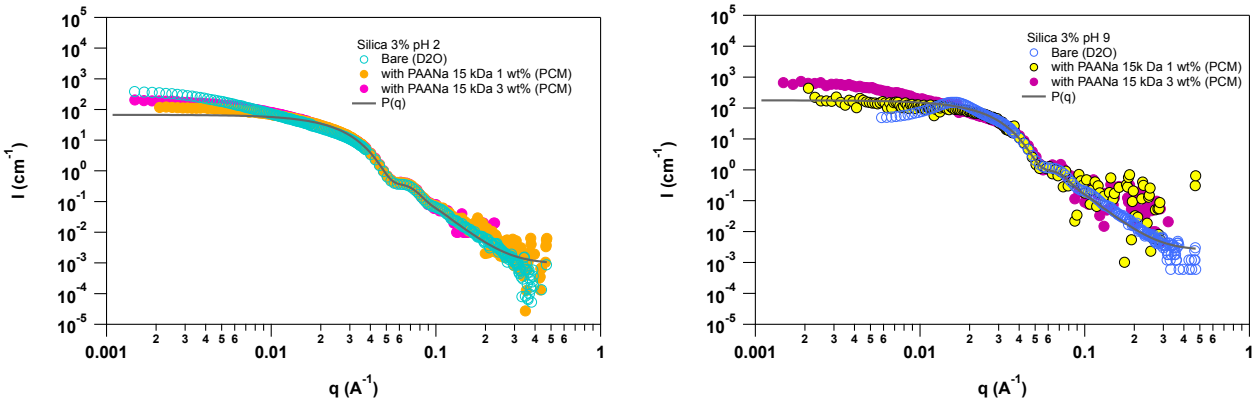

Figure 7.11: Left: SANS data of silica LS ϕ 3% (D_2O pH 2, light blue circles), silica plus PAANa 15 kDa 1 *wt%* (PAANa contrast match (PCM) pH 2, pink points), and plus PAANa 15 kDa 3 *wt%* (PCM pH 2, orange points). Right: SANS data of silica LS ϕ 3% (D_2O pH 9, dark blue circle), silica LS plus PAANa 15 kDa 1 *wt%* (PCM pH 9, yellow points), and plus ϕ 3% PAANa 15 kDa 3 *wt%* (PCM pH 9, purple points). T 298 K.

At pH = 2 (left graph), with the addition of 1 wt% of PAANa the plateau at small q decreases with respect to the system of bare silica, which suggests the presence of smaller aggregates than without polyelectrolytes. Increasing the concentration of PAANa from 1 wt% to 3 *wt%* produces an intermediate situation.

At pH = 9 (right graph), the addition of PAANa causes the appearance of attractive interaction between nanoparticles, that increases with the concentration of PAANa. From a repulsive interaction without polyacrylate, the interactions become more and more attractive as the concentration of polyacrylate increases. This concentration dependence tends to confirm the presence of a notable depletion interaction at high pH.

The data reported in Fig. 7.12 are related to the same systems at pH 2 (left graph) and pH 9 (right graph), but in D_2O as a solvent. The data of bare silica, are compared with the data of silica with different concentrations of PAANa 15 kDa (1, 3, and 9 wt%). In D_2O, the scattered intensity comes from all objects in solution, so because the complexity of the system only a qualitative analysis of the next measurements is done.

At pH = 2, we do not observe significant variations of the data at medium and low q, for the lowest PAANa concentration studied (1 and 3 wt%) suggesting that the main contribution to the scattered intensity comes from the silica nanoparticles. However, a higher PAA concentration (9 wt%) is available for this contrast. The data displays a different shape without the appearance of a plateau at low q, and a change of curvature at intermediate q. This may be related to the

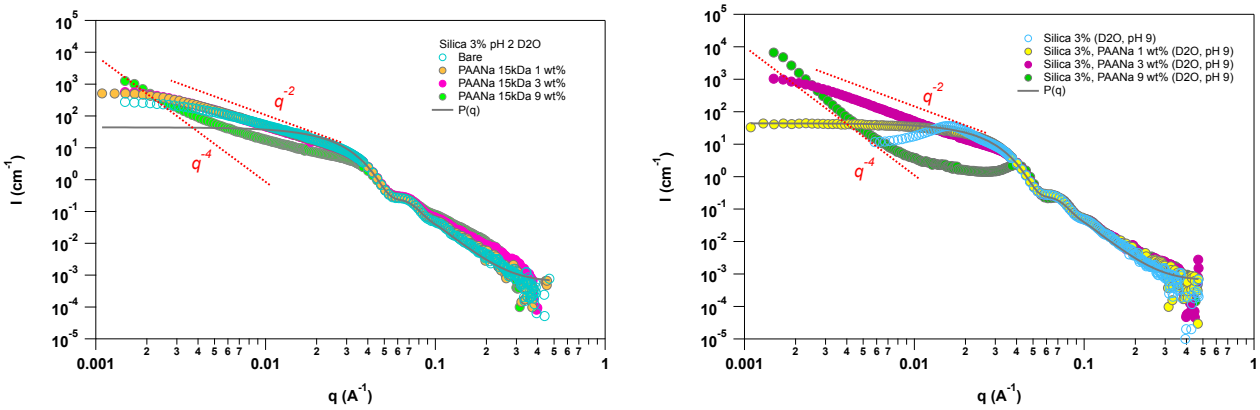

Figure 7.12: Left: SANS data of silica LS ϕ 3% (D_2O pH 2, light blue circles), silica LS plus PAANa 15 kDa in D_2O pH 9 1 *wt%* (orange points), 3 *wt%* (pink points), and 9 *wt%* (light green points) Right: SANS data of silica LS ϕ 3% (D_2O pH 9, dark blue circles), silica LS plus PAANa 15 kDa in D_2O pH 9 1 *wt%* (yellow points), 3 *wt%* (purple points), and 9 *wt%* (green points). T 298 K.

formation of larger aggregates of silica particles. The change of slope also suggest the formation of more compact structure than for the lower concentrations.

At pH = 9, the effects of PAANa concentration is strikingly visible not only from the data (Fig. 7.12 on the right) and but also from the macroscopic aspect of the sample (Fig. 7.13).

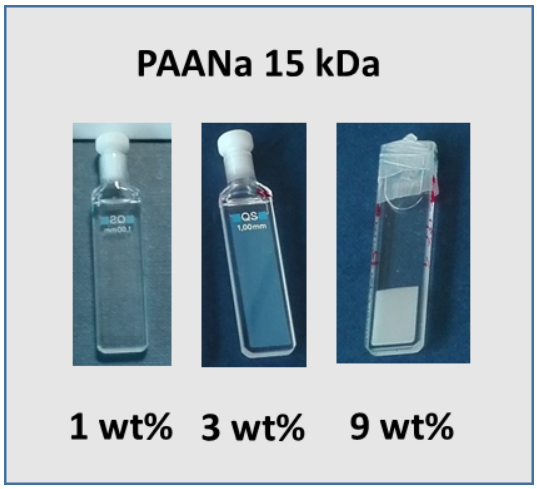

Figure 7.13: Sample used for SANS experiments . From left to right: Silica LS ϕ 3 % plus PAANa 15 kDa in D_2O pH 9 1 *wt%*, 3 *wt%*, and 9 *wt%*. pH 9.

In Fig. 7.13, the sample of silica LS with the different PAANa concentrations at pH = 9 are shown. At low PAANa concentrations (1 *wt%*), the system seems stable, the sample is transparent and exhibit a low-q plateau very close to the $P(q)$ of the silica nanoparticles. This stable suspension is close to the samples used for the diffusion measurements (chapter 6).

Increasing the concentration of PAANa (3 wt%), the sample becomes slightly turbid. From the scattered intensity we see the formation of large fractal aggregates, with the low q behaviour of the scattering intensity close to $I(q) \sim q^{-2}$ [311–313]. For the highest PAANa concentration (9 *wt%*), there exist a macroscopic phase separation in the sample, which a silica nanoparticle rich phase at the bottom. Only this strongly turbid sediment was measured and displays interesting features. There is well defined peak observed at $q = 0.04$ Å^{-1} ($d = 15.7$ nm) which corresponds to the distance of two nanoparticles in contact. Furthermore, at low q, the data display a strong slope close to $I(q) \sim q^{-4}$, like a second Porod regime due to a sharp interface. Like the behaviour observed at high q due to the phase boundary between silica nanoparticle and solution, at low q this sharp increase corresponds to the phase boundary between the phase of sedimented silica nanoparticle and the other phase.

To sum up, at pH = 9, the presence of PAANa causes a strong attraction between the nanoparticles, which increase as the concentration of polyacrylate increases. The presence of depletion makes the dispersion of nanoparticles unstable and lead to an aggregation even a phase separation if the concentration is high enough. This phase separation is predicted by the theory of depletion [82]. However, no restabilisation at high polymer concentration due to polyelectrolyte-polyelectrolyte repulsion was observed contrary to other systems [314, 315]

The pH dependence of the depletion may related also to the different conformation of the PAANa a different pH. As seen in Eq.1.31 and 1.32, the depletion intensity increases with the radius of the depletant, as we will see in section 7.5.3.

7.5.2 | Different point of view: the help of the contrast match

In this section, using the contrast variation techniques, we isolate the contributions arising from the silica nanoparticle only (polymer contrast match PCM), or from the polyelectrolyte only (silica contrast match, SCM). The data at three different contrasts (full contrast,PCM, and SCM) for the system of silica $\phi = 3\%$ with 3 wt% of PAANa at pH = 2 and 9 are reported in Fig.7.14.

At pH = 2, the data measured in SCM seems to have the same behaviour of the data of the system in PCM a medium q. This could be related to the polymer absorbed on the surface of the silica, that have the same large scale correlation observed for the silica. However, because

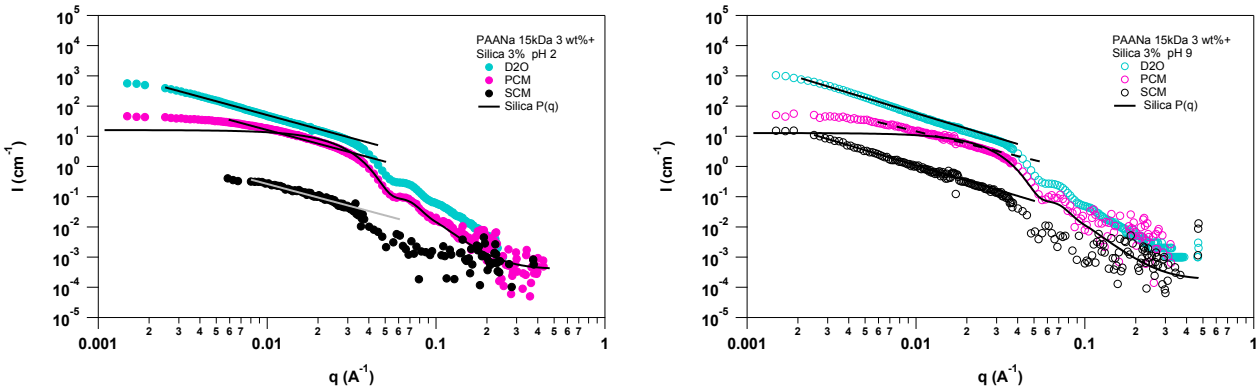

Figure 7.14: SANS data of silica LS ϕ=3% + PAANa at 3 *wt%* at pH 2 (left graph) and pH 9 (right graph) at different contrast match. In full contrast (D_2O, blue symbols), polymer contrast match (PCM, pink symbols), silica contrast match (SCM, black symbols). Power law fit of the data a medium q. The form factor of the silica is reported (black line).

of their low intensity these measurements might be affected by remaining silica intensity, as a result an unequivocal interpretation can not be done. The data at intermediate q have been fitted with a power law, and an exponent of 1.5 has been found for the three contrasts.

At pH = 9, the signal arising from the measurements of silica particles only (PCM), points out the formation of aggregates of silica. As seen in the previous section, at high pH the concentration of 3 wt% of PAANa is enough to cause the aggregation of the silica particles. The signal of only PAANa a low q (SCM), is different than that observed for the system in silica (PCM) where a plateau a low q is observed. The data a low q have been fitted with a power law and an exponent of 1.7 has been found for the system in D_2O and SCM. This higher exponent at high pH indicates the formation of more compact aggregates than in low pH and a stronger repulsion of the polyacrylate.

To verify the presence of PAANa adsorbed on the surface of silica nanoparticles, the data have been represented in $I(q)q^4$ vs q. If a sharp interface exists between the sphere and the solvent, in the asymptotic Porod regime ($q \rightarrow +\infty$), the scattering intensity decreases steeply as $I(q) \sim q^{-4}$. In the presence of a corona, the decrease is slower $I(q) \sim q^{-2}$. As a result, $I(q)q^4$ should tend to a plateau value for the first case and to a parabolic regime for the second [316]. In Fig. 7.15, the curves corresponding to the silica particles only (PCM) certainly tends towards a plateau with some oscillations. The curves corresponding to the polyelectrolytes only (SCM) are unfortunately too noisy due to the small scattering intensity of the polyelectrolyte. They cannot be exploited quantitatively. The scattering curves determined in D_2O can also be used in

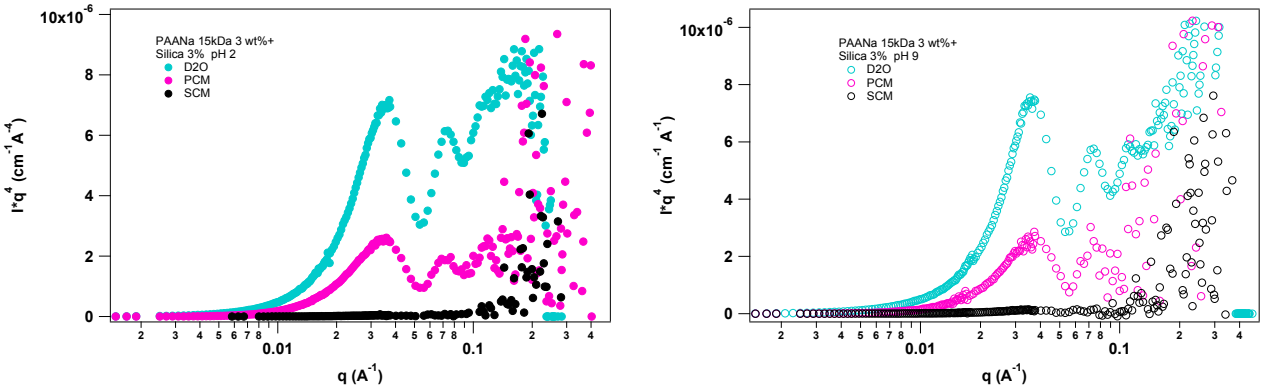

Figure 7.15: $I(q)q^4$ vs q representation of SANS data of silica LS ϕ=3% + PAANa at 3 *wt%* at pH 2 (left graph, points) and pH 9 (right graph, circles) at different contrast match. In full contrast (D_2O, blue symbols), polymer contrast match (PCM, pink symbols), silica contrast match (SCM, black symbols).

principle. From 7.15, while at pH = 9 the curve seems to tend to a plateau value, the curve at pH = 2 shows a slight increase with q that might ascribed to a corona contribution. However, if the signal to noise ratio is not an issue for these data, they contain all the scatterers contribution, including the cross terms. Their quantitative calculation is then difficult.

In Fig. 7.16, the scattering intensity of the polyacrylate only (SCM) is displayed for a higher concentration of PAANa (9 wt%). The scattering curves confirms the previous observations. At pH = 2, a power law with an exponent smaller than 2 is observed. At pH = 9, at low q a strong increase with a q^{-4} scaling is representative of the phase separation described above (Fig. 7.16, left).

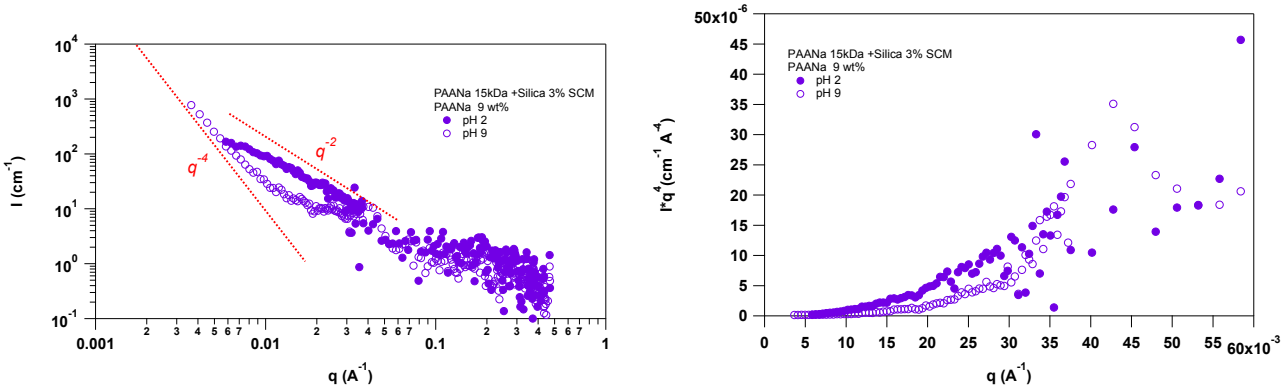

Figure 7.16: SANS data of silica LS ϕ=3% + PAANa at 9*wt%* at pH 2 (purple points) and pH 9 (purple circles) in SCM. On the right the same data in a $I(q)q^4$ vs q representation. T=298 K.

The representation $I(q)q^4$ vs q for these data is plotted in Fig. 7.16 (right). Unfortunately, it does not provide any supplementary information on the existence of a corona of adsorbed

polymer, even for this higher concentration.

7.5.3 | Effect of the size of the polyacrylate

In this section, we investigate the effect of the size of PAANa on the stability of the silica nanoparticles. The study of this dependence will help us to investigate the contribution of the depletion phenomenon to the total interaction between silica particles in the presence of PAANa. Since the depletion volume increases with the volume of the depletant (see Eq.1.31), the strength of the depletion increase with it. Furthermore, the range of depletion interaction increases also with the radius of gyration of the polymer as seen in Eq. 1.32.

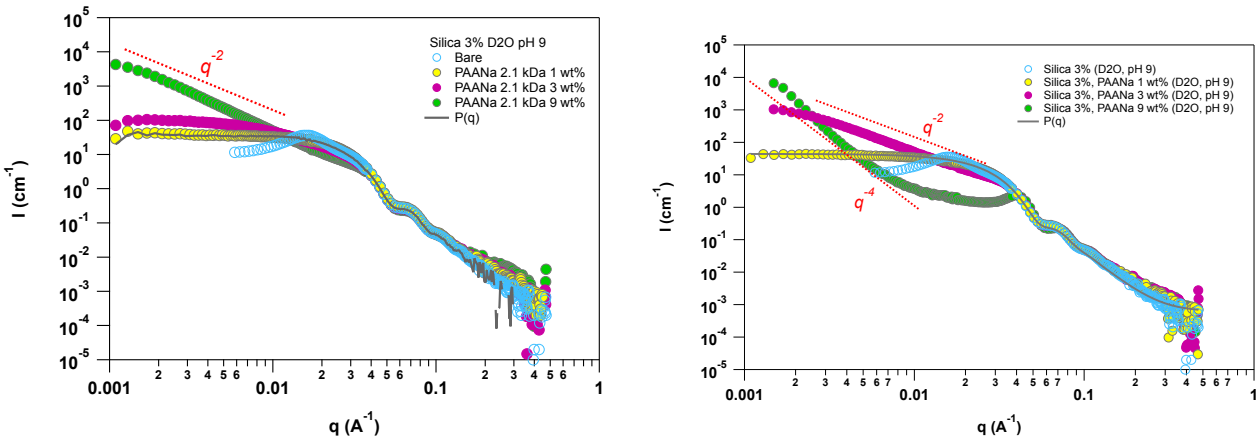

Figure 7.17: Left: SANS data of silica LS ϕ 3% (D_2O pH 9, dark blue circles), silica LS D_2O pH 9 and its form factor $P(q)$ (black line), plus PAANa 2.1 kDa 1 *wt%* (yellow points), 3 *wt%* (purple points), and 9 *wt%* (green points). Right: same configurations than left graph in presence of PAANa 15 kDa. T 298 K.

The behaviour of silica LS at $\phi = 3\%$ in the presence of PAANa of different molecular weight (2.1 and 15 kDa) is studied. For the two systems, the pH is fixed at 9, and the concentration of the PAANa is varied from 1 to 9 wt%. In Fig. 7.17 the scattering data of the system of silica and PAANa 2.1 kDa (left graph) and 15 kDa (right graph) are shown. We observe that the increase of the attractive interaction is size dependent. The presence of attractive interaction caused by the PAANa is stronger in presence of the 15 kDa chain. The addition of low amount of PAANa (1 %) in both cases, reduces the total repulsion between silica particles without causing the aggregation of the particles, as also the transparent solutions in Fig.7.13 and Fig.7.18 prove. The scattering intensity in both cases is very close to the form factor.

The addition of 3 wt% of PAANa increases the attractive interactions, and causes the formation of large silica aggregate only in presence of 15 kDa. Smaller aggregates are formed in the presence of 2.1 kDa PAANa in the same conditions. At high concentration of PAANa, there are aggregates for both sizes, and in case of the 15 kDa PAANa, there is even a phase separation as discussed earlier. The macroscopic aspect of the samples, Fig.7.13 for PAANa 15 kDa and Fig. 7.18 for PAA 2.1 kDa, is consistent with the scattering curves.

Figure 7.18: Sample used for SANS experiments . From left to right: Silica LS ϕ 3 % plus PAANa 2.1 kDa in D_2O pH 9 1 *wt%*, 3 *wt%*, and 9 *wt%*. pH 9.

To conclude, as expected in the case of depletion interactions, the intensity of this attractive interaction increases with the length of the chain. This statement is in favour of the depletion nature of the interactions between nanoparticles caused by the presence of PAANa.

Summary of Chapter 7

In this chapter we have studied the phase behaviour of silica particles in the presence of polyelectrolytes using small-angle neutron scattering (SANS).
The presence of polyelectrolyte particles in colloidal suspensions can alter the interactions between particles and affect the stability of the system. If the adsorption of polyelectrolytes on the surface of nanoparticles causes a stabilization of the nanoparticles through steric effects and electrostatic repulsions conversely, unabsorbed polyelectrolytes generate depletion induced interaction which is attractive.
In the last months of this thesis, we took advantage of beam time on the D33 spectrometer of the Laue-Langevin Institute (Grenoble) to study the structure of these systems by SANS. This technique allows the access to the suspension structure on the length scales ranging from 1 to 1000 nm. Thanks to SANS, we have studied the average conformation of chains and their dispersion state. Mainly, we focused on the effect of the concentration and size of polyelectrolytes on the stability of the silica nanoparticles.
At high pH, the presence of PAANa causes a strong attraction between the nanoparticles, which increases as the concentration of polyacrylate raises. The presence of depletion makes the dispersion of nanoparticles unstable and lead to an aggregation or even a phase separation if the concentration is high enough. The increase of this attractive interaction with the concentration of the polyelectrolyte, is in agreement with the depletion nature of the attractive interactions induced by the presence of the PAANa. However, no restabilisation at high polymer concentration due to polyelectrolyte-polyelectrolyte repulsion was observed contrary to other systems.
The aggregation effect is not present at low polyelectrolyte concentration (1%), in the conditions used in diffusion NMR experiments.

Conclusion

In this thesis, we have investigated the modification of the dynamics properties of short polyelectrolytes in presence of charged nanoparticles.

To study this problem we have designed an experimental system made of carboxylate molecules of various sizes, from a simple carboxylate (propionate) up to polyelectrolytes (sodium polyacrylate, PAANa), in aqueous dispersions of silica nanoparticles of different sizes and surface charges. Both polyelectrolytes and nanoparticles are negatively charged at high pH. We have chosen the polyacrylic acid (PAA) because it is widely used, and due its simple structure it can be seen as a polymer model. In particular, we have focused on short polyacrylate chain since so far, the vast majority of studies have been carried out on long chain polyelectrolytes.

To study this system we have used mainly the diffusion NMR technique. Thanks to this technique and to a data treatment, developed in the present work, that considers the dispersity $Đ$ of the polyelectrolytes, we have quantified the self-diffusion of polyelectrolytes on a length scale of 10-100 μm. The data treatment has been applied on a different system in the following work [155].

The structural changes of carboxylate molecules and the variation of their dynamics in a dilute regime have been studied by the evolution of the chemical shift δ and the diffusion coefficient. The two NMR observables have been compared to assess the consequences of the ionisation and to investigate the influence of the polyelectrolyte molar mass.

The charging process of the chain, governed by pH of the solution, has a noticeable effect on the chemical shift δ and the diffusion coefficient D. While simple carboxylic acids are well described by the Henderson-Hasselbalch equation, the latter equation fails unambiguously for the evolution of the same quantities measured for the polyelectrolytes.

As the length of the chain increases, the deprotonation degree β, the chemical shift δ, and the diffusion coefficient D give rise to significant differences not observed for the simple carboxylic

acids. Whereas δ has a variation with pH independent of the chain length, the ionisation degree and the diffusion coefficient display opposite molecular weight dependences.

The diffusion coefficient of the short polyacrylate depends strongly on the pH. At low pH, a compact conformation is observed, while at high pH the chain adopts a flexible rod conformation. The amplitude of the change of diffusion coefficient with the pH is found to be higher as the molar mass increases.

Even short polyelectrolytes singularly differ from simple carboxylic acids. They tend to behave like long chain polyelectrolytes but with noticeable differences due to their small size compared to the persistence length. Their ionization process and its effect on diffusion cannot be easily derived by a single parameter study, since several phenomena are at play.

The impact of charged obstacles on the dynamics of the polyelectrolytes have been investigated, by the study of the self-diffusion coefficient at different volume fractions of obstacles ϕ. Furthermore, the influence of the interaction between diffuser and obstacle, has been studied by the modification of the electrostatic repulsion by salt addition or pH variation.

The increase of the volume fraction of the crowding particles causes a linear decrease of the diffusion coefficient of all studied oligomers and polyelectrolytes, in the range of ϕ studied. The physical volume of the obstacles, is not enough to explain the decrease of the diffusion coefficient of the chain with ϕ. Other proprieties, as the size of the diffuser and the interactions between diffusers and obstacles, have to be considered to understand the behaviour of the diffusion coefficient.

The role played by the electrostatic interactions have been pointed out by the addition of salt or pH variation. The addition of salt enhances the diffusion of the PAANa, due to the reduction of the intra-chains PAANa interactions and of the obstacles-PAANa repulsions. By pH variation, the charge of surface of the objects have been changed. At high pH, the effect of the repulsion is predominant while at low pH, a behaviour close to the pure obstruction due to the physical volume of the obstacles is recovered, even if a contribution of adsorption cannot be completely overlooked.

A cell-model was used to solve numerically the diffusion equation in a DLVO interaction potential between obstacles and diffusers. A semi-quantitative agreement with the experimental data is found especially at high ionic strength. However, the model cannot render satisfactorily

the details of the observed diffusion coefficient. A more detailed implementation of all the interactions and of the dynamics of the obstacles is to consider together with the numerical simulation of the system with mesoscopic techniques such as Brownian Dynamics or MPCD.

In the last months of this thesis, we took advantage of beam time on the D33 spectrometer of the Laue-Langevin Institute (Grenoble) to study the structure of these system by small angle neutron scattering (SANS). We have investigated how the presence of polyelectrolytes modifies the phase behaviour of silica particles by using SANS.

The effect of the addition of the weak polyelectrolyte is found to be strongly dependent on pH. At high pH, where silica nanoparticle suspensions are stable, due to the strong electrostatic repulsion, the addition of PAANa causes a strong attraction between the nanoparticles, which increases with the concentration of polyacrylate. This depletion interaction leads to an aggregation of the silica nanoparticles and even to a phase separation if the concentration of polyacrylate is high enough. The increase of this attractive interaction with the concentration of the polyelectrolyte, is in agreement with the depletion nature of the attractive interactions induced by the presence of the PAANa. However, this effect is not present in the conditions used during the measurement of diffusion coefficients done by NMR.

The analysis of SANS data have to be completed with the other measured systems, that have not been shown due to the short interval since the experiments. The effect of the silica concentration and a preliminary study on the kinetic of the aggregation phenomena are some of the other problems investigated.

Perspectives

The weak polyelectrolytes and the silica nanoparticles have allowed us to look at the contribution and the role of the different properties of the system on the dynamics of the short polyelectrolytes. In the following, we list some investigations that may be done to deepen the knowledge on the subject and as continuation:

- The study an analogous system of the one studied here with strong polyelectrolytes may help to separate more clearly the effects arising from the obstacles and from the diffuser.

- More generally in these complex systems other species can be studied such as the solvent [198], and the counterions whose dynamics contains a wealth of information on the interactions in the system.

- The use of the NMR relaxation time measurements of the chain in the different environments discussed in the present thesis, would give a complementary understanding of the phenomena at play on a shorter time scale. It might be valuable to study the polyacrylate conformation and the potential adsorption on the silica surface at low pH values.

- Studying the kinetic of the aggregation processes on long time scale, that arises when the system of PAANa and silica are mixed, to characterise the time scale as a function of the system properties. These phenomena have been observed preliminarily during the SANS experiment, but not presented in this manuscript.

- If the absorption and electrokinetic characteristics of alumina suspensions in presence of polyacrylic acid as a dispersant have been studied [14], the study of the dynamics of the PAA in presence of attractive obstacle could be another interesting complementary work.

Appendix A

Static light scattering

The SLS is based on the time-average intensity of scattered light. The intensity of light scattered as function of sample concentration c, provides the molecular weight M_w, and the 2nd virial coefficient A_2 which describes particles-solvent interactions [317].

For particles larger than $\lambda_0/50 \cdot n_0$, where λ_0 is wavelength of the incident light in the vacuum and n_0 is the refractive index of the solution, the intensity is reduced due to destructive interference among rays scattered by different part of the particles, this is the Mie scattering.

In the opposite case, for molecules smaller then $\lambda_0/50 \cdot n_0$ (=16 nm in our case=, the scattering particle can be assumed like a single dipole. This condition is respected by the PAANa studied here. In this case the molecular weight is determined by measuring the sample at different concentrations, applying the Rayleigh equation [142]. In this approximation, the equation describes the intensity of light scattered by particles in solution can be described by a virial coefficient expansion:

$$\frac{Kc}{R_\theta} = \frac{1}{M_w} + 2A_2c + 3A_3c^2 \tag{A.1}$$

where K is the optical constant, c is the concentration, R_θ the Rayleigh ratio (the ratio of scattered light to incident light of the sample per unit volume of solution detected), M_w the weight average molecular mass, and A_x the virial coefficients. In the approximation of small concentrations, it is possible to stop the expansion at the first order in c.

The optical constant K, is given by:

$$K = \frac{4\pi^2}{\lambda_0^2 N_A}\left(n_0\frac{\mathrm{d}n}{\mathrm{d}c}\right)^2 \tag{A.2}$$

where λ_0 is incident laser wavelength (633 nm), N_A Avogadro's constant, n_0 solvent refractive index (1.3363 [318]), and dn/dc the differential index increment (0.175 ml g^{-1} in case of PAANa and water [12, 319]). The Rayleigh ratio is calculated using a standard Rayleigh ratio value, the one of toluene. The expression of Rayleigh ratio calculated with a toluene standard is:

$$R_\theta = \frac{I_A n_0^2}{I_T n_T^2} R_T \tag{A.3}$$

where I_A is the residual scattered intensity corrected of the solvent signal; I_T is toluene scattering intensity (210 kcps); n_T toluene refractive index (1.4961), and R_T Rayleigh ratio of toluene at 298 K and 633 nm (2.737×10^{-5} cm^{-1}, [28]).

The A_2 coefficient describes the interaction among particles. When $A_2 > 0$ particles tend to stay as a stable solution: particle-solvent interaction is stronger than particle-particle interaction strength. When $A_2 < 0$ the particle may aggregate: particle-particle interaction is stronger than particle-solvent interaction strength. When $A = 0$ the particle-particle interaction is equivalent to particle-solvent interaction.

Polyelectrolytes In order to characterise the averaged molecular weight M_w and also have information about the interactions of the system, SLS measurements have been conducted on polyelectrolytes. Thanks to the second virial coefficient the particles interactions are studied. The systems studied here are PAANa samples of 5.1 and 8 kDa.

The experiment was carried out at different PAANa mass concentrations (from 0.1 to 1 *wt %*) in water solutions of 0.1 and 1.5 M NaCl a pH$\approx$ 8 and T=298 K. The samples were filtered with 0.1 μm MILLEX VV filter. The final intensity, corrected with the solvent intensity and dark counts, is used to calculate the Rayleigh ratio. Using the Eq. A.2 and A.3 with the following parameters: λ_0 = 633 nm; n_0=1.3363 [28]; dn/dc = 0.175 ml g^{-1} [12, 28, 319], $R_T = 2.737 \times 10^{-5}$ cm^{-1} [28]; n_T = 1.4961; I_T = 210 kcps. The Kc/R_θ is calculated and it is plotted versus the concentration in Fig. A.1.

From the fit in Fig.A.1 M_w and the A_2 are obtained and they are reported in table A.1. A_2 decreases with the salt concentration and tends to zero, this means that particle-particle interactions are favored with the addition of salt. The value found at 0.1 M shows that an 0.1 M solution represents a good solvent. Then a water solution 1.5 M NaCl reppresent a condition of $\theta-$solvent as also confirmed by Schweins et al. [28]. In a good solvent, the interaction

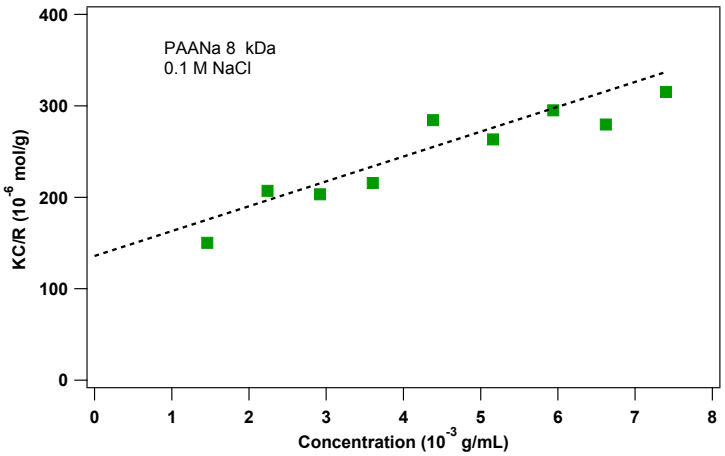

Figure A.1: SLS measure of PAANa 8 kDa in solution of 0.1 M NaCl. Kc/R_θ (mol/l) (green squares) a different concentration c (g/ml) fitted with Eq. A.1. pH≈ 8, T = 298 K.

between monomer and solvent is energetically favourable, and the polymer tends to expand. In a θ solvent, the chain have a nearly ideal conformation, the interactions inter-chains have the same weight than the interaction monomer-solvent [40].

M by furnisher (kDa)	C_{NaCl} (mol L^{-1})	M_w from fit (kDa)	A_2 from fit (mol cm^3 g^{-2})
8	0.1	7.4±0.9	0.012
8	1.5	5.5±0.3	0.005
5.1	0.1	13±3	0.016
5.1	1.5	4.3±0.9	0.007

Table A.1: Parameters found by of SLS data in Fig A.1 as a function of concentration of the PAANa 8 kDa (Sigma-Aldrich) at 0.1 and 1.5 M NaCl in water solution, a pH≈ 8. M_w is the molecular weight with the errors obtained from the fit and A_2 is the second virial coefficient. Experiments are carried out at T = 298 K.

The values of M_w obtained in this analysis are not considered for the rest of the analysis, because the large discrepancy from the value of the furnisher and of the SEC measurements (section 4.1.2).

Bibliography

[1] M. Hess, R. G. Jones, J. Kahovec, T. Kitayama, P. Kratochvil, P. Kubisa, W. Mormann, R. F. T. Stepto, D. Tabak, J. Vohlidal, and E. S. Wilks. Terminology of polymers containing ionizable or ionic groups and of polymers containing ions - (IUPAC recommendations 2006). *Pure and Applied Chemistry*, 78(11):2067–2074, 2006.

[2] M. Hara. *Polyelectrolytes: Science and Technology*. CRC Press, 1992.

[3] R. M. Fuoss. Polyelectrolytes. *Discussions of the Faraday Society*, 11(0):125–134, 1951.

[4] J. Koetz and S. Kosmella. *Polyelectrolytes and Nanoparticles*. Springer, 2007.

[5] C. L. Cooper, P. L. Dubin, A. B. Kayitmazer, and S. Turksen. Polyelectrolyte-protein complexes. *Current Opinion in Colloid & Interface Science*, 10(1-2):52–78, 2005.

[6] A. V. Dobrynin, R. H. Colby, and M. Rubinstein. Scaling Theory of Polyelectrolyte Solutions. *Macromolecules*, 28(6):1859–1871, 1995.

[7] A. V. Dobrynin and M. Rubinstein. Theory of polyelectrolytes in solutions and at surfaces. *Prog. Polym. Sci.*, 30(11):1049–1118, 2005.

[8] Y. Gong, L. Xie, H. Li, and Y. Wang. Sustainable and scalable production of monodisperse and highly uniform colloidal carbonaceous spheres using sodium polyacrylate as the dispersant. *Chem. Commun.*, 50(84):12633–12636, 2014.

[9] X. Jiang, Y. Y., C. Wang, and X. Tian. Decolorization of anionic dye solutions using the hydrophobically modified polyelectrolytes containing beta-cyclodextrin moieties. *Chem. Eng. J.*, 253: 183–189, 2014.

[10] W. Xu, P. A. Ledin, F. A. Plamper, C. V. Synatschke, A. H. E. Müller, and V. V. Tsukruk. Multiresponsive Microcapsules Based on Multilayer Assembly of Star Polyelectrolytes. *Macromolecules*, 47(22):7858–7868, 2014.

[11] C. Yi, R. Hu, H. Ren, X. Hu, S. Wang, X. Gong, and Y. Cao. Protonation process of conjugated polyelectrolytes on enhanced power conversion efficiency in the inverted polymer solar cells. *J. Photonics Energy*, 4:043099–043108, 2014.

[12] J. Brandrup, E. H. Immergut, and E. A. Grulke. *Polymer Handbook*, volume 2. Wiley Interscience, New York, 4 edition, 1999.

[13] P. Knappe, R. Bienert, S. Weidner, and A. F. Thuenemann. Poly(acrylic acid): A combined analysis with field-flow fractionation and SAXS. *Macromol. Chem. Phys.*, 211(19):2148–2153, 2010.

[14] D. Santhiya, G. Nandini, S. Subramanian, K. Natarajan, and S. Malghan. Effect of polymer molecular weight on the absorption of polyacrylic acid at the alumina-water interface. *Colloids Surfaces A Physicochem. Eng. Asp.*, 133(1-2):157–163, 1998.

[15] K. R. Rogan, A. C. Bentham, G. W. A. Beard, I. A. George, and D. R. Skuse. Sodium polyacrylate mediated dispersion of calcite. In *Trends Colloid Interface Sci. VIII*, Progress in Colloid & Polymer Science, pages 97–102. Steinkopff, Darmstadt, 1994.

[16] E. Laarz and L. Bergström. The effect of anionic polyelectrolytes on the properties of aqueous silicon nitride suspensions. *J. Eur. Ceram. Soc.*, 20:431–440, 2000.

[17] G. M. Roger, S. Durand-Vidal, O. Bernard, G. Mériguet, S. Altmann, and P. Turq. Characterization of humic substances and polyacrylic acid: A high precision conductimetry study. *Colloids Surf., A*, 356(1-3):51–57, 2010.

[18] B. Bolto and J. Gregory. Organic polyelectrolytes in water treatment. *Water Res.*, 41(11):2301–2324, 2007.

[19] D. P. Wang, M. Q. Yang, Z.-x. Dong, S.-q. Bo, and X. L. Ji. Interaction between poly (ethylene oxide) and silica nanoparticles in dilute solutions. *Chinese Journal of Polymer Science*, 31(9): 1290–1298, 2013.

[20] G. Schmidt and M. M. Malwitz. Properties of polymer and nanoparticle composites. *Current Opinion in Colloid & Interface Science*, 8(1):103–108, 2003.

[21] W. P. Cao, Q.-B. Ren, and M.-B. Luo. Translocation of polymers into crowded media with dynamic attractive nanoparticles. *Physical Review E*, 92(1):012603, 2015.

[22] T. Ando and J. Skolnick. Crowding and hydrodynamic interactions likely dominate in vivo macromolecular motion. *Proc. Natl. Acad. Sci. U.S.A.*, 107(43):18457–18462, 2010.

[23] J. Buffle and R. R. DeVitre. *Chemical and biological regulation of aquatic systems*. CRC Press, 1993.

[24] R. Krishnamoorti, R. A. Vaia, and E. P. Giannelis. Structure and dynamics of polymer-layered silicate nanocomposites. *Chemistry of Materials*, 8(8):1728–1734, 1996.

[25] J. A. Dix and A. S. Verkman. Crowding effects on diffusion in solutions and cells. In *Annual Review of Biophysics*, volume 37, pages 247–263. Annual Reviews, 2008.

[26] G. Kwon, B. J. Sung, and A. Yethiraj. Dynamics in crowded environments: is non-Gaussian Brownian diffusion normal? *J. Phys. Chem. B*, 118(28):8128–34, 2014.

[27] A. Laguecir, S. Ulrich, J. Labille, N. Fatin-Rouge, S. Stoll, and J. Buffle. Size and pH effect on electrical and conformational behavior of poly(acrylic acid): Simulation and experiment. *Eur. Polym. J.*, 42(5):1135–1144, 2006.

[28] R. Schweins, J. Hollmann, and K. Huber. Dilute solution behaviour of sodium polyacrylate chains in aqueous NaCl solutions. *Polymer*, 44(23):7131–7141, 2003.

[29] G. Gonzalez, J. C. de la Cal, and J. M. Asua. Flocculation efficiency of blends of short and long chain polyelectrolytes. *Colloids and Surfaces A: Physicochemical and Engineering Aspects*, 385 (1-3):166–170, 2011.

[30] S. Yu, X. Xu, C. Yigit, M. van der Giet, W. Zidek, J. Jankowski, J. Dzubiella, and M. Ballauff. Interaction of human serum albumin with short polyelectrolytes: a study by calorimetry and computer simulations. *Soft Matter*, 11(23):4630–4639, 2015.

[31] W. Price. *NMR Studies of Translational Motion: Principles and Applications*. Cambridge Molecular Science. Cambridge University Press, 2009.

[32] U. Scheler. Nmr on polyelectrolytes. *Current Opinion in Colloid & Interface Science*, 14(3):212 – 215, 2009.

[33] P. T. Callaghan. *Principles of nuclear magnetic resonance microscopy*. Oxford University Press on Demand, 1993.

[34] T. Kitayama and K. Hatada. *NMR spectroscopy of polymers*. Springer Science & Business Media, 2013.

[35] P. Stilbs. Fourier transform pulsed-gradient spin-echo studies of molecular diffusion. *Progress in Nuclear Magnetic Resonance Spectroscopy*, 19(1):1–45, 1987.

[36] W. S. Price. Pulsed-field gradient nuclear magnetic resonance as a tool for studying translational diffusion: Part II. Experimental aspects. *Concepts in Magnetic Resonance*, 10(4):197–237, 1998.

[37] S. Ji and J. Y. Walz. Depletion Flocculation Induced by Synergistic Effects of Nanoparticles and Polymers. *The Journal of Physical Chemistry B*, 117(51):16602–16609, 2013.

[38] K. K. Das and P. Somasundaran. A kinetic investigation of the flocculation of alumina with polyacrylic acid. *J. Colloid Interface Sci.*, 271(1):102–109, 2004.

[39] P. G. de Gennes. *Scaling Concepts in Polymer Physics*. Cornell University Press, Ithaca, NY, 1979.

[40] M. Rubinstein and R. H. Colby. *Polymer Physics*. OUP Oxford, 2003.

[41] R. Hunter. *Foundations of colloid science*. Oxford University Press, 2001.

[42] T. Honegger and D. Peyrade. Dielectrophoretic properties of engineered protein patterned colloidal particles. *Biomicrofluidics*, 6(4):044115, 2012.

[43] L. Jacot-Descombes, C. Martin-Olmos, M. R. Gullo, V. J. Cadarso, G. Mermoud, L. G. Villanueva, M. Mastrangeli, A. Martinoli, and J. Brugger. Fluid-mediated parallel self-assembly of polymeric micro-capsules for liquid encapsulation and release. *Soft Matter*, 9(41):9931, 2013.

[44] J. Ma, Y. Wang, X. Zhang, and H. Huang. Filtration of protein colloids by fibrous membranes: A mechanistic investigation using packed bed filtration approach. *Colloids and Surfaces A: Physicochemical and Engineering Aspects*, 502:44–53, 2016.

[45] B. J. Le Reverend, I. T. Norton, P. W. Cox, and F. Spyropoulos. Colloidal aspects of eating. *Current Opinion in Colloid & Interface Science*, 15(1-2):84–89, 2010.

[46] E. Hückel and P. Debye. The theory of electrolytes: I. lowering of freezing point and related phenomena. *Phys. Z.*, 24, 1923.

[47] L. Belloni. Ionic condensation and charge renormalization in colloidal suspensions. *Colloids and Surfaces a-Physicochemical and Engineering Aspects*, 140(1-3):227–243, 1998.

[48] L. Bocquet, E. Trizac, and M. Aubouy. Effective charge saturation in colloidal suspensions. *J. Chem. Phys.*, 117(17):8138, 2002.

[49] V. Vlachy. Ionic effects beyond poisson-boltzmann theory. *Annu. Rev. Phys. Chem.*, 50(1):145–165, 1999.

[50] H. Yukawa. On the interaction of elementary particles. i. *Nippon Sugaku-Buturigakkwai Kizi Dai 3 Ki*, 17(0):48–57, 1935.

[51] E. Werwey and J. T. G. Overbeek. Theory of the stability of lyophobic colloids, 1948.

[52] V. Dahirel and M. Jardat. Effective interactions between charged nanoparticles in water: What is left from the DLVO theory? *Curr. Opin. Colloid Interface Sci.*, 15(1-2):2–7, 2010.

[53] B. Derjaguin and L. Landau. Theory of the stability of strongly charged lyophobic sols and of the adhesion of strongly charged particles in solutions of electrolytes. *Acta Physico Chemica URSS*, 14:633, 1941.

[54] H. Hamaker. The london-van der waals attraction between spherical particles. *physica*, 4(10): 1058–1072, 1937.

[55] F. London. The general theory of molecular forces. *Trans. Faraday Soc.*, 33:8b–26, 1937.

[56] A. Delgado, F. Gonzalez, G.lez-Caballero, R. Hunter, L. Koopal, and J. Lyklema. Measurement and interpretation of electrokinetic phenomena. *Journal of Colloid and Interface Science*, 309(2): 194–224, 2007.

[57] J. Israelachvili. *Intermolecular and Surface Forces*. Academic Press, London, 1991.

[58] R. F. T. Stepto. Dispersity in polymer science (IUPAC Recommendations 2009). *Pure Appl. Chem.*, 81(2):351–353, 2009.

[59] J. Viéville, M. Tanty, and M.-A. Delsuc. Polydispersity index of polymers revealed by DOSY NMR. *J. Magn. Reson.*, 212(1):169–173, 2011.

[60] I. Teraoka. *Polymer Solutions: An Introduction to Physical Properties*. John Wiley & Sons, New York, 2002.

[61] P. T. Callaghan and J. Lelievre. The size and shape of amylopectin: A study using pulsed-field gradient nuclear magnetic resonance. *Biopolymers*, 24(3):441–460, 1985.

[62] D. Reith, B. Müller, F. Müller-Plathe, and S. Wiegand. How does the chain extension of poly (acrylic acid) scale in aqueous solution? a combined study with light scattering and computer simulation. *J. Chem. Phys.*, 116(20):9100–9106, 2002.

[63] T. Odijk and A. Houwaart. Theory of Excluded-Volume Effect of a Polyelectrolyte in a 1-1 Electrolyte Solution. *Journal of Polymer Science Part B-Polymer Physics*, 16(4):627–639, 1978.

[64] P. J. Flory. *Principles of Polymer Chemistry*. Cornell University Press, 1953.

[65] J.-L. Barrat and J.-F. Joanny. Persistence Length of Polyelectrolyte Chains. *EPL (Europhysics Letters)*, 24(5):333, 1993.

[66] S. W. Cranford and M. J. Buehler. Variation of Weak Polyelectrolyte Persistence Length through an Electrostatic Contour Length. *Macromolecules*, 45(19):8067–8082, 2012.

[67] A. V. Dobrynin. Theory and simulations of charged polymers: From solution properties to polymeric nanomaterials. *Current Opinion in Colloid & Interface Science*, 13(6):376–388, 2008.

[68] J. C. Voegel, G. Decher, and P. Schaaf. Polyelectrolyte multilayer films in the biotechnology field. *Actualite Chimique*, (11-12):30–38, 2003.

[69] H. Schiessel. The physics of chromatin. *Journal of Physics-Condensed Matter*, 15(19):R699–R774, 2003.

[70] J. L. Lutkenhaus and P. T. Hammond. Electrochemically enabled polyelectrolyte multilayer devices: from fuel cells to sensors. *Soft Matter*, 3(7):804–816, 2007.

[71] M. Doi and S. F. Edwards. *The theory of polymer dynamics*. Clarendon Press, 1986.

[72] T. Odijk. Possible Scaling Relations for Semidilute Polyelectrolyte Solutions. *Macromolecules*, 12(4):688–693, 1979.

[73] M. Mandel. The potentiometric titration of weak polyacids. *Eur. Polym. J.*, 6:807–822, 1970.

[74] L. Shi, F. Carn, F. Boué, and E. Buhler. Role of the ratio of biopolyelectrolyte persistence length to nanoparticle size in the structural tuning of electrostatic complexes. *Phys. Rev. E*, 94(3):032504, 2016.

[75] Y. Muroga, I. Noda, and M. Nagasawa. Investigation of local conformations of polyelectrolytes in aqueous solution by small-angle x-ray scattering. 1. Local conformations of poly(sodium acrylates). *Macromolecules*, 18(8):1576–1579, 1985.

[76] Q. Liao, A. V. Dobrynin, and M. Rubinstein. Molecular Dynamics Simulations of Polyelectrolyte Solutions: Nonuniform Stretching of Chains and Scaling Behavior. *Macromolecules*, 36(9): 3386–3398, 2003.

[77] U. Böhme, B. Hänel, and U. Scheler. *Influence of the Counterions on the Behaviour of Polyelectrolytes*, volume 138 of *Progress in Colloid and Polymer Science*. Springer Berlin Heidelberg, 2011.

[78] H. Lekkerkerker and A. Stroobants. The phase behaviour of colloid-polymer and colloid-colloid mixtures. In L. Garrido, editor, *Complex Fluids*, volume 415 of *Lecture Notes in Physics*, pages 1–13. Springer Berlin Heidelberg, Berlin, Heidelberg, 1993.

[79] O. Spalla. Nanoparticle interactions with polymers and polyelectrolytes. *Curr. Opin. Colloid Interface Sci.*, 7(3-4):179–185, 2002.

[80] R. Tuinier, J. Rieger, and C. de Kruif. Depletion-induced phase separation in colloid polymer mixtures. *Adv. Colloid Interface Sci.*, 103(1):1–31, 2003.

[81] M. Peláez-Fernández, A. Moncho-Jordá, and J. Callejas-Fernández. Charged colloid-polymer mixtures: A study on electrostatic depletion attraction. *J. Chem. Phys.*, 134(5):054905, 2011.

[82] H. N. Lekkerkerker and R. Tuinier. *Colloids and the Depletion Interaction*, volume 833 of *Lecture NoteFalses in Physics*. Springer Netherlands, Dordrecht, 2011.

[83] A. Fuchs and E. Killmann. Adsorption of polyelectrolytes on colloidal latex particles, electrostatic interactions and stability behaviour. *Colloid and Polymer Science*, 279(1):53–60, 2001.

[84] M. Wisniewska, K. Terpilowski, S. Chibowski, T. Urban, V. I. Zarko, and V. M. Gun'ko. Stability of Colloidal Silica Modified by Macromolecular Polyacrylic Acid (PAA) - Application of Turbidymetry Method. *Journal of Macromolecular Science Part a-Pure and Applied Chemistry*, 50(6): 639–643, 2013.

[85] D. Bauer, H. Buchhammer, A. Fuchs, W. Jaeger, E. Killmann, K. Lunkwitz, R. Rehmet, and S. Schwarz. Stability of colloidal silica, sikron and polystyrene latex influenced by the adsorption of polycations of different charge density. *Colloids and Surfaces A: Physicochemical and Engineering Aspects*, 156(1-3):291–305, 1999.

[86] L. Shi, F. Carn, F. Boué, G. Mosser, and E. Buhler. Control over the electrostatic self-assembly of nanoparticle semiflexible biopolyelectrolyte complexes. *Soft Matter*, 9(20):5004, 2013.

[87] Y. Adachi and T. Matsumoto. Dynamics of initial stage flocculation of polystyrene latex spheres with polyelectrolytes. *Colloids Surf. A*, 113(3):229–236, 1996.

[88] R. Dunleavey-Routh and B. Vincent. Aggregate morphology and aggregation rate constants for silica dispersions in the presence of salt and polyelectrolyte. *Journal of Colloid and Interface Science*, 309(1):119–125, 2007.

[89] I. Szilagyi, G. Trefalt, A. Tiraferri, P. Maroni, and M. Borkovec. Polyelectrolyte adsorption, interparticle forces, and colloidal aggregation. *Soft Matter*, 10(15):2479–2502, 2014.

[90] F. Oosawa and S. Asakura. On Interaction between Two Bodies Immersed in a Solution of Macromolecules. *J. Chem. Phys.*, 22(7):1255, 1954.

[91] A. Vrij. Polymers at Interfaces and the Interactions in Colloidal Dispersions. *Pure Appl. Chem.*, 48(4):471–483, 1976.

[92] E. S. Pagac, R. D. Tilton, and D. C. Prieve. Depletion attraction caused by unadsorbed polyelectrolytes. *Langmuir*, 14(18):5106–5112, 1998.

[93] P. Hiemenz and R. Rajagopalan. Electrophoresis and other electrokinetic phenomena. *Principles of colloid and surface chemistry*, 3:534–574, 1977.

[94] R. Fuoss and U. Strauss. Electrostatic Interaction of Polyelectrolytes and Simple Electrolytes. *Journal of Polymer Science*, 3(4):602–603, 1948.

[95] J. Cohen, Z. Priel, and Y. Rabin. Viscosity of Dilute Poly-Electrolyte Solutions. *The Journal of Chemical Physics*, 88(11):7111–7116, 1988.

[96] P. E. R. Jr. A Theory of the Linear Viscoelastic Properties of Dilute Solutions of Coiling Polymers. *The Journal of Chemical Physics*, 21(7):1272–1280, 1953.

[97] B. Zimm. Dynamics of Polymer Molecules in Dilute Solution - Viscoelasticity, Flow Birefringence and Dielectric Loss. *The Journal of Chemical Physics*, 24(2):269–278, 1956.

[98] G. Weill and J. des Cloizeaux. Dynamics of polymers in dilute solutions : an explanation of anomalous indices by cross-over effects. *Journal de Physique*, 40(1):99–105, 1979.

[99] P. T. Callaghan and D. N. Pinder. Self-diffusion of random-coil polystyrene determined by pulsed field gradient nuclear magnetic-resonance - dependence on concentration and molar mass. *Macromolecules*, 14(5):1334–1340, 1981.

[100] D. K. Wilkins, S. B. Grimshaw, V. Receveur, C. M. Dobson, J. A. Jones, and L. J. Smith. Hydrodynamic radii of native and denatured proteins measured by pulse field gradient NMR techniques. *Biochemistry*, 38(50):16424–16431, 1999.

[101] J. G. Kirkwood and J. Riseman. The Intrinsic Viscosities and Diffusion Constants of Flexible Macromolecules in Solution. *The Journal of Chemical Physics*, 16(6):565–573, 1948.

[102] B. Dünweg. Molecular dynamics algorithms and hydrodynamic screening. *The Journal of Chemical Physics*, 99(9):6977–6982, 1993.

[103] R. Chang and A. Yethiraj. Brownian dynamics simulations of salt-free polyelectrolyte solutions. *The Journal of Chemical Physics*, 116(12):5284–5298, 2002.

[104] T. Zhou and S. B. Chen. Computer simulations of diffusion and dynamics of short-chain polyelectrolytes. *The Journal of Chemical Physics*, 124(3):034904, 2006.

[105] K. Grass and C. Holm. Polyelectrolytes in electric fields: measuring the dynamical effective charge and effective friction. *Soft Matter*, 5:2079–2092, 2009.

[106] H. Kielman and J. Leyte. Nuclear Magnetic-Relaxation of P-31 in Aqueous Orthophosphate Solutions. *Berichte Der Bunsen-Gesellschaft-Physical Chemistry Chemical Physics*, 79(12): 1201–1205, 1975.

[107] K. Zero and B. Ware. Mobilities of Poly-L-Lysine Molecules in Low-Salt Solutions. *The Journal of Chemical Physics*, 80(4):1610–1616, 1984.

[108] F. J. M. Schipper and J. C. Leyte. Mass transport in polyelectrolyte solutions. *Journal of Physics: Condensed Matter*, 11(6):1409, 1999.

[109] M. Tokuyama and I. Oppenheim. Dynamics of Hard-Sphere Suspensions. *Physical Review E*, 50 (1):R16–R19, 1994.

[110] L. Liu, J. Chen, W. Chen, L. Li, and L. An. Diffusion behavior of polyelectrolytes in dilute solution: coupling effects of hydrodynamic and Coulomb interactions. *Science China Chemistry*, 57(7):1048–1052, 2014.

[111] H.-X. Zhou, G. Rivas, and A. P. Minton. Macromolecular crowding and confinement: Biochemical, biophysical, and potential physiological consequences. In *Annual Review of Biophysics*, volume 37, pages 375–397. Annual Reviews, 2008.

[112] R. Pecora. Dynamics of Biological Polyelectrolytes. *Macromolecular Symposia*, 229(1):18–23, 2005.

[113] G.-W. Li, O. G. Berg, and J. Elf. Effects of macromolecular crowding and DNA looping on gene regulation kinetics. *Nature Physics*, 5(4):294–297, 2009.

[114] I. Pastor, L. Pitulice, C. Balcells, E. Vilaseca, S. Madurga, A. Isvoran, M. Cascante, and F. Mas. Effect of crowding by Dextrans in enzymatic reactions. *Biophysical Chemistry*, 185:8–13, 2014.

[115] E. Bartsch. Diffusion in concentrated colloidal suspensions and glasses. *Curr. Opin. Colloid Interface Sci.*, 3(6):577–585, 1998.

[116] S.-J. E. Lee and A. K. Chakraborty. Sequence dependence of polymer dynamics in quenched disordered media: Weak attraction facilitates transport. *The Journal of Chemical Physics*, 117(23): 10869–10876, 2002.

[117] T. Odijk. Protein-macromolecule interactions. *Macromolecules*, 29(5):1842–1843, 1996.

[118] D. S. Banks and C. F. Anomalous diffusion of proteins due to molecular crowding. *Biophys. J.*, 89 (5):2960–2971, 2005.

[119] P. Polanowski and A. Sikorski. Simulation of diffusion in a crowded environment. *Soft Matter*, 10: 3597–607, 2014.

[120] S. K. Ghosh, A. G. Cherstvy, and R. Metzler. Non-universal tracer diffusion in crowded media of non-inert obstacles. *Phys. Chem. Chem. Phys.*, 17(3):1847–1858, 2015.

[121] F. Roosen-Runge, M. Hennig, F. Zhang, R. M. J. Jacobs, M. Sztucki, H. Schober, T. Seydel, and F. Schreiber. Protein self-diffusion in crowded solutions. *Proc. Natl. Acad. Sci. U.S.A.*, 108(29): 11815–11820, 2011.

[122] P. G. de Gennes. Reptation of a Polymer Chain in Presence of Fixed Obstacles. *The Journal of Chemical Physics*, 55(2):572, 1971.

[123] A. Baumgartner and M. Muthukumar. A Trapped Polymer-Chain in Random Porous-Media. *The Journal of Chemical Physics*, 87(5):3082–3088, 1987.

[124] M. Muthukumar and A. Baumgaertner. Diffusion of a polymer chain in random media. *Macromolecules*, 22(4):1941–1946, 1989.

[125] E. Vilaseca, A. Isvoran, S. Madurga, I. Pastor, J. L. Garcés, and F. Mas. New insights into diffusion in 3d crowded media by Monte Carlo simulations: effect of size, mobility and spatial distribution of obstacles. *Physical Chemistry Chemical Physics*, 13(16):7396–7407, 2011.

[126] H. N. W. Lekkerkerker and J. K. G. Dhont. On the calculation of the self-diffusion coefficient of interacting Brownian particles. *The Journal of Chemical Physics*, 80(11):5790–5792, 1984.

[127] B. Jönsson and H. Wennerström. Thermodynamics of Ionic Amphiphile-Water Systems. *Journal of Colloid and Interface Science*, 80(2):482–496, 1981.

[128] A. H. Muhr and J. M. V. Blanshard. Diffusion in gels. *Polymer*, 23(7):1012–1026, 1982.

[129] J. H. Wang. Theory of the Self-diffusion of Water in Protein Solutions. A New Method for Studying the Hydration and Shape of Protein Molecules. *Journal of the American Chemical Society*, 76(19): 4755–4763, 1954.

[130] E. Cheever, F. D. Blum, K. R. Foster, and R. A. Mackay. Self-diffusion of water in ionic and nonionic microemulsions. *J. Colloid Interface Sci.*, 104(1):121–129, 1985.

[131] P. Venema, R. P. W. J. Struis, J. C. Leyte, and D. Bedeaux. The effective self-diffusion coefficient of solvent molecules in colloidal crystals. *Journal of Colloid and Interface Science*, 141(2):360–373, 1991.

[132] R. Bai, P. J. Basser, R. M. Briber, and F. Horkay. NMR Water Self-Diffusion and Relaxation Studies on Sodium Polyacrylate Solutions and Gels in Physiologic Ionic Solutions. *J. Appl. Polym. Sci.*, 131(6):1–7, 2014.

[133] G. M. Bell. Self-diffusion of ions in the electric fields of spherical particles. *Trans. Faraday Soc.*, 60:1752–1759, 1964.

[134] M. Blees and J. Leyte. The Effective Translational Self-Diffusion Coefficient of Small Molecules in Colloidal Crystals of Spherical-Particles. *Journal of Colloid and Interface Science*, 166(1): 118–127, 1994.

[135] J. Feng-Hua Wang, Y. Shang, L. Zhou, H.-X., H. Liu, and Y. Hu. Translocation of Polymer Through a Nanopore Studied by Langevin Dynamics: Effect of the Friction Coefficient. *Chinese Journal of Chemical Engineering*, 20(2):231–238, 2012.

[136] H. Fricke. A Mathematical Treatment of the Electric Conductivity and Capacity of Disperse Systems I. The Electric Conductivity of a Suspension of Homogeneous Spheroids. *Physical Review*, 24(5):575–587, 1924.

[137] J. C. Maxwell. *A treatise on electricity and magnetism*. Oxford : Clarendon Press, 1873.

[138] L. Masaro and X. X. Zhu. Physical models of diffusion for polymer solutions, gels and solids. *Progress in Polymer Science*, 24(5):731–775, 1999.

[139] R. Waggoner, F. Blum, and J. Macelroy. Dependence of the Solvent Diffusion-Coefficient on Concentration in Polymer-Solutions. *Macromolecules*, 26(25):6841–6848, 1993.

[140] J. S. Mackie and P. Meares. The Diffusion of Electrolytes in a Cation-Exchange Resin Membrane. I. Theoretical. *Proceedings of the Royal Society of London A: Mathematical, Physical and Engineering Sciences*, 232(1191):498–509, 1955.

[141] S. Pickup and F. D. Blum. Self-diffusion of toluene in polystyrene solutions. *Macromolecules*, 22 (10):3961–3968, 1989.

[142] C. S. Johnson and D. A. Gabriel. *Laser Light Scattering*. Courier Dover Publications, 1994.

[143] T. L. Hill. *An Introduction to Statistical Thermodynamics*. Courier Corporation, 1960.

[144] B. Jönsson, H. Wennerström, P. G. Nilsson, and P. Linse. Self-diffusion of small molecules in colloidal systems. *Colloid and Polymer Science*, 264(1):77–88, 1986.

[145] M. Blees and J. Leyte. Self-Diffusion of Small Hydrophobic Molecules in Aqueous Poly(n-Butylacrylate Acrylic-Acid) Latex Dispersions. *Journal of Colloid and Interface Science*, 157(2): 355–360, 1993.

[146] M. V. Smoluchowski. Über Brownsche Molekularbewegung unter Einwirkung äußerer Kräfte und deren Zusammenhang mit der verallgemeinerten Diffusionsgleichung. *Ann. Phys.*, 353(24): 1103–1112, 1916.

[147] J. H. Huang, Z. F. Mao, and C. J. Qian. Dynamic Monte Carlo study on the polymer chain in random media filled with nanoparticles. *Polymer*, 47(8):2928–2932, 2006.

[148] G. G. Putzel, M. Tagliazucchi, and I. Szleifer. Nonmonotonic Diffusion of Particles Among Larger Attractive Crowding Spheres. *Physical Review Letters*, 113(13):138302, 2014.

[149] G. M. Bell and A. J. Dunning. Counter-ion self-diffusion in a concentrated micellar system. *Trans. Faraday Soc.*, 66:500–508, 1970.

[150] D. Chan and B. Halle. The Smoluchowski-Poisson-Boltzmann description of ion diffusion at charged interfaces. *Biophys. J.*, 46(3):387–407, 1984.

[151] L. Belloni, M. Drifford, and P. Turq. Counterion diffusion in polyelectrolyte solutions. *Chemical physics*, 83(1):147–154, 1984.

[152] L. G. Nilsson, L. Nordenskioeld, P. Stilbs, and W. H. Braunlin. Macroscopic counterion diffusion in solutions of cylindrical polyelectrolytes. *The Journal of Physical Chemistry*, 89(15):3385–3391, 1985.

[153] N. Fatin-Rouge, A. Milon, J. Buffle, R. R. Goulet, and A. Tessier. Diffusion and Partitioning of Solutes in Agarose Hydrogels: The Relative Influence of Electrostatic and Specific Interactions. *J. Phys. Chem. B*, 107(44):12126–12137, 2003.

[154] L. H. Lucas and C. K. Larive. Measuring ligand-protein binding using NMR diffusion experiments. *Concepts Magn. Reson.*, 20A(1):24–41, 2004.

[155] G. Hostnik, M. Bončina, C. Dolce, G. Mériguet, A.-L. Rollet, and J. Cerar. Influence of counterions on the conformation of conjugated polyelectrolytes: the case of poly(thiophen-3-ylacetic acid). *Phys. Chem. Chem. Phys.*, 18(36):25036–25047, 2016.

[156] J. Vrentas and J. Duda. Diffusion in Polymer-Solvent Systems .2. Predictive Theory for Dependence of Diffusion-Coefficients on Temperature, Concentration, and Molecular-Weight. *Journal of Polymer Science Part B-Polymer Physics*, 15(3):417–439, 1977.

[157] N. Peppas and C. Reinhart. Solute Diffusion in Swollen Membranes .1. a New Theory. *Journal of Membrane Science*, 15(3):275–287, 1983.

[158] T. O'Leary. Concentration dependence of protein diffusion. *Biophys. J.*, 52(1):137–139, 1987.

[159] N. Muramatsu and a. P. Minton. Tracer diffusion of globular proteins in concentrated protein solutions. *Proc. Natl. Acad. Sci. U.S.A.*, 85(9):2984–2988, 1988.

[160] J. Han and J. Herzfeld. Macromolecular diffusion in crowded solutions. *Biophys. J.*, 65(3): 1155–61, 1993.

[161] G. Nägele, J. K. G. Dhont, and G. Meier. Diffusion in Colloidal and Polymeric systems. In P. Heitjans and J. Kärger, editors, *Diffusion in Condensed Matter*, chapter 16, pages 620–715. Springer-Verlag, Berlin/Heidelberg, 2005.

[162] J. K. G. Dhont. *An Introduction to Dynamics of Colloids*. Elsevier, 1996.

[163] N. Yoshida. Concentration dependence of the self-diffusion coefficient of hard spheres in solution. *Chem. Phys. Lett.*, 101(6):555–561, 1983.

[164] N. Yoshida. Calculation of the self-diffusion coefficient of interacting Brownian particles based on the time-independent Smoluchowski equation. *J. Chem. Phys.*, 83(9):4786, 1985.

[165] S. Hanna, W. Hess, and R. Klein. Self-diffusion of spherical Brownian particles with hard-core interaction. *Physica A*, 111(1-2):181–199, 1982.

[166] P. Bernadó, J. García de la Torre, and M. Pons. Macromolecular crowding in biological systems: hydrodynamics and NMR methods. *J. Mol. Recognit.*, 17(5):397–407, 2004.

[167] G. Nägele and P. Baur. Long-time dynamics of charged colloidal suspensions: hydrodynamic interaction effects. *Physica A*, 245(3-4):297–336, 1997.

[168] M. G. McPhie and G. Nägele. Long-time self-diffusion of charged colloidal particles: electrokinetic and hydrodynamic interaction effects. *J. Chem. Phys.*, 127(3):034906, 2007.

[169] J.-F. Dufrêche, M. Jardat, P. Turq, and B. Bagchi. Electrostatic Relaxation and Hydrodynamic Interactions for Self-Diffusion of Ions in Electrolyte Solutions. *J. Phys. Chem. B*, 112(33): 10264–10271, 2008.

[170] M. Jardat, O. Bernard, P. Turq, and G. R. Kneller. Transport coefficients of electrolyte solutions from Smart Brownian dynamics simulations. *J. Chem. Phys.*, 110(16):7993, 1999.

[171] M. Jardat, S. Durand-Vidal, N. Da Mota, and P. Turq. Transport coefficients of aqueous dodecyltrimethylammonium bromide solutions: comparison between experiments, analytical calculations and numerical simulations. *J. Chem. Phys.*, 120(13):6268–73, 2004.

[172] G. Batôt, V. Dahirel, G. Mériguet, a. a. Louis, and M. Jardat. Dynamics of solutes with hydrodynamic interactions: Comparison between Brownian dynamics and stochastic rotation dynamics simulations. *Phys. Rev. E*, 88(4):043304, 2013.

[173] M. Jardat, B. Hribar-Lee, and V. Vlachy. Self-diffusion coefficients of ions in the presence of charged obstacles. *Phys. Chem. Chem. Phys.*, 10(3):449, 2008.

[174] M. Długosz and J. Trylska. Diffusion in crowded biological environments: applications of Brownian dynamics. *BMC Biophys.*, 4:3, 2011.

[175] T. Stylianopoulos, M.-Z. Poh, N. Insin, M. G. Bawendi, D. Fukumura, L. L. Munn, and R. K. Jain. Diffusion of particles in the extracellular matrix: the effect of repulsive electrostatic interactions. *Biophys. J.*, 99(5):1342–9, 2010.

[176] C. Echeverria and R. Kapral. Macromolecular dynamics in crowded environments. *J. Chem. Phys.*, 132(10):104902, 2010.

[177] A. Tomilov, A. Videcoq, T. Chartier, T. Ala-Nissilä, and I. Vattulainen. Tracer diffusion in colloidal suspensions under dilute and crowded conditions with hydrodynamic interactions. *J. Chem. Phys.*, 137(1):014503, 2012.

[178] G. Nägele and J. K. G. Dhont. Tracer-diffusion in colloidal mixtures: A mode-coupling scheme with hydrodynamic interactions. *J. Chem. Phys.*, 108(22):9566, 1998.

[179] G. Nägele, M. Medina-Noyola, J. L. Arauz-Lara, and R. Klein. A simple theory for the self-diffusion coefficients in binary mixtures of highly charged spherical macroions. In *New Trends Colloid Sci.*, volume 73 of *Progress in Colloid & Polymer Science*, pages 5–9. Steinkopff, Darmstadt, 1987.

[180] J. L. Arauz-Lara, H. Ruiz-Estrada, M. Medina-Noyola, G. Nägele, and R. Klein. Tracer-diffusion in binary mixtures of charged spherical macroparticles. In *Trends Colloid Interface Sci. V*, volume 84 of *Progress in Colloid & Polymer Science*, pages 377–380. Steinkopff, Darmstadt, 1991.

[181] J. L. Arauz-Lara, H. Ruiz-Estrada, and M. Medina-Noyola. Tracer Diffusion in Colloidal Mixtures. *J. Colloid Interface Sci.*, 171(1):127–133, 1995.

[182] S. Balayssac, S. Trefi, V. Gilard, M. Malet-Martino, R. Martino, and M.-a. Delsuc. 2D and 3D DOSY 1H NMR, a useful tool for analysis of complex mixtures: application to herbal drugs or dietary supplements for erectile dysfunction. *J. Pharm. Biomed. Anal.*, 50(4):602–12, 2009.

[183] J. Vaysse, S. Balayssac, V. Gilard, D. Desoubdzanne, M. Malet-Martino, and R. Martino. Analysis of adulterated herbal medicines and dietary supplements marketed for weight loss by DOSY 1 H-NMR. *Food Addit. Contam. Part A*, 27(7):903–916, 2010.

[184] J. Vaysse, V. Gilard, S. Balayssac, C. Zedde, R. Martino, and M. Malet-Martino. Identification of a novel sildenafil analogue in an adulterated herbal supplement. *J. Pharm. Biomed. Anal.*, 59(1): 58–66, 2012.

[185] F. Ribot, V. Escax, C. Roiland, C. Sanchez, J. C. Martins, M. Biesemans, I. Verbruggen, and R. Willem. In situ evaluation of interfacial affinity in CeO2 based hybrid nanoparticles by pulsed field gradient NMR. *Chem. Commun.*, 3(8):1019–21, 2005.

[186] L. Van Lokeren, G. Maheut, F. Ribot, V. Escax, I. Verbruggen, C. Sanchez, J. C. Martins, M. Biesemans, and R. Willem. Characterization of titanium dioxide nanoparticles dispersed in organic ligand solutions by using a diffusion-ordered spectroscopy-based strategy. *Chem. Eur. J*, 13(24): 6957–66, 2007.

[187] A. Guillermo and M. Bardet. In Situ Pulsed-Field Gradient NMR Determination of the Size of Oil Bodies in Vegetable Seeds. Analysis of the Effect of the Gradient Pulse Length. *Anal. Chem.*, 79 (17):6718–6726, 2007.

[188] K. László, A. Guillermo, A. Fluerasu, A. Moussaïd, and E. Geissler. Microphase Structure of Poly(N -isopropylacrylamide) Hydrogels As Seen by Small- and Wide-Angle X-ray Scattering and Pulsed Field Gradient NMR. *Langmuir*, 26(6):4415–4420, 2010.

[189] Q. Berrod, S. Lyonnard, A. Guillermo, J. Ollivier, B. Frick, A. Manseri, B. Améduri, and G. Gébel. Nanostructure and Transport Properties of Proton Conducting Self-Assembled Perfluorinated Surfactants: A Bottom-Up Approach toward PFSA Fuel Cell Membranes. *Macromolecules*, 48 (17):6166–6176, 2015.

[190] P. Hagmann, L. Jonasson, P. Maeder, J.-P. Thiran, V. J. Wedeen, and R. Meuli. Understanding Diffusion MR Imaging Techniques: From Scalar Diffusion-weighted Imaging to Diffusion Tensor Imaging and Beyond. *RadioGraphics*, 26(suppl_1):S205–S223, 2006.

[191] A. A. Sapega, D. P. Sokolow, T. J. Graham, and B. Chance. Phosphorus nuclear magnetic resonance: a non-invasive technique for the study of muscle bioenergetics during exercise. *Medicine and science in sports and exercise*, 19(4):410–420, 1987.

[192] P. J. Hore. *Nuclear magnetic resonance*. Oxford University Press, Oxford; New York, 1995.

[193] P. Callaghan. *Translational Dynamics and Magnetic Resonance: Principles of Pulsed Gradient Spin Echo NMR*. OUP Oxford, 2011.

[194] D. Pristinski, V. Kozlovskaya, and S. A. Sukhishvili. Fluorescence correlation spectroscopy studies of diffusion of a weak polyelectrolyte in aqueous solutions. *J. Chem. Phys.*, 122(1):14907, 2005.

[195] R. McDonough, R. Cueto, G. D. J. Phillies, P. S. Russo, D. Dorman, and K. A. Streletzky. Fluorescent Labeling Can Alter Polymer Solution Dynamics. *Macromolecules*, 48(19):7245–7255, 2015.

[196] M. Sedlák. Structure and dynamics of polyelectrolyte solutions by light scattering. In T. Radeva, editor, *Physical chemistry of polyelectrolytes*, Surfactant Science, pages 1–58. Marcel Dekker, Inc, New York, 2001.

[197] C. J. Jameson. Understanding NMR chemical shift. *Annu. Rev. Phys. Chem.*, 47(1):135–169, 1996.

[198] C. L. Cooper, T. Cosgrove, J. S. v. Duijneveldt, M. Murray, and S. W. Prescott. The use of solvent relaxation NMR to study colloidal suspensions. *Soft Matter*, 9(30):7211–7228, 2013.

[199] D. Canet and P. Mutzenhardt. Relaxation in Nuclear Magnetic Resonance, General. In R. A. Meyers, editor, *Encycl. Anal. Chem.*, pages 12265–12291. John Wiley & Sons, Ltd, Chichester, UK, 2000.

[200] P. Hore, J. Jones, and S. Wimperis. *NMR: The Toolkit: how Pulse Sequences Work*. Oxford University Press, USA, 2015.

[201] R. L. Vold, J. S. Waugh, M. P. Klein, and D. E. Phelps. Measurement of Spin Relaxation in Complex Systems. *J. Chem. Phys.*, 48(8):3831–3832, 1968.

[202] E. L. Hahn. Spin Echoes. *Physical Review*, 80(4):580–594, 1950.

[203] H. Y. Carr and E. M. Purcell. Effects of Diffusion on Free Precession in Nuclear Magnetic Resonance Experiments. *Phys. Rev.*, 94(3):630–638, 1954.

[204] S. Meiboom and D. Gill. Modified Spin-Echo Method for Measuring Nuclear Relaxation Times. *Rev. Sci. Instrum.*, 29(8):688–691, 1958.

[205] R. Kimmich. Molecular Dynamics in Polymers. In *Principles of Soft-Matter Dynamics*, chapter 5, pages 373–498. Springer Netherlands, Dordrecht, 2012.

[206] C. S. Johnson. Diffusion ordered nuclear magnetic resonance spectroscopy: principles and applications. *Progress in Nuclear Magnetic Resonance Spectroscopy*, 34(3-4):203–256, 1999.

[207] E. O. Stejskal and J. E. Tanner. *The Journal of Chemical Physics*, 42(1):288–292, 1965.

[208] S. Mori and J. Zhang. Principles of diffusion tensor imaging and its applications to basic neuroscience research. *Neuron*, 51(5):527–539, 2006.

[209] E. O. Stejskal. Use of Spin Echoes in a Pulsed Magnetic-Field Gradient to Study Anisotropic, Restricted Diffusion and Flow. *The Journal of Chemical Physics*, 43(10):3597, 1965.

[210] J. E. Tanner. Use of the Stimulated Echo in NMR Diffusion Studies. *J. Chem. Phys.*, 52(5):2523, 1970.

[211] D. H. Wu, A. D. Chen, and C. S. Johnson. An improved diffusion-ordered spectroscopy experiment incorporating bipolar-gradient pulses. *J. Magn. Reson., Ser. A*, 115(2):260–264, 1995.

[212] R. Karlicek and I. Lowe. A modified pulsed gradient technique for measuring diffusion in the presence of large background gradients. *J. Magn. Reson.*, 37(1):75–91, 1980.

[213] E. Fordham, S. Gibbs, and L. Hall. Partially restricted diffusion in a permeable sandstone: Observations by stimulated echo PFG NMR. *Magn. Reson. Imaging*, 12(2):279–284, 1994.

[214] G. Zheng and W. S. Price. Solvent signal suppression in NMR. *Prog. Nucl. Magn. Reson. Spectrosc.*, 56(3):267–288, 2010.

[215] M. Piotto, V. Saudek, and V. Sklenář. Gradient-tailored excitation for single-quantum nmr spectroscopy of aqueous solutions. *Journal of biomolecular NMR*, 2(6):661–665, 1992.

[216] G. A. Morris and R. Freeman. Enhancement of nuclear magnetic resonance signals by polarization transfer. *Journal of the American Chemical Society*, 101(3):760–762, 1979.

[217] D. Li, R. Hopson, W. Li, J. Liu, and P. G. Williard. 13c inept diffusion-ordered nmr spectroscopy (dosy) with internal references. *Organic letters*, 10(5):909–911, 2008.

[218] J. A. Aguilar, R. W. Adams, M. Nilsson, and G. A. Morris. Suppressing exchange effects in diffusion-ordered nmr spectroscopy. *Journal of Magnetic Resonance*, 238:16–19, 2014.

[219] G. A. Morris. Diffusion-Ordered Spectroscopy (DOSY). In D. M. Grant and R. K. Harris, editors, *Adv. NMR*, Encyclopedia of Nuclear Magnetic Resonance Volume, pages 35–44. John Wiley & Sons, 2002.

[220] A. Jerschow and N. Müller. Suppression of Convection Artifacts in Stimulated-Echo Diffusion Experiments. Double-Stimulated-Echo Experiments. *J. Magn. Reson.*, 125(2):372–375, 1997.

[221] Y. Shrot and L. Frydman. Single-scan 2d dosy nmr spectroscopy. *Journal of Magnetic Resonance*, 195(2):226–231, 2008.

[222] W. S. Price. Pulsed-field gradient nuclear magnetic resonance as a tool for studying translational diffusion: Part 1. basic theory. *Concepts Magn. Reson.*, 9(5):299–336, 1997.

[223] M. Holz and H. Weingartner. Calibration in Accurate Spin-Echo Self-Diffusion Measurements Using H-1 and Less-Common Nuclei. *Journal of Magnetic Resonance*, 92(1):115–125, 1991.

[224] M. Holz, S. R. H., and A. Sacco. Temperature-dependent self-diffusion coefficients of water and six selected molecular liquids for calibration in accurate 1H NMR PFG measurements. *Phys. Chem. Chem. Phys.*, 2(20):4740–4742, 2000.

[225] R. T. Mckay. Recent Advances in Solvent Suppression for Solution NMR: A Practical Reference. *Annu. Reports NMR Spectrosc.*, 66:33–76, 2009.

[226] W. van Megen and S. M. Underwood. Tracer diffusion in concentrated colloidal dispersions. II. Non-Gaussian effects. *J. Chem. Phys.*, 88(12):7841–7846, 1988.

[227] B. Håkansson, M. Nydén, and O. Söderman. The influence of polymer molecular-weight distributions on pulsed field gradient nuclear magnetic resonance self-diffusion experiments. *Colloid Polym. Sci.*, 278(5):399–405, 2000.

[228] M. G. Oostwal, M. H. Blees, J. De Bleijser, and J. C. Leyte. Chain self-diffusion in aqueous salt-free solutions of sodium poly(styrenesulfonate). *Macromolecules*, 26(26):7300–7308, 1993.

[229] H. Walderhaug, O. Söderman, and D. Topgaard. Self-diffusion in polymer systems studied by magnetic field-gradient spin-echo NMR methods. *Prog. Nucl. Magn. Reson. Spectrosc.*, 56(4): 406–425, 2010.

[230] M. Röding, D. Bernin, J. Jonasson, A. Sarkka, D. Topgaard, M. Rudemo, and M. Nyden. The gamma distribution model for pulsed-field gradient NMR studies of molecular-weight distributions of polymers. *Journal of Magnetic Resonance*, 222:105–111, 2012.

[231] A. Chen, D. Wu, and C. S. Johnson. Determination of Molecular Weight Distributions for Polymers by Diffusion-Ordered NMR. *J. Am. Chem. Soc.*, 117(30):7965–7970, 1995.

[232] W. Li, H. Chung, C. Daeffler, J. a. Johnson, and R. H. Grubbs. Application of (1)H DOSY for Facile Measurement of Polymer Molecular Weights. *Macromolecules*, 45(24):9595–9603, 2012.

[233] P. T. Callaghan and D. N. Pinder. A pulsed field gradient NMR study of self-diffusion in a polydisperse polymer system: dextran in water. *Macromolecules*, 16(6):968–973, 1983.

[234] K. Terao. *Poly(acrylic acid) (PAA)*. Springer, Berlin, Heidelberg, 2014.

[235] N. Ise, T. Okubo, K. Yamamoto, H. Kawai, T. Hashimoto, M. Fujimura, and Y. Hiragi. Ordered structure in dilute solutions of ionic biopolymers. 2. Small-angle X-ray scattering study of sodium polyacrylate solution. *J. Am. Chem. Soc.*, 102(27):7901–7906, 1980.

[236] J. Kestin, H. Khalifa, and R. Correia. Tables of the Dynamic and Kinematic Viscosity of Aqueous Nacl Solutions. *J. Phys. Chem. Ref. Data*, 10(1):71–87, 1981.

[237] T. Saito, K. Shimada, and S. Kinugasa. Determination of the size of a polystyrene nanosphere by the pulsed field gradient nuclear magnetic resonance method. *Langmuir*, 20(11):4779–4781, 2004.

[238] E. A. Litmanovich, S. O. Zakharchenko, and G. V. Stoichev. Influence of chain charge and complexation on the overlap and entanglements formation in poly (acrylic acid) salt-containing aqueous solutions. *The Journal of Physical Chemistry B*, 111(29):8567–8571, 2007.

[239] T. Cosgrove and P. Griffiths. The Critical Overlap Concentration Measured by Pulsed-Field Gradient Nuclear-Magnetic-Resonance Techniques. *Polymer*, 35(3):509–513, 1994.

[240] S. Forster, M. Schmidt, and M. Antonietti. Static and Dynamic Light-Scattering by Aqueous Polyelectrolyte Solutions - Effect of Molecular-Weight, Charge-Density and Added Salt. *Polymer*, 31(5):781–792, 1990.

[241] A. Topp, L. Belkoura, and D. Woermann. Dynamic Light Scattering Experiments with Aqueous Solutions of Polyelectrolytes of Low Charge Density Along the Polymer Chain in the Presence of Salt. *Berichte der Bunsengesellschaft für physikalische Chemie*, 99(5):730–735, 1995.

[242] R. Pecora. *Dynamic Light Scattering*. Springer US, Boston, MA, 1985.

[243] A. Sadeghpour, A. Vaccaro, S. Rentsch, and M. Borkovec. Influence of alkali metal counterions on the charging behavior of poly(acrylic acid). *Polymer*, 50(16):3950–3954, 2009.

[244] L. J. Henderson. Concerning the relationship between the strength of acids and their capacity to preserve neutrality. *American Journal of Physiology–Legacy Content*, 21(2):173–179, 1908.

[245] K. A. Hasselbalch. *Die Berechnung der Wasserstoffzahl des Blutes aus der freien und gebundenen Kohlensäure desselben, und die Sauerstoffbindung des Blutes als Funktion der Wasserstoffzahl*. Julius Springer, 1916.

[246] M. Borkovec, B. Jönsson, and G. J. M. Koper. Ionization Processes and Proton Binding in Polyprotic Systems: Small Molecules, Proteins, Interfaces, and Polyelectrolytes. In *Surface and Colloid Science*, volume 16, pages 99–339. Springer US, Boston, MA, 2001.

[247] V. V. Annenkov, V. A. Kruglova, and N. L. Mazyar. Analysis of the potentiometric titration curves within the framework of the theory of the "neighbor effect". *J. Polym. Sci. Part B Polym. Phys.*, 36 (6):931–936, 1998.

[248] F. Carnal, S. Ulrich, and S. Stoll. Influence of Explicit Ions on Titration Curves and Conformations of Flexible Polyelectrolytes: A Monte Carlo Study. *Macromolecules*, 43(5):2544–2553, 2010.

[249] M. Ullner, B. Jönsson, and P.-O. Widmark. Conformational properties and apparent dissociation constants of titrating polyelectrolytes: Monte Carlo simulation and scaling arguments. *J. Chem. Phys.*, 100(4):3365, 1994.

[250] M. Ullner, B. Jönsson, B.on, B. Söderberg, and C. Peterson. A Monte Carlo study of titrating polyelectrolytes. *J. Chem. Phys.*, 104(8):3048–3057, 1996.

[251] R. Arnold. The titration of polymeric acids. *J. Colloid Sci.*, 12(6):549–556, 1957.

[252] G. S. Manning. Limiting Laws and Counterion Condensation in Polyelectrolyte Solutions I. Colligative Properties. *J. Chem. Phys.*, 51(3):924–933, 1969.

[253] M. Barisik, S. Atalay, A. Beskok, and S. Qian. Size Dependent Surface Charge Properties of Silica Nanoparticles. *J. Phys. Chem. C*, 118(4):1836–1842, 2014.

[254] S. Stoll. The Importance of Zeta Potential Measurements & Role of Ionic Strength in Flocculation Processes. *Water Technol.*, 4(1):1–5, 2013.

[255] N. Spanos, P. G. Klepetsanis, and P. K. Koutsoukos. Calculation of zeta-potentials form electrokinetic data. In *Encycl. Surf. Colloid Sci.*, pages 829–845. Taylor & Francis, 2002.

[256] O. A. Hickey, T. N. Shendruk, J. L. Harden, and G. W. Slater. Simulations of Free-Solution Electrophoresis of Polyelectrolytes with a Finite Debye Length Using the Debye-Hüuckel Approximation. *Physical Review Letters*, 109(9):098302, 2012.

[257] P. Attard, D. Antelmi, and I. Larson. Comparison of the Zeta Potential with the Diffuse Layer Potential from Charge Titration. *Langmuir*, 16(4):1542–1552, 2000.

[258] J. Spevacek, M. Suchoparek, and S. Alalawi. Characterization of the Stereochemical Structure of Poly(acrylic Acid). *Polymer*, 36(21):4125–4130, 1995.

[259] D. S. Wishart, C. G. Bigam, J. Yao, F. Abildgaard, H. J. Dyson, E. Oldfield, J. L. Markley, and B. D. Sykes. 1h, 13c and 15n chemical shift referencing in biomolecular NMR. *Journal of Biomolecular NMR*, 6(2):135–140, 1995.

[260] J. Bezencon, M. B. W., B. Cutting, M. Smiesko, B. Wagner, M. Kansy, and B. Ernst. pK(a) determination by H-1 NMR spectroscopy - An old methodology revisited. *Journal of Pharmaceutical and Biomedical Analysis*, 93:147–155, 2014.

[261] T. Tynkkynen, M. Tiainen, P. Soininen, and R. Laatikainen. From proton nuclear magnetic resonance spectra to ph. assessment of ^{1}H NMR pH indicator compound set for deuterium oxide solutions. *Anal. Chim. Acta*, 648(1):105–12, 2009.

[262] D. P. Cistola, D. M. Small, and J. A. Hamilton. Ionization behavior of aqueous short-chain carboxylic acids: a carbon-13 NMR study. *J. Lipid Res.*, 23(5):795–799, 1982.

[263] C. Chang, D. D. Muccio, and T. St. Pierre. Determination of the tacticity and analysis of the pH titration of poly(acrylic acid) by proton and carbon-13 NMR. *Macromolecules*, 18(11):2154–2157, 1985.

[264] W. G. Schneider, H. J. Bernstein, and J. A. Pople. Proton Magnetic Resonance Chemical Shift of Free (Gaseous) and Associated (Liquid) Hydride Molecules. *J. Chem. Phys.*, 28(4):601, 1958.

[265] A. Buckingham. Chemical Shifts in the Nuclear Magnetic Resonance Spectra of Molecules Containing Polar Groups. *Can. J. Chem.*, 38(2):300–307, 1960.

[266] W.-M. Kulicke and C. Clasen. *Viscosimetry of polymers and polyelectrolytes*. Springer Science & Business Media, 2013.

[267] Y. Mylonas, G. Staikos, and M. Ullner. Chain conformation and intermolecular interaction of partially neutralized poly(acrylic acid) in dilute aqueous solutions. *Polymer*, 40(24):6841–6847, 1999.

[268] D. J. Ramsay and K. S. Schmitz. Quasi-Elastic Light Scattering and Fluorescence Photobleaching Recovery Studies on Poly(lysine) Dynamics. *Macromolecules*, 18(12):2422–2429, 1985.

[269] A. Sehgal and T. a. P. Seery. Polyelectrolyte Self-Diffusion: Fluorescence Recovery after Photobleaching of Sodium Poly(styrenesulfonate) in N -Methylformamide. *Macromolecules*, 36(26): 10056–10062, 2003.

[270] L. Onsager. Theories and problems of liquid diffusion. *Ann. N. Y. Acad. Sci.*, 46:241–65, 1945.

[271] O. Bernard, W. Kunz, P. Turq, and L. Blum. Self-Diffusion in Electrolyte Solutions Using the Mean Spherical Approximation. *J. Phys. Chem.*, 96(1):398–403, 1992.

[272] M. R. Wright. *An Introduction to Aqueous Electrolyte Solutions*. Wiley-Blackwell, Chichester, England ; Hoboken, NJ :, 2007.

[273] T. Swift, L. Swanson, M. Geoghegan, and S. Rimmer. The pH-responsive behaviour of poly(acrylic acid) in aqueous solution is dependent on molar mass. *Soft Matter*, 2016.

[274] L. Dunn and R. Stokes. The diffusion of monocarboxylic acids in aqueous solution at 25. *Aust. J. Chem.*, 18(3):285–296, 1965.

[275] W. J. Albery, A. R. Greenwood, and R. F. Kibble. Diffusion coefficients of carboxylic acids. *Trans. Faraday Soc.*, 63:360–368, 1967.

[276] G. Ramanathan. Counterion condensation in micellar and colloidal solutions. *The Journal of Chemical Physics*, 88(6):3887–3892, 1988.

[277] C. Flood, T. Cosgrove, Y. Espidel, I. Howell, and P. Revell. Sodium polyacrylate adsorption onto anionic and cationic silica in the presence of salts. *Langmuir*, 23(11):6191–6197, 2007.

[278] F. Boué. Les polymères comme matériaux désordonnés: l'apport de la diffusion de neutrons. *J. Phys. IV Fr.*, 111:211–241, 2003.

[279] C. D. Dewhurst. D33 a third small-angle neutron scattering instrument at the institut laue langevin. *Measurement Science and Technology*, 19(3):034007, 2008.

[280] J. Schweizer. Que peut-on voir avec des neutrons? Une introduction pour des non spécialistes. *J. Phys. IV*, 130:3–35, 2005.

[281] J. Teixeira. Introduction à la diffusion de neutrons. *École thématique de la Société Française de Neutronique*, 12:1–9, 2007.

[282] G. L. Squires. *Introduction to the Theory of Thermal Neutron Scattering*. Cambridge University Press, 2012.

[283] J. Cotton. Introduction to scattering experiments. In P. Lindner and T. Zemb, editors, *Neutron, X-ray and light scattering : introduction to an investigative tool for colloidal and polymeric systems*, pages 3–19. Elsevier B.V., 1991.

[284] I. Grillo. Small-Angle Neutron Scattering and Applications in Soft Condensed Matter. In *Soft Matter Characterization*, pages 723–782. Springer Netherlands, Dordrecht, 2008.

[285] J. Cotton. Variations on contrast in SANS: determination of self and distinct correlation functions. *Adv. Colloid Interface Sci.*, 69(1-3):1–29, 1996.

[286] J. Cotton. DNPA : introduction et variations sur le contraste. *J. Phys. IV Fr.*, 9:21–49, 1999.

[287] N. Ise and T. Okubo. Partial molal volume of polyelectrolytes. *J. Am. Chem. Soc.*, 90(17): 4527–4533, 1968.

[288] K. Hiraoka, H. Shin, and T. Yokoyama. Density measurements of poly(acrylic acid) sodium salts. *Polym. Bull.*, 8(7-8):211–216, 1982.

[289] A. Moussaid, F. Schosseler, J. P. Munch, and S. J. Candau. Structure of polyacrylic acid and polymethacrylic acid solutions : a small angle neutron scattering study. *Journal de Physique II*, 3 (4):573–594, 1993.

[290] J. Combet, P. Lorchat, and M. Rawiso. Salt-free aqueous solutions of polyelectrolytes: Small angle X-ray and neutron scattering characterization. *Eur. Phys. J. Spec. Top.*, 213:243–265, 2012.

[291] H. Benoit. La diffusion de la lumiere par des macromolecules en chaines en solution dans un bon solvant. *Comptes Rendus Hebdomadaires des Seances de l'Academie des Sciences.*, 245(25): 2244–2247, 1957.

[292] B. Hammouda. *SANS from homogeneous polymer mixtures: A unified overview*, pages 87–133. Springer Berlin Heidelberg, Berlin, Heidelberg, 1993.

[293] B. Hammouda, D. L. Ho, and S. Kline. Insight into Clustering in Poly(ethylene oxide) Solutions. *Macromolecules*, 37(18):6932–6937, 2004.

[294] N. Volk, D. Vollmer, M. Schmidt, W. Oppermann, and K. Huber. Conformation and Phase Diagrams of Flexible Polyelectrolytes. In *Adv. Polym. Sci.*, volume 166, chapter 2, pages 29–65. Springer, 2004.

[295] M. Benmouna and a. Z. Akcasu. Temperature Effects on the Dynamic Structure Factor in Dilute Polymer Solutions. *Macromolecules*, 11(6):1187–1192, 1978.

[296] A. Z. Akcasu and M. Benmouna. Concentration Effects on the Dynamic Structure Factor in Polymer Solutions. *Macromolecules*, 11(6):1193–1198, 1978.

[297] A. Guinier and G. Fournet. *Small-angle scattering of X-rays*. Wiley, 1955.

[298] J. S. Pedersen, D. Posselt, and K. Mortensen. Analytical treatment of the resolution function for small-angle scattering. *J. Appl. Crystallogr.*, 23(4):321–333, 1990.

[299] P. Lindner and T. Zemb. Neutron, x-ray and light scattering: introduction to an investigative tool for colloidal and polymeric systems. 96(6):839–839, 1991.

[300] J. B. Hayter and J. Penfold. An analytic structure factor for macroion solutions. *Molecular Physics*, 42(1):109–118, 1981.

[301] J.-P. Hansen and J. B. Hayter. A rescaled MSA structure factor for dilute charged colloidal dispersions. *Molecular Physics*, 46(3):651–656, 1982.

[302] J.-P. Hansen and I. R. McDonald. Distribution-function Theories. In *Theory of Simple Liquids*, pages 78–108. Elsevier, London ; Orlando :, 3 edition, 2006.

[303] M. Kotlarchyk and S.-H. Chen. Analysis of small angle neutron scattering spectra from polydisperse interacting colloids. *The Journal of chemical physics*, 79(5):2461–2469, 1983.

[304] M. J. Pond, J. R. Errington, and T. M. Truskett. Implications of the effective one-component analysis of pair correlations in colloidal fluids with polydispersity. *J. Chem. Phys.*, 135(12): 124513, 2011.

[305] R. Sharma and K. Sharma. The structure factor and the transport properties of dense fluids having molecules with square well potential, a possible generalization. *Physica A: Statistical Mechanics and its Applications*, 89(1):213–218, 1977.

[306] R. J. Baxter. Percus-Yevick Equation for Hard Spheres with Surface Adhesion. *J. Chem. Phys.*, 49 (6):2770, 1968.

[307] R. K. Iler. *The chemistry of silica : solubility, polymerization, colloid and surface properties, and biochemistry*. Wiley New York, 1979.

[308] J. J. Valle-Delgado, J. A. Molina-Bolívar, F. Galisteo-González, M. J. Gálvez-Ruiz, A. Feiler, and M. W. Rutland. Hydration forces between silica surfaces: Experimental data and predictions from different theories. *J. Chem. Phys.*, 123(3):034708, 2005.

[309] M. van der Linden, B. O. Conchúir, E. Spigone, A. Niranjan, A. Zaccone, and P. Cicuta. Microscopic Origin of the Hofmeister Effect in Gelation Kinetics of Colloidal Silica. *J. Phys. Chem. Lett.*, 6(15):2881–2887, 2015.

[310] A. J. Milling and B. Vincent. Depletion forces between silica surfaces in solutions of poly(acrylic acid). *J. Chem. Soc. Faraday Trans.*, 93(17):3179–3183, 1997.

[311] T. Freltoft, J. K. Kjems, and S. K. Sinha. Power-law correlations and finite-size effects in silica particle aggregates studied by small-angle neutron scattering. *Phys. Rev. B*, 33(1):269–275, 1986.

[312] P. W. Rouw and C. G. de Kruif. Adhesive hard-sphere colloidal dispersions: Fractal structures and fractal growth in silica dispersions. *Phys. Rev. A*, 39(10):5399–5408, 1989.

[313] J. Hyeon-Lee, G. Beaucage, S. E. Pratsinis, and S. Vemury. Fractal Analysis of Flame-Synthesized Nanostructured Silica and Titania Powders Using Small-Angle X-ray Scattering. *Langmuir*, 14 (20):5751–5756, 1998.

[314] S. Kim, K. Hyun, J. Y. Moon, C. Clasen, and K. H. Ahn. Depletion Stabilization in Nanoparticle-Polymer Suspensions: Multi-Length-Scale Analysis of Microstructure. *Langmuir*, 31(6):1892–1900, 2015.

[315] S. Kumar, V. K. Aswal, and J. Kohlbrecher. Small-Angle Neutron Scattering Study of Interplay of Attractive and Repulsive Interactions in Nanoparticle-Polymer System. *Langmuir*, 32(6): 1450–1459, 2016.

[316] D. Lairez. Introduction à la diffusion de neutrons aux petits angles. *J. Phys. IV*, 103:253–290, 2003.

[317] D. S. Poche, P. S. Russo, B. Fong, E. Temyanko, and H. Ricks. Teaching light scattering to exemplify and reinforce basic principles. *Journal of Chemical Education*, 76(11):1534–1538, 1999.

[318] T. O. Goldsmith. *The refractive index of water for electro-magnetic waves eight to twenty-four centimenters in length*. Cornell Univ., 1936.

[319] American Polymer Standards Corporation. Light scattering dn/dc values. URL `http://www.ampolymer.com/dndc.html`.

Diffusion of polyelectrolytes in dispersions of nanoparticles

Polyelectrolytes are a particular class of polymers with ionizable repetition units that dissociate in polar solvents, such as water, leading to macro-ions and counterions. Solutions and materials made of polyelectrolytes are extensively used in several formulations and in industrial, biological and environmental processes. For a better insight into these systems, the properties of polyelectrolytes in the presence of other particles have to be studied in more detail.
This work deals with the modification of the dynamic properties of short polyelectrolytes in the presence of charged silica nanoparticles. To study this problem, we design an experimental system made of carboxylate molecules of various sizes, from a simple carboxylate (propionate) up to short polyelectrolytes (sodium polyacrylate, PAANa), diffusing in aqueous dispersions of silica nanoparticles of different size and surface charge. Both polyelectrolytes and nanoparticles are negatively charged at high pH. The self-diffusion of the molecules is investigated using NMR diffusion experiments, which monitors the Brownian motions of individual molecules on 10-1000 ms timescale (10-100 μm lengthscale).
This work also investigates how the presence of polyelectrolytes modifies the phase behaviour of silica particles by using small angle neutron scattering.

Keywords: Polyelectrolytes, crowded media, PAANa, silica, diffusion NMR, SANS.

Diffusion de polyélectrolytes dans des dispersions de nanoparticules

Les polyélectrolytes sont des polymères avec des unités de répétition ionisables qui dans un solvant polaire, comme l'eau, se dissocient en libérant des contre-ions. Les polyélectrolytes, du fait leur présence dans de nombreuses formulations, de leur rôle dans les processus industriels, les milieux biologiques et environnementaux, sont le sujet d'un grand nombre d'études. Aussi, pour mieux comprendre et mettre à profit les polyélectrolytes, leurs propriétés en présence d'autres composés doivent être étudiées plus en détails.
Ce travail se concentre sur la modification des propriétés dynamiques de polyélectrolytes courts en présence de nanoparticules de silice chargées. Pour cette étude, nous avons conçu un système expérimental constitué de diffuseurs dispersés au sein d'obstacles chargés. Les diffuseurs sont des molécules de type carboxylate de différentes tailles : des carboxylates simples jusqu'aux polyélectrolytes (polyacrylate de sodium, PAANa) courts. Les obstacles sont des nanoparticules de silice de différentes tailles et charges de surface. Les polyélectrolytes et les nanoparticules sont chargés négativement à pH élevé. L'autodiffusion des molécules est étudiée principalement par diffusion RMN, technique qui permet d'étudier les mouvements browniens de molécules sur une échelle de temps de 10-1000 ms (10-100 μ m en échelle spatiale).
Ce travail examine également comment la présence de polyélectrolytes modifie les interactions entre particules de silice en utilisant la diffusion de neutrons aux petits angles.

Mots clefs : Polyélectrolyte, milieu encombré, PAANa, silice, diffusométrie RMN, DNPA.